General Order Coupled-Cluster in the 4-Component Framework

Inaugural-Dissertation

zur

Erlangung des Doktorgrades der

Mathematisch-Naturwissenschaftlichen Fakultät

der Heinreich-Heine-Universität Düsseldorf

vorgelegt von

Lasse Kragh Sørensen

aus Guldager (Dänemark)

Düsseldorf 2009

Aus dem Institut für Theoretische Chemie und Computerchemie

der Heinreich-Heine-Universität Düsseldorf

Gedruckt mit Genehmigung der

Mathematisch-Naturwissenschaftlichen Fakultät

der Heinreich-Heine-Universität Düsseldorf

Referent:	Prof. Dr. Christel M. Marian
Korreferent:	Prof. Dr. Jeppe Olsen
Externer Referent	Prof. Dr. Michael Dolg

Tag der mündlichen Prüfung: 27.01.2010

So it goes.

Kurt Vonnegut, Jr.

Slaughterhouse-Five, or The Children's Crusade: A Duty-Dance With Death

Zusammefassung

Die Entwicklung eines Generalized-Active-Space (GAS) Coupled-Cluster (CC) Programmes für die Anwendung in der relativistischen Elektronenstrukturtheorie steht im Mittelpunkt dieser Arbeit. Anwendungen an kleinen molekularen Systemen, welche schwere Elemente enthalten, nummerische Untersuchungen der Grenzen des gegenwärtigen Ansatzes und Näherungsmodelle, welche ebenfalls in dieser Arbeit präsentiert werden, stellen natürliche Erweiterungen zu diesem Punkt dar. Die Entwicklung des General-Order CC Programmes wurde hierbei in drei aufeinanderfolgenden Ausführungsschritten durchgeführt. Bei dem ersten handelt es sich um die Verwirklichung einer Schnittstelle zwischen dem LUCIA Programm und dem DIRAC Programmpaket. Diese Schnittstelle ermöglicht es, mit dem nichtrelativistischen GAS CC Programm von Jeppe Olsen Rechnungen im relativistischen, spinfreien Formalismus des DIRAC Programmpaketes durchzuführen. Der zweite Schritt umfasst die Adaptierung eines konfigurationswechselwirkungsbasierten (CI) General-Order CC Programmes auf den vollrelativistischen Formalismus. Mit diesem Programm konnten somit die ersten Rechnungen präsentiert werden, welche iterative Dreifachanregungen (CCSDT) im vollrelativistischen Rahmen beinhalten. Im letzten Schritt wurde die Implementierung eines effizienten, vollrelativistischen GAS CC Programmes, welches auf den Eigenschaften von Kommutatoren beruht, umgesetzt. Mit Hilfe dieses neuen, effizienten Programmes war es möglich, eine umfangreiche Behandlung der Korrelation, bei der die CC Hierarchie erst bei den vollen iterativen Vierfachanregungen (CCSDTQ) abgeschnitten wurde, zu betreiben. Dies überschreitet deutlich die Möglichkeiten bereits existierender Programme. Alle drei in dieser Arbeit entwickelten Programme erlauben als einen Spezialfall eine zustandsselektive (SS) Multireferenz (MR) CC Entwicklung durchzuführen. Auf dieser Basis war es daher nicht nur möglich, die ersten SSMRCC Rechnungen im vollrelativistischen Formalismus durchzuführen, sondern darüber hinaus auch die CC Entwicklung bis zu vollständig iterativen Dreifachanregungen (MRCCSDT) fortzuführen. Desweiteren wurden mehrere Näherungen, welche auf umgedrehten Kramersprojektion, unvollständigen formalen Modellräumen (CC(n_m)) und angenäherten Core-Valenzkorrelationsmodellen beruhen, in die neuen Programme integriert. Ziel dieser Näherungen ist es, die Rechenzeit bei gleichbleibender Genauigkeit signifikant zu vermindern. Alle Programme, die in dieser Arbeit entwickelt wurden, werden in der Zukunft als Teil des DIRAC Programmpakets der wissenschaftlichen Gemeinschaft zur Verfügung stehen.

Die Anwendungen, welche in dieser Arbeit präsentiert wurden, befassen sich mit der genauen Ermittlung spektroskopischer Eigenschaften kleiner Moleküle mit schweren Elementen in ihren Grund- und elektronisch angeregten Zuständen. Hierbei konnte durch späteres Abschneiden der CC Hierarchie und durch Anwendung des GAS Konzeptes in Rechnungen mit extensiven, unkontrahierten Basissätzen eine hohe Genauigkeit erzielt werden. Um die Einsatzmöglichkeiten der realisierten Programme zu untersuchen und um spektroskopische Daten zu erhalten, wurden mehrere Vergleichsstudien an den HBr, BiH und LiCs Molekülen durchgeführt. Für LiCs wurden neben den elektronischen Eigenschafen des elektronischen Grundzustandes auch skalarrelativistische- und Spin-Bahn Effekte auf diesen umfassend untersucht. Anhand von präzisen CC und CI Potentialflächen und daraus abgeleiteter vibronischer Spektren konnte für das RbYb Molekül ein verbessertes Laser-getriebenes Zwei-Schritt Schema zur experimentellen Präparation des Moleküls in seinem rovibronischen Grundzustand ausgehend von ultrakalten Rb und Yb Atomen aufgestellt werden. In den Arbeiten am molekularen Kation $(RbBa)^+$ wurde der Einfluss energetisch niedrigliegender Ba $6s^1 5d^1$ Zustände auf einen möglichen Ladungstransfermechanismus unter Beteiligung strahlungsloser Prozesse in Stoßexperimenten ultrakalter Rb Atome und Ba^+ Ionen herausgestrichen.

Darüber hinaus wurden umfassende, systematische Studien über die Auswirkungen der Basisatzgröße, das Abschneidens des virtuellen Raums und der Korrelation von Elektronen des äußeren Cores an den HBr und LiCs Molekülen durchgeführt. Intention dieser Studien war es, herauszuarbeiten, wie bei zukünftigen Rechnungen an molekularen Systemen mit schweren Atomen eine systematische Verbesserung der Ergebnisse zu erlangen ist, ohne sich dabei gefälliger Fehlerkompensation zu bedienen.

Summary

The development of a generalized active space (GAS) coupled-cluster (CC) code for the use in relativistic electronic-structure theory is in the center of this thesis. Application to small molecular systems containing heavy elements along numerical investigation of the limitations of the current approach and approximative schemes also presented in this work have all been natural extensions of this center. The development and implementation of the general order coupled-cluster codes was performed in three separate steps. The first step comprised the implementation of an interface of the LUCIA code to the DIRAC program package. This interface allowed to perform calculations within the relativistic spin-free framework of DIRAC using the non-relativistic generalized active space coupled-cluster code of Jeppe Olsen. The second step was the adaptation of a general order coupled-cluster code based on configuration-interaction expansions to the fully relativistic framework. With this code the first coupled-cluster calculations including iterative triples (CCSDT) in the fully relativistic framework could be presented. The final step encompassed the implementation of an efficient generalized active space coupled-cluster code in the four-component framework based on the property of commutators. With the new efficient code extensive correlation treatment outperforming previous implementations has been demonstrated by truncating the coupled-cluster hierarchy at the fully iterative quadruples (CCSDTQ). All the methods described above can, as a special case, perform a state-selective multireference coupled-cluster expansion. The first of its kind, in a fully relativistic framework, were performed with these codes. Moreover, the first multireference calculations containing fully iterative triples (MRCCSDT) have been performed. Several approximation methods based on the flipping of the Kramers projection, incomplete formal model spaces (CC(n_m)) and approximative core-valence correlation schemes have been implemented. These aim at a reduction of the computational time while still maintaining the accuracy. The newly implemented codes will be made available to the scientific community in a future release of the DIRAC program package.

The applications presented in this thesis are concerned with an accurate determination of ground- and excited-state spectroscopic properties of small molecules containing heavy elements. Very high accuracy was achieved in this context by extending the truncation in the coupled-cluster hierarchy, applying the concept of generalized active spaces

and making use of extensive uncontracted basis sets. Several benchmark studies have been performed on the molecules HBr, BiH and LiCs to demonstrate the capabilities of the implemented methods and to obtain accurate spectroscopic data. For LiCs scalar-relativistic and spin-orbit effects on the ground state were studied comprehensively along with electric properties. On the basis of accurate CC and CI potential energy curves and the derived vibrational data a revised laser-driven two-step mechanism was proposed to prepare RbYb molecules in their rovibronic ground state under laboratory conditions using ultracold Rb and Yb atoms. In the studies of the molecular cation $(RbBa)^+$ it has been discussed how the energetically low-lying Ba $6s^15d^1$ states could possibly contribute to a non-radiative charge-transfer mechanism in collision experiments of ultracold Rb atoms and Ba^+ ions.

Extensive systematic studies of the effect of basis set size, truncation of virtual space along with outer-core correlation have been conducted for the molecules HBr and LiCs, demonstrating how systematic improvement of theoretical studies of molecular systems containing heavy atoms can be achieved. These studies will thus help to guide future calculations to systematically improve towards the right answer for the right reason.

Contents

Introduction

The understanding and solution of classic and quantized many-body equations has been at the core of theoretical physics and chemistry since the emergence of classical Newtonian physics and even more with the development of quantum mechanics in the early 20th century and still today presents a formidable challenge to the various communities. The solutions presented to these equations have rarely been in a closed algebraic form except for the simplest cases or when special starting conditions are applied. For the most parts an approximative form or not a closed form has been put forward in an attempt to solve these coupled partial differential equations with a given accuracy and precision. The more elegant of these methods have a systematic way of increasing the accuracy and precision to an, in principle, arbitrary level. One of these methods, namely the coupled-cluster method, has been the focus of this work.

The theory of relativity and the attempt to combine this with quantum mechanics gave rise to another more fundamental problem, namely, the formulation of the exact quantized many-body equations. The first Lorentz invariant one-particle quantized equation was the Klein-Gordon equation which can be used to describe spin-0 particles like pions [1]. Not much later P.A.M. Dirac formulated his famous equation [2], bearing his name, describing spin-$\frac{1}{2}$ particles. However, the extension from one-particle [1] equation to a proper many-body equation has proven exceedingly difficult and to date no proper Hamiltonians has been formulated. This has lead to the formulation of effective many-body Hamiltonians as the Dirac-Coulomb Hamiltonian and the likes. Unlike for the solution of these equations there is no way of improving the Hamiltonian in a systematic manner until, in principle, the exact one is found.

In the last decades with the rapid development of fast and large computers with ample computational power has enabled numerical investigations of the various approxi-

[1] In the Dirac hole theory there is no true one-particle equation.

mative solutions. In the quantum chemistry community there are two main branches. The *ab initio* branch which with its systematic methods like perturbation theory, configuration interaction (CI) and coupled cluster (CC) has shown that chemical accuracy[2] is possible with higher level of approximation. These methods unfortunately have a steep scaling with regards to the approximation level of the hierarchy. Therefore, chemical accuracy and going to higher levels in the hierarchy is only possible for small molecules. The other branch include methods like Density Functional Theory (DFT) and Molecular Mechanics (MM) which have a much more favorable scaling with respect to system size. They cannot, however, yield exact results since they rely on external parameters. Attempts have been made to combine the two branches in hybrid methods like the DFT/MRCI to try and get the best of both branches or embedding schemes like QM/MM methods for very large molecules where only a small part of the molecule is of interest.

For the *ab initio* methods it has become customary to truncate these methods at the second order, due to the steep scaling, thereby making the familiar methods like MP2, CISD and CCSD. In recent years the size extensive method CCSD and approximations of this like CC2 and RI-CC2 have gained much attention in the calculation of medium sized molecules. Very recent developments in the screening of integrals for the MP2 method have enabled linear scaling with regards to system size thus making this method available to large and very large molecules. These lower-order approximation methods are, however, not what is desired if one is looking for chemical accuracy. The fastest converging of these methods with respect to the excitation level is the coupled-cluster method. The coupled-cluster method has therefore also received the greatest attention when it comes to reaching chemical accuracy. The direct implementation of higher-order methods has, however, proven to be rather demanding due to the rapid increase of the number of matrix elements to be programmed and debugged. It is, however, obvious that general order programs cannot be generated by explicit programming of matrix elements to all but the very lightest of elements. To make methods of general order it is therefore necessary to develop a completely different strategy where one avoids these explicit matrix elements and instead focuses on the general contraction of operators. Such codes have, however, been scarce and have not until recently been developed in the non-relativistic framework [3–6] and are yet to be distributed to a wider audience than the developers

[2]Chemical accuracy defined as 1 kcal/mol in thermochemistry.

and collaborators of these.

The work presented in this thesis is a general-order coupled-cluster code adapted to relativistic framework based on the Dirac-Coulomb Hamiltonian. Besides being of general order the code also incorporates the generalized active space (GAS) concept. The GAS is a generalization of the complete active space (CAS) or restricted active space (RAS) and enables a completely free division of Kramers pairs[3] into subspaces of Kramers pairs and any desired (and allowed) excitation between these. This very general way of allowing and restricting excitations between Kramers pairs also makes the program able to perform state-selective multireference coupled-cluster calculations making this the first general-order coupled-cluster and multireference coupled-cluster program for the relativistic framework. The calculations presented in this thesis have therefore also been novel since these types of calculations have not previously been possible with existing codes. The programs have primarily been developed to calculate highly accurate potential energy surfaces where these are needed. An example of this kind of application is in the field of ultracold molecules where several molecules have been examined. With methods and programs capable of performing extensive correlation treatments well-defined error bars for a given calculation can be found. This is of great importance to enhance the predictive power of the calculations. Good error bars are at the moment only known for closed-shell molecules of the first and second row[4] and only until the CCSD(T) level. An investigation with molecules including heavy elements is therefore needed to guide the calculations.

Layout of this thesis

The thesis can be divided into three parts:

I The first part is concerned with developing the physical framework that we are working in. This means introducing relativistic effects, relativistic quantum chemistry and the different types of multireference coupled-cluster correlation methods. This part lays the foundation for the development.

II In the second part the programs, their concepts and their implementation is presented. The development of quantum chemistry codes will be sketched and new

[3] In the non-relativistic framework this would be orbitals.

[4] From Li to Ar.

approximation methods proposed.

III In the final part applications of the newly implemented codes along with interesting investigations on ultracold molecules is shown. Finally, a critical numerical look is taken at the usual approximations done for molecules containing heavy elements.

Chapter 1

Heavy Elements

The aim of this chapter is to give the unfamiliar reader to relativistic contributions of electron structure theory a short overview of the effects of scalar relativity, spin-orbit and other smaller effects on atoms and molecules. The chapter is written to show when inadequacies will arise in the non-relativistic Hamiltonian and then a more accurate Hamiltonian like the Dirac-Coulomb or others will be needed. The chapter is written from a primarily phenomenological viewpoint and is meant to be readable even without a deeper understanding of the underlying equations and methods. The equations are therefore partially saved for later in the theory section on relativity in chapter 2 though not completely and the reader is therefore encouraged to study the book from W. Greiner *Relativistic quantum mechanics* [1] for a thorough introduction to the Dirac equation. The extension to atomic and molecular many-body equation and the methods of solving these is very well covered in the book from Dyall and Fægri *Introduction to Relativistic Quantum Chemistry* [7] or the older book by Moss *Advanced Molecular Quantum Mechanics* [8]. The more interested reader would be referred to Pyykkö's paper [9] on the various relativistic effects and the more contemporary books from Dyall and Fægri [7] and Reiher and Wolf [10] which also cover recent developments in the field of relativistic quantum chemistry. These three sources contains all the main material written in this chapter and would all serve as a very good introduction to relativistic effects in atoms and molecules.

Firstly we will briefly look at where heavy elements used in physics an chemistry which has been relevant for this work before proceeding to the relativistic effects.

1.1 Heavy Elements in Physics and Chemistry

The primary function of this section is to give an example of where heavy elements are used in physics and chemistry. The focus will be on uses where highly accurate potential surfaces are needed and the on calculations done in this work.

A prime example is in the rapidly developing field of cold and ultra cold molecules where very accurate potential energy curves are needed to interpret lines in spectra and to find possible mechanisms to reach the rovibronic ground state or the knowledge of electric properties for trapping or further manipulations. Several molecules like the LiCs, RbYb and $RbBa^+$ presented in Sections 9.3, 9.6, 9.4 and 9.5 have been examined in this field which was inspired by a recent/ongoing collaboration with the group of Axel Görlitz which does experiments in this field.

Other very active fields of research are in the actinide chemistry where the $5f$ electrons make for very interesting and complicated chemistry. Here one often finds a multiconfigurational character of the wave function and would therefore also be an obvious area of application of the multireference coupled-cluster method. The complexity of many of the molecules is however a study on its own and therefore beyond the scope of this thesis.

Another important, though not so active, field is the chemistry of the p block elements. Since these have the largest spin-orbit splitting in the periodic system these are ideal for the *a priori* inclusion of spin-orbit coupling which comes naturally in the 4-component framework. Work on these systems is presented in Sections 9.1, 9.2 and 9.6. An explanation for why the p-block elements have the largest spin-orbit splitting can be found in Section 1.2.1.3.

1.1.1 Ultra Cold Molecules

A large fraction of investigated systems in the (ultra-)cold molecular sciences is comprised by alkali metal diatomics like the LiCs, see Sections 9.3 and 9.6. These alkali dimers were the first to gain attention since there was already a prior knowledge of how to cool these atoms for a later production of a molecule and because these molecules often exhibit a dipole moment which makes them suitable for a later manipulation.

A new class of hetero-nuclear diatomics like the RbYb, see Section 9.4, may be trapped due to their unpaired electron(s) and manipulated using magnetic fields [11].

They are, for example, promising candidates for an experimental search for a permanent electric dipole moment of the electron or for producing lattice-spin models [12] for quantum computing.

Other classes of charged hetero-nuclear diatomics like the $RbBa^+$ formed from an alkali and an alkaline earth metal. With a charged molecule intermolecular charge-transfer processes could be studied. Other interesting fields of research would be study of mesoscopic molecular ions in Bose-Einstein condensates (BEC) [13] where the BEC is doped with few ions. This will have a longer range potential of C_4/r^4 than the van der Waals interaction of C_6/r^6 that is seen in the neutral hetero-nuclear molecules.

A number of groundbreaking achievements has been reported from the field of cold and ultra-cold molecules, and ongoing investigations bear the potential for yet further findings of fundamental importance [14]. These range from the production of BECs [15] to the striving for a controlled chemistry at the quantum level [16] and the possibility of testing, e.g., fundamental symmetries in nature through measurements of a postulated electric dipole moment (EDM) of an electron [17, 18] or the space-time variation of fundamental constants such as the fine-structure constant α [19, 20]. The experimental work for producing (ultra-)cold molecules has to the date been conducted in a variety of ways, such as photoassociation (PA) [21], buffer gas cooling (sympathetic cooling) [22], Stark deceleration of polar molecules via time-modulated electric fields [23] and magnetically tunable Feshbach resonances [24].

Theoretical contributions to the field of (ultra-)cold molecules are of value in many different respects. Among the most important is the determination of accurate molecular potential energy curves (PECs) of ground and relevant electronically excited states. These potentials are often required to be known both at short and long range [21]. At long range, atom-atom interactions are typically evaluated by perturbation theory, whereas at short range advanced methods of molecular electronic structure theory come into play. In addition to the spectral constants which may be extracted directly from the short-range potentials (equilibrium bond lengths, harmonic vibrational frequencies, dissociation and excitation energies) [25–27], vibrational states and Franck-Condon factors (FCFs) [28], molecule formation rates [29], and electric properties such as permanent EDM [30, 31], transition dipole moments [32], and static polarizabilities are of interest and have been determined by theoretical methods.

1.2 Relativistic Effects in Atoms and Molecules

This section is written to show what effect the most dominant relativistic contributions have on atoms and the molecular structure. These effects are "independent" of which Hamiltonian is used and will therefore be discussed from a Hamiltonian more resembling the one known from the Schrödinger equation namely the Breit-Pauli Hamiltonian.

1.2.1 Primary Concepts

Much of quantum chemistry has primarily been concerned about solving the time independent many-body electronic Schrödinger equation[1] for molecules consisting of the first two rows of atoms. The equation comes from the time dependent many-body Schrödinger equation where time has been factorized out and then the Born-Oppenheimer approximation has been invoked to separate electronic and nuclear coordinates to a final equation for electrons in a static electric field of nuclear charges. The equation is easily generalized to any molecule and the Hamiltonian can in it's most general form be written as

$$\hat{H} = \hat{T} + V = \sum_{i}^{N} \frac{1}{2m} \hat{\boldsymbol{p}}_i^2 - \sum_{i}^{N} \sum_{A}^{M} \frac{Z_A}{r_{iA}} + \sum_{j>i}^{N} \frac{1}{r_{ij}} \tag{1.1}$$

where the first term is the kinetic energy of the electrons, second the Coulomb interaction of electrons and nuclei and finally the electron-electron Coulomb interaction. The most obvious thing missing from the equation is any reference to spin. Therefore an additional postulate of spin is needed[2]. While this Hamiltonian can give accurate spectroscopic prediction for the light elements it will fail for electronic transitions between states with different spin (since these will always be trivially zero) and it will also fail already in the prediction of the ground state of many heavy atoms and molecules. An example of such a failure to predict the correct state is seen in the BiH molecule which is due to incorrect prediction of the Bi ground state. The correct ground state of BiH is 0^+ and not the $^3\Sigma^-$ predicted from non-relativistic theory. Calculations on the BiH molecule is presented in Section 9.2.

[1] Hereon just the Schrödinger equation

[2] In the limit of $\lim c \to \infty$ for the Dirac equation the Schrödinger equation can be recovered in a two component form (spinor) where spin is naturally included. This is the Lévy-Leblond equation [33]

To compare with the Schrödinger equation I choose the Breit-Pauli Hamiltonian, which can be constructed either by a Foldy-Wouthuysen transformation or an elimination of the small component, this Hamiltonian is correct to $O(c^{-2})$ and contains the most important relativistic effects[3]. With the elimination of the small component the Breit-Pauli Hamiltonian can be written in a form more comparable to the Schrödinger equation in 1.1

$$\begin{aligned}
\hat{H}^{BP} &= \sum_{i}^{N}\left[\frac{1}{2m}\hat{\boldsymbol{p}}_i^2 - \frac{1}{8m^3c^2}\hat{\boldsymbol{p}}_i^4 - \sum_{A}^{M}\Big(\frac{Z_A}{r_{iA}} + \frac{\pi\hbar^2 Z_A}{2m^2c^2}\delta(\boldsymbol{r}_{iA}) + \frac{Z_A}{2m^2c^2r_{iA}^3}\boldsymbol{s}_i\cdot\boldsymbol{l}_i\Big)\right] \quad (1.2)\\
&+ \sum_{j>i}^{N}\left[\frac{1}{r_{ij}} - \frac{1}{m^2c^2r_{ij}^3}(\boldsymbol{s}_i+2\boldsymbol{s}_j)\cdot\boldsymbol{r}_{ij}\times\boldsymbol{p}_i - \frac{\pi\hbar^2}{m^2c^2}\delta(\boldsymbol{r}_{ij})\right.\\
&- \frac{1}{2m^2c^2}\Big(\frac{1}{r_{ij}}\boldsymbol{p}_i\cdot\boldsymbol{p}_j + \frac{1}{r_{ij}^3}(\boldsymbol{r}_{ij}(\boldsymbol{r}_{ij}\cdot\boldsymbol{p}_j)\cdot\boldsymbol{p}_i\Big) - \frac{8\pi}{3m^2c^2}(\boldsymbol{s}_i\cdot\boldsymbol{s}_j)\delta(\boldsymbol{r}_{ij})\\
&+ \left.\frac{1}{m^2c^2}\Big(\frac{(\boldsymbol{s}_i\cdot\boldsymbol{s}_j)}{r_{ij}^3} - \frac{3(\boldsymbol{s}_i\cdot\boldsymbol{r}_{ij})(\boldsymbol{s}_j\cdot\boldsymbol{r}_{ij})}{r_{ij}^5}\Big)\right]
\end{aligned}$$

where one finds additional one- and two-electron contributions. The most important of these additional contributions are the three extra one-electron terms which are the mass-velocity, Darwin and the spin-orbit term, respectively, in line one of Eq. 1.2. The additional two-electron terms are spin-same- and spin-other-orbit, Darwin, retarded orbit-orbit interaction, Fermi contact and the spin-spin dipole interaction.

The mass-velocity and the one- and two-electron Darwin terms are together referred to as the scalar relativistic effects. These together with the one-electron spin-orbit and spin-same-orbit terms originate from the Coulomb interaction. The spin-dependent part of the Gaunt interaction gives the spin-other-orbit, Fermi contact and the spin-spin dipole terms. The spin-free part of the Gaunt term is partially canceled by the gauge term from the Breit interaction but still leaves the first part of the retarded orbit-orbit interaction. The second part comes from the gauge term[4]. To the order $O(c^{-2})$ the gauge term does not contain any spin-dependent terms. All these additional terms arise from the picture change when going from the Dirac picture to the Schrödinger picture [34].

[3]This is the more modern derivation of the Breit-Pauli Hamiltonian. Originally the Pauli Hamiltonian was constructed by Pauli before the Dirac equation was formulated.

[4]Both the Gaunt and the gauge term do contain more terms, like a two-electron Darwin term, which however cancels

1.2.1.1 Direct and Indirect Relativistic Effects

Going from the Schrödinger equation to a relativistic Hamiltonian a plethora of additional terms appears as shown in Eq. 1.2. The contribution from these additional terms are called the direct relativistic effects. However, due to the direct effects on each electron, the potential (screening) of all other electrons changes and this change is called the indirect relativistic effect. Which effect dominates is very dependent on the angular momentum l of the sub-shell since the higher angular momentum shell does not penetrate the core region like the lower ones do [35].

While the direct relativistic effects cause contraction and stabilization of the atomic orbitals, this effect is really only important for the s and p orbitals since only these have significant probability density close to the core region where the direct effects are large. d and f orbitals, on the other hand, have only very little direct relativistic effects since they do not penetrate the core region. These direct effects originate primarily from the one-electron scalar relativistic effects which can in Eq. 1.2 be seen to be very localized in and around the core region.

The indirect effects will come from both the contraction of the core orbitals but even more important contraction of semi-core/valence orbitals. The contraction of the core s and p orbitals only have small destabilization influence on the valence s and p since these have their radial maximum well outside the core region. The d and f orbitals will not experience any significant effect of the core contraction since they lie outside the core. d and f orbitals will, however, experience a strong destabilization from contracted orbitals with a radial maximum in the same region as the d and f orbitals which in particular are the s and p orbitals in the semi-core/valence region [35]. Hence the relativistically contracted s and p orbitals will cause an indirect destabilization of valence electrons whereas the d and f orbitals will actually cause an indirect stabilization due to a poorer shielding of the nuclei.

To summarize the s orbital is dominated by direct relativistic effects and will therefore contract and be stabilized. For the p orbitals the direct and the indirect contributions approximately cancel. If one looks at the $p_{1/2}$ and $p_{3/2}$ subshells of the p orbital it is then seen that the $p_{1/2}$ has a larger dynamic effects than the $p_{3/2}$ which means that there usually will be a small contraction and stabilization of the $p_{1/2}$ and opposite the $p_{3/2}$. The d

and f orbitals are dominated by the indirect relativistic effects and will therefore always expand and be destabilized.

1.2.1.2 Scalar Relativistic Effects

The scalar relativistic contributions come primarily from the one-electron Darwin and the mass-velocity term. As is seen from Eq. 1.2 and mentioned in Section 1.2.1.1 they affect primarily orbitals with significant electron density in and around the nuclei and hence will therefore primarily affect the s orbitals which are contracted and stabilized. The scalar relativistic effects can have a large influence on the bond length as shown for LiCs in Section 9.3 which involves a σ bond. While scalar relativistic effects change the magnitude of a bond it, however, does not alter the symmetry since no mixing of states with different spins are involved. This means it can easily be included in a non-relativistic code either directly or as a perturbation. This is discussed further in section 2. Since the largest part of the bond contraction comes from the dynamics and not the orbital contraction [34–37] non-relativistic orbitals can therefore be used for light elements. This stabilization of the s orbitals is often called the "inert pair" effect since even in the valence shell for the heavy p block elements the s orbitals helps to stabilize the $n-2$ oxidation state of an n electron valence system.

That the Darwin and mass-velocity term are the most significant scalar relativistic contributions comes from the fact that they are the lowest order corrections. The mass-velocity is the lowest order correction of the kinetic energy and the Darwin term to the external charge distribution, which is here the nuclear charge. The Darwin potential is furthermore related to the *Zitterbewegung* which causes a smearing of the charge in the Pauli representation of the of the Compton wavelength $\lambda_c = \hbar/mc$.

1.2.1.3 Spin-Orbit Effects

With the inclusion of spin-orbit effect a lift of degeneracy in all orbitals with $l > 0$ is experienced which splits into two degenerate subshells depending on the spin s being parallel or anti-parallel with the angular momentum l. These new subshells then depend on the total angular momentum j according to

$$\boldsymbol{j} = \boldsymbol{l} + \boldsymbol{s}. \tag{1.3}$$

The p orbitals then split into a $p_{1/2}$ and a $p_{3/2}$ subshells where the $p_{1/2}$ is lower in energy than the $p_{3/2}$ which is evident from the sign of the one-electron spin-orbit operator in the Breit-Pauli Hamiltonian in Eq. 1.2. Likewise is the d orbital split into $d_{3/2}$ and $d_{5/2}$ and the f into $f_{5/2}$ and $f_{7/2}$ where the lowest j value is lowest in energy.

Like with the scalar relativistic effects it is also the one-electron term that dominates the spin-orbit splitting and again does the penetration of the orbital play the largest role in the size of the spin-orbit splitting. While one naively might expect, from the expression of the one-electron spin-orbit term in Eq. 1.2, that the spin-orbit splitting would increase with increasing angular momentum l since the angular integral $\boldsymbol{l} \cdot \boldsymbol{s}$ increases this is, however, not the case. The reason for this is the radial part of the spin-orbit coupling that decreases dramatically with increasing l due to the inability of orbitals of higher angular momentum to penetrate the core region. Hence one therefore see the opposite with the largest spin-orbit splitting in the p block and the smallest in the f block.

The one-electron spin-orbit operator scales approximately as Z^4 [38] and is thus of increasing importance for heavy elements[5]. The scaling of the two-electron spin-orbit terms are however not so clear. The one-electron originate from the interaction with the nuclei while the two-electron is caused by the motion of the other electrons. This difference is also seen in the importance of the various spin-orbit terms with increasing Z. For the light elements the relative error is significantly larger when not including the two-electron spin-orbit terms than for the heavy elements. This occurs because the one- and two-electron spin-orbit splitting is closer in size for the light element than for the heavy ones. For the heavy elements the one-electron term is the dominating term so while the two-electron term also increases with Z its relative size to the one-electron terms decreases. The absolute error made by not including the two-electron term, of course, increases with Z thereby making it essential for accurate calculations.

[5]For a comparison of light and heavy elements with this scaling the comparison always has to be between the same shell.

Chapter 2

Dirac Equation and Effective Many-Body Hamiltonians

The first part of this chapter will be kept rather short and only gives a very short overview of parts of relativistic quantum mechanics. This is primarily done since there already exist many good text books on the subjects touched upon here. For a rigorous introduction to the Dirac equation the excellent book by Greiner [1] would be highly recommended. For a slightly faster introduction the book by Moss [8], Messiah [39], or Schweber [40] would be recommended where the last one contains also a bit of a historical introduction. Going beyond the Dirac equation for a single electron to atoms and molecules the book by Dyall and Fægri [7] would be highly recommended. Other books here would also include the first of the two volume book by Schwerdtfeger [41] and Reiher and Wolf [10].

2.1 The Dirac Equation and It's Usage in Electronic Structure Theory

The Dirac equation [2] was first proposed by P. A. M. Dirac in 1928 in an attempt to find a covariant form of the free particle time dependent Schrödinger equation

$$\imath\hbar\frac{\partial\Psi}{\partial t} = \hat{H}\Psi = \sum_{i}^{3}\frac{\hat{p}_i^2}{2m_0}\Psi \tag{2.1}$$

with a positive definite probability density, a problem that had occurred with the Klein-Gordon equation. At the time neither the charge density nor the fact that the Klein-Gordon equation was completely useless for electrons, since it describes spin-0 particles, was known. Although not accepted at once due to difficulties in interpretation it soon showed to have predictive power not seen before with the discovery of the anti-particle of the electron, namely the positron, in 1932 [42].

First thought to only have very little influence on atoms and molecules, except for the core electrons of heavy elements, it was not until much later, in the seventies, that this was shown to not be the case. In the seventies more systematic studies pioneered by P. Pyykkö, K. Pitzer and J. P. Desclaux showed that relativistic effects did indeed have a significant influence on the valence of heavy atoms and therefore also on the bonding of these. Very nice reviews on this subject written by Pyykkö can be found in [9] and Pitzer in [43] plus a complete tabulation of all atoms in [44] by Desclaux.

Today it is recognized that for accurate calculations of heavy elements codes including relativistic effects are needed. In the past two to three decades there has therefore been a large effort in developing codes for this purpose. Some of the codes developed are MOLFDIR [45], MOLCAS [46], SPOCK [47, 48], TURBOMOLE [49], CIDBG [50], SOCI [51], MAGIC [52], ACES II [53], GAMESS [54, 55], CIPSI [56] and DIRAC [57] which all in one form or another can either include relativistic contributions or is directly based on the Dirac equation.

2.1.1 The Dirac Equation

The derivation of the Dirac equation will follow the historical approach though many of the intermediate steps will be left out and only the main features will be kept in.

Because the free-particle time-dependent Schrödinger equation contains second derivatives with respect to space and first derivatives with respect to time it treats time and space on different footing unlike the Lorentz transformation. It is then obvious that the time-dependent Schrödinger equation (2.1) is not Lorentz invariant. Because of the asymmetry between time and space it will be necessary to formulate a new equation to combine special relativity and quantum mechanics. The search is therefore for an equation which is of first derivative in both time and space to ensure Lorentz invariance. Hence an equation

of the form

$$\imath\hbar\frac{\partial\Psi}{\partial t} = \hat{H}\Psi\big[\frac{\hbar c}{\imath}\big(\hat{\alpha}_1\frac{\partial}{\partial x^1} + \hat{\alpha}_2\frac{\partial}{\partial x^2} + \hat{\alpha}_3\frac{\partial}{\partial x^3}\big) + \hat{\beta}m_0c^2\big]\Psi \tag{2.2}$$

where the coefficients $\hat{\alpha}_i$ and $\hat{\beta}$ is to be decided. As already indicated in Eq. 2.2 the coefficients are not simple numbers but matrices which means Ψ cannot be a simple scalar but must be column vector. By analyzing the algebra of $\hat{\alpha}_i$ and $\hat{\beta}$ it can be shown that this is anticommutative and that the minimum dimension of the matrices which fulfill this algebra will be four. Hence Ψ will then be a four-vector or four-component vector and methods derived directly from the Dirac equation will be four-component methods [1]. In the standard representation $\hat{\alpha}_i$ and $\hat{\beta}$ take the form

$$\hat{\alpha}_i = \begin{pmatrix} 0 & \hat{\sigma}_i \\ \hat{\sigma}_i & 0 \end{pmatrix}, \quad i = 1,2,3; \qquad \hat{\beta} = \begin{pmatrix} \mathbf{1} & 0 \\ 0 & -\mathbf{1} \end{pmatrix} \tag{2.3}$$

where $\hat{\sigma}_i$ are the Pauli matrices and $\mathbf{1}$ is here a 2×2 unit matrix. With the Pauli matrices

$$\hat{\sigma}_1 = \begin{pmatrix} 0 & 1 \\ 1 & 0 \end{pmatrix}; \quad \hat{\sigma}_2 = \begin{pmatrix} 0 & -i \\ i & 0 \end{pmatrix}; \quad \hat{\sigma}_3 = \begin{pmatrix} 1 & 0 \\ 0 & -1 \end{pmatrix}. \tag{2.4}$$

Since we are normally as a start interested in looking for stationary states which are eigenfunctions of a time independent Hamiltonian we will separate off the time dependent part. Since the form of Eq. 2.2 is the same as for the time dependent Schrödinger equation (2.1) the separation follows analogously

$$\Psi(\vec{r},t) = \Psi(\vec{r})\theta(t) \tag{2.5}$$

where the temporal part is

$$\theta(t) = e^{Et/\imath\hbar}. \tag{2.6}$$

[1] It can be debated if a method which makes a transformation that block diagonalizes the Dirac equation can be called a four-component method since to solve the equations there only the components in a given block will be necessary. The author here prefers that any method based directly on the Dirac equation is a four-component method.

We furthermore notice the Eq. 2.2 will then have a positive definite probability density

$$\rho(x) = \Psi^\dagger(x)\Psi(x) > 0 \tag{2.7}$$

since there is no time coordinate or derivative entering the density. This also means we can be sure to have stationary states in any inertial reference frame as long as the Hamiltonian is Lorentz invariant despite the fact that the Lorentz transformation mixes space and time. With the separation of the temporal coordinate Eq. 2.2 transforms into the time independent free Dirac equation

$$\epsilon\Psi(x) = \hat{H}\Psi(x) = (c\hat{\alpha}\cdot\hat{p} + m_0c^2\hat{\beta})\Psi(x) \tag{2.8}$$

which is seen to be a regular eigenvalue problem. The solutions to Eq. 2.8 are

$$\epsilon = \pm E_p, \qquad E_p = c\sqrt{\hat{\mathbf{p}}^2 + m_0^2c^2} \tag{2.9}$$

which is recognized as the relativistic energy from the special relativity theory and is then conserved. The $\pm E_p$ in Eq. 2.9 suggests that the spectrum of the momentum eigenstates will have positive and negative eigenvalues as shown in Figure 2.1. The continuum spectrum of the Dirac equation in Figure 2.1 is a general feature of this and we will always have these solutions below $-mc^2$ and above mc^2 in addition to any discrete solutions in between for bound states. The negative energy solutions shown in Eq. 2.9 and Figure 2.1 are connected with particles of the same mass but opposite charge of the electron, hence the positron. This means the Dirac equation can describe both electrons and positrons only depending on the sign of the charge and the two solutions are related by a charge conjugation. The later discovery of the positron [42] has been seen as one of the great success of Dirac equation and opened the door for the anti-particles and that these can be described in the same equation as the particle. The Dirac equation therefore also immediately gives a lower bound of $2mc^2$ for the pair creation phenomenon where an electron and a positron is spontaneously created.

The four-component wave function, which can describe both electrons or positrons, we will divide into two bispinors of a large and a small component

Figure 2.1: The spectrum of the free Dirac equation

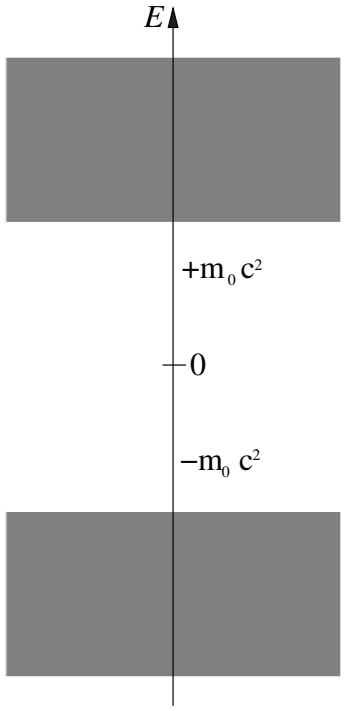

$$\Psi(\mathbf{r},t) = \begin{pmatrix} \Psi_1(\mathbf{r},t) \\ \Psi_2(\mathbf{r},t) \\ \Psi_3(\mathbf{r},t) \\ \Psi_4(\mathbf{r},t) \end{pmatrix} = \begin{pmatrix} \Psi^L(\mathbf{r},t) \\ \Psi^S(\mathbf{r},t) \end{pmatrix}. \tag{2.10}$$

If we then want to describe electrons (as we do) and we are not in the ultra-relativistic case (meaning $p \ll mc$) the large component will be the dominant part of the wave function, hence the large component. For positrons one could also define a large component but in the context of this thesis and in general in quantum chemistry we are interested in the electronic structure and the large component will therefore always refer to the electronic part.

Having an infinite number of negative energy solutions immediately presents a problem when there is any interaction with a radiation field (see Eq. 2.11) since this will connect the positive and negative energy states. This interaction will give an infinite transition probability from the positive to the negative energy continuum meaning any state would immediately make a spontaneous emission of photons as the energy would go to minus infinity. This of course is not a physically acceptable solution since it would mean that there would be no stable matter in contrast to observation. We furthermore

observe that if we have more than one particle it will be possible to make an infinite number of degenerate states where one particle is excited to a positive energy state and another de-excited to the negative energy state. Therefore the system would dissolve into the two continua. This last problem is usually called continuum dissolution [58] or Brown-Ravenhall disease [59]. To overcome these problems the vacuum has to be redefined and a normal-ordered Hamiltonian has to be used in a similar way also done in QED [7].

2.1.2 Many-Body Hamiltonians

The extension of the free particle Dirac equation 2.8 to a to a particle in an external electromagnetic field proceeds with the regular minimal coupling scheme for an electromagnetic interaction

$$\mathbf{p} \rightarrow \mathbf{p} - \mathbf{qA} \qquad \mathbf{E} \rightarrow \mathbf{E} + \mathbf{q}\phi \tag{2.11}$$

where the external scalar ϕ and vector $\mathbf{A}$ potentials are introduced. Introducing Eq. 2.11 into the Eq. 2.8 gives the Hamiltonian for the interaction of an electron with an external field

$$\hat{H} = c\hat{\alpha} \cdot \hat{\mathbf{p}} + mc^2\hat{\beta} + ec\hat{\alpha} \cdot \hat{\mathbf{A}} - e\phi \tag{2.12}$$

In electronic structure theory we are, however, interested in a many-body Hamiltonian and not just a single particle in an electric field. While the extension from one to many particles is straight forward for the Schrödinger equation this is not so for the Dirac equation and to date no exact equation has been formulated. We will therefore make due with an approximative equation like the Dirac-Coulomb equation, which is the one that has been used in the calculations for this thesis, or the extension Dirac-Coulomb-Breit. These two equations are both formulated within the Born-Oppenheimer approximation where the nuclear coordinates have been separated off and what remains to solve is the electronic equation. The stationary nuclei will then only enter the electronic equation as a generator of a stationary electric field, i.e. the nuclei will be viewed as a classical particle while the electrons remains quantum mechanical. For a hydrogen-like system this would

make ϕ of Eq. 2.12 the regular nuclear Coulomb potential of Z/r_{iA} [2]. The Hamiltonian for the hydrogen-like atom then becomes

$$\hat{H} = c\hat{\alpha} \cdot \hat{\mathbf{p}} + mc^2\hat{\beta} - eZ/r_{iA} \tag{2.13}$$

where we notice the vector potential disappear since the nucleus only enters as a static electric field. This is a consequence of the Born-Oppenheimer approximation. The Hamiltonian for the hydrogen-like system is seen to be easy to generalize for many non-interacting electrons and will therefore be used as part of the one-electron operator in the Dirac-Coulomb and Dirac-Coulomb-Breit equations describing the kinetic energy and external field. By invoking the Born-Oppenheimer approximation and using Eq. 2.13 for the one-electron part we have fixed the reference frame to the Born-Oppenheimer frames where only the center of origin of the coordinate system can be moved or the axis rotated. If we had chosen a coordinate system moving relative to the Born-Oppenheimer frames the one-electron equation in 2.13 would also then have to be extended by the vector potential $\mathbf{A}$ from the minimal coupling in 2.11 and to be made Lorentz invariant. We are therefore limited to the Born-Oppenheimer frames.

The extension from the hydrogen-like atom to helium-like atoms is not trivial since the regular Coulomb potential is not Lorentz invariant because it is an instantaneous interaction which does not account for the finite transmission speed of the interaction. Hence the Coulomb interaction has to be extended by retardation terms which account for the finite interaction speed of c for electromagnetic interactions. We will therefore limit the discussion to only include an approximate interaction known as the Breit interaction [60] which is valid for low energies. The Breit interaction can in the Coulomb gauge be written as

$$V_{Breit} = \frac{q_1 q_2}{4\pi\epsilon_0}\Big(\frac{1}{r_{12}} - \frac{\hat{\alpha_1} \cdot \hat{\alpha_2}}{2r_{12}} - \frac{1}{2}\frac{(\hat{\alpha_1} \cdot \mathbf{r_{12}})(\hat{\alpha_2} \cdot \mathbf{r_{12}})}{r_{12}^3}\Big) + O(c^{-4}) \tag{2.14}$$

where the first term is the regular Coulomb interaction, second the Gaunt [61] and lastly the gauge term[3]. This electromagnetic interaction is correct to the order $O(c^{-2})$

[2] In actuality a point nucleus is not employed since it contains a singularity at the center. In DIRAC a nucleus spanned by two Gaussians is used instead.

[3] The gauge term does not appear in Feynman gauge but does in Coulomb gauge and is hence named the gauge term.

and in actual quantum chemical calculations does not appear to be the limiting factor for the accuracy. It can be shown that the Coulomb interaction contains spin-same-orbit term (see Eq. 1.2) while the Gaunt term is needed for the spin-other-orbit term [62]. The one-electron spin-orbit term is contained in the one-electron operator from Eq. 2.13.

With the one-electron and two-electron operator we can write the Dirac-Coulomb Hamiltonian as used in the calculation presented

$$\hat{H}_{DC} = \sum_i (c\hat{\alpha}_\mathbf{i} \cdot \hat{\mathbf{p}}_\mathbf{i} + mc^2\hat{\beta} + \sum_A \hat{V}_{iA}^{nuc}) + \frac{1}{2}\sum_{i\neq j}\frac{1}{r_{ij}} \tag{2.15}$$

where the nuclei is no longer a point charge. Including the Gaunt term is possible at the Hartree-Fock level (see Section 9.5) but at the moment no transformed integrals are available so the spin-other-orbit term cannot be included at the correlated level. As we shall see in Section 9 that although the Dirac-Coulomb Hamiltonian does not contain any retardation effects it is capable of giving very accurate predictions for molecular structures and properties when used in conjunction with large basis sets and high level *ab initio* methods.

2.1.3 Dyall's Spin-Free Hamiltonian

As shown in Section 1.2.1 we can separate relativistic contributions into scalar relativistic and spin-orbit contributions. While spin-orbit interaction mixes spin and space thereby losing the spin symmetry, scalar relativistic does not do this. A spin-free Hamiltonian could therefore be interesting to assess the magnitude of the spin-orbit coupling and scalar relativistic contributions which can be done by comparing with results from the Dirac-Coulomb Hamiltonian in Eq. 2.15 and with a Lévy-Leblond Hamiltonian (see Section 4.2.3). Such a comparison has been made for the LiCs molecule in Section 9.3 where it is found that while scalar relativistic effects are absolutely essential for a correct description of the ground state, spin-orbit contributions are minimal. That spin-orbit contributions can be very small for the ground state is also seen for the RbYb and $(RbBa)^+$ in Sections 9.4 and 9.5, respectively. A spin-free Hamiltonian will furthermore have the advantage that the regular point group symmetry can be used, is significantly cheaper to use in calculations, as will be shown in Sections 2.2.1 and 7, and easier to implement (see Section 6.1). Extensions to include spin-orbit *a posteriori* could be done by diagonalizing an

effective spin-orbit operator in the basis of the spin-free states. This could be a way to save computational power if the spin-orbit contribution is small.

The spin-free Hamiltonian we will focus on is the one suggested by Kutzelnigg [63] and Dyall [7, 64] which consists of a similarity transformation of the Dirac-Coulomb Hamiltonian to a Hamiltonian where there is an exact separation of spin-dependent and spin-independent terms. Let us start from the Dirac equation written in the bispinor form shown in Eq. 2.10

$$\begin{pmatrix} \hat{V} & c\hat{\sigma}\cdot\hat{\mathbf{p}} \\ c\hat{\sigma}\cdot\hat{\mathbf{p}} & \hat{V}-2mc^2 \end{pmatrix} \begin{pmatrix} \psi^L \\ \psi^S \end{pmatrix} = E \begin{pmatrix} \psi^L \\ \psi^S \end{pmatrix}, \tag{2.16}$$

where $\hat{\alpha}$ is written with the Pauli matrices from 2.3. To perform the transformation we insert

$$\hat{\tau} = \begin{pmatrix} 1 & 0 \\ 0 & (\alpha/2)(\hat{\sigma}\cdot\mathbf{p}) \end{pmatrix} \tag{2.17}$$

into a Hamiltonian $\tilde{h}_D$

$$\tilde{h}_D = \hat{\tau} h_D \hat{\tau} \tag{2.18}$$

which can rigorously be separated into a spin-free and a spin-dependent part

$$\tilde{h}_D = \begin{pmatrix} \hat{V} & \hat{T} \\ \hat{T} & (\alpha^2/4)(\mathbf{p}\cdot\hat{V}\mathbf{p}) - \hat{T} \end{pmatrix} + \begin{pmatrix} 0 & 0 \\ 0 & (\alpha^2/4)\imath\sigma\cdot(\mathbf{p}\hat{V})\times\mathbf{p} \end{pmatrix}. \tag{2.19}$$

by applying the Dirac identity

$$(\hat{\sigma}\cdot\mathbf{u})(\hat{\sigma}\cdot\mathbf{v}) = \mathbf{u}\cdot\mathbf{v} + \imath\hat{\sigma}\cdot\mathbf{u}\times\mathbf{v}. \tag{2.20}$$

Where in Eq. 2.19 the kinetic energy operator $T = \mathbf{p}^2/(2m)$ is inserted. The spin-free Dirac Hamiltonian is now obtained by omitting the second term on the right-hand side of Eq. 2.19 which contains the spin-orbit operator in the lower right block. This choice of transformation leads to the following equation:

$$(\tilde{h}_D^{sf} + \tilde{g}_{1,2}^{C,sf})\tilde{\Psi} = \tilde{G}E\tilde{\Psi} \tag{2.21}$$

with

$$\tilde{h}_D^{sf} = \begin{pmatrix} \hat{V} & \hat{T} \\ \hat{T} & (\alpha^2/4)(\mathbf{p}\cdot\hat{V}\mathbf{p}) - \hat{T} \end{pmatrix} \tag{2.22}$$

$$\tilde{g}_{1,2}^{C,sf} = \begin{pmatrix} P_1^+ & P_1^- \end{pmatrix} \begin{pmatrix} \frac{1}{r_{12}} & \frac{\alpha^2}{4}\mathbf{p}_2 \cdot \frac{1}{r_{12}}\mathbf{p}_2 \\ \frac{\alpha^2}{4}\mathbf{p}_1(\frac{1}{r_{12}})\mathbf{p}_1 & \frac{\alpha^2}{16}\mathbf{p}_2[\mathbf{p}_1 \cdot \frac{1}{r_{12}}\mathbf{p}_1]\mathbf{p}_2 \end{pmatrix} \begin{pmatrix} P_1^+ \\ P_1^- \end{pmatrix}, \tag{2.23}$$

where $\tilde{h}_D^{sf}$ is the spin-free one-electron Hamiltonian and $\tilde{g}_{1,2}^{C,sf}$ the corresponding spin-free two-electron Hamiltonian. $\tilde{G}, P_k^+$, and P_k^- denote a metric and the projectors onto the large and small component parts of the wave function, respectively

$$\tilde{G} = \begin{pmatrix} 1 & 0 \\ 0 & \frac{\alpha}{2}T \end{pmatrix}, \qquad P_k^+ = \begin{pmatrix} 1 & 0 \\ 0 & 0 \end{pmatrix}, \qquad P_k^- = \begin{pmatrix} 0 & 0 \\ 0 & 1 \end{pmatrix}. \tag{2.24}$$

This transformation does not require any expansion parameter for the separation and is therefore exact. As there is no unique separation scheme, the results obtained in different spin-orbit free formalisms may differ in principle [65], although in many practical cases this appears to be of no importance [66]. Hence, we expect the spectroscopic properties derived with the spin-free Dirac-Coulomb equation to be similar to those obtained from a unitary-transformed Dirac equation (without spin-orbit) to infinite order. The price paid for the exact decomposition is that the solutions of the spin-free Dirac-Coulomb equations still have four components. This makes the Self-Consistent-Field step computationally more expensive than standard "scalar"-relativistic approaches that neglect the small component. However, the spin-free Dirac-Coulomb equations have the same spin-factorization as in the non-relativistic case. Therefore, a non-relativistic correlation code based on regular point group symmetry can be used with a set of orbitals optimized in the spin-free Dirac-Coulomb framework. Since the computational demand of highly accurate calculations on small heavy-element compounds is dominated by the dynamic correlation step, the four-component Self-Consistent-Field calculations and integral transformations do not lead to significant increases of the total computation time. On the contrary the savings done using the spin-free Dirac-Coulomb over the Dirac-Coulomb Hamiltonian are very significant in particular when going to higher than coupled cluster single doubles as will be seen in Sections 2.2.1 and 7. This spin-free Hamiltonian has been used in the implementation of the spin-free general order coupled cluster code in Section 6.4 and in almost all applications presented in this thesis in Section 9.

2.2 Symmetry of the Dirac-Coulomb Hamiltonian

Group theory has proven to be a very powerful tool in physics and chemistry giving great insight into the system just by knowing its symmetry. In this way group theory can help to exploit the symmetry by giving selection rules or block diagonalization just from knowing the irreducible representation of the spinors and wave function. Therefore in calculations symmetry is able to greatly reduce the computation time since the problem can be reduced to smaller blocks which individually can be diagonalized much faster. Due to the spin-orbit mixing of spin and space, we lose the very simple yet important spin symmetry in the relativistic case. To regain some of the lost symmetry blocking from the spin symmetry, we will introduce the time reversal symmetry and show how this can be used for a formalism in conjunction with double group symmetry.

2.2.1 Time Reversal Symmetry

I will in this section first try to show how time reversal symmetry can be used to relate spinors. With these relations I will try to introduce auxiliary quantum numbers and operators. These operators, although they do have meaning, are *not* observables and are there to aid the formalism and illustrate the additional work that has to be done going from a non-relativistic or spin-free Hamiltonian to the Dirac-Coulomb Hamiltonian. I will show how we in this formalism easily can arrive at a minimum number of elementary operators which then has to be multiplied by some integral or amplitude. This formalism will then be used on the Dirac-Coulomb Hamiltonian along with also the time reversal properties of the integrals to show how the Hamiltonian is constructed at an upper level of the implemented code. Although Section 3 is a large coupled cluster section the generalization of the cluster operators will be done is this section. For the most part the following section will be kept in the second quantization language. For the reader unfamiliar with this language I would recommend the book by Helgaker, Jørgensen and Olsen [67] for a solid background on this and the book by Dyall and Fægri [7] for the extension to the relativistic framework. The work done in these sections are to a large degree new development I have derived for my thesis and published in [68].

2.2.1.1 Time Reversal Symmetry and Spinors

In the absence of external magnetic fields the time reversal operator $\hat{K}$ will commute with the Dirac-Coulomb Hamiltonian and the one particle Dirac operator, and $\hat{K}$ can therefore be used as a symmetry operator. Since a time-reversal operation leaves positions invariant but changes signs of velocities and momenta

$$\hat{K}\mathbf{r}\hat{K} = \mathbf{r} \qquad \hat{K}\mathbf{p}\hat{K} = -\mathbf{p} \tag{2.25}$$

$\hat{K}$ will be a antiunitary operator

$$\hat{K}c = c^*\hat{K} \quad \hat{K}^\dagger = \hat{K}^{-1}. \tag{2.26}$$

The phase is usually chosen such that the time reversal operator has the following form

$$\hat{K} = \imath\hat{\mathbf{\Sigma}}_y\hat{K}_0 = -\imath \begin{pmatrix} \hat{\sigma}_y & 0 \\ 0 & \hat{\sigma}_y \end{pmatrix} \hat{K}_0 \tag{2.27}$$

where $\hat{\sigma}_y$ is the usual Pauli spin matrix and $\hat{K}_0$ a complex conjugation operator.

It can be shown that the time-reversal operator transforms a spinor ϕ_p as

$$\hat{K}\phi_p = \phi_{\bar{p}} \quad \hat{K}\phi_{\bar{p}} = -\phi_p \tag{2.28}$$

The spinor $\phi_{\bar{p}}$ is then the time-reversed conjugate of ϕ_p. These spinors can be shown to be linearly independent and hence can be orthonormalized

$$\langle\phi_{\bar{p}}|\phi_p\rangle = 0. \tag{2.29}$$

The pair $(\phi_p, \phi_{\bar{p}})$ is then said to form a *Kramers pair* and ϕ_p and $\phi_{\bar{p}}$ is denoted the unbarred and barred spinor, respectively. For the fermion case (odd number of electrons) the Kramers pair $(\phi_p, \phi_{\bar{p}})$ form a degenerate pair: Kramers' theorem [69] state that in systems of half-integer spin the energy levels are at least doubly degenerate and any degeneracy even-fold.

The Kramers pairs will in the following be used as the spinor basis. By working in a basis of Kramers-paired spinors we can recover part of the computational savings the now lost spin symmetry would otherwise give. This will furthermore also allow us to develop a formalism based on excitations between barred and unbarred spinors and approximations to these. The notion of Kramers-restricted will then be used for any method where the spinors will appear as Kramers pairs.

In the language of second quantization, Eq.(2.28) can be written as relations for creation-operators

$$\hat{K}a_p^\dagger = a_{\bar{p}}^\dagger \hat{K} \quad \hat{K}a_{\bar{p}}^\dagger = -a_p^\dagger \hat{K} \tag{2.30}$$

and by taking the adjoints of the relations in Eq.(2.30) and using Eq.(2.26) one obtains the relations for the corresponding annihilation operators

$$\hat{K}a_p = a_{\bar{p}} \hat{K} \quad \hat{K}a_{\bar{p}} = -a_p \hat{K} \tag{2.31}$$

The operator $\hat{K}$ being an antiunitary operator is not an observable and will not have a corresponding eigenvalue K.

An auxiliary quantum number M_k can, however, be introduced to classify the different spinors of a Kramers pair. M_k is introduced as the relativistic equivalent to the non-relativistic projection of spin M_s and is therefore also referred to the Kramers projection of the spinors[4]. To define M_k we introduce the Kramers projection operator

$$\hat{K}_z = \frac{1}{2}(\sum_p a_p^\dagger a_p - \sum_{\bar{p}} a_{\bar{p}}^\dagger a_{\bar{p}}) \tag{2.32}$$

The value M_k of the Kramers projection for an occupation number vector $|0\rangle$ is then defined as

$$\hat{K}_z|0\rangle = M_k|0\rangle \tag{2.33}$$

and the change ΔM_k of Kramers projection of a product of creation and annihilation operators $\hat{O}$ is defined as the eigenvalue

$$[\hat{K}_z, \hat{O}_{N,\Delta M_k}] = \Delta M_k \hat{O}_{N,\Delta M_k} \tag{2.34}$$

[4]Notice in general will a many particle wave function not have a well defined Kramers projection.

provided $\hat{O}$ has a well-defined change in Kramers projection. We will in Section 2.2.1.3 elaborate more on the meaning of this. As ΔM_k denotes the change of Kramers projection it is also called the Kramers flip. The value of ΔM_k is thus $\frac{1}{2}$ for $a_p^\dagger$ and $a_{\bar{p}}$ whereas ΔM_k is $-\frac{1}{2}$ for $a_{\bar{p}}^\dagger$ and a_p

In the next subsection we will discuss Kramers projections for strings of creation and annihilation operators.

2.2.1.2 Time Reversal and the Elementary Operator Strings

With the knowledge of the transformation properties of the creation and annihilation operators, general operators can be considered. For an operator string we are interested in the change of the Kramers projection. For this we introduce the notation of an elementary operator class $\hat{O}_{(N,\Delta M_k)}$ where N is the particle rank and ΔM_k is the change in Kramers projection. Although this does not uniquely define a main particle operator class (except for $N = \pm\Delta M_k$) it will later serve to divide general main particle operators classes into sets of operator division classes to construct new approximative schemes. An elementary one-particle operator string $a_p^\dagger a_q$ belongs to operator division class $\hat{O}_{1,0}$ since we annihilate and create an unbarred spinor. The other possible one-particle operator strings are

$$a_{\bar{p}}^\dagger a_q \in \hat{O}_{1,-1} \quad a_p^\dagger a_{\bar{q}} \in \hat{O}_{1,1} \quad a_{\bar{p}}^\dagger a_{\bar{q}} \in \hat{O}_{1,0} \tag{2.35}$$

where we observe also a flipping of the Kramers projection. For a general operator string containing N^c and $\bar{N}^c$ unbarred and barred creation operators, respectively, and N^a and $\bar{N}^a$ unbarred and barred annihilation operators, respectively, one obtains

$$\Delta M_k = \tfrac{1}{2}(N^c - \bar{N}^c + \bar{N}^a - N^a) \tag{2.36}$$

$$N = \tfrac{1}{2}(N^c + \bar{N}^c + \bar{N}^a + N^a). \tag{2.37}$$

Conservation of the number of electrons requires

$$N^c + \bar{N}^c = N^a + \bar{N}^a. \tag{2.38}$$

In this way any elementary particle operator string can be placed into an operator division class depending on the particle rank N and the Kramers flip ΔM_k.

2.2.1.3 From a General Operator to a Kramers Restricted Operator

Before moving to the Hamilton- or the cluster operator we will first briefly show how an operator written in the general Kramers unrestricted form may be written in the Kramers restricted form. Using upper case letters for general (barred and unbarred) spinors and assuming that the dimension of the spinor basis is $2N$, a general Kramers unrestricted one-particle operator has the form

$$\hat{O}_1 = \sum_{PQ}^{2N} O_{PQ} a_P^\dagger a_Q \tag{2.39}$$

Assuming time reversal symmetry for the one-particle operator in Eq. 2.39 we can then write $\hat{O}_1$ in the one-particle operator in the Kramers restricted form.

$$\hat{O}_1 = \sum_{pq}^{N} (O_{pq} a_p^\dagger a_q + O_{\bar{p}\bar{q}} a_{\bar{p}}^\dagger a_{\bar{q}} + O_{\bar{p}q} a_{\bar{p}}^\dagger a_q + O_{p\bar{q}} a_p^\dagger a_{\bar{q}}) \tag{2.40}$$

We see that the Kramers restricted one-particle operator is the sum of all possible operator classes

$$\hat{O}_1 = \sum_{\Delta M_k=-1}^{1} \hat{O}_{1,\Delta M_k} \tag{2.41}$$

Likewise we can rewrite an two-particle operator from the Kramers unrestricted form

$$\hat{O}_2 = \frac{1}{2} \sum_{PQRS}^{2N} (PQ|RS) a_P^\dagger a_R^\dagger a_S a_Q \tag{2.42}$$

to the Kramers restricted form

$$\begin{aligned}
\hat{O}_2 = \frac{1}{2} \sum_{pqrs}^{N} & (pq|rs) a_p^\dagger a_r^\dagger a_s a_q + (\bar{p}q|rs) a_{\bar{p}}^\dagger a_r^\dagger a_s a_q + (p\bar{q}|rs) a_p^\dagger a_r^\dagger a_s a_{\bar{q}} + (pq|\bar{r}s) a_p^\dagger a_{\bar{r}}^\dagger a_s a_q \\
& + (pq|r\bar{s}) a_p^\dagger a_r^\dagger a_{\bar{s}} a_q + (\bar{p}\bar{q}|rs) a_{\bar{p}}^\dagger a_r^\dagger a_s a_{\bar{q}} + (\bar{p}q|\bar{r}s) a_{\bar{p}}^\dagger a_{\bar{r}}^\dagger a_s a_q + (\bar{p}q|r\bar{s}) a_{\bar{p}}^\dagger a_r^\dagger a_{\bar{s}} a_q \\
& + (p\bar{q}|\bar{r}s) a_p^\dagger a_{\bar{r}}^\dagger a_s a_{\bar{q}} + (p\bar{q}|r\bar{s}) a_p^\dagger a_r^\dagger a_{\bar{s}} a_{\bar{q}} + (pq|\bar{r}\bar{s}) a_p^\dagger a_{\bar{r}}^\dagger a_{\bar{s}} a_q + (\bar{p}\bar{q}|\bar{r}s) a_{\bar{p}}^\dagger a_{\bar{r}}^\dagger a_s a_{\bar{q}} \\
& + (\bar{p}\bar{q}|r\bar{s}) a_{\bar{p}}^\dagger a_r^\dagger a_{\bar{s}} a_{\bar{q}} + (\bar{p}q|\bar{r}\bar{s}) a_{\bar{p}}^\dagger a_{\bar{r}}^\dagger a_{\bar{s}} a_q + (p\bar{q}|\bar{r}\bar{s}) a_p^\dagger a_{\bar{r}}^\dagger a_{\bar{s}} a_{\bar{q}} + (\bar{p}\bar{q}|\bar{r}\bar{s}) a_{\bar{p}}^\dagger a_{\bar{r}}^\dagger a_{\bar{s}} a_{\bar{q}}
\end{aligned} \tag{2.43}$$

Following this recipe any n-particle operator can easily be written using time reversal symmetry and can always be decomposed into operator division classes of elementary operator strings

$$\hat{O}_N = \sum_{\Delta M_k=-N}^{N} \hat{O}_{N,\Delta M_k}. \tag{2.44}$$

This decomposition is not restricted to normal-ordered particle operators strings but will work for any operator string and can therefore also be used for the cluster operators as encountered in 2.2.2. The auxiliary quantum number M_k will therefore serve to define restricted excitation manifolds of cluster operators which leads additional ways to define other approximation schemes in the truncation of CC hierarchy (see Section 8.1).

If an operator, like the Dirac-Coulomb Hamiltonian or the cluster operator, consists of several different particle number operators one can write equation 2.44 as

$$\hat{O} = \sum_{N=N_{min}}^{N_{max}} \hat{O}_N = \sum_{N=N_{min}}^{N_{max}} \sum_{\Delta M_k=-N}^{N} \hat{O}_{N,\Delta M_k} \tag{2.45}$$

or if one is only interested in a given ΔM_k one can write

$$\hat{O} = \sum_{\Delta M_k=-N_{max}}^{N_{max}} \hat{O}_{\Delta M_k} = \sum_{\Delta M_k=-N_{max}}^{N_{max}} \sum_{N\geq|\Delta M_k|\geq N_{min}}^{N_{max}} \hat{O}_{N,\Delta M_k} \tag{2.46}$$

In Eq. 2.43 we observe that several elementary operator strings within a given operator division class can be related by anti commutation and a renaming of indices. In the operator division class $\hat{O}_{2,-1}$ the two elementary operator strings

$$a_{\bar{p}}^{\dagger} a_r^{\dagger} a_s a_q \wedge a_p^{\dagger} a_{\bar{r}}^{\dagger} a_s a_q \tag{2.47}$$

are seen to be related. Since it is advantages to calculate only the minimum number elementary operator strings we will bring about a reduction in the number of elementary operator strings by making use of the interchanging of integration variables, the anti commutation relationship of second quantized operators and a renaming of indices. As an example we take the two-particle operator from the Hamiltonian from Eq. 2.43 which can be written as

$$
\begin{aligned}
\hat{O}_{+2} &= \frac{1}{2}\sum_{pqrs}^{N}(p\bar{q}|r\bar{s})a_p^\dagger a_r^\dagger a_{\bar{s}} a_{\bar{q}} \\
\hat{O}_{+1} &= \sum_{pqrs}^{N}((p\bar{q}|rs)a_p^\dagger a_r^\dagger a_s a_{\bar{q}} + (p\bar{q}|\bar{r}\bar{s})a_p^\dagger a_{\bar{r}}^\dagger a_{\bar{s}} a_{\bar{q}}) \\
\hat{O}_{0} &= \frac{1}{2}\sum_{pqrs}^{N}((pq|rs)a_p^\dagger a_r^\dagger a_s a_q + (\bar{p}\bar{q}|\bar{r}\bar{s})a_{\bar{p}}^\dagger a_{\bar{r}}^\dagger a_{\bar{s}} a_{\bar{q}} + 2((pq|\bar{r}\bar{s}) - (p\bar{s}|\bar{r}q))a_p^\dagger a_{\bar{r}}^\dagger a_{\bar{s}} a_q) \\
\hat{O}_{-1} &= \sum_{pqrs}^{N}((\bar{p}q|rs)a_{\bar{p}}^\dagger a_r^\dagger a_s a_q + (\bar{p}q|\bar{r}\bar{s})a_{\bar{p}}^\dagger a_{\bar{r}}^\dagger a_{\bar{s}} a_q)) \\
\hat{O}_{-2} &= \frac{1}{2}\sum_{pqrs}^{N}(\bar{p}q|\bar{r}s)a_{\bar{p}}^\dagger a_{\bar{r}}^\dagger a_s a_q
\end{aligned}
\tag{2.48}
$$

when written in the form shown in Eq. 2.46 and where we have made use of integral symmetry shown in Eq. 2.57.

By writing an operator in the above form shown in Eq. 2.48, we obtain a bijective mapping between the operator strings and the string representation of what we will define as the main operator class. This can also be seen by adding the number of barred and unbarred indices for a given operator division class $\hat{O}_{N,\Delta M_k}$ using Eqs. 2.36 and 2.38. By doing this a main operator class can then be uniquely defined

$$
\hat{O}_{N,\Delta M_k,M_{ub}} \tag{2.49}
$$

where

$$
M_{ub} = \frac{N^c + N^a}{2} - \frac{\bar{N}^c + \bar{N}^a}{2} \tag{2.50}
$$

and where we have introduced a second difference between operators under time reversal symmetry, namely the difference between the number of barred and unbarred operators.

It can then easily be shown that the minimum number of main operator classes for a given operator $\hat{O}_N$ will be

$$
D_{N,\Delta M_k,M_{ub}} = (N+1)(N+2) - (N+1) = (N+1)^2 \tag{2.51}
$$

by using the Eq. 2.36 and the constraints in 2.38. We see that by writing an N-electron operator in the main operator class form we have reduced the number of types of operator strings from 2^{2N} to $(N+1)^2$. In the real and complex groups (see Section 2.2.3) this is further reduced to $(N+1)^2 - N^2/2$ since the odd flipping of the Kramers projection falls out due to symmetry. This however is still significantly above the $(N+1)$ seen in the non-relativistic framework.

We notice that even though the motivation was writing a number conserving operator in the main operator class form this form also work for any string of elementary operators with a small extension. On can therefore introduce the change in the number of particles

$$\Delta N = \frac{N^c + \bar{N}^c}{2} - \frac{N^a + \bar{N}^a}{2} \tag{2.52}$$

to give a general main class form

$$\hat{O}_{N,\Delta M_k,M_{ub},\Delta N} \tag{2.53}$$

for any operator string. If the ΔN is omitted we assume it is zero and therefore a regular particle operator.

2.2.1.4 Time Reversal Symmetry and the Dirac-Coulomb Hamiltonian

We will now examine how the formalism of main operator classes $\hat{O}_{N,\Delta M_k,M_{ub}}$ may be used to rewrite relativistic Hamiltonians, in particular the Dirac-Coulomb Hamiltonian, in a compact form. By using symmetry relations of integrals and operators, the complexity of the Hamiltonian will be significantly reduced. Specifically, we shall demonstrate that a simple addition of integrals leads to significant simplifications compared to our previously reported CC [70] and the CI [71–73] algorithms.

The Dirac-Coulomb Hamiltonian is in the Kramers unrestricted form

$$\hat{H} = \sum_{PQ}^{2N} h_{PQ} a_P^\dagger a_Q + \frac{1}{2} \sum_{PQRS}^{2N} (PQ|RS) a_P^\dagger a_R^\dagger a_S a_Q \tag{2.54}$$

This Hamiltonian can be simplified using the Kramers restricted basis. By using that $\hat{K}$ commutes with the Hamiltonian and $\hat{h}$ and is antiunitary, see Eqs. 2.26 and 2.28, one obtains for the one-electron integrals

$$h_{\bar{p},\bar{q}} = \langle\bar{\phi}_p|\hat{h}|\bar{\phi}_q\rangle = \langle\hat{K}\phi_p|\hat{h}|\hat{K}\phi_q\rangle = \langle\phi_p|\hat{K}^\dagger\hat{h}\hat{K}|\phi_q\rangle^* = \langle\phi_p|\hat{h}|\phi_q\rangle^* = h^*_{p,q} = h_{q,p} \tag{2.55}$$

and

$$\begin{aligned} h_{\bar{p},q} &= \langle\bar{\phi}_p|\hat{h}|\phi_q\rangle = \langle\hat{K}\phi_p|\hat{h}|\phi_q\rangle = \langle\phi_p|\hat{K}^\dagger\hat{h}\hat{K}\hat{K}^\dagger|\phi_q\rangle^* \\ &= \langle\phi_p|\hat{h}\hat{K}^\dagger|\phi_q\rangle^* = -\langle\phi_p|\hat{h}|\bar{\phi}_q\rangle^* = -h^*_{p,\bar{q}} = -h_{\bar{q},p} \end{aligned} \tag{2.56}$$

By using time reversal symmetry we can half the number of integrals needed and by exploiting that $\hat{h}$ is a Hermitian operator we can further half the number of integrals, so all in all only one fourth of the one electron integrals are needed.

Reducing the number of two-particle integrals is of significantly larger interest since this will give much larger computational savings. These integrals can, just like the one-particle integrals, be reduced by a factor of four. This is most elegantly done by using the Kramers permutation operator as shown in [7]. The following relations for the two particle integrals can then be shown

$$\begin{aligned} (pq|rs) &= (pq|\bar{s}\bar{r}) = (\bar{q}\bar{p}|rs) = (\bar{q}\bar{p}|\bar{s}\bar{r}) \\ (\bar{p}q|rs) &= (\bar{p}q|\bar{s}\bar{r}) = -(\bar{q}p|rs) = -(\bar{q}p|\bar{s}\bar{r}) \\ (\bar{p}q|\bar{r}s) &= -(\bar{p}q|\bar{s}r) = -(\bar{q}p|\bar{r}s) = (\bar{q}p|\bar{s}r) \\ (\bar{p}q|r\bar{s}) &= -(\bar{p}q|s\bar{r}) = -(\bar{q}p|r\bar{s}) = (\bar{q}p|s\bar{r}) \end{aligned} \tag{2.57}$$

By inserting Eqs. 2.56 and 2.57 in Eq. 2.54, using the elementary anticommutation relations of creation and annihilation operators and reordering the terms according to N and ΔM_k as shown in Eq. 2.48 one obtains

$$\hat{H} = \sum_{\Delta M_K=-2}^{2} \hat{H}_{\Delta M_K} \tag{2.58}$$

with

$$\begin{aligned}
\hat{H}_{+2} &= \frac{1}{2}\sum_{pqrs}^{N}(p\bar{q}|r\bar{s})a_p^\dagger a_r^\dagger a_{\bar{s}} a_{\bar{q}} \\
\hat{H}_{+1} &= \sum_{pq}^{N} h_{p\bar{q}} a_p^\dagger a_{\bar{q}} + \sum_{pqrs}^{N}((p\bar{q}|rs)a_p^\dagger a_r^\dagger a_s a_{\bar{q}} + (p\bar{q}|\bar{r}\bar{s})a_p^\dagger a_{\bar{r}}^\dagger a_{\bar{s}} a_{\bar{q}}) \\
\hat{H}_0 &= \sum_{pq}^{N} h_{pq} a_p^\dagger a_q + h_{\bar{p}\bar{q}} a_{\bar{p}}^\dagger a_{\bar{q}} \qquad (2.59) \\
&+ \frac{1}{2}\sum_{pqrs}^{N}((pq|rs)a_p^\dagger a_r^\dagger a_s a_q + (\bar{p}\bar{q}|\bar{r}\bar{s})a_{\bar{p}}^\dagger a_{\bar{r}}^\dagger a_{\bar{s}} a_{\bar{q}} + 2((pq|\bar{r}\bar{s}) - (p\bar{s}|\bar{r}q))a_p^\dagger a_{\bar{r}}^\dagger a_{\bar{s}} a_q) \\
\hat{H}_{-1} &= \sum_{pq}^{N} h_{\bar{p}q} a_{\bar{p}}^\dagger a_q + \sum_{pqrs}^{N}((\bar{p}q|rs)a_{\bar{p}}^\dagger a_r^\dagger a_s a_q + (\bar{p}q|\bar{r}\bar{s})a_{\bar{p}}^\dagger a_{\bar{r}}^\dagger a_{\bar{s}} a_q)) \\
\hat{H}_{-2} &= \frac{1}{2}\sum_{pqrs}^{N}(\bar{p}q|\bar{r}s)a_{\bar{p}}^\dagger a_{\bar{r}}^\dagger a_s a_q \qquad (2.60)
\end{aligned}$$

By combining the integrals as $(pq|\bar{r}\bar{s}) - (p\bar{s}|\bar{r}q)$ for the operator $a_p^\dagger a_{\bar{r}}^\dagger a_{\bar{s}} a_q$ we have accomplished a reduction in the number of operator strings in comparison to previous CC [70] and CI [71–73].

2.2.2 Kramers Restricted Coupled Cluster

We will now turn to the single reference coupled cluster theory and show what happens to the basic equations when applying time reversal symmetry. In the coupled cluster theory the wave function is parametrized by an exponential ansatz

$$|CC\rangle = \exp(\hat{T})|HF\rangle \qquad (2.61)$$

working on an N-particle reference function. In the similarity transformed coupled cluster the energy and amplitude equations become

$$\langle HF|\exp(-\hat{T})\hat{H}\exp(\hat{T})|HF\rangle = E \qquad (2.62)$$

$$\langle\mu|\exp(-\hat{T})\hat{H}\exp(\hat{T})|HF\rangle = \langle\mu|\exp(-\hat{T})E\exp(\hat{T})|HF\rangle = 0 \qquad (2.63)$$

respectively.

The operator $\hat{T}$ is restricted to excitations from spinors occupied in $|HF\rangle$ to spinors unoccupied in $|HF\rangle$. The inclusion of all such excitations into $\hat{T}$ leads to the full coupled-cluster model which solves the Schrödinger equations in the defined one-electron basis. However, the operator $\hat{T}$ is typically restricted compared to the full operator. The standard form of such truncations is to include into $\hat{T}$ all excitations up to a given maximum excitation level $m \leq N$

$$\hat{T} = \sum_{i=1}^{m} \hat{T}_i \tag{2.64}$$

where $\hat{T}_i$ is an m-fold excitation operator. The operator $\hat{T}_i$ is a general i-fold excitation operator

$$\hat{T}_i = \sum_{\mu} t_{\mu i} \hat{\tau}_{\mu i} \tag{2.65}$$

where $\hat{\tau}_{\mu i}$ is an elementary i-fold excitation operator and $t_{\mu i}$ is the corresponding amplitude. Consider as an example the case where at most double excitations are included, $m = 2$. Using the standard notation of I, J and A, B for occupied and virtual spinors, respectively, and using $2O$ and $2V$ the number of occupied and virtual spinors, respectively, the Kramers unrestricted single- and double excitation coupled cluster operators are

$$\begin{aligned} \hat{T}_1 &= \sum_{\mu} t_{1\mu} \hat{\tau}_{1\mu} = \sum_{I,A}^{2O,2V} t_I^A \hat{\tau}_I^A \\ \hat{T}_2 &= \sum_{\mu} t_{2\mu} \hat{\tau}_{2\mu} = \sum_{I \leq J, A \leq B}^{2O,2V} t_{IJ}^{AB} \hat{\tau}_{IJ}^{AB} \end{aligned} \tag{2.66}$$

The above form contains the independent coupled cluster coefficients, for example t_{IJ}^{AB} with $I \leq J, A \leq B$. It is sometimes convenient to introduce forms of the coupled cluster operators where the sums instead are over unrestricted indices. The double excitation operator may then be expressed as

$$\begin{aligned} \hat{T}_2 &= \sum_{\mu} t_{2\mu} \hat{\tau}_{2\mu} = \sum_{I \leq J, A \leq B}^{2O,2V} t_{IJ}^{AB} \hat{\tau}_{IJ}^{AB} \\ &= \frac{1}{4} \sum_{IJ,AB}^{2O,2V} t_{IJ}^{AB} \hat{\tau}_{IJ}^{AB} \end{aligned} \tag{2.67}$$

where the additional amplitudes are related to the independent amplitudes by simple sign changes, depending on the number of permutations

$$-T_{IJ}^{BA} = -T_{JI}^{AB} = T_{JI}^{BA} = T_{IJ}^{AB} \tag{2.68}$$

Introducing the division of the spinors into barred and unbarred, and assuming that the number of barred spinors equals the number of unbarred spinors in both the occupied and virtual spaces, the single- and double- excitations operators become

$$\hat{T}_1 = \sum_{i,a}^{O,V} (t_i^a \hat{\tau}_i^a + t_{\bar{i}}^a \hat{\tau}_{\bar{i}}^a + t_i^{\bar{a}} \hat{\tau}_i^{\bar{a}} + t_{\bar{i}}^{\bar{a}} \hat{\tau}_{\bar{i}}^{\bar{a}}) \tag{2.69}$$

$$\begin{aligned} \hat{T}_2 = \frac{1}{4} \sum_{ij,ab}^{O,V} (& t_{ij}^{ab} \hat{\tau}_{ij}^{ab} + 2t_{\bar{i}j}^{ab} \hat{\tau}_{\bar{i}j}^{ab} + 2t_{i\bar{j}}^{ab} \hat{\tau}_{i\bar{j}}^{ab} + 2t_{ij}^{\bar{a}b} \hat{\tau}_{ij}^{\bar{a}b} \\ & + 2t_{ij}^{a\bar{b}} \hat{\tau}_{ij}^{a\bar{b}} + t_{\bar{i}\bar{j}}^{ab} \hat{\tau}_{\bar{i}\bar{j}}^{ab} + 4t_{\bar{i}j}^{\bar{a}b} \hat{\tau}_{\bar{i}j}^{\bar{a}b} + 4t_{\bar{i}j}^{a\bar{b}} \hat{\tau}_{\bar{i}j}^{a\bar{b}} \\ & + 4t_{i\bar{j}}^{\bar{a}b} \hat{\tau}_{i\bar{j}}^{\bar{a}b} + 4t_{i\bar{j}}^{a\bar{b}} \hat{\tau}_{i\bar{j}}^{a\bar{b}} + t_{ij}^{\bar{a}\bar{b}} \hat{\tau}_{ij}^{\bar{a}\bar{b}} + 2t_{\bar{i}\bar{j}}^{\bar{a}b} \hat{\tau}_{\bar{i}\bar{j}}^{\bar{a}b} \\ & + 2t_{\bar{i}\bar{j}}^{a\bar{b}} \hat{\tau}_{\bar{i}\bar{j}}^{a\bar{b}} + 2t_{\bar{i}j}^{\bar{a}\bar{b}} \hat{\tau}_{\bar{i}j}^{\bar{a}\bar{b}} + 2t_{i\bar{j}}^{\bar{a}\bar{b}} \hat{\tau}_{i\bar{j}}^{\bar{a}\bar{b}} + t_{\bar{i}\bar{j}}^{\bar{a}\bar{b}} \hat{\tau}_{\bar{i}\bar{j}}^{\bar{a}\bar{b}}) \end{aligned} \tag{2.70}$$

The coupled cluster excitation operators may be divided into the main operator class form, just as the operators in the Hamiltonian, 2.49, which again will lead to a reduction in the number of operator strings to be considered. For example, the $\hat{T}_2$ cluster operator may be split into a sum of five operators, each with a specific ΔM_k form

$$\begin{aligned} \hat{T}_{2,+2} &= \frac{1}{4} \sum_{ij,ab}^{N,V} t_{\bar{i}\bar{j}}^{ab} \hat{\tau}_{\bar{i}\bar{j}}^{ab} \\ \hat{T}_{2,+1} &= \frac{1}{2} \sum_{ij,ab}^{N,V} (t_{\bar{i}j}^{\bar{a}b} + t_{\bar{j}\bar{i}}^{b\bar{a}}) \hat{\tau}_{\bar{i}j}^{\bar{a}b} + (t_{i\bar{j}}^{ab} + t_{\bar{j}i}^{ba}) \hat{\tau}_{i\bar{j}}^{ab} = \sum_{ij,ab}^{N,V} t_{\bar{i}j}^{\bar{a}b} \hat{\tau}_{\bar{i}j}^{\bar{a}b} + t_{i\bar{j}}^{ab} \hat{\tau}_{i\bar{j}}^{ab} \\ \hat{T}_{2,0} &= \frac{1}{4} \sum_{ij,ab}^{N,V} t_{ij}^{ab} \hat{\tau}_{ij}^{ab} + t_{\bar{i}\bar{j}}^{\bar{a}\bar{b}} \hat{\tau}_{\bar{i}\bar{j}}^{\bar{a}\bar{b}} + 4(t_{\bar{i}j}^{\bar{a}b} + t_{\bar{j}\bar{i}}^{b\bar{a}} - t_{\bar{i}j}^{b\bar{a}} - t_{\bar{j}\bar{i}}^{\bar{a}b}) \hat{\tau}_{\bar{i}j}^{\bar{a}b} \\ &= \frac{1}{4} \sum_{ij,ab}^{N,V} t_{ij}^{ab} \hat{\tau}_{ij}^{ab} + t_{\bar{i}\bar{j}}^{\bar{a}\bar{b}} \hat{\tau}_{\bar{i}\bar{j}}^{\bar{a}\bar{b}} + 16 t_{\bar{i}j}^{\bar{a}b} \hat{\tau}_{\bar{i}j}^{\bar{a}b} \\ \hat{T}_{2,-1} &= \frac{1}{2} \sum_{ij,ab}^{N,V} (t_{\bar{i}j}^{\bar{a}\bar{b}} + t_{\bar{j}\bar{i}}^{\bar{b}\bar{a}}) \hat{\tau}_{\bar{i}j}^{\bar{a}\bar{b}} + (t_{ij}^{\bar{a}b} + t_{ji}^{b\bar{a}}) \hat{\tau}_{ij}^{\bar{a}b} = \sum_{ij,ab}^{N,V} t_{\bar{i}j}^{\bar{a}\bar{b}} \hat{\tau}_{\bar{i}j}^{\bar{a}\bar{b}} + t_{ij}^{\bar{a}b} \hat{\tau}_{ij}^{\bar{a}b} \\ \hat{T}_{2,-2} &= \frac{1}{4} \sum_{ij,ab}^{N,V} t_{ij}^{\bar{a}\bar{b}} \hat{\tau}_{ij}^{\bar{a}\bar{b}} \end{aligned} \tag{2.71}$$

where it has been used that pure excitation operators commutes and that the amplitudes are antisymmetric with respect to index interchange, Eq. 2.68.

Assuming that the reference single determinant is a closed-shell determinant consisting of Kramers pairs, further reduction in the number of amplitudes can be reached by requiring that $\hat{K}$ commutes with $\hat{T}$. We then get the familiar relations shown in [74, 75] between amplitudes of $\hat{T}_1$ and $\hat{T}_2$ with different number of barred/unbarred indices and different Kramers projection.

$$t_i^a = t_{\bar{i}}^{\bar{a}^*} \quad t_i^{\bar{a}} = -t_{\bar{i}}^{a^*} \tag{2.72}$$

$$t_{ij}^{ab} = t_{\bar{i}\bar{j}}^{\bar{a}\bar{b}^*} \quad t_{ij}^{\bar{a}\bar{b}} = t_{\bar{i}\bar{j}}^{ab^*} \quad t_{\bar{i}j}^{\bar{a}b} = t_{i\bar{j}}^{a\bar{b}^*} \quad t_{ij}^{a\bar{b}} = -t_{\bar{i}\bar{j}}^{\bar{a}b^*} \tag{2.73}$$

These relations are easily generalized to operators with higher particle rank since the time-reversal symmetry for an amplitude depends on the values of $N, \Delta M_k$ and M_{ub} for the corresponding operator as

$$t_{N,\Delta M_k,M_{ub}} = (-1)^{|\Delta M_k|} t^*_{N,-\Delta M_k,-M_{ub}} \tag{2.74}$$

where $t_{N,\Delta M_k,M_{ub}}$ is the amplitude for the main cluster operator class $\hat{\tau}_{N,\Delta M_k,M_{ub}}$. In the current implementation the time reversal symmetry between the amplitudes is not exploited. It should be noted that in the open-shell case by not demanding that $\hat{K}$ commutes with $\hat{T}$ will lead to Kramers contamination which shares similarities to the non-relativistic spin contamination[5]. Instead, demanding Eq. 2.74 also to be valid in the open-shell case will lead to a Kramers adapted formalism which will be non-commutative since there will be at least one cluster operator which will not be a pure excitation operator. In the Kramers adapted case we will then no longer see a truncation of the nested commutators after the fourth order but instead after the eighth order.

Dividing the cluster operator into the operator division class form also opens up for an alternative truncation of the coupled cluster hierarchy namely one based not only on the excitation level m, as shown in Eq. 2.64, but also in ΔM_k. Here the possibility has been

[5] We keep in mind that the many-particle wave function will not have a well-defined Kramers projection and therefore only similarities.

implemented to truncate $\hat{T}$ at excitation level and Kramers flip, hence at $\hat{T}_{m\leq N,|\Delta M_k|\leq m}$. The truncation with ΔM_k is taken at $\pm\Delta M_k$ to conserve the time reversal symmetry of the wave function. This kind of approximation would be particularly interesting for molecules with small spin-orbit contributions. Although implemented a numerical investigation of this additional approximation has not yet been undertaken. This type of approximation will be discussed in more detail in Section 8.1

2.2.3 Double Group Symmetry

In the relativistic theory spin and space ($j = l + s$) have been combined. We can therefore no longer use the regular point groups since these only contains operations on space. We must therefore use the double point groups which is a group constructed from the direct product of the non-relativistic point group and the evident subgroup $\{E, \bar{E}\}$ where $\bar{E}$ represents a rotation through 2π and E a rotation through 4π. While the order of the group is $2n$, the number of irreps in the double group is not necessarily doubled. The extension gives rise to a new set of irreps which are called fermion irreps. These change sign under the $\bar{E}$ operation and therefore describe half-integer j values. The regular point group irreps are the boson irreps and describe integer j values. Another consequence that follows from the fact that each element does not form a class of its own is that the double groups in general are non-abelian. Therefore special care has to be taken when doing a symmetry multiplication which gives an added complication to the regular point groups implemented in quantum chemistry packages.

Taking also time reversal symmetry into account it can be shown that for the Hamiltonian:

- Groups with only quaternion fermion irreps, all integrals are nonzero and complex
- Groups with only complex fermion irreps, all integrals with an odd number of bars are zero and the rest complex
- Groups with only real fermion irreps, all integrals with an odd number of bars are zero and the rest real

This means for non-quaternion groups $\hat{H}_{\Delta M_k=\pm 1}$ will be zero thereby halving the minimum number of integrals and significantly reducing the number of main operator

classes. The commutator driven coupled cluster program (see Section 6.3) is at the present state limited to the real binary double groups ($D_{2h}^{\star}, D_{2}^{\star}$ and $C_{2v}^{\star}$). This is currently being extended to the complex-valued double groups ($C_{2h}^{\star}, C_{2}^{\star}, C_{s}^{\star}$) which has already been accomplished for the CI-driven coupled cluster in Section 6.2. Since the molecules of interest to be treated with highly correlated methods typically show high symmetry it is advantageous to start with the real groups.

2.2.3.1 Additional Blocking from Time-Reversal Symmetry

As long as the spinor $\phi_{\bar{p}}$ and its time-reversed conjugate of ϕ_p belong to different irreducible representation it is easy to see that working in a basis of Kramers pairs will give an additional symmetry blocking. If, however, they belong to the same irreducible representation, the reduction is not obvious since the double point group does not offer any blocking. It can, however, be shown that there exists a unitary transformation of the spinors in a Kramers paired basis that will block diagonalize these even when belonging to the same irreducible representation. The example for this blocking is taken from [7] and will only here be shown in an abridged form.

We will reduce the problem to the diagonalization of a 2×2 matrix since this is sufficient to get the block diagonalization of a single Kramers pair. A generalization of this example will then lead to a block diagonalization of all Kramers pairs. For clarity we will only do this for an operator that is symmetric under time reversal symmetry

$$\hat{\mathbf{\Omega}} = \hat{K}\hat{\mathbf{\Omega}}\hat{K}^{-1} \tag{2.75}$$

since the operators we are interested in here are symmetric. The operator $\hat{\mathbf{\Omega}}$ is then

$$\hat{\mathbf{\Omega}} = \begin{pmatrix} \Omega_{pq} & \Omega_{p\bar{q}} \\ \Omega_{\bar{p}q} & \Omega_{\bar{p}\bar{q}} \end{pmatrix} = \begin{pmatrix} \Omega_{pq} & \Omega_{p\bar{q}} \\ -\Omega_{p\bar{q}}^{*} & \Omega_{pq}^{*} \end{pmatrix} \tag{2.76}$$

where the relations derived in Eqs. 2.55 and 2.56 have been used. It is seen that the operator $\hat{\mathbf{\Omega}}$ in Eq. 2.76 can be diagonalized by the quaternion unitary matrix

$$\hat{\mathbf{u}} = \frac{1}{\sqrt{2}} \begin{pmatrix} 1 & j \\ j & 1 \end{pmatrix} \tag{2.77}$$

giving

$$\hat{\mathbf{u}}^{\dagger}\hat{\mathbf{\Omega}}\hat{\mathbf{u}} = \begin{pmatrix} \Omega_{pq} + \Omega_{p\bar{q}}j & 0 \\ 0 & \Omega^{*}_{pq} - \Omega^{*}_{p\bar{q}}j \end{pmatrix} = \begin{pmatrix} Q & 0 \\ 0 & -kQk \end{pmatrix} \tag{2.78}$$

where Q is a quaternion number. The eigenvalue is now seen to be degenerate as they should be according to Kramers' theorem [69] (see Section 2.2.1.1) and a symmetry blocking of the matrix $\hat{\mathbf{\Omega}}$ is accomplished.

2.3 Basis Sets

A fundamental step in quantum chemistry is the expansion of the wave function in a (finite) set of known functions and thereby transforming the partial differential problem to a matrix problem. The expansion in Gaussian type orbitals with fast evaluation of integrals has made it possible to approach a complete expansion of the wave function in a systematic way. This whole machinery developed in the non-relativistic framework we would like to take over to the relativistic framework. There are, however, some questions arising, namely how should the expansion for the small component be done since there does not seem to be a straight-forward approach from non-relativistic theory. Second the contracted non-relativistic basis sets are grouped after l. However, we know that all orbitals with $l > 0$ are split by spin-orbit interaction (see Section 1.2.1.3) where the $l+1/2$ and $l - 1/2$ components contract/expand differently. This means their radial maximum are shifted away from each other. The question is then whether the contracted basis set approach will still work or whether it needs to be modified. These issues will briefly be elucidated in the following two sections. An excellent discussion of these problems by Dyall and Fægri can be found in [7] and [76] which goes into significantly more detail than what is presented here.

2.3.1 Kinetic Balance

The early four-component results had sometimes shown unpredictable results where the energy was very basis set dependent. This was traced back to how the expansions for the large and the small component was individually done. To have stable results it has been

shown that the expansion for the large and the small component should be performed in a balanced way, a way called kinetic balance [77]. To illustrate how this is done we take a part of Eq. 2.16 and rearrange it such that we can find a relation between the large and the small component

$$\psi^S = (E - V + 2mc^2)^{-1} c(\hat{\sigma} \cdot \hat{p})\psi^L. \tag{2.79}$$

If it is now assumed that the kinetic energy is significantly smaller than $2mc^2$, i.e. we have $E - V \ll 2mc^2$, Eq. 2.79 can be written as

$$\psi^S = (2mc)^{-1}(\hat{\sigma} \cdot \hat{p})\psi^L. \tag{2.80}$$

Eq. 2.80 is then the equation for the kinetic balance between the large and the small component. We here see that the two bispinors then will be related though the kinetic energy operator $\hat{\sigma} \cdot \hat{p}$. With the kinetic balance it can be shown that the kinetic energy approaches the non-relativistic limit in a correct fashion [7] and that the kinetic energy is a maximum [78].

We, however, also notice that when the large component is expanded in Gaussians the number of small component functions is significantly larger. This is seen by using a differential operator on a p-type spherical Gaussian

$$\frac{d}{dr} r e^{-\eta r^2} = (1 - 2\eta r^2) e^{-\eta r^2} \tag{2.81}$$

giving and s- and d-type spherical Gaussian. So, despite the fact that the small component is localized close to the nuclei and does not contribute much to the chemistry, the kinetic balance requires that the basis set for the small component is significantly larger than that of the large component. We also notice that the exponents are the same and if they are left so we say we have restricted kinetic balance. This restricted kinetic balance has been used in all calculation presented in this thesis.

Furthermore we also see that when an exponent of an s- and d-type Gaussian are the same they will both create a p-type Gaussian with the same exponent and hence create linear dependency in the basis set of the small component. It is therefore necessary to be able to eliminate potential linear dependencies that may arise from the kinetic balance in

the small component. This linear dependency in the small component can however also be exploited to reduce the number of functions for the small component by deliberately choosing the exponent of functions of angular momentum l and $l+2$ to be the same. This for instance is done in the family and dual family basis sets and the linear dependencies are then removed whereby the number of functions for the small component is reduced.

2.3.2 Uncontracted Basis Sets

Working with primitive Gaussian were in non-relativistic calculations found to take up an excess amount of disk space since the number of Gaussians needed, in comparison to, for instance Slater type orbitals, was greatly increased. To circumvent this problem of having large data files to be handled and stored, two approaches were put forward. One was the direct approach where the data is recomputed when needed and hence not stored on disk (for a review see [79]) the other one is to "compress" the data by contracting the Gaussians as discussed in [80]. With the contracted Gaussians several primitive Gaussians are combined to one single function by a fixed linear combination which thereby reduces the dimension of the Fock matrix.

As mentioned in the introduction to this section, this contraction scheme is done for each l value individually. However, in the relativistic framework it would then be unclear how this contraction should be performed, if contracted after l, since all orbitals with $l > 0$ are split by spin-orbit interaction with components having different radial functions. An alternative could be a contraction after j. This, however, creates an "additional" basis set compared to the l contracted which will be almost identical for light elements and could therefore cause linear dependencies or numerical instability [7]. It has furthermore been demonstrated that even for one-electron systems the straight-forward scheme where first the large component is contracted and then the kinetic balance is applied to get a contracted small component is problematic [81]. We are therefore left with using uncontracted basis sets which has been employed in all calculations throughout this thesis.

Chapter 3

Coupled-Cluster Theory

The coupled-cluster method represents the most successful approach to accurate many-electron molecular wave functions. This is due to it being size-extensive and having a faster convergence with respect to the excitation level than the CI approach. The coupled-cluster method is however a single-reference approach and it therefore requires the problem at hand to be fairly accurately described by a single determinant wave function. Wave functions with degenerate or near degenerate cannot be described or if possible at least very slow convergence with higher order is observed [67].

Molecules containing heavy elements often has these degeneracies or near degeneracies due to their partly filled p-, d- and f-shells[1]. The extension of the single-reference coupled-cluster wave function to a multireference wave function is, unlike CI, not a straightforward matter and to date no consensus has been reached on which way of extending is the preferred one. These extensions along with the single-reference coupled-cluster has been the topic of many larger review papers like [82–84]. The approach presented in this work is the state-selective multireference coupled-cluster method. The author has however also spent a significant amount of time studying other types of multireference coupled-cluster methods and has therefore also included the derivation of the two common branches of multireference coupled-cluster methods in some detail in a different way than normally presented. This has in part been done to show the relationship between the various methods and how they can be derived from a common framework of

[1] What is degenerate or near degenerate may differ depending on taking a non-relativistic approach to a relativistic one. An example of this is BiH which has been calculated in this work.

effective Hamiltonians. A framework which is also shared by multireference perturbation theory [85].

3.1 Coupled-Cluster Theory

In this chapter the elementary equations will be derived for the single-reference coupled-cluster wave function and its most known multireference and pseudo multireference extensions. A brief discussion on the pro and cons will also be given to highlight the difficulty in extending the single-reference coupled-cluster method to a multireference method but also to give a perspective of what could and should be improved for a given extension for it being the method of choice.

The starting point for any of these correlation models is the independent-particle model. This model is in our case always the Hartree-Fock (HF) or Dirac-Coulomb Hartree-Fock (DCHF) model which describes the uncorrelated motion of the electrons. The correlated methods are a refinement of this model where the correlated motion of the electrons is carried out in virtual excitations from occupied to unoccupied spinors[2]. Each excitation is then associated with an amplitude which gives the probability that a particular excitation will occur as a result of a given electron-electron interaction. In the CI method this probability would be represented by the linear coefficients C_i from the variationally optimized linear combination of Slater determinants

$$|C\rangle = \sum_i C_i |i\rangle. \tag{3.1}$$

In the coupled-cluster method one obtains the C_i coefficients indirectly by the non-linear coupled-cluster amplitudes t_μ from

$$|CC\rangle = \Big[\prod_\mu (1 + t_\mu \hat{\tau}_\mu)\Big]|HF\rangle. \tag{3.2}$$

In Section 3.1.1 it will be seen that unlike in the CI method the excitations in the coupled-cluster method can lead to the same determinant so in the coupled-cluster method one can not only talk about excitations but also the processes of excitations. The understanding of these processes for excitations can lead to effective approximations of the coupled cluster hierarchy[3], appropriate choices of multireference expansions but more fundamentally

[2] Non-relativistic this would be spin orbitals

[3] like CC2 and CCSD(T)

the way the correlated electrons interact with each other. This last part gives meaning to questions like 'Will the interaction of two electrons be better described via a double excitation of both electrons or from the interaction of the already excited electrons in specific virtual spinors' or 'Will four electron interactions predominantly be from the direct excitation all four electron, the pairwise excitation and interaction or from interaction one at a time in four given virtual spinors[4]'. The answer to the first of these questions can be found by comparing the amplitude t_{ij}^{ab} to the product of $t_i^a t_j^b$, where i,j,k... denotes occupied spinors and a,b,c... unoccupied. The second question is found likewise by comparing t_{ijkl}^{abcd} to $t_{ij}^{ab} t_{kl}^{cd}$ and $t_i^a t_j^b t_k^c t_l^d$, respectively. What is in general found here is that double excitation in both cases is very important and, as will be evident in 3.1.1.4, is key to the success of the coupled-cluster method.

3.1.1 Single-Reference Coupled Cluster

3.1.1.1 Recent Developments for the Single-Reference Coupled-Cluster Method

The single-reference coupled-cluster has proven very successful in systems dominated by a single determinant and it's hierarchy has been extensively investigated in [4, 67, 86–88]. Despite a faster order by order convergence than the CI method the convergence is still rather slow and higher than doubles is needed for very accurate potential energy surfaces. A goal in quantum chemistry has for a long time been to reach chemical accuracy which is defined to be 1 kcal mol^{-1}. This however has turned out to be a not so easy task since not only does this require higher excitations but also very large basis sets due to the slow convergence also in the one-particle sector [89].

The large expense of trying to achieve chemical accuracy for light closed-shell molecules is shown in [90] where it is there demonstrated the need for very large basis sets and higher-order correlation treatment to achieve this accuracy. For the convergence of the basis sets there exists an estimate of this convergence to the basis set limit of X^{-3}, where X is the cardinal number in the correlation-consistent basis sets from Dunning [91–93]. Although there is not a similar estimate for the excitation level of the cluster operator, schemes for extrapolating the correlation contribution has been proposed [94–97] with very good success. These extrapolation methods consist of large series of calculations where the

[4]This would be spin orbital in non-relativistic theory

basis set cardinal number is successively increased first for the Hartree-Fock calculation, then the same is repeated for the first step in the coupled-cluster hierarchy CCSD onto CCSD(T), CCSDT and further until a limit for the basis set cardinal number is found. This limit is typically the limit of the computational hardware or a simple time limit due to the large increase in timings with every step. From these smaller calculations the result of a larger calculation is then extrapolated which will have a higher accuracy and precision than the performed calculations. So far this has only really been developed for the first-row elements and to extend this scheme to heavy elements extrapolation with respect to outer-core/inner-valence correlation effects needs to be carefully looked at. The need for outer-core/inner-valence polarization/correlation is demonstrated for molecules containing atoms from the second row in [98] and from all application sections in this thesis (see Section 9) it is obvious that this only increases with nuclear charge. The extrapolation schemes, of course, also require, in the development, very accurate experimental data which is harder to come by for the heavy elements.

Since higher excitations has turned out to be necessary and that including excitations higher than either full iterative triples or perturbative triples the need for general order program arose. This is also partly due to the fact that explicit programming of the various matrix elements for higher than triples is rather cumbersome and difficult to debug. Two such general-order programs have recently been presented in the non-relativistic framework. One by M. Kállay *et al.* [5, 6] and by J. Olsen [3, 99] where the codes from J. Olsen have served as the basis for the development of this work.

3.1.1.2 Formal Development of Single-Reference Coupled Cluster

Before the formal development of the coupled-cluster theory can proceed a few definitions of spinor and Kramers pair indices have to be given. The convention chosen here is $i, j, k, l, \ldots$ will designate spinors which are initially occupied in the reference determinant. $a, b, c, d, \ldots$ will be reserved for the initially unoccupied spinors. Few mixed or general indices $m, n, o, p, \ldots$ will be used. The Greek indices μ, ν will be the label for a general-order excitation operator.

The effect of any correlation operator working on any state can be written as

$$|\rangle \rightarrow (1 + t_\mu \hat{\tau}_\mu)|\rangle \tag{3.3}$$

where $\hat{\tau}_\mu$ is a general excitation operator and t_μ the associated amplitude. If one then forms the product of such correlation operator working on a given reference the coupled-cluster wave function appears

$$|CC\rangle = \Big[\prod_\mu (1 + t_\mu \hat{\tau}_\mu)\Big]|HF\rangle. \tag{3.4}$$

This wave function not only describes the correlation effect by excitations like the CI wave function in Eq. 3.1 but also by processes coming from the products of $\hat{\tau}_\mu$ in the wave function. Another very important aspect of this product form is that this immediately leads to a size-extensive formalism (see Section 3.1.1.4) for any-order truncation[5]. This means for two non-interacting subsystems the energy is additive separable[6] and the wave operator multiplicative separable. From a computational viewpoint this means compound and fragments will calculated with the same accuracy in the limit of non-interacting systems and there will be a "comparable accuracy" with increasing system size.

Due to the fact that the excitation operators $\hat{\tau}_\mu$ and $\hat{\tau}_\nu$ always excite from a set of occupied spinors these operators will commute

$$[\hat{\tau}_\mu, \hat{\tau}_\nu] = 0 \tag{3.5}$$

and using the fact that two excitations cannot excite from the same occupied spinor

$$\hat{\tau}_\mu \hat{\tau}_\mu = 0 \tag{3.6}$$

one can do the following expansion of 3.4

$$|CC\rangle = \Big(1 + \sum_\mu t_\mu \hat{\tau}_\mu + \sum_{\mu\nu} t_\mu t_\nu \hat{\tau}_\mu \hat{\tau}_\nu + \dots\Big)|HF\rangle \tag{3.7}$$

$$|CC\rangle = |HF\rangle + \sum_\mu t_\mu |\mu\rangle + \sum_{\mu\nu} t_\mu t_\nu |\mu\nu\rangle + \dots \tag{3.8}$$

keeping in mind there will be no $\hat{\tau}_\mu \hat{\tau}_\mu$ from the product form. It is seen from Eq. 3.8 that the determinants $|\mu\nu\rangle$ can be reached in several different ways either the direct way or in a product form

$$|\mu\nu\rangle = \hat{\tau}_{\mu\nu}|HF\rangle = \hat{\tau}_\mu \hat{\tau}_\nu |HF\rangle. \tag{3.9}$$

[5] Any exact wave function is also size-extensive.

[6] For the energy alone this is also called size-consistency and is needed for the correlation energy at a given truncation level to be proportional to system size.

Therefore we cannot associate an amplitude and excitation operator to a single determinant since both amplitude and operator will also be part of other determinants. This therefore leads to processes of ways a determinant can be reached. An example could be the triples amplitude

$$t_{\mu\nu\eta}^{total} = t_{\mu\nu\eta} + t_{\mu\nu}t_{\eta} + t_{\mu}t_{\nu\eta} + \cdots + t_{\mu}t_{\nu}t_{\eta} \tag{3.10}$$

which is comprised of the direct triple amplitude, products of double excitations with a single excitation and of three single excitations. The amplitude $t_{\mu\nu\eta}$ is here called the connected cluster amplitude and the products disconnected cluster amplitudes.

The most known form for the coupled-cluster wave function is, however, not the product form but the exponential one. From Eq. 3.6 one sees that the correlation operator in Eq. 3.3 can also be written in the exponential form

$$1 + t_{\mu}\hat{\tau}_{\mu} = \exp(t_{\mu}\hat{\tau}_{\mu}) = \sum_{n=0}^{\infty} \frac{1}{n!}(t_{\mu}\hat{\tau}_{\mu})^n \tag{3.11}$$

since all quadratic and higher order vanishes due to Eq. 3.6 and due to the commutation of the cluster operators in Eq. 3.5 we can use the exponential relation for commutative operators

$$\exp(\hat{A})\exp(\hat{B}) = \exp(\hat{A} + \hat{B}). \tag{3.12}$$

The familiar exponential ansatz then comes when one writes the cluster operator like

$$\hat{T} = \sum_{\mu} t_{\mu}\hat{\tau}_{\mu} \tag{3.13}$$

and inserts it with Eq. 3.11 in Eq. 3.4 to get

$$|CC\rangle = \exp(\hat{T})|HF\rangle \tag{3.14}$$

The regular coupled-cluster hierarchy is introduced by dividing the $\hat{T}$ from Eq. 3.13 into operators consisting of single, double, triple and so on excitation operators

$$\hat{T} = \hat{T}_1 + \hat{T}_2 + \ldots + \hat{T}_N. \tag{3.15}$$

3.1.1.3 Solving the Coupled-Cluster Equations

From Eq. 3.8 it is seen that $\hat{\tau}_{\mu}$ gives contributions to not only to determinants of the same excitation level as $\hat{\tau}_{\mu}$ but also to all higher determinants from the FCI wave function

and that even a truncation at a given level in the coupled-cluster hierarchy will still yield contributions from all determinants. This means a variational treatment of the coupled-cluster equations would be a major undertaking since it would entail all determinants of the FCI wave function with also higher products of variational parameters. The number of parameters would for the truncated coupled-cluster be smaller than the FCI but still involve all determinants. The full coupled-cluster (FCC) wave function would still have the same number of parameters as the FCI wave function. It is therefore obvious that the coupled-cluster wave function will not be solved variationally[7] and another approach is needed.

The given equation to be solved is written as

$$\hat{H}\exp(\hat{T})|HF\rangle = E\exp(\hat{T})|HF\rangle \tag{3.16}$$

and is then projected onto the reference determinant and the projection manifold

$$\langle\mu| = \langle HF|\hat{\tau}_\mu^\dagger. \tag{3.17}$$

The unlinked coupled-cluster equations[8] for the energy and the amplitudes then become

$$\langle HF|\hat{H}\exp(\hat{T})|HF\rangle = E \tag{3.18}$$

$$\langle\mu|\hat{H}\exp(\hat{T})|HF\rangle = E\langle\mu|\exp(\hat{T})|HF\rangle = 0 \tag{3.19}$$

The more common form is the linked coupled-cluster equations or also called similarity transformed coupled-cluster where Eq. 3.16 is multiplied by $\exp(-\hat{T})$ to give

$$\exp(-\hat{T})\hat{H}\exp(\hat{T})|HF\rangle = E\exp(-\hat{T})\exp(\hat{T})|HF\rangle = E|HF\rangle \tag{3.20}$$

Here one can view $\exp(-\hat{T})\hat{H}\exp(\hat{T})$ as an effective non-Hermitian similarity transformed Hamiltonian working on a model state. Doing again the projection with Eq. 3.17 on Eq. 3.20 the energy and amplitude equation then becomes

$$\langle HF|\exp(-\hat{T})\hat{H}\exp(\hat{T})|HF\rangle = E \tag{3.21}$$

$$\langle\mu|\exp(-\hat{T})\hat{H}\exp(\hat{T})|HF\rangle = \langle\mu|\exp(-\hat{T})E\exp(\hat{T})|HF\rangle = 0 \tag{3.22}$$

[7] This can be done but only for small systems

[8] This terminology comes from perturbation theory and refers to the appearance of unlinked diagrams in the perturbation theory.

Despite different appearance the result of the two approaches are the same if the excitation manifold is closed under deexcitations, see also Section 5.1.1. In this work the focus has been on the linked coupled-cluster equations so therefore will only it be discussed further. An argument and a possible algorithm for the unlinked case will be discussed in Section 6.2.2 for the CI driven coupled-cluster algorithm.

The coupled-cluster energy is only directly determined by double excitations

$$E = \langle HF|\exp(-\hat{T})\hat{H}\exp(\hat{T})|HF\rangle = \langle HF|\hat{H}\exp(\hat{T})|HF\rangle \tag{3.23}$$

$$= \langle HF|\hat{H}\Big(1+\hat{T}_2+\frac{1}{2}\hat{T}_1^2\Big)|HF\rangle \tag{3.24}$$

since the Hamilton operator is a two-particle operator and the single excitations drop out due to Brillouin's theorem. The higher-order excitations only give an indirect contribution to the energy.
For the amplitude equation the similarity-transformed Hamiltonian is expanded with the Baker-Campbell-Hausdorff (BCH) expansion

$$\exp(-\hat{T})\hat{H}\exp(\hat{T}) = \hat{H}+[\hat{H},\hat{T}]+\frac{1}{2}[[\hat{H},\hat{T}],\hat{T}] \tag{3.25}$$

$$+ \frac{1}{6}[[[\hat{H},\hat{T}],\hat{T}],\hat{T}]+\frac{1}{24}[[[[\hat{H},\hat{T}],\hat{T}],\hat{T}],\hat{T}]. \tag{3.26}$$

This expansion terminates after the fourth order since the Hamiltonian is a two-particle operator[9] and every commutator reduces the deexcitation rank of this by $\frac{1}{2}$ down to zero.

This termination after fourth order we will see being important for the CI-based coupled-cluster code in Section 6.2.2 where it will be evident that for this type of implementation the linked coupled-cluster equations are preferred. For the commutator-based coupled-cluster program this can of course only be valid for the linked coupled-cluster equations since it is the only case commutators appear. A preference for the linked over the unlinked coupled-cluster equations is, however, not as evident. From a implementation viewpoint the linked coupled-cluster equations may seem simpler since there will only appear up to the fourth order commutator and from this only a definite number of ways these can be ordered. This means there are steps where all cases can be programmed explicitly. A further elucidation of this will be shown in Section 6.3.

[9] This is then a rank 2 operator.

3.1.1.4 Why does Coupled Cluster Perform better than Configuration Interaction?

While the CI and the coupled-cluster method has the same scaling of O^nV^{n+2}, where O represents the occupied spinors and V the unoccupied spinors in the reference determinant and n is the largest excitation level included in the hierarchy[10], the performance of the two methods is very different. For correlation of few electrons the difference is small, which is demonstrated in Section 9.1 for HBr, but the difference between the CI and the coupled-cluster method increases with the number of electrons correlated[11], also shown in Section 9.1.

This increasing difference between truncated CI and coupled-cluster with system size stems from the fact that coupled-cluster is size-extensive and CI not. This means coupled-cluster at a given truncation level can give comparable good calculations[12] for small systems as well as large systems while CI cannot. For CI to deliver the same result for a large system as for a small one the truncation in the CI expansion will necessarily have to be larger for the large system than for the small one. Exactly how much higher in the hierarchy can, however, not be said. This means getting very exact atomization energies with CI will be difficult since the subsystems are calculated with higher accuracy than the compound system. In turn this also translates into heavy element calculations and large molecules where many electrons have to be correlated. The usefulness of the CI method would be questionable, since it would rarely be possible to increase the hierarchy so much it would be in competition with the coupled-cluster method.

The natural question of course also arises to why does the coupled cluster method perform better than the CI method. This can be seen by comparing the CI hierarchy to

[10] This is under the assumption of $O, V \gg n$.

[11] It should be noted that the difference between CISD and CCSD, of course, will be greater than the multireference calculations presented in Section 9.1 since the CISD and CCSD calculations will be further from FCI.

[12] Comparable good calculations is a rather vague term since size-extensivity is not really defined for large but not periodic systems [100]. The problem with these systems is that there can not be any counting arguments used or no limits taken since the system cannot be divided into any repeating units. Although only defined for an infinite insulating periodic system the concept does seem to hold some value even for molecular systems. However coupled cluster will also like CI degrade in accuracy with increasing system size, just not as fast.

the cluster operators in Eq. 3.13

$$\hat{C}_0 = 1 \tag{3.27}$$

$$\hat{C}_1 = \hat{T}_1 \tag{3.28}$$

$$\hat{C}_2 = \hat{T}_2 + \frac{1}{2!}\hat{T}_1^2 \tag{3.29}$$

$$\hat{C}_3 = \hat{T}_3 + \hat{T}_1\hat{T}_2 + \frac{1}{3!}\hat{T}_1^3 \tag{3.30}$$

$$\hat{C}_4 = \hat{T}_4 + \hat{T}_1\hat{T}_3 + \frac{1}{2!}\hat{T}_2^2 + \frac{1}{2!}\hat{T}_1^2\hat{T}_2 + \frac{1}{4!}\hat{T}_1^4. \tag{3.31}$$

Where when compared to the CCSD amplitude equation

$$\begin{aligned} &\langle\mu_1|\hat{H}|HF\rangle + \langle\mu_1|[\hat{H},\hat{T}_1]|HF\rangle + \langle\mu_1|[\hat{H},\hat{T}_2]|HF\rangle + \frac{1}{2!}\langle\mu_1|[[\hat{H},\hat{T}_1],\hat{T}_1]|HF\rangle \\ +\ &\langle\mu_1|[[\hat{H},\hat{T}_1],\hat{T}_2]|HF\rangle + \frac{1}{3!}\langle\mu_1|[[[\hat{H},\hat{T}_1],\hat{T}_1],\hat{T}_1]|HF\rangle = 0 \end{aligned} \tag{3.32}$$

$$\begin{aligned} &\langle\mu_2|\hat{H}|HF\rangle + \langle\mu_2|[\hat{H},\hat{T}_1]|HF\rangle + \langle\mu_2|[\hat{H},\hat{T}_2]|HF\rangle + \frac{1}{2!}\langle\mu_2|[[\hat{H},\hat{T}_1],\hat{T}_1]|HF\rangle \\ +\ &\langle\mu_2|[[\hat{H},\hat{T}_1],\hat{T}_2]|HF\rangle + \frac{1}{2!}\langle\mu_2|[[\hat{H},\hat{T}_2],\hat{T}_2]|HF\rangle + \frac{1}{3!}\langle\mu_2|[[[\hat{H},\hat{T}_1],\hat{T}_1],\hat{T}_1]|HF\rangle \\ +\ &\frac{1}{2!}\langle\mu_2|[[[\hat{H},\hat{T}_1],\hat{T}_1],\hat{T}_2]|HF\rangle + \frac{1}{4!}\langle\mu_2|[[[[\hat{H},\hat{T}_1],\hat{T}_1],\hat{T}_1],\hat{T}_1]|HF\rangle = 0 \end{aligned} \tag{3.33}$$

it is seen that in these equations not only do $\hat{T}_1$ and $\hat{T}_2$ appear linearly but also as products. Products, which first appear later compared in the CI hierarchy. So even if these products do not give the exact triples or quadruples they do give a very good approximation of these. So despite the fact that the truncated coupled-cluster equations do not give exact single, doubles,..., it does give weight to all determinants and a very good approximate contribution to the nearest higher excited determinants in the CI hierarchy. This is much more important than delivering the exact CI coefficients at any given order and that is really why the coupled-cluster method is so successful.

Of these products $\hat{T}_2^2$ is particularly important since this term will typically give the vast contribution to the very important quadruples excitations and this with a scaling of O^2N^4 in comparison to the full T_4 with O^4N^6. In general will the disconnected amplitudes from $\hat{T}_2^n$ give the most important contribution to the higher CI hierarchy but still with

only the O^2N^4 scaling which is a tremendous saving in comparison with the effort that would have to be put into a CI calculation. This is also most likely the term which is the dominating factor in the good scaling of coupled-cluster with respect to system size.

Triples contributions, on the other hand, are not that well described by CCSD since $\hat{T}_3$ is there the most important excitation operator. The triples contribution is, however, significantly smaller than the doubles and normally around the same size as the quadruples in the CI hierarchy. This means the triples will normally[13] only give a small contribution in a CI calculation. To be better than CCSD one would have to go to CISDTQ, and this would only be slightly better since the majority of the quadruples contribution is already in the CCSD calculation. In general CI will need an excitation level of plus two in comparison to the coupled-cluster excitation level since all odd excitation levels normally only give around the same contribution as the next even excitation level[14].

3.1.2 Model Spaces and Effective Hamiltonians

The purpose of this section is to introduce the concepts of model spaces, effective Hamiltonians, wave operators plus building a common framework to be able to make short derivations of the Hilbert-space and Fock-space coupled-cluster methods. The section will be very general and can be used for any method where one would try to construct only a part of the full spectrum with an effective operator working on some reference model states. This will also serve in showing the similarity in the development of any multireference perturbation or coupled-cluster theory since the only difference is the ansatz for the wave operator. The consequence of choosing wave operators with different properties such as conserving commutations relations, state independent, norm- and symmetry conserving and Hermiticity is explored extensively in two rather exhausting but very rewarding articles by V. Hurtubise and K. F. Freed [101, 102]. In [101, 102] it is also shown that

[13]Triples can be important in systems where correlation dramatically changes the electron density where then additional orbital relaxation comes in via the triples.

[14]This only seems to hold for smaller molecules since it can be shown that any truncated CI calculation contribution to the correlation energy will tend to zero when the number of electrons goes to infinity [67]. This has been shown for when the number of non-interacting systems will go to infinity and this will also be true in the case of interacting systems since CI is not size-consistent. For coupled-cluster on the other hand the correlation energy remains constant due to size-consistency in the non-interacting case. It is however not exactly clear what happens in the case of interacting systems.

despite there being an infinite number of ways to construct the wave operator there is however a final number of classifications of these.

The idea of effective Hamiltonians is built on partitioning the full space into a model space and an orthogonal complementary space designated P- and Q-space, respectively. With this partitioning a space of low dimension P is generated where an effective operator can be diagonalized and give the exact eigenvalues of the full problem for any state in the model space. This effective operator only operates in the model space but brings in all the contributions from the complementary Q-space. So instead of solving the full problem for all states the problem is reduced to only solving it for those inside the model space.

3.1.2.1 General Framework for Effective Hamiltonians

An effective Hamiltonian $\hat{H}_{eff}$ is defined to operate in a model space P_0 of finite dimension spanned by reference model functions $|\phi_{\mu,0}\rangle$ and there generate the exact eigenvalues E_μ for the full problem for all states μ in the model space P[15]

$$\hat{H}_{eff}|\phi_{\mu,0}\rangle = E_\mu|\phi_{\mu,0}\rangle \qquad \mu \in P. \tag{3.34}$$

This is a very general definition and would also include the similarity transformed coupled-cluster in Eq. 3.20 where the effective Hamiltonian

$$\hat{H}_{eff} = \exp(-\hat{T})\hat{H}\exp(\hat{T}) \tag{3.35}$$

would operate on the reference model space $|HF\rangle$ to generate the exact eigenvalue E

$$\exp(-\hat{T})\hat{H}\exp(\hat{T})|HF\rangle = \hat{H}_{eff}|HF\rangle = E|HF\rangle \tag{3.36}$$

in this model space.

The wave operator $\hat{k}$ is defined as the operator that transform the reference model eigenstates $|\phi_{\mu,0}\rangle$ to the exact eigenstates $|\phi_\mu\rangle$

$$\hat{k}|\phi_{\mu,0}\rangle = |\phi_\mu\rangle \qquad \mu \in P. \tag{3.37}$$

Here it should be noted that $\hat{k}$ is only defined for the model space and will not give any information on the complementary Q-space.

[15]Notice it does not matter if it is here written P or P_0 since we will later demand that there will be a bijective mapping between these two model spaces. So no function in P will be linearly independent of P_0 and vice versa.

We will furthermore assume that there exists a bijective mapping between the reference model space $|\phi_{\mu,0}\rangle$ and the exact states $|\phi_\mu\rangle$. This means there will also exist another linear operator $\hat{l}$ that maps the exact states back onto the reference states in the model space

$$\hat{l}|\phi_\mu\rangle = |\phi_{\mu,0}\rangle \qquad \mu \in P \tag{3.38}$$

which again only operates inside the model space.

At the same time we will also define the projection operators for the reference eigenfunctions and the exact ones for both the P- and Q-space. For the reference eigenfunctions the projectors will be denoted $\hat{P}_0$ and $\hat{Q}_0$ for the projection onto the model space and the complementary space, respectively. Likewise will the projectors from the exact eigenfunctions be denoted $\hat{P}$ and $\hat{Q}$. These will be written in the common way

$$\begin{aligned}
\hat{P}_0 &= \sum_{\mu}^{n} |\bar{\phi}_{\mu,0}\rangle\langle\phi_{\mu,0}| \\
\hat{Q}_0 &= \sum_{\nu>n} |\bar{\phi}_{\nu,0}\rangle\langle\phi_{\nu,0}| \\
\hat{P} &= \sum_{\mu}^{n} |\bar{\phi}_{\mu}\rangle\langle\phi_{\mu}| \\
\hat{Q} &= \sum_{\nu>n} |\bar{\phi}_{\nu}\rangle\langle\phi_{\nu}|
\end{aligned} \tag{3.39}$$

where $|\phi_{\mu,0}\rangle$ is a reference model space determinant, n is the size of the model space and $\bar{\phi}$ shows there may be a difference between left and right eigenvectors, when using a bi-orthogonal expansion, which is dependent on the choice of $\hat{k}, \hat{l}$. The projectors are related through

$$\hat{P}_0 + \hat{Q}_0 = \hat{1}. \tag{3.40}$$

The remaining projectors and relations can be written likewise.

A few relations between the projectors and the wave operators can be derived to illustrate that the wave operator only operates inside the model space.

$$\hat{k}\hat{P}_0 = \hat{k} = \hat{P}\hat{k} \tag{3.41}$$

$$\hat{k}\hat{Q}_0 = 0 = \hat{Q}\hat{k} \tag{3.42}$$

$$\hat{l}\hat{P} = \hat{l} = \hat{P}_0\hat{l} \tag{3.43}$$

$$\hat{l}\hat{Q} = 0 = \hat{Q}_0\hat{l} \tag{3.44}$$

$$\hat{l}\hat{k} = \hat{P}_0 \tag{3.45}$$

$$\hat{k}\hat{l} = \hat{P} \tag{3.46}$$

These equations follow directly from the definitions of the mappings. Eqs. 3.45 and 3.46 follow from Eqs. 3.37 and 3.38. From these two equations it is also seen that $\hat{l}$ is both a left and a right inverse of $\hat{k}$ and vice versa.

The effective Hamiltonian in the reference model space will then be

$$\hat{H}_{eff}|\phi_{\mu,0}\rangle = \hat{l}\hat{H}\hat{k}|\phi_{\mu,0}\rangle = E_\mu|\phi_{\mu,0}\rangle \qquad \mu \in P. \tag{3.47}$$

There will from this effective Hamiltonian be an infinite number of different ways to generate it. The various properties this effective Hamiltonian will get are depending on the wave operator $\hat{k}$ and its inverse $\hat{l}$. The numerable choices and properties can be found in [101]. With a quick glance back at the single-reference coupled-cluster it is seen that the wave operator $\hat{k}$ in this case of a one-dimensional model space becomes $\exp(\hat{T})$ and its inverse $\hat{l}$ is $\exp(-\hat{T})$ in the similarity transformed case. From this it is also clear that the effective Hamiltonian for the linked coupled-cluster will not be a Hermitian[16] since

$$(\exp(\hat{T}))^\dagger \neq \exp(-\hat{T}). \tag{3.48}$$

For the unlinked coupled-cluster the wave operator is the same but the inverse is just the projection operator P_0.

The effective Hamiltonian presented in Eqs. 3.34 and 3.47 can also be viewed as a similarity transformation of the complete Hamiltonian

$$\hat{H}_{sim} = \hat{\omega}^{-1}\hat{H}\hat{\omega} \tag{3.49}$$

which block diagonalizes the complete Hamiltonian in a P- and Q-space like[17]

$$\hat{H}_{sim} = \hat{P}_0\hat{H}_{sim}\hat{P}_0 + \hat{Q}_0\hat{H}_{sim}\hat{Q}_0. \tag{3.50}$$

[16]For an Hermitian effective Hamiltonian the transformation should be unitary. For the coupled-cluster method this would lead to the unitary coupled-cluster method.

[17]This formulation could also be used to decouple the large and the small component in the Dirac equation.

The only part of 3.50 that is used for the effective Hamiltonian is then

$$\hat{H}_{eff} = \hat{P}_0 \hat{H}_{sim} \hat{P}_0 \tag{3.51}$$

which gives the exact eigenvalues for the states in the model space when diagonalized. The actual wave operator that is being looked for will the be of the form

$$\hat{\omega} = \hat{\Omega} \hat{P}_0 \tag{3.52}$$

so that only an $\hat{\Omega}$ ansatz and an inverse have to be found.

3.1.3 Hilbert-Space Coupled Cluster

In the author's opinion the Hilbert-space coupled-cluster formulation is from an algebraic viewpoint by far the most elegant and appealing since it offers a natural extension of the single-reference coupled-cluster method. This, however, does not necessarily matter for the performance of the method since despite its elegance it is a rather difficult method to work with in practice and causes great convergence problems of the model space due to intruder states.

The method was the second of the genuine multireference coupled-cluster methods to be proposed after the Fock-space coupled-cluster method (see Section 3.1.4). This was done in 1981 by B. Jeziorski and H. J. Monkhorst [103]. Although proposed some time ago only few codes have been developed and most calculations presented have been on very small systems since it was quickly realized that it was very difficult, if not often impossible, to converge the model space. In recent developments this intruder state problem has been solved by introducing a buffer-space between the model space and the complementary space [104]. This, however, introduces indirect corrections to the states in the model space which cannot be solved by increasing the correlation level. To counteract this correction an extrapolation method has been proposed [104] in a similar way also done for Fock-space coupled cluster.

3.1.3.1 Formal Development of Hilbert-Space Coupled Cluster

The derivation of the working equations will here be kept to a minimum since this is mostly for comparing the working equations with the equations later derived in 3.1.5.1. The

discussion of incomplete reference spaces, the appearance of connected and disconnected diagrams[18] will be left for the interested reader in [103]. The notation will be the same as in Sections 3.1.1.2 and 3.1.2.1.

The Hilbert-space coupled-cluster is a Bloch type of effective Hamiltonian which means it will be in the $2a$ (K, L) category from [101]. It will have unity normalized reference right eigenvectors and a non-Hermitian effective Hamiltonian. The true right eigenvectors are, however, not normalized and a normalization factor comes in. It is also worth noticing that there has been chosen the bi-orthonormality condition

$$\langle \bar{\phi}_{\mu,0} | \phi_{\nu,0} \rangle = \langle \phi_{\mu,0} | \bar{\phi}_{\nu,0} \rangle = 0 \tag{3.53}$$

where the left and right eigenvectors are normalized on each other. This is typically part of what is called intermediate normalization where the rest is shown in Eq. 3.56.

The ansatz for the wave operator will here be

$$\hat{k} = \hat{\Omega}\hat{P}_0 = \sum_{\mu} \hat{\Omega}_{\mu}\hat{P}_{\mu} = \sum_{\mu} \exp(\hat{T}_{\mu})\hat{P}_{\mu} \qquad \mu \in P \tag{3.54}$$

where it is seen that every reference function in the model space has its own exponential expansion $\exp(\hat{T}_{\mu})$. This is in the author's opinion the most straight forward extension of the single-reference coupled-cluster method since it easily seen to reduce to the single-reference coupled-cluster method when the dimension of the model space is one. This proposal of a separate wave operator for each state in the model space makes this a state-universal approach. The inverse operator is here just the product of the projection operators of the model spaces

$$\hat{l} = \hat{P}_0\hat{P} = \sum_{\mu\nu}^{n} |\phi_{\mu,0}\rangle\langle\phi_{\mu,0}|\phi_{\nu}\rangle\langle\phi_{\nu}| \qquad \mu, \nu \in P \tag{3.55}$$

which means for a one dimensional model space that the coupled-cluster energy equations 3.18 and 3.21 are recovered. With the intermediate normalization of the wave function

$$\langle \phi_{\mu,0} | \phi_{\nu} \rangle = \delta_{\mu\nu} \tag{3.56}$$

[18] A theory with only connected diagrams or with cancellation of all disconnected diagrams is size-extensive. The diagrammatical technique stems from perturbation theory.

the inverse operator takes the form

$$\hat{l} = \sum_{\mu}^{n} |\phi_{\mu,0}\rangle\langle\phi_{\mu}| \qquad \mu \in P \tag{3.57}$$

and the wave operator becomes idempotent

$$\hat{k}^2 = \sum_{\mu\nu} |\phi_{\mu}\rangle\langle\phi_{\mu,0}|\phi_{\nu}\rangle\langle\phi_{\nu,0}| = \sum_{\mu} |\phi_{\mu}\rangle\langle\phi_{\mu,0}| = \hat{k}. \tag{3.58}$$

It should also be noted that the excitation operator $\hat{T}_{\mu}$ does not create any excitations inside the model space only to the outside so each state becomes a Fermi vacuum. These choices of wave operators can also be confirmed to satisfy the equations 3.41 to 3.46. The interaction of the states inside the model space comes in by diagonalizing the effective Hamiltonian in the model space. This means any exact state in the model space can be written as

$$|\phi_{\nu}\rangle = \sum_{\mu} c_{\nu\mu} \exp(\hat{T}_{\mu})|\phi_{\mu,0}\rangle \qquad \mu,\nu \in P \tag{3.59}$$

The amplitudes are determined by projecting against the Bloch equation. The Bloch equation can easily be derived from the exact equation

$$\hat{H}|\phi_{\mu}\rangle = \hat{H}\hat{k}|\phi_{\mu,0}\rangle = E_{\mu}|\phi_{\mu}\rangle = E_{\mu}\hat{k}|\phi_{\mu,0}\rangle \tag{3.60}$$

by multiplying with the wave operator from left

$$\hat{k}\hat{H}|\phi_{\mu}\rangle = \hat{k}\hat{H}\hat{k}|\phi_{\mu,0}\rangle = E_{\mu}\hat{k}|\phi_{\mu}\rangle = E_{\mu}\hat{k}^2|\phi_{\mu,0}\rangle \tag{3.61}$$

and using the idempotency of the wave operator in Eq. 3.58 the Bloch equation appears

$$\hat{k}\hat{H}\hat{k} = \hat{H}\hat{k}. \tag{3.62}$$

Multiplying the Bloch equation 3.62 by $|\phi_{\mu,0}\rangle$ from the right and by $\exp(-\hat{T}_{\mu})$ from the left and then projecting against all determinants in the complementary space Q yields

$$\langle\phi_{\mu,0}|\hat{\tau}_{\mu}\exp(-\hat{T}_{\mu})\hat{k}\hat{H}\hat{k}|\phi_{\mu,0}\rangle = \langle\phi_{\mu,0}|\hat{\tau}_{\mu}\exp(-\hat{T}_{\mu})\hat{H}\hat{k}|\phi_{\mu,0}\rangle \tag{3.63}$$

$$\langle\phi_{\mu,0}|\hat{\tau}_{\mu}\exp(-\hat{T}_{\mu})\sum_{\nu}\exp(\hat{T}_{\nu})\hat{P}_{\nu}\hat{H}\sum_{\eta}\exp(\hat{T}_{\eta})\hat{P}_{\eta}|\phi_{\mu,0}\rangle = \langle\phi_{\mu,0}|\hat{\tau}_{\mu}\exp(-\hat{T}_{\mu})\hat{H}\sum_{\nu}\exp(\hat{T}_{\nu})\hat{P}_{\nu}|\phi_{\mu,0}\rangle \tag{3.64}$$

$$\sum_{\nu\neq\mu}\langle\phi_{\mu,0}|\hat{\tau}_\mu\exp(-\hat{T}_\mu)\exp(\hat{T}_\nu)|\phi_{\nu,0}\rangle\langle\phi_{\nu,0}|\exp(-\hat{T}_\mu)\hat{H}\exp(\hat{T}_\mu)|\phi_{\nu,0}\rangle = \langle\phi_{\mu,0}|\hat{\tau}_\mu\exp(-\hat{T}_\mu)\hat{H}\exp(\hat{T}_\mu)|\phi_{\mu,0}\rangle. \quad (3.65)$$

It is again noted that this expression will reduce to the linked coupled-cluster equations in Section 3.1.1.2 for a model space with a dimension of one since the left-hand side becomes zero. But what also is evident from Eq. 3.65 is the fact that all states in the model space have to be optimized simultaneously since the amplitudes of all the other states t_ν in the model space are included in optimizing the state t_μ. This makes the procedure more cumbersome and very sensitive to any problems in the optimization step since all other states will be directly affected by this. Since it is often not possible to converge the states in the model space due to intruders, the development of the Hilbert space coupled-cluster has been scarce and mostly dominated by pilot codes.

A recent flavor of the Hilbert-space coupled-cluster method dubbed Mukherjee coupled cluster has been proposed where a resolution of identity is inserted into Eq. 3.65 between $\exp(-\hat{T}_\mu)$ and the effective Hamiltonian. This, however, leaves the equations under-determined. By imposing a condition on the equations, the under-determinedness can be resolved. This variant has received more attention and codes have been developed [105, 106] with significant success.

3.1.4 Fock-Space Coupled Cluster

The first genuine multireference coupled-cluster approach to be proposed was done in 1975 by D. Mukherjee, R. K. Moitra and A. Mukhopadhyay [107] and has been the most successful since then. This approach assumes the same wave operator for the whole model space, unlike the Hilbert space coupled-cluster which has a separate wave operator for each state in the model space. This assumption then makes the Fock-space coupled cluster a valence-universal approach. This is also the only approach along with the state-selective multireference coupled-cluster method which has been adapted to the relativistic framework [108, 109] and also for non-relativistic codes to include higher than doubles excitations [110]. The state-selective multireference coupled-cluster method presented in this work is, however, the only one to have both relativity and higher than double excitations included simultaneously. While the initial formulation which is presented here suffers from having to start from a closed shell molecule, the intermediate Fock-Space

coupled-cluster method and mixed sector presented in [109,111] is capable of starting from a quasi closed-shell molecule making the sector of interest closer to the starting sector. The idea of the mixed sector approach is in particular aimed at heavy elements where spin-orbit splitting can give quasi closed shells such as $p_{1/2}$ and $d_{3/2}$ and will therefore only work if the spin-orbit splitting is sufficiently large.

3.1.4.1 Formal Development of Fock-Space Coupled Cluster

Before the algebraic development of the Fock-Space Coupled-Cluster method can commence there is first a need to extend the conventions of notation from Section 3.1.1.2. To understand this notation the particle-hole formalism will first be introduced. The particle-hole formalism can be used when there exists a preferred reference determinant for a redefinition of the vacuum to this reference determinant, which will now be referred to as the Fermi vacuum. The annihilation operators of the reference determinant will be called hole creation operators and creation operators hole annihilation operator. For the annihilation and creation of the unoccupied virtuals these will retain their usual name, namely annihilation and creation of particles. To extend this preferred reference to a multireference formalism a model space, that will be called the valence orbitals, consisting of active holes and particles will be defined. The letters $\bar{i}, \bar{j}, \bar{k}, \bar{l}, \ldots$ will designate inactive holes and $\bar{a}, \bar{b}, \bar{c}, \bar{d}, \ldots$ the inactive particles. The Greek letters $\iota, \kappa, \lambda \ldots$ will be reserved for active holes and $\alpha, \beta, \gamma \ldots$ for active particles. The set of active and inactive particles (holes) combined is symbolized by the letters $i, j, k, l, \ldots$ ($a, b, c, d, \ldots$) as shown in Section 3.1.1.2. Additionally the letters $\bar{\bar{i}}, \bar{\bar{j}}, \bar{\bar{k}}, \bar{\bar{l}}, \ldots$ will be for inactive holes and all valence levels (active holes and particles) and correspondingly $\bar{\bar{a}}, \bar{\bar{b}}, \bar{\bar{c}}, \bar{\bar{d}}, \ldots$ will be for inactive particles and all valence levels. The valence levels are the active holes and particles. For general indices $m, n, o, p, \ldots$ will still be used and μ, ν for general order excitations. This division is also illustrated in Figure 3.1. The reason for adding these many new indices which are combinations of the inactive and active particles and holes is to create shorter and more compact looking equations.

The Fock-space coupled-cluster method is also of the type (K, L) category from [101]. While not directly a Bloch type of effective Hamiltonian since several model spaces have to be considered simultaneously[19], the Bloch equation 3.62 will, however, be used in the

[19] In practice this will be successively in an embedding scheme.

Figure 3.1: The indices for the Fock-space coupled-cluster method.

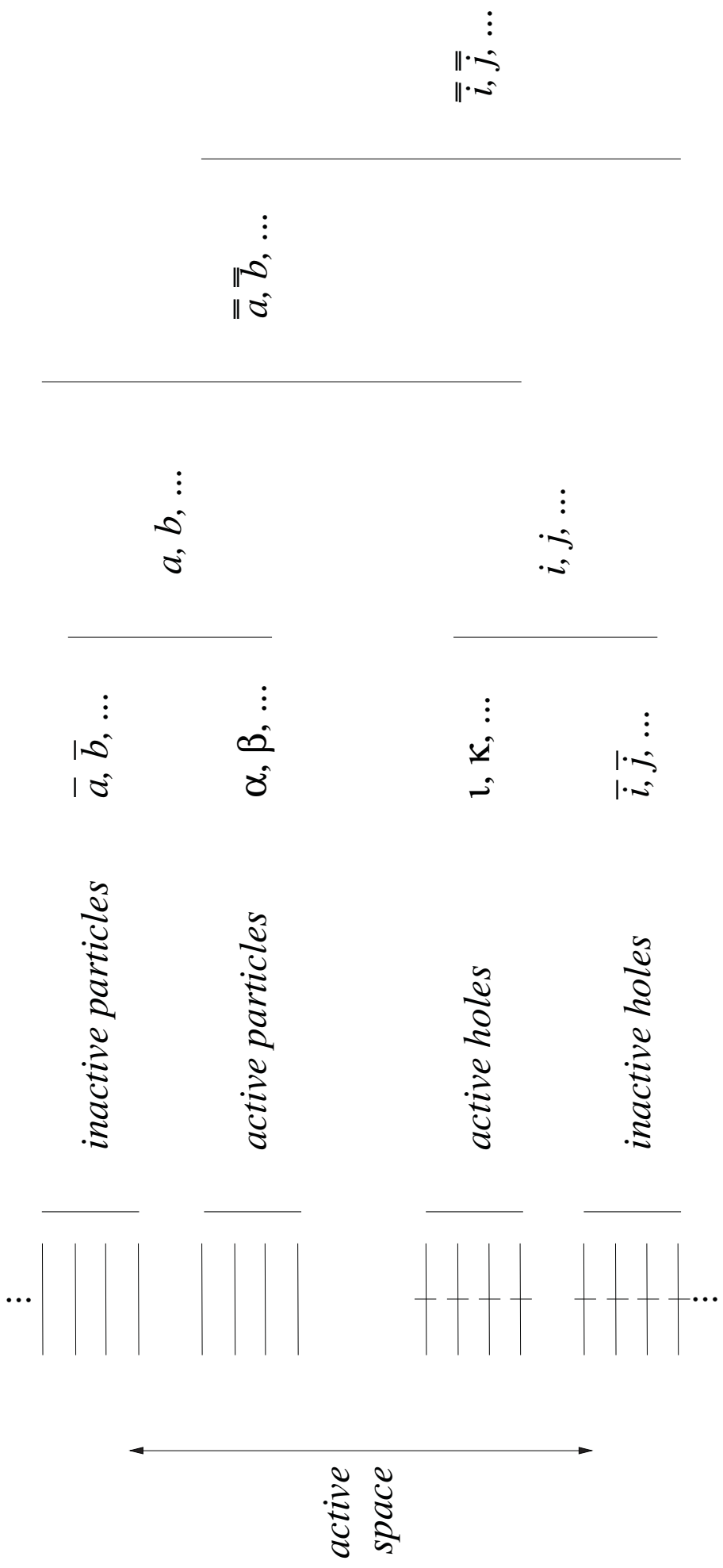

derivation. The need to consider several model spaces also within same the same fixed N-electron Hilbert space, but with different number of active holes and particles, stems from the insistence of valence universality and will become clear later.

Unlike in the state-universal Hilbert-space coupled-cluster method in Section 3.1.3 where several vacua, one for each state in the model space are defined, we will in the valence-universal Fock-space coupled-cluster method assume a common vacuum for all states in the model space. The consequence of just one vacuum for all states results in having to include in the model space all determinants corresponding to a variable number of electrons. For a complete model space all determinants from zero to the number of valence levels have to be taken into consideration. Here, the number of valence levels (N_v) are

$$N_v = N_{ah} + N_{ap} \tag{3.66}$$

the sum of the number of active holes (N_{ah}) and particles (N_{ap}). With the variable number of electrons we see that this coupled-cluster method is no longer confined to a N-particle Hilbert space like the other methods but will move in the Fock space. This also means that not only will the neutral atom or molecule be calculated but also ionized and electron attached states as well.

With the single vacuum also follows just one wave operator. The ansatz in Fock-space coupled cluster for the wave operator is

$$\hat{k} = \hat{\Omega}\hat{P}_0 = \{\exp(\hat{S})\}\hat{P}_0 \tag{3.67}$$

where the curly braces indicate that the cluster operator $\hat{S}$[20] is normal ordered and $\hat{P}_0$ projects onto all states in the Fock space model space. The cluster operator in the Fock-space coupled-cluster method has the same expansion as shown in Eq. 3.15, however, a different form

$$\hat{S}_N = \frac{1}{(n!)^2} \sum_{\bar{\bar{a}},\bar{\bar{b}},\ldots\bar{\bar{i}},\bar{\bar{j}},\ldots}{}' s^{\bar{\bar{a}},\bar{\bar{b}},\ldots}_{\bar{\bar{i}},\bar{\bar{j}},\ldots} \bar{\bar{a}}^\dagger \bar{\bar{b}}^\dagger \ldots \bar{\bar{j}}^\dagger \bar{\bar{i}}^\dagger \tag{3.68}$$

where the summation runs not just over the hole and particle $(i, j, \ldots, a, a \ldots)$ indices separated but also includes the active holes. The prime, however, indicates that no excitation within the model space is taking place. Furthermore, as it is seen from Figure 3.1, the double barred indices overlap within the valence which could lead to possible contraction amongst the cluster operators i.e. a non-commutative formalism. This, however, has

[20] In the Fock-space coupled-cluster method the cluster operator is normally designated with $\hat{S}$.

been resolved by using a normal-ordered ansatz for the cluster operator [112] where all annihilation operators appear to the right of the creation operators with respect to the Fermi vacuum.

To get to a set of working equations we will separate the projection operator $\hat{P}_0$ into sectors depending on the number of valence indices (n)

$$\hat{P}_0 = \hat{P}_0^{(0)} + \hat{P}_0^{(1)} + \hat{P}_0^{(2)} + \ldots \hat{P}_0^{(N_v)}. \tag{3.69}$$

Each of these n-valence sectors can be further divided depending on the number of particle k and hole l valence indices

$$\hat{P}_0^{(n)} = \sum_{k=0}^{n} \sum_{l=0}^{n-k} \hat{P}_0^{(k,l)} \tag{3.70}$$

and each $\hat{P}_0^{(k,l)}$ will then project onto a space where k particles and l holes have been created in the valence space. This same sector structure can also be applied to the cluster operator $\hat{S}$. For a truncated coupled cluster scheme at a given level n, the general structure of the cluster operator in this sector form then becomes

$$\hat{S}^{(n)} = \sum_{k=0}^{n} \sum_{l=0}^{n-k} \hat{S}^{(k,l)} = \sum_{k=0}^{n} \sum_{l=0}^{n-k} \Big(\sum_{i=0}^{k} \sum_{j=0}^{l} \hat{S}^{(i,j)} \Big) \tag{3.71}$$

where it is noticed that the cluster operator has a part in all sectors up to n. We notice here that although the $(0,0)$ and $(1,1)$ sectors are different they belong to the same N electron Hilbert space and the $(1,1)$ sector contains in fact just the singly excited states in the model space of the $(0,0)$ sector. Likewise the $(2,2)$ sector will then comprised of the doubly excited states of the $(0,0)$ sector. There, furthermore, exists a hierarchical structure for the cluster operator

$$\hat{S}^{(p,q)} \hat{P}_0^{(i,j)} = 0 \qquad \forall \quad p > i \vee q > j. \tag{3.72}$$

The structure in Eq. 3.72 is quite evident since a cluster operator from the sector (p,q) will contain p annihilation operators in the active particle space and q creation operators in the active hole space. If the projection operator does not allow for enough annihilation or creation in a given active space, the contribution will be trivially zero as shown by Eq. 3.72. From Eq. 3.71 it can be seen that if the truncation of the cluster operator at n is smaller than the number of levels in the valence space N_v we will be working with an incomplete model space since we will then not consider sectors higher

than n. This also means that to reach higher sectors in Fock-space coupled cluster higher excitation levels from the cluster operator are needed. These are at the moment only implemented up to triples in the non-relativistic framework [110].

With the sector structure in place and using the intermediate normalization (see Eq. 3.56) and the wave operator ansatz in Eq. 3.67 we can write the Fock-space equations

$$\hat{H}\{\exp(\hat{S})\}\hat{P}_0 = \{\exp(\hat{S})\}\hat{P}_0\hat{H}^{eff}\hat{P}_0 \tag{3.73}$$

which has been written with a slight modification to the Bloch equation in 3.62

$$\hat{k}\hat{l}\hat{H}\hat{k} = \hat{H}\hat{k} \tag{3.74}$$

and in terms of the effective operator in Eq. 3.47. Written in terms of the sectors Eq. 3.73 can be written as

$$\hat{H}\{\exp(\hat{S}^{(k,l)})\}\hat{P}_0^{(k,l)} = \{\exp(\hat{S}^{(k,l)})\}\hat{P}_0^{(k,l)}\hat{H}^{eff}\hat{P}_0^{(k,l)} \tag{3.75}$$

where $\hat{S}^{(k,l)}$ is defined in Eq. 3.71 and $\hat{P}_0^{(k,l)}$ in Eq. 3.70. The Bloch equation for the Fock-space coupled-cluster equations in Eq. 3.75 is solved by projecting onto the complementary space

$$\hat{Q}_0^{(k,l)}\hat{H}\{\exp(\hat{S}^{(k,l)})\}\hat{P}_0^{(k,l)} = \hat{Q}_0^{(k,l)}\{\exp(\hat{S}^{(k,l)})\}\hat{P}_0^{(k,l)}\hat{H}^{eff}\hat{P}_0^{(k,l)}. \tag{3.76}$$

Normally the $(0,0)$ sector is separated off by a similarity transformation. This, however, is not done here.

Looking a little closer at the equations to be solved in Eq. 3.76 it becomes evident that certain sectors are under-determined, i.e. the number of amplitudes is greater than the number of equations. An example of this is the $(1,1)$ sector

$$\langle\phi_\iota^{\bar{a}}|\hat{S}|\phi_\iota^{\alpha}\rangle = \langle\phi_\iota^{\bar{a}}|\sum_{\bar{b}\beta} s_\beta^{\bar{b}}\bar{b}^\dagger\beta + \sum_{\bar{b}\beta\kappa} s_{\beta\kappa}^{\bar{b}\kappa}\bar{b}^\dagger\kappa^\dagger\kappa\beta|\phi_\iota^{\alpha}\rangle = s_\alpha^{\bar{a}} + s_{\alpha\kappa}^{\bar{a}\kappa} \tag{3.77}$$

where it is seen that from one equation we get two undetermined amplitudes. To solve this problem it is noticed that the amplitude $s_\alpha^{\bar{a}}$ also appears in the lower $(1,0)$ sector

$$\langle\phi^{\bar{a}}|\hat{S}|\phi^{\alpha}\rangle = \langle\phi^{\bar{a}}|\sum_{\bar{b}\beta} s_\beta^{\bar{b}}\bar{b}^\dagger\beta\hat{S}|\phi^{\alpha}\rangle = s_\alpha^{\bar{a}} \tag{3.78}$$

which is then used again in the higher sector in Eq. 3.77 so that the number of equations and amplitudes in the $(1,1)$ sector becomes identical. The $s_\alpha^{\bar{a}}$ amplitudes in Eq. 3.77 is

then referred to as spectator amplitudes since they are not optimized in that equation. By solving the Fock-space equations in this way one arrives at the subsystem embedding scheme [113]. In the subsystem embedding scheme all sectors are solved individually and all sectors lying lower than the (n, m) sector must be solved before the (n, m) sector. By solving the Fock-space coupled-cluster equation sector by sector we get an unrelaxed set of equations where the influence on $s_{\alpha}^{\bar{a}}$ of taking in $s_{\alpha\nu}^{\bar{a}\nu}$ is neglected in the above example. For getting the influence on the amplitudes in the (1,0) sector ($s_{\alpha}^{\bar{a}}$) of including the (1,1) sector ($s_{\alpha\nu}^{\bar{a}\nu}$) one would have to solve all the Fock-space equations simultaneously. This simultaneous solution has, however, proven to be numerically more unstable than the sector-by-sector solution. The subsystem embedding scheme is, however, not without convergence problems and can be very difficult to converge on an entire potential energy surface. It has furthermore been very difficult to get to sectors beyond $k, l > 2$ due to convergence problems in lower sectors and because of the need to include higher excitations. To alleviate these problems the intermediate Hamiltonian approach has been put forward (results can be seen in [109, 111]) where a buffer space is introduced into the model space with an approximate interaction. To recover this approximate interaction the extrapolated Fock-space coupled cluster was put forward [114].

Besides the problems with convergence and reaching higher sectors, the orbital space used in all sectors is the same, meaning that the same orbital space will have to be able to describe not only neutral but also charged states from electron attachment and detachment (particles and holes in the valence). This means a very flexible basis set will have to be used since the differences between neutral and charged states can be significant. Hence a slower convergence with respect to basis set size could be expected. A second, but connected problem, is the subsystem embedding scheme where spectator amplitudes taken from other sectors appear in higher sectors. The results of the higher sectors then depend on how well the amplitudes in the lower sector have been determined. A propagation of errors though the sectors is then expected. An error which is expected to be closely connected to how well the basis set is able to describe the various neutral and charged sectors of Fock space. Reaching higher sectors therefore seems to be exceedingly difficult and it will be immensely difficult to extend the methods beyond the $k, l > 2$ sectors. A further problem to this extension of sectors is the need to include higher excitations where the scaling of the coupled-cluster method at some point also will become problematic. If

larger model spaces are considered along with higher excitations then the scaling factor, i.e. the number of times a calculation in a (k, l) sector have to be performed, will also prove to be a bottleneck of the method. This in particular if the mixed sector approach cannot be used and the starting sector and the sector of interest lie far apart.

Despite these concerns by the author about the Fock-space coupled-cluster method it is to date the most successful of the multireference coupled-cluster methods for both the ground and excited states. The applicability of the method at present state does not appear to be universal but on the systems where it can be used it is very accurate.

3.1.5 State-Selective Multireference Coupled Cluster

The state-selective multireference coupled-cluster method that will be focused on is the method suggested by Oliphant and Adamowicz [115, 116] in 1991. This method can be considered a special case of the more general generalized active space coupled-cluster method discussed in Section 5 and the publications [30, 68, 117]. The idea of the method is to retain some of the simplicity of the single-reference coupled-cluster method and try to avoid some of the difficulties described for the multireference coupled-cluster methods in Sections 3.1.3 and 3.1.4. The way this has been accomplished is very similar to how a multireference configuration interaction method could be formulated. While the multireference configuration interaction method would be a genuine multireference method, the state-selective multireference coupled-cluster method is not. The method is a pseudo multireference method since it is not invariant to the chosen Fermi vacuum. As already mentioned in Section 3.1.1.1 this method has received a great deal of attention in the non-relativistic framework where also general-order codes have been developed [3, 5, 6, 99]. The extension of this method[21] to the spin-free and fully relativistic framework has been the central theme in my Ph.D. work. With this method we have also been the first to publish fully relativistic coupled-cluster calculations with fully iterative triples and soon also quadruples and multireference calculations with fully iterative triples as can be seen in Section 9.2.

[21] Actually it is the more general generalized active space coupled-cluster method.

3.1.5.1 Formal Development of State-Selective Multireference Coupled-Cluster

The formal development of the state-selective multireference coupled-cluster method is like the similarity-transformed single-reference coupled-cluster method in 3.1.1.2. Hence the wave operator will then be the same as in Eq. 3.35, the truncation scheme will, however, not follow the scheme indicated in Eq. 3.15, where the truncation of the cluster operator follows a certain excitation level. It will instead include those higher excitations that would make it look like there existed several reference determinants all with a given level of truncation of the cluster operator.

To explain how the different truncation scheme of the cluster operator works we will have to introduce the some of the indices also used for the Fock-space coupled-cluster method in Section 3.1.4.1. From Figure 3.1 we will use the indices $\bar{i}, \bar{j}, \bar{k}, \bar{l}, \ldots$ and $\bar{a}, \bar{b}, \bar{c}, \bar{d}, \ldots$ for the inactive holes and particles, respectively. For the active holes and particles we will use $\iota, \kappa, \lambda \ldots$ and $\alpha, \beta, \gamma \ldots$, respectively. The combined set of active and inactive particles (holes) is symbolized by the letters $i, j, k, l, \ldots$ ($a, b, c, d, \ldots$) as shown in Section 3.1.1.2.

The derivation of the equations will be done in a way that illustrates the idea behind the method. The way presented is perhaps not the simplest but in the author's opinion more illustrative than other derivations and the connection to the Hilbert-space coupled-cluster method is clearer. The aim of the method is to create a formal model space but retain the simplicity of the single-reference coupled-cluster method. To formally create a method that resembles the Hilbert-space coupled-cluster method in Section 3.1.3 but without making a Fermi vacuum for each individual state in the model space. Hence to get away from the Hilbert space ansatz for the wave operator in Eq. 3.54 where every reference has its own wave operator to one common wave operator for all states in the model space. This means having just one Fermi vacuum like Fock-space coupled-cluster method but wanting to stay within the Hilbert space. For this one can pursue a variant of the single-reference coupled-cluster method where the cluster operator is partitioned into an internal and an external part

$$\hat{T} = \hat{T}^{int} + \hat{T}^{ext}. \tag{3.79}$$

The internal part $\hat{T}^{int}$ will then only contain valence indices (see Figure 3.1) while the external $\hat{T}^{ext}$ will contain at least one inactive hole or particle index. To show how we

from the division of the cluster operator in Eq. 3.79 immediately get to a multireference like method we can write

$$|\phi\rangle = \exp(\hat{T})|\phi_0\rangle = \exp(\hat{T}^{int} + \hat{T}^{ext})|\phi_0\rangle = \exp(\hat{T}^{ext})\exp(\hat{T}^{int})|\phi_0\rangle = \exp(\hat{T}^{ext})|\phi_0^{int}\rangle \tag{3.80}$$

where it is seen $\exp(\hat{T}^{int})$ generates the formal reference $|\phi_0^{int}\rangle$ and a single cluster operator $\exp(\hat{T}^{ext})$ is used for the entire formal model space. $\exp(\hat{T}^{ext})$ in this picture then works as a formal wave operator. In the separation of $\hat{T}^{int}$ and $\hat{T}^{ext}$ we have used that the cluster operator for the single-reference coupled cluster is commutative (see Eq. 3.5) since it is a pure excitation operator. With the same wave operator as in the single-reference coupled-cluster method[22] we will then have commutation between $\hat{T}^{int}$ and $\hat{T}^{ext}$

$$[\hat{T}^{int}, \hat{T}^{ext}] = 0. \tag{3.81}$$

The exact form of the internal cluster operator will be

$$\hat{T}^{int} = \sum_{p=1}^{M} \hat{T}_p^{int} = \hat{T}_1^{int} + \hat{T}_2^{int} + \cdots + \hat{T}_M^{int} \qquad M = min(N_{ah}, N_{ap}) \tag{3.82}$$

which is the part that creates all possible excitations inside the valence space. N_{ah} and N_{ap} are here the number of active holes and particles, respectively. The $\hat{T}^{int}$ in Eq. 3.82 will in the state-selective multireference coupled-cluster method not be truncated but used in its entirety. In the generalized active space coupled-cluster method discussed in Section 5 and as shown in Section 8.2 truncations of $\hat{T}^{int}$ makes it possible to create the CC(n_m) methods [118].

As an example, the $\hat{T}_2^{int}$ operator will then be

$$\hat{T}_2^{int} = \frac{1}{4}\sum_{\iota\kappa,\alpha\beta}^{N_{ah},N_{ap}} \hat{T}_{\iota\kappa}^{\alpha\beta} = \frac{1}{4}\sum_{\iota\kappa,\alpha\beta}^{N_{ah},N_{ap}} t_{\iota\kappa}^{\alpha\beta}\hat{\tau}_{\iota\kappa}^{\alpha\beta} \tag{3.83}$$

in terms of amplitude $t_{\iota\kappa}^{\alpha\beta}$ multiplied by second quantized excitation operator $\hat{\tau}_{\iota\kappa}^{\alpha\beta}$. The external cluster operator can then be written as

$$\hat{T}^{ext} = \hat{T} - \hat{T}^{int} \tag{3.84}$$

which contains the remaining excitations. We notice here that, unlike in the Hilbert-space coupled-cluster method, we here have a formal wave operator that also contains

[22]Notice the wave operator is the same as the single-reference coupled-cluster method while the formal wave operator is $\exp(\hat{T}^{ext})$.

excitations in the valence space though always at least one inactive index, but still only one for all formal references. The expansion of the external cluster operator is written a little differently

$$\hat{T}^{ext} = \sum_{p=1}^{N_{ah}+N_{ih}} \hat{T}_p^{ext} = \hat{T}_1^{ext} + \hat{T}_2^{ext} + \cdots + \hat{T}_{N_{ah}+N_{ih}}^{ext} \tag{3.85}$$

where N_{ih} is the number of inactive holes[23] and the excitation level x of $\hat{T}_x^{ext}$ refers to the maximum number of either inactive hole or particle indices (see Figure 3.1). By choosing to divide the external cluster operator in a way that the index x no longer refers to the excitation level but to the maximum number of either inactive hole or particle indices, the operator $\hat{T}_x^{ext}$ then becomes a sum of excitation operators of different excitation level. At a given level of truncation M we then do not get the equality in Eq. 3.79

$$\hat{T}_M \neq \hat{T}_M^{int} + \hat{T}_M^{ext} \tag{3.86}$$

since $\hat{T}_M^{int}$ is not truncated and therefore always written as $\hat{T}^{int}$ which can contain excitations greater than M. The external cluster operator $\hat{T}_M^{ext}$ will contain excitations greater than M, namely the sum of the internal and external excitations. The external excitation operator can then be written as

$$\hat{\tau}^{ext} = (1 + \hat{\tau}^{int})\hat{\tau}^{in} = (1 + \hat{\tau}^{int}) \sum_{p}^{N_{ah}+N_{ih}} \hat{\tau}_p^{in} \tag{3.87}$$

where the inactive excitation operator $\hat{\tau}^{in}$ is a sum of two excitation operators

$$\hat{\tau}^{in} = \hat{\tau}_{ih}^{ap,ip} + \hat{\tau}_{ah}^{ip} \tag{3.88}$$

which all contain at least one inactive index. Here ap and ip denote the number of active and inactive particle indices, respectively. We see with $\hat{T}_x^{ext}$ written this way we get a complete parametrization of all possible configurations. The truncation of the cluster operator in the state-selective multireference coupled-cluster method is then truncated in $\hat{T}^{ext}$. A truncation at $\hat{T}_2^{ext}$ would then give a MRCCSD calculation. The amplitude for the external cluster operator can then more easily be found when the external excitation operator in Eq. 3.87 is written out in it entirety.

With this division of the cluster operator from the single-reference coupled-cluster method we have achieved to formulate a formal reference with a formal wave operator

[23] We notice $N_{ah} + N_{ih}$ is equal to the total number of holes i.e. electrons.

Figure 3.2: Example of a MRCCSD space for the state-selective multireference coupled-cluster method

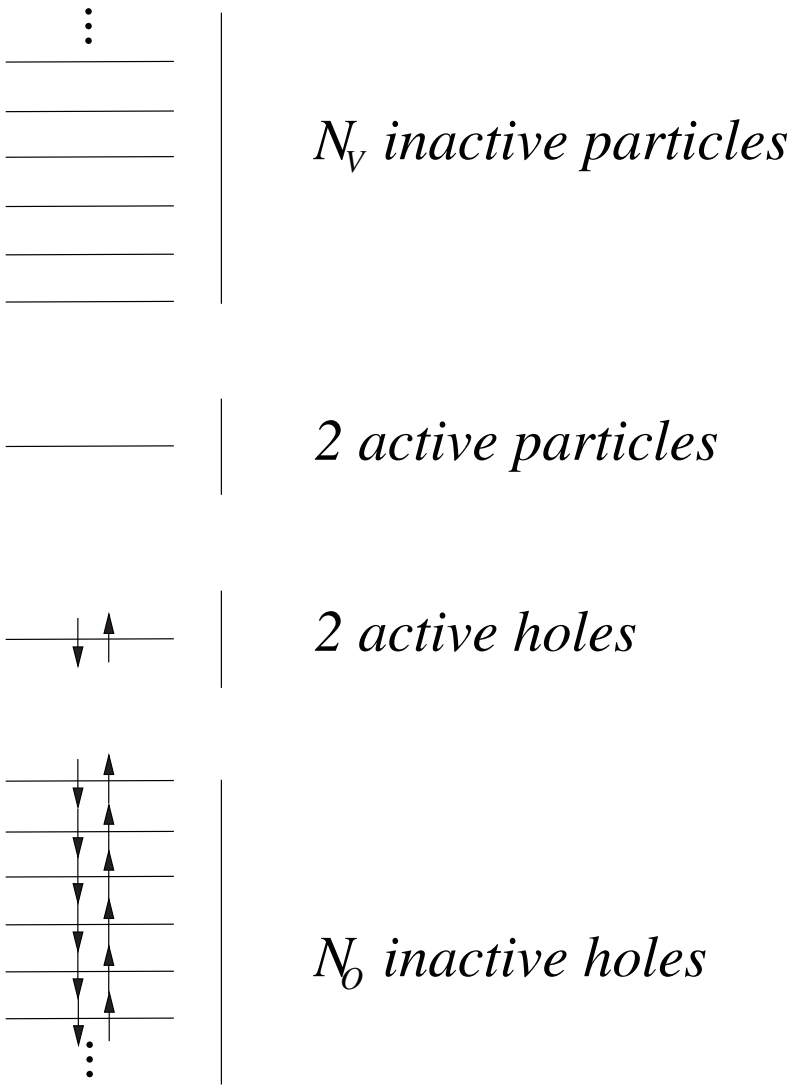

which resembles a multireference coupled-cluster method. The difference is that the formal wave operator now contains excitations inside the formal model space and that in the truncation of this higher internal excitations combined with external are present since the truncation is in the maximal number of either inactive hole or particle indices[24].

To illustrate how the final cluster operator will look like in a state-selective multireference coupled-cluster calculation, I will give a small example of a MRCCSD calculation. In this example we will have N_o inactive holes, two active holes, two active particles and N_v number of inactive particles as illustrated in Figure 3.2.

The internal cluster operator is seen to have up to double excitations since the minimum of active holes or particles is two (see Eq. 3.82). The double excitations will

[24]Total number of inactive indices can be larger, the individual not.

take the same form as shown in Eq. 3.83 which along with the single excitations will give

$$\hat{T}^{int} = \hat{T}_1^{int} + \hat{T}_2^{int} = \sum_{\iota,\alpha} \hat{T}_\iota^\alpha + \frac{1}{4} \sum_{\iota\kappa,\alpha\beta} \hat{T}_{\iota\kappa}^{\alpha\beta} \tag{3.89}$$

Finding the external excitation operator we first use Eq. 3.88 to find the inactive excitation operator $\hat{\tau}^{in}$. We here see that the maximum number of inactive indices is two since the truncation is done at the singles doubles level and the number of active particles is also two. The inactive excitation operator then becomes

$$\hat{\tau}^{in} = \hat{\tau}_1^{in} + \hat{\tau}_2^{in} \tag{3.90}$$

where $\hat{\tau}_1^{in}$ is

$$\hat{\tau}_1^{in} = \sum_{\bar{i},\alpha} \hat{\tau}_{\bar{i}}^\alpha + \sum_{\bar{i},\bar{a}} \hat{\tau}_{\bar{i}}^{\bar{a}} + \sum_{\iota,\bar{a}} \hat{\tau}_\iota^{\bar{a}} = \sum_{\bar{i},a} \hat{\tau}_{\bar{i}}^a + \sum_{\iota,\bar{a}} \hat{\tau}_\iota^{\bar{a}} \tag{3.91}$$

and $\hat{\tau}_2^{in}$

$$\hat{\tau}_2^{in} = \frac{1}{4} \sum_{\bar{i}\bar{j},\alpha\beta} \hat{\tau}_{\bar{i}\bar{j}}^{\alpha\beta} + \frac{1}{2} \sum_{\bar{i}\bar{j},\alpha\bar{a}} \hat{\tau}_{\bar{i}\bar{j}}^{\alpha\bar{a}} + \frac{1}{4} \sum_{\bar{i}\bar{j},\bar{a}\bar{b}} \hat{\tau}_{\bar{i}\bar{j}}^{\bar{a}\bar{b}} + \frac{1}{4} \sum_{\iota\kappa,\bar{a}\bar{b}} \hat{\tau}_{\iota\kappa}^{\bar{a}\bar{b}} = \frac{1}{4} \sum_{\bar{i}\bar{j},ab} \hat{\tau}_{\bar{i}\bar{j}}^{ab} + \frac{1}{4} \sum_{\iota\kappa,\bar{a}\bar{b}} \hat{\tau}_{\iota\kappa}^{\bar{a}\bar{b}} \tag{3.92}$$

where it has been possible to combine some of the indices due to the fact that the internal excitation level equals the external. Building the external excitation operator

$$\hat{\tau}^{ext} = (1 + \hat{\tau}_1^{int} + \hat{\tau}_2^{int})(\hat{\tau}_1^{in} + \hat{\tau}_2^{in}) \tag{3.93}$$

we will collect these in parts of excitations from the reference determinant. We see that in this case we will have a maximum of fourfold excitations

$$\hat{\tau}_1^{ext} = \hat{\tau}_1^{in} \tag{3.94}$$

$$\hat{\tau}_2^{ext} = \hat{\tau}_2^{in} + \hat{\tau}_1^{int}\hat{\tau}_1^{in} \tag{3.95}$$

$$\hat{\tau}_3^{ext} = \hat{\tau}_1^{int}\hat{\tau}_2^{in} + \hat{\tau}_2^{int}\hat{\tau}_1^{in} \tag{3.96}$$

$$\hat{\tau}_4^{ext} = \hat{\tau}_2^{int}\hat{\tau}_2^{in} \tag{3.97}$$

where all excitations higher than two are made up of products of the inactive and internal excitations. Knowing the external excitation operator, the amplitudes for this can then also be written down. I will here just show one example of this for the double excitation of Eq. 3.95

$$\hat{T}_2^{ext} = \frac{1}{4} \sum_{\bar{i}\bar{j},ab} \hat{T}_{\bar{i}\bar{j}}^{ab} + \frac{1}{4} \sum_{\iota\kappa,\bar{a}\bar{b}} \hat{T}_{\iota\kappa}^{\bar{a}\bar{b}} + \sum_{\bar{i}\iota,\alpha a} \hat{T}_{\bar{i}\iota}^{\alpha a} + \frac{1}{2} \sum_{\iota\kappa,\alpha\bar{a}} \hat{T}_{\iota\kappa}^{\alpha\bar{a}} \tag{3.98}$$

where we notice that the only thing missing in the external doubles is the internal doubles excitations. Adding the internal and external cluster operator we then find the cluster operator to be

$$\hat{T} = \hat{T}_1 + \hat{T}_2 + \hat{T}^{\alpha\beta\bar{a}}_{\iota\kappa\bar{i}} + \hat{T}^{\alpha\bar{a}\bar{b}}_{\iota\kappa\bar{i}} + \hat{T}^{\alpha\beta\bar{a}}_{\iota\bar{i}\bar{j}} + \hat{T}^{\alpha\bar{a}\bar{b}}_{\iota\bar{i}\bar{j}} + \hat{T}^{\alpha\beta\bar{a}\bar{b}}_{\iota\kappa\bar{i}\bar{j}} \tag{3.99}$$

where we notice that we have an additional term ($\hat{T}^{\alpha\bar{a}\bar{b}}_{\iota\bar{i}\bar{j}}$) compared to the original papers from Oliphant and Adamowicz [115,116] which is because they only considered two reference determinants. The observation made in Eq. 3.99 that the complete $\hat{T}_1$ and $\hat{T}_2$ appear in the final expression for the cluster operator is a general observation for a MRCCSD. All higher cluster operators will then also only appear as products of internal and external excitations where the maximum excitation level will be the sum of the maximal internal and external level. These higher terms in the cluster operator will then also appear in the projection manifold (see Eq. 3.17) to give a fully determined set of equations.

The terms in Eq. 3.99 do have a meaningful explanation in a formal multireference coupled-cluster formalism and do show many similarities to the genuine multireference coupled-cluster methods, here in particular the Hilbert-space coupled-cluster method. $\hat{T}^{\alpha\beta\bar{a}}_{\iota\kappa\bar{i}}$ and $\hat{T}^{\alpha\beta\bar{a}\bar{b}}_{\iota\kappa\bar{i}\bar{j}}$ is the orbital relaxation and correlation of a doubly excited determinant from the reference determinant. $\hat{T}^{\alpha\bar{a}\bar{b}}_{\iota\bar{i}\bar{j}}$ is the correlation of a singly excited determinant. The orbital relaxation of this is in $\hat{T}_2$. The two remaining terms describe the cross correlation and relaxation of the inactive holes and the valence. The relation to multireference configuration interaction is also immediately noted from Eq. 3.99 where we see that the multireference configuration interaction wave function will just be $1 + \hat{T}$ where the amplitudes have to be replaced with the CI coefficients.

The extension of the state-selective multireference coupled-cluster method presented here to a fully relativistic framework all happens by extending the cluster operator to include flipping of the Kramers projection as shown in Section 2.2.2. The formalism itself does not change, so conclusions drawn at the non-relativistic level are therefore expected to carry over to the fully relativistic framework. The method has shown itself as numerically stable for both ground and excited states [118–121]. We here notice that unlike the genuine multireference coupled-cluster methods either a linear response or equation-of-motion module must be used to get the excited states since the method, like the single-reference coupled-cluster method, is a ground-state method. The obvious drawback of the method is the lack of invariance to the Fermi vacuum which means the

results will be dependent of which reference determinant is chosen for a coupled-cluster expansion. This lack of Fermi invariance leads to symmetry breaking of the wave function. In the non-relativistic framework it has been shown that this can lead to larger overlaps between different states[25] and spin projection errors compared to other multireference coupled cluster methods [122]. A yet unaddressed problem connected with the equation length will be dealt with in Section 7.1 where it will be shown that this can be problematic, in particular in the relativistic case.

[25]Unlike MRCI, MRCC or CC will not necessarily give exactly orthogonal states except in the limit of FCC. The overlap is just a measure of the accuracy of the wave function.

Chapter 4

DIRAC Program Package

This chapter is primarily meant to give non-experts a little bit of an insight into what goes into making a new module in a program package and how the modules therein are linked together. The second function of this chapter is also to document what other modules may have been used and to which purpose.

Before any correlation code can be used it will need one or more external programs/modules to calculate the starting conditions for the code since this is not present in a correlation code. This will typically be a program/module to do a Hartree-Fock calculation and subsequently an integral transformation step to deliver the needed integrals for the correlation code. Sometimes one may opt for a stand alone code with an interface to one or more programs that can deliver the needed information. This however is not the path chosen for the code presented in this work. This code has become a module, named ARDUCCA[1], in the larger quantum chemistry package DIRAC [57].

4.1 DIRAC

The DIRAC program computes molecular properties using relativistic quantum chemical methods. It is named after P. A. M. Dirac[2], the father of relativistic electronic structure theory. The DIRAC program code is distributed freely to academic researchers and can be obtained by contacting Hans Jørgen Aagaard Jensen. A new release for DIRAC2008 [57]

[1] AaRhus DÜsseldorf Coupled Cluster Algorithm

[2] P.A.M. DIRAC : Program for Atomic and Molecular Direct Iterative Relativistic All-electron Calculations

is now available. The program consists of many modules bundled together in one program package which can be used as one or as stand-alone modules. The modules used in this thesis are the Dirac-Hartree-Fock module [123, 124], MOLTRA - Integral transformation module, RELCCSD [74,125] - Coupled cluster module and the LUCIAREL [71,72] module which is a GAS CI module. A variety of different Hamiltonians is also available and has been used in this work like the Dirac-Coulomb- , a spin-free- [64] and the Lévy-Leblond [33] Hamiltonian. All these and my usage of them will be very briefly described in the subsequent subsections. For a more complete list of modules both released and unreleased, their documentation plus contact informations the reader is encouraged to visit the DIRAC wiki page at http://wiki.chem.vu.nl/dirac/index.php/Dirac_Program .

This program suite has served as the basis for the further development of the non-relativistic GAS coupled cluster code from Jeppe Olsen [99]. The developments done in this thesis is therefore now a module in DIRAC and will at some point in the future be released for users. At the moment, however, the program resides on the developers version until a final version can be released.

4.2 The Hamiltonians

To elucidate various relativistic effects like the ones shown in Section 9.3 a set of different Hamiltonians has been employed. This has been done by performing the same type of correlation calculation but employing different types of Hamiltonians.

4.2.1 The Dirac-Coulomb Hamiltonian

The Dirac-Coulomb Hamiltonian (see also Sections 2.1.2 and 2.2.1.4) is the standard Hamiltonian in relativistic electronic structure theory and is a 4-component Hamiltonian containing the most important relativistic effects. In this Hamiltonian the electron-electron interaction is approximated by the usual Coulomb interaction known from non-relativistic quantum mechanics. Additionally, the Born-Oppenheimer approximation is also used so the electron-nuclei interaction is then just a static field. The Dirac-Coulomb Hamiltonian, however, contains the scalar relativistic effects like the Darwin and the mass-velocity term but also spin-orbit coupling in the form of the spin-same-orbit term. For

a more correct electron-electron interaction the Dirac-Coulomb-Breit Hamiltonian would be the next step where an additional current-current interaction and a gauge term [7] is added to the electron-electron interaction. At the moment only the current-current interaction, also known as the Gaunt interaction [61], can be used at the DCHF level. Work is being done to also have transformed integrals of this. A correlation code for the Dirac-Coulomb Hamiltonian has been the final goal of this thesis and will be presented in Sections 9.2 and 9.1. These correlation codes are, however, more complicated and cumbersome than the ones presented for the spin-free- and the Lévy-Leblond Hamiltonian. The additional complication stems from the spin-orbit contribution which requires much additional work in implementing but also in the use of the codes. The inherent problem is described in further details in Sections 7 and 2.2.1.

4.2.2 The Spin-Free Hamiltonian

The spin-free Hamiltonian in `DIRAC` is the one presented by Dyall in [64]. The separation of the Hamiltonian into a spin-free and a spin-dependent part is not unique [65] but there does not appear to be any significant differences between the different ways of partitioning the Hamiltonian [66]. In Dyall's formalism the spin-dependent part is neglected keeping just the scalar relativistic part and neglecting the spin-orbit part. In practice this has the advantage that spin and space can again be separated just like in the non-relativistic framework. This means, with an interface, a non-relativistic correlation code can used which is what has been described in Sections 6.1 and 9.3. In the correlation step, for the coupled cluster, this has the advantage that the cluster operator no longer flips the Kramers projection as shown in Sections 9.1, 9.2 and 7, reducing the number of amplitudes and connections. The disadvantage of this Hamiltonian, is of course, that it cannot be used on systems where the spin-orbit contribution becomes significant. It can, however, be employed for many systems used in the field of cold and ultra-cold molecules with very good accuracy. In these systems the electronic ground state typically exhibits 0^+ symmetry and is well separated from the electronically excited states at the equilibrium geometry. Hence, the inaccuracy of the correlation treatment and basis set deficiencies by far outweighs spin-orbit effects. The spin-orbit contribution can therefore be estimated by doing a CCSD using the Dirac-Coulomb Hamiltonian and then adding this correction to the spin-free curve since the changes introduced by spin-orbit interaction in these systems

will be almost independent of basis-set size and correlation level as seen in Sections 9.1 and 9.3.

4.2.3 The Lévy-Leblond Hamiltonian

The Lévy-Leblond Hamiltonian [33] is the non-relativistic limit of the Dirac-Coulomb Hamiltonian which then includes spin but not spin-orbit or any other relativistic contributions. With the interface for the spin-free Hamiltonian, the Lévy-Leblond Hamiltonian can immediately also be used. This Hamiltonian has only been used when trying to assess scalar relativistic contributions as shown in Section 9.3.

With these three Hamiltonians it is possible to assess the scalar relativistic and spin-orbit contributions like shown in Section 9.3. These contributions are however not completely decoupled, like a perturbation, since the relativistic effects are optimized along with all other effects. Using each Hamiltonian however does give a very good insight into the different contributions.

4.3 The Modules

The modules that is briefly presented in the following sections are just a few of the modules in DIRAC but these are the ones that have been used in this thesis and not programmed by the author. The Dirac-Fock and the integral transformation module MOLTRA have of course been used extensively since these are the two first steps before any correlation calculation can begin.

4.3.1 Dirac-Fock

The Dirac-Fock [124] has always been the first step done in any calculation presented in this thesis and corresponds to the Hartree-Fock step in a non-relativistic framework. This is also the only part of the code that has four-components like the Dirac-equation and usually also the only step where all electrons and virtuals are treated. Since the Dirac-Fock operator is not bounded from below the electronic ground state can thus be viewed as an excited state in the spectrum of the Dirac-Coulomb Hamiltonian. The usual

minimization procedure from the variational principle cannot be applied and is replaced by a minmax procedure [126].

4.3.2 MOLTRA

This module transforms integrals from the scalar AO basis to integrals in the molecular spinor basis and thereby provides the integrals for the correlation code. This is a rather time consuming step due to heavy I/O with writing both the transformed and half-transformed integrals to disc. This step is largely increased for the 4-component methods, due to the very large basis set needed for the small component which in turn is needed for kinetic balance of the basis set (see Section 2.3.1).

4.3.3 RELCCSD

RELCCSD [74,125] is a coupled-cluster module capable of performing CCSD and CCSD(T) calculations using all the different types of Hamiltonians described in 4.2. Since the matrix elements are here explicitly programmed it is therefore faster in doing CCSD calculations than the more general order code programmed by the author. It is, however, limited to this and the CCSD(T) calculations. This module has been very useful for the larger LiCs calculations presented in Section 9.6 but also for debugging of the general-order coupled-cluster code.

4.3.4 LUCIAREL

LUCIAREL [71, 72] is a general-order CI code which also includes the GAS concept as shown in Sections 9.4 and 9.5. This is an adaptation of the non-relativistic code by Olsen [127] to the relativistic framework. This code is the forerunner to the first relativistic version of the GAS coupled-cluster (see Sections 6.2 and 9.1) since the latter is driven by a modified version of this CI-code done by the author. The code has also been used for comparisons of CI and CC calculations like those shown in Section 9.1 and for applications on molecules used in the ultra-cold regime like RbYb and $(RbBa)^+$ as shown in Sections 9.4 and 9.5, respectively.

Chapter 5

Concepts of the Codes

With a general code capable of higher excitations a host of new concepts needs to be introduced. This chapter will mainly focus on introducing these. These concepts were first introduced[1] for the non-relativistic general-order Configuration Interaction (CI) program LUCIA [127] by Jeppe Olsen. A multireference configuration interaction (MRCI) and a state selective multireference coupled-cluster method can be formulated in the same framework which can be seen by the close relation between these methods as shown in Section 3.1.5. The concepts from the generalized active space CI can then be taken over to the generalized active space coupled-cluster method.

5.1 Concepts in ARDUCCA

The concepts of the Generalized Active Space (GAS), excitation class formalism, string based operators and the evaluation of these are independent of the code being non-relativistic, spin-free or fully relativistic. The only things changing between these three are the number of integrals and the number of classes rather than the concept. They will therefore be introduced here first since this is a common integral part of all the codes presented in Section 6.

[1] In these codes

5.1.1 Generalized Active Space (GAS)

The standard two-fold partitioning of the spinor space into occupied unoccupied parts is not sufficient to define, for example, the state-selective multireference expansions originally suggested by Adamowicz [115, 116] and shown in Section 6.3. One of the possible strategies for obtaining more general expansions functions is the Generalized Active Space (GAS) approach which has been developed both for CI and CC methods. In the GAS approach, the spinor space is first divided into a number of subspaces. This is a generalization of the more familiar Complete Active Space (CAS) and Restricted Active Space (RAS) approaches which allows for completely free choice of subspaces and excitations between these. This allows for complex and physically motivated truncation schemes of the cluster operator like the CC(n_m) [118] presented in Section 8.2 and variations of this like the ones shown for the GASCI in Sections 9.4 and 9.5.

In the current context of coupled-cluster expansions with commuting excitation operators, the subspaces are required to contain only occupied or virtual Kramers pairs. To exploit time reversal symmetry and restrictions, it is in the following further assumed that each subspace consists of pairs of barred and unbarred spinors. An example of such a partitioning of the spinor space is illustrated in Figure 5.1 where occupied and unoccupied spinor spaces are divided into two subspaces each.

Excitations from the occupied to the unoccupied spinor spaces are next specified, and a set of commuting excitation operators defining the CC expansion is thereby defined. The corresponding coupled-cluster equations will be manifestly size-extensive provided the excitation manifold is closed under deexcitation. An excitation manifold is closed under deexcitation if for any pair of excitation operators $\hat{\mathcal{O}}_1, \hat{\mathcal{O}}_2$ there is another excitation operator $\hat{\mathcal{O}}_3$ in the manifold such that $\hat{\mathcal{O}}_1^\dagger \hat{\mathcal{O}}_2 |HF\rangle = \hat{\mathcal{O}}_3 |HF\rangle$ [67].

The GAS is a very useful concept which can help to reduce the computational cost and still make very accurate calculations [5, 118] by selecting the Kramers pair subspaces so that the most important amplitudes are included. Due to the large flexibility it can, however, be difficult to make a direct comparison to the regular CC hierarchy without larger comparative studies. Important special cases the of GAS CC expansions are the state-selective multireference coupled-cluster method [115, 116] and the $CC(n_m)$ approach [118], see Sections 3.1.5 and 8.2, respectively. Other approaches of the GAS concept have

Figure 5.1: Example of division of occupied and unoccupied Kramers pairs into subspaces for the generalized active space coupled-cluster method

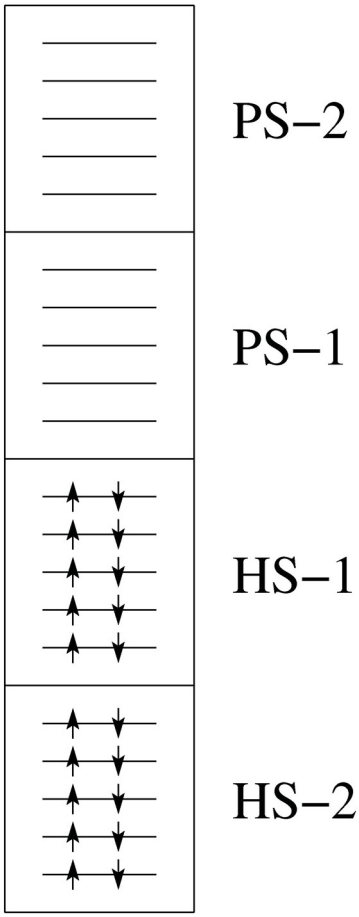

also been in use for the GAS CI codes and are presented in Sections 9.4 and 9.5.

5.1.2 Excitation Class Formalism and String Based Operators

In this section we will try to make the connection between the main operator classes and the generalized active space. The aim will be to show how the main operator classes can be divided into strings or classes when the orbital space is divided. This is the final division and the strings/classes are the entities programmed in the code and which drive it. The entries in these strings represent the number of second-quantized operators in a given generalized active space and will be explained in greater detail below.

To illustrate how a main operator class splits into several classes we will start out by the simplest example possible, namely the division of the Kramers pair space into two Kramers pair subspaces with the $\hat{O}_{1,0,1}$ main operator class. When dividing the Kramers

pair space into Kramers pair subspaces we see we will need to define another operator class since the sum over the indices for the main operator class will be restricted. First we will therefore examine what happens to a main operator class when the Kramers pair space is divided into two Kramers pair subspaces. We will here focus on the operator since the integral or amplitude follows from the operator due to the indexing of the amplitude or integral being the same. Therefore omitting the integral for the $\hat{O}_{1,0,1}$ main operator class we see that by dividing our Kramers pairs into occupied and virtuals the $\hat{O}_{1,0,1}$ main operator class will split into four terms

$$\sum_{p,q}^{N} a_p^\dagger a_q = \sum_{p}^{m}\sum_{q}^{m} a_p^\dagger a_q + \sum_{p>m}^{N}\sum_{q>m}^{N} a_p^\dagger a_q + \sum_{p}^{m}\sum_{q>m}^{N} a_p^\dagger a_q + \sum_{p>m}^{N}\sum_{q}^{m} a_p^\dagger a_q \qquad N > m \quad (5.1)$$

where the first m spinors would be in the first subspace (occupied) and the remaining $N - m$ in the second subspace (virtual).

Before generalizing this splitting of the Kramers pairs into subspaces we see that from the first division into occupied and virtuals we can extract information like the down rank of a class and whether it is a hole or particle that will be contracted in the reduction of the class. This is shown for the $\hat{O}_{1,0,1}$ main operator class in Table 5.1. Knowing the down rank of a class it is immediately possible to find the minimum and maximum number of commutators in the Baker-Cambell-Hausdorff (BCH) expansion which is also shown for $\hat{O}_{1,0,1}$ in Table 5.1. The general rule is zero commutators for down rank zero and a minimum of one and maximum of two times the down rank for all other possible down ranks. Since, for a linked formalism, each commutator will reduce the down rank of the Hamiltonian a minimum of one half and a maximum of the down rank. This immediately helps to identify the number cluster operator classes there has to be looped over in Section 6.3. It should be noted that since the cluster operator is a pure excitation operator it will have a down rank of zero and therefore for the single division of Kramers pairs into occupied and virtuals will leave the main operator class and the class identical.

Table 5.1: The splitting of the main operator class $\hat{O}_{1,0,1}$ into classes when dividing the Kramers pair space into occupied m and virtuals $N-m$. The down rank and the number of holes or particles that needs to be contracted to reduce the rank to zero and the number of commutators needed for this is shown.

Operator	Rank	Hole	Particle	# Commutators
$\sum_{p}^{m}\sum_{q}^{m} a_p^\dagger a_q$	$\frac{1}{2}$	1	0	1
$\sum_{p>m}^{N}\sum_{q>m}^{N} a_p^\dagger a_q$	$\frac{1}{2}$	0	1	1
$\sum_{p}^{m}\sum_{q>m}^{N} a_p^\dagger a_q$	1	1	1	1-2
$\sum_{p>m}^{N}\sum_{q}^{m} a_p^\dagger a_q$	0	0	0	0

The operator classes will be written in the CAAB (creator alpha, creator beta, annihilator alpha, annihilator beta)[2] form which is a string of second-quantized operators which represents a given class. The length of such string will be the number of generalized active spaces multiplied by four ($N_{GAS} \times 4$), where N_{GAS} is the number of generalized active spaces and the entries denotes the number of second-quantized operators of a given type that will be in a given GAS. The CAAB form will for the $\hat{O}_{1,0,1}$, shown in Eq. 5.1, be written as

$$\sum_{p}^{m}\sum_{q}^{m} a_p^\dagger a_q + \sum_{p>m}^{N}\sum_{q>m}^{N} a_p^\dagger a_q + \sum_{p}^{m}\sum_{q>m}^{N} a_p^\dagger a_q + \sum_{p>m}^{N}\sum_{q}^{m} a_p^\dagger a_q \tag{5.2}$$

CA	1	0	0	1	1	0	0	1
CB	0	0	0	0	0	0	0	0
AA	1	0	0	1	0	1	1	0
AB	0	0	0	0	0	0	0	0

(5.3)

where in the line with CA is the number of unbarred (alpha) creation operators in a GAS, CB the number of barred (beta) creation operators and AA and AB the unbarred and barred annihilation operators. Above each string the corresponding algebraic expression

[2] In the fully relativistic case this will then be creator unbarred, creator barred, annihilator unbarred, annihilator barred.

is written to highlight the connection between these. We see that the indices have been dropped in the CAAB form so we can no longer for $\hat{O}_{N\geq 2}$ see which two indices belong to the same electron. This can be seen by writing the operator $\hat{O}_{2,0,2}$ in the CAAB form

$$\begin{array}{lcccccccccccccccc}
CA & 2 & 0 & 0 & 2 & 2 & 0 & 0 & 2 & 2 & 0 & 0 & 2 & 1 & 1 & 1 & 1 & 1 & 1 \\
CB & 0 & 0 & 0 & 0 & 0 & 0 & 0 & 0 & 0 & 0 & 0 & 0 & 0 & 0 & 0 & 0 & 0 & 0 \\
AA & 2 & 0 & 0 & 2 & 0 & 2 & 2 & 0 & 1 & 1 & 1 & 1 & 0 & 2 & 2 & 0 & 1 & 1 \\
AB & 0 & 0 & 0 & 0 & 0 & 0 & 0 & 0 & 0 & 0 & 0 & 0 & 0 & 0 & 0 & 0 & 0 & 0
\end{array} \tag{5.4}$$

where we find nine operators instead of the expected 16 from the sums in Eq. 5.1, which stems from dropping the connection to the indices and instead introducing a canonical ordering. The connection to Eq. 5.1 becomes apparent when writing the CAAB operator

$$\begin{array}{lcc}
CA & 2 & 0 \\
CB & 0 & 0 \\
AA & 1 & 1 \\
AB & 0 & 0
\end{array} \tag{5.5}$$

as the sums of two operators (here for the Hamiltonian)

$$\sum_{prs\leq m,q>m}^{m,N} a_p^\dagger a_r^\dagger a_s a_q + \sum_{pqr\leq m,s>m}^{m,N} a_p^\dagger a_r^\dagger a_s a_q \qquad N > m \tag{5.6}$$

where in the first term the index q belongs to the second GAS whereas in the second it is the index s. If the integral is included and the anti-commutation relationship of second-quantized operators is applied along with a renaming of indices, it is seen that the CAAB operator in Eq. 5.5 is equal to

$$\sum_{prq\leq m,s>m}^{m,N} ((pq|rs) - (ps|rq))a_p^\dagger a_r^\dagger a_s a_q \tag{5.7}$$

so the indices for the same electron can come in as an exchange integral. This does not happen to the cluster operator in the first division of spinors into occupied and virtuals since it is a deexcitation rank zero operator.

In the GAS formalism the Kramers pairs can be divided into any number of GASs. It is therefore of interest to know the number of operators in the CAAB form. This can

give information on code design and an easy comparison between relativistic and non-relativistic string-based methods. If there is a single overall excitation level in all GASs the number of classes in the CAAB form from a general main operator class can the be shown to be

$$N_{CAAB} = \begin{pmatrix} N_{GAS} + N^c - 1 \\ N_{GAS} - 1 \end{pmatrix} \times \begin{pmatrix} N_{GAS} + \bar{N}^c - 1 \\ N_{GAS} - 1 \end{pmatrix} \times \begin{pmatrix} N_{GAS} + N^a - 1 \\ N_{GAS} - 1 \end{pmatrix} \times \begin{pmatrix} N_{GAS} + \bar{N}^a - 1 \\ N_{GAS} - 1 \end{pmatrix} \tag{5.8}$$

where N_{CAAB} is the number of classes in the CAAB form, N_{GAS} the number of GASs and $N^c, \bar{N}^c, N^a, \bar{N}^a$ the number of unbarred and barred creation and annihilation operators, respectively, as defined in Eq. 2.36. These classes, written in the CAAB form, can then be written as

$$\hat{O}_{N,\Delta M_k,M_{ub}} = \sum_{2N_i=1}^{N_{GAS}} \hat{S}^{2N_i}_{N,\Delta M_k,M_{ub}} \quad x_1 \geq x_2 \geq \ldots \geq x_N \tag{5.9}$$

where $2N_i$ is the number of indices summed over in $(N^c, \bar{N}^c, N^a, \bar{N}^a)$ order and in all x_i (like N^c) every successive index inside x_i is smaller or equal to the one before. Taking the above example for $\hat{O}_{2,0,2}$ it can then be written as

$$\hat{O}_{2,0,2} = \sum_{a_1 a_2 c_1 c_2=1}^{N_{GAS}} \hat{S}^{a_1 a_2 c_1 c_2}_{2,0,2} \quad a_1 \geq a_2 \quad c_1 \geq c_2. \tag{5.10}$$

For higher operators like $\hat{O}_{4,2,1}$, the operator classes in the CAAB form can then also easily be found

$$\hat{O}_{4,2,1} = \sum_{a_1 a_2 a_3 b_1 c_1 c_2 d_1 d_2=1}^{N_{GAS}} \hat{S}^{a_1 a_2 a_3 b_1 c_1 c_2 d_1 d_2}_{4,2,1} \quad a_1 \geq a_2 \geq a_3 \quad c_1 \geq c_2 \quad d_1 \geq d_2 \tag{5.11}$$

which appear in a four-particle interaction. We have here for clarity named the indices (a_n, b_n, c_n, d_n) for the indices appearing in $(N^c, \bar{N}^c, N^a, \bar{N}^a)$. As it can be seen the number of classes of operators increases rapidly with N_{GAS} and the excitation level. To utilize the full capacity of the GAS concept it is, for the code design, therefore important to have a fast evaluation of which Hamiltonian operator class a given cluster operator class can be contracted with.

Since the cluster operator is a pure excitation operator it has a down rank of zero we can abridge the CAAB form shown in Eq. 5.9 to

$$\hat{T}_{N,\Delta M_k,M_{ub}} = \sum_{NC_i=N_{GO}+1}^{N_{GV}+N_{GO}} \sum_{NA_i=1}^{N_{GO}} \hat{T}^{NC_i+NA_i}_{N,\Delta M_k,M_{ub}} \quad x_1 \geq x_2 \geq \ldots \geq x_N x \tag{5.12}$$

where N_{GO} denotes the GASs with the occupied Kramers pairs and N_{GV} the virtual and the summation has been split into the number of creator indices NC_i and annihilator indices NA_i. With this restriction of the loops for the elementary operator, the number of cluster operators in the CAAB form is significantly lower than the general operator in the CAAB form for the same particle rank. This can be seen by comparing Eq. 5.8 with

$$N_{CAABT} = \left(\begin{array}{c} N_{GV} + N^c - 1 \\ N_{GV} - 1 \end{array} \right) \times \left(\begin{array}{c} N_{GV} + \bar{N}^c - 1 \\ N_{GV} - 1 \end{array} \right) \times \left(\begin{array}{c} N_{GO} + N^a - 1 \\ N_{GO} - 1 \end{array} \right) \times \left(\begin{array}{c} N_{GO} + \bar{N}^a - 1 \\ N_{GO} - 1 \end{array} \right) \tag{5.13}$$

since $N_{GAS} = N_{GV} + N_{GO}$. The cluster operator can, however, contain higher than double excitations and, as can be seen from Table 6.1, therefore also contain more classes than the Hamiltonian.

The GAS concept, however, also allows that a cluster operator $\hat{T}_n$ can be truncated in certain GASs which is needed to perform for instance a state-selective multireference coupled-cluster calculation. This, however, does not change the CAAB form in Eq. 5.12. Since such a truncation occurs in the main operator class form it does however put a restriction on the indices. Therefore the main operator class form for a truncated operator has to be extended with N_{GAS} indices to show the truncation of the sums. We will then write a truncated main cluster operator class as $\hat{T}^{N_{GAS}}_{N,\Delta M_k,M_{ub}}$ where the N_{GAS} indices denotes the maximum number of holes or particles in a given GAS (depending on occupied or virtual). These indices are written as $NGAS = (GAS1, GAS2, \ldots, GASN)$ and the restriction for the number of elementary operators in a given GASJ

$$(\sum_{o=1}^{N_i} \hat{o} \in GASJ) \leq NGAS(J) \tag{5.14}$$

where $\hat{o}$ is either a creation or annihilation operator of a CAAB operator and N_i the total number of these. The truncated main operator class will then get the following CAAB form

$$\hat{T}^{N_{GAS}}_{N,\Delta M_k,M_{ub}} = \sum_{NC_i=N_{GO}+1}^{N_{GV}+N_{GO}} \sum_{NA_i=1}^{N_{GO}} \hat{T}^{NC_i+NA_i,N_{GAS}}_{N,\Delta M_k,M_{ub}} \quad x_i \quad x_1 \geq x_2 \geq \ldots \geq x_N x \tag{5.15}$$

where the N_{GAS} indices give a restriction on the number of occupied or virtual indices in a given GAS.

The general scheme of dividing operators can then be summarized

$$\hat{O} \supseteq \hat{O}_N \supseteq \hat{O}_{N,\Delta M_k} \supsetneq \hat{O}_{N,\Delta M_k,M_{ub}} \supseteq \hat{S}^{2N_i}_{N,\Delta M_k,M_{ub}} \tag{5.16}$$

where every division forms a subset of operators from the previous. The approximations from the truncation in the regular hierarchy of the cluster operator $\hat{T}$ are done at the $\hat{O}$ level giving a sum of $\hat{T}_N$ operators. The ΔM_k truncation scheme is done at the operator division level $\hat{O}_{N,\Delta M_k}$ whereas the restriction from input is done at the main operator level $\hat{O}_{N,\Delta M_k,M_{ub}}$ which finally determines the classes and the structure of the CAAB operators $\hat{S}^{2N_i}_{N,\Delta M_k,M_{ub}}$.

Chapter 6

Computational Structure

In this chapter I will first start out by giving a documentation of the algorithm of the codes and what changes are needed for an adaptation to the relativistic framework. Further, three sections have been introduced to explain why the linked coupled-cluster formalism (see Section 3.1.1.3) is preferred in the CI-driven coupled-cluster code, a solution for a reduction of overhead in the commutator-based coupled-cluster and how the integral handling works. The second part of the chapter is devoted to the documentation of the input to both the spin-free and the fully relativistic codes.

Currently the ARDUCCA module is residing on a branch of the developers version of the DIRAC [57] program package. On this branch there exist three general order spin-free coupled-cluster programs and two fully relativistic programs. The spin-free coupled-cluster code works via an interface to the spin-free integrals. The inner workings of these codes will not be discussed here since this work originates from Jeppe Olsen [3, 99] and this discussion would furthermore be duplicated in the description of the fully relativistic codes. The fully relativistic codes will be discussed in greater detail in Sections 6.2 and 6.3 where the algorithm for two of the spin-free codes also will become evident.

6.1 Documentation of Spin-Free Coupled-Cluster Code

The implementation of the spin-free coupled-cluster codes is primarily a technical issue of writing an interface to fetch spin-free integrals from the `DIRAC` program. We have in Section 2.1.3 seen that Dyall's spin-free Hamiltonian has the same spin factorization

as a non-relativistic Hamiltonian and regular point group symmetry can be used. This means that at the correlated level the only difference in the Hamiltonian is the addition of one- and two-electron scalar relativistic integrals to the regular one- and two-electron integrals. At the correlated level there will then be no difference in the structure of the Hamiltonian and the cluster operator classes[1]. A non-relativistic code can therefore be interfaced directly by just fetching the new integrals. For the implementation of the spin-free coupled-cluster code a regular `DIRAC` input has been interfaced for the input and transfer of information on common blocks along with the appropriate integrals[2].

6.2 Documentation of CI-based Coupled-Cluster Code

The documentation of the CI-driven coupled-cluster code will follow the one also presented in [70] but will have some additional comments. As was seen in the input in Section 6.4 this type of coupled-cluster approach requires an extended vector and the reason for that will be shown in Section 6.2.1. Since this uses the CI-Hamiltonian which is not as compactly programmed as the CC-Hamiltonian in Eq. 2.59, some additional main operator classes are here present. The method can use the first two approximations shown in Section 8 but not the last since defining the mixed core-valence correlation approximation is not straight forward with two different set of cluster operators. This code is, however, the less efficient of the two and the mixed core-valence correlation approximation would therefore not be applicable anyway. The work with adding the non-relativistic code to the program and getting the external setup will not be described as is the change to double group symmetry and the adaptation to 64 bits systems[3].

The current implementation treats the real-valued and some of the complex-valued double groups (C_{2h}^*, C_2^*, and C_s^*). This means complex algebra has been added throughout the non-relativistic code. This is done by splitting all vectors into a real and an imaginary part and then handling these separately. The complex algebra is only used if the double point group belongs to the complex-valued double groups which was not the case previ-

[1] It will be the same main operator classes used.

[2] It is in fact an interface to the whole of the LUCIA code [127]. This means that in the spin-free case there is also a GAS CI code like the LUCITA module [128] included. The CI-driven coupled-cluster code is here using the ARDUCCA CI code.

[3] This is heavily inspired by the adaptation on the trunk performed by Stefan Knecht.

ously for the underlying CI code. The remaining groups, the so-called quaternion-matrix groups (C_i^* and C_1^*), require modifications in the configuration-interaction program [72] and are not implemented yet, see Section 2.2.3 for definition of the groups.

6.2.1 Implementation of the CI-based Coupled-Cluster Code

The essential quantity to be evaluated in the course of a coupled-cluster optimization is the coupled-cluster vector function Ω_μ for a given element μ of the excitation manifold:

$$\Omega_\mu = \left\langle \mu \left| e^{-\hat{T}} \hat{H} e^{\hat{T}} \right| \mathrm{Ref} \right\rangle \tag{6.1}$$

The cluster operators $\hat{T} = \sum_m \hat{T}_m$ are now generalized to the relativistic framework, which entails the possibility of flipping the Kramers projection along with the excitation as shown in Section 2.2.2.

The evaluation of the CC vector function proceeds in an analogous fashion as described in reference [3], where the CC vector function is obtained in four steps which are based on CI expansions and string manipulations. Although this formalism is rather inefficient, it allows the generation of a general relativistic CC code by reusing much of the code which has previously been developed for relativistic CI [72, 73]. Furthermore, the developed code may be used in calculations where only a small number of electrons is correlated, and provides a test code for the more advanced and efficient relativistic CC codes presented in Section 6.3.

In the following, we first consider the general features of this CI-based vector function implementation as also mentioned in reference [3] and then review the four required steps in the evaluation where in both cases some additional information will be added to the published version in [70].

As we only have to consider terms inside the projection manifold $\langle\mu|$ this means $e^{-\hat{T}}\hat{H}e^{\hat{T}}\,|\mathrm{Ref}\rangle$ can be restricted to this. Seeing that $e^{-\hat{T}}$ contains the identity operator, which does not increase the excitation of the state it is acting on, the configuration space spanned by $\hat{H}e^{\hat{T}}\,|\mathrm{Ref}\rangle$ must be restricted to the space of the projection manifold $\langle\mu|$. Since the Hamiltonian is an operator with a maximum de-excitation (down) rank of 2, this implies that the evaluation of $\hat{H}$ acting on $e^{\hat{T}}\,|\mathrm{Ref}\rangle$ has to be determined in a space with a maximum excitation level increased by 2 relative to the excitation manifold. In

Figure 6.1: Reduced linear transformation step for the CI-based evaluation of the CC vector function. $\underline{\mathbf{c}}^{\text{ext}}$ is a reference vector from the extended space which is projected onto a reduced space $\underline{\sigma}^{\text{red}}$ defined by the CC excitation manifold.

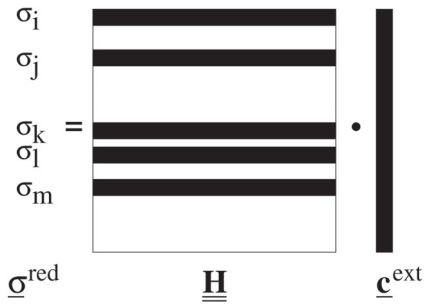

the $\hat{H}e^{\hat{T}}\,|\text{Ref}\rangle$ step the space is then reduced to the one spanned by $\langle\mu|$. For example, in a CCSD calculation the expression $e^{\hat{T}}\,|\text{Ref}\rangle$ can be restricted to at most quadruple excitations. We illustrate the linear transformation step $\hat{H}e^{\hat{T}}\,|\text{Ref}\rangle$ in Figure 6.1 where we see $\hat{H}$ working on a extended vector $e^{\hat{T}}\,|\text{Ref}\rangle$.

The computational scaling of this procedure is given as $O^{n+2}\,V^{n+2}$ where O is the number of occupied spinors, V the number of virtual spinors and n is the highest CC excitation level in the calculation. This is to be compared to a CC implementation with an optimal scaling as $O^n\,V^{n+2}$ such as the commutator driven implementation in Section 6.3. The higher scaling of the CI-based coupled cluster is caused by the Hamiltonian being used on an extended vector. This reduced efficiency therefore limits the number of electrons which may be correlated (roughly up to 10 or 12) and the size of the employed one-particle basis sets (roughly up to triple-zeta quality). Due to the use of the efficient direct CI technique based on Generalized Active Space expansions [72, 73] fairly large calculations with more than 1×10^8 Slater determinants in the extended space are nevertheless possible.

In the following, I will describe the relativistic implementation focusing on the individual steps required for the CC vector function. These steps are also shown in Figure 6.2 along with the setup routines and the iterative procedure.

Step 1:

$|a\rangle = e^{\hat{T}}\,|\text{Ref}\rangle$, expansion of the reference vector.

$$\begin{aligned} |a\rangle &= \left(\sum_{n=0}\frac{1}{n!}\hat{T}^n\right)|\text{Ref}\rangle \\ &= |\text{Ref}\rangle + \hat{T}\,|\text{Ref}\rangle + \frac{1}{2!}\hat{T}\left\{\hat{T}\,|\text{Ref}\rangle\right\} + \frac{1}{3!}\ldots \end{aligned} \tag{6.2}$$

Figure 6.2: Overview of the CI-driven coupled-cluster code.

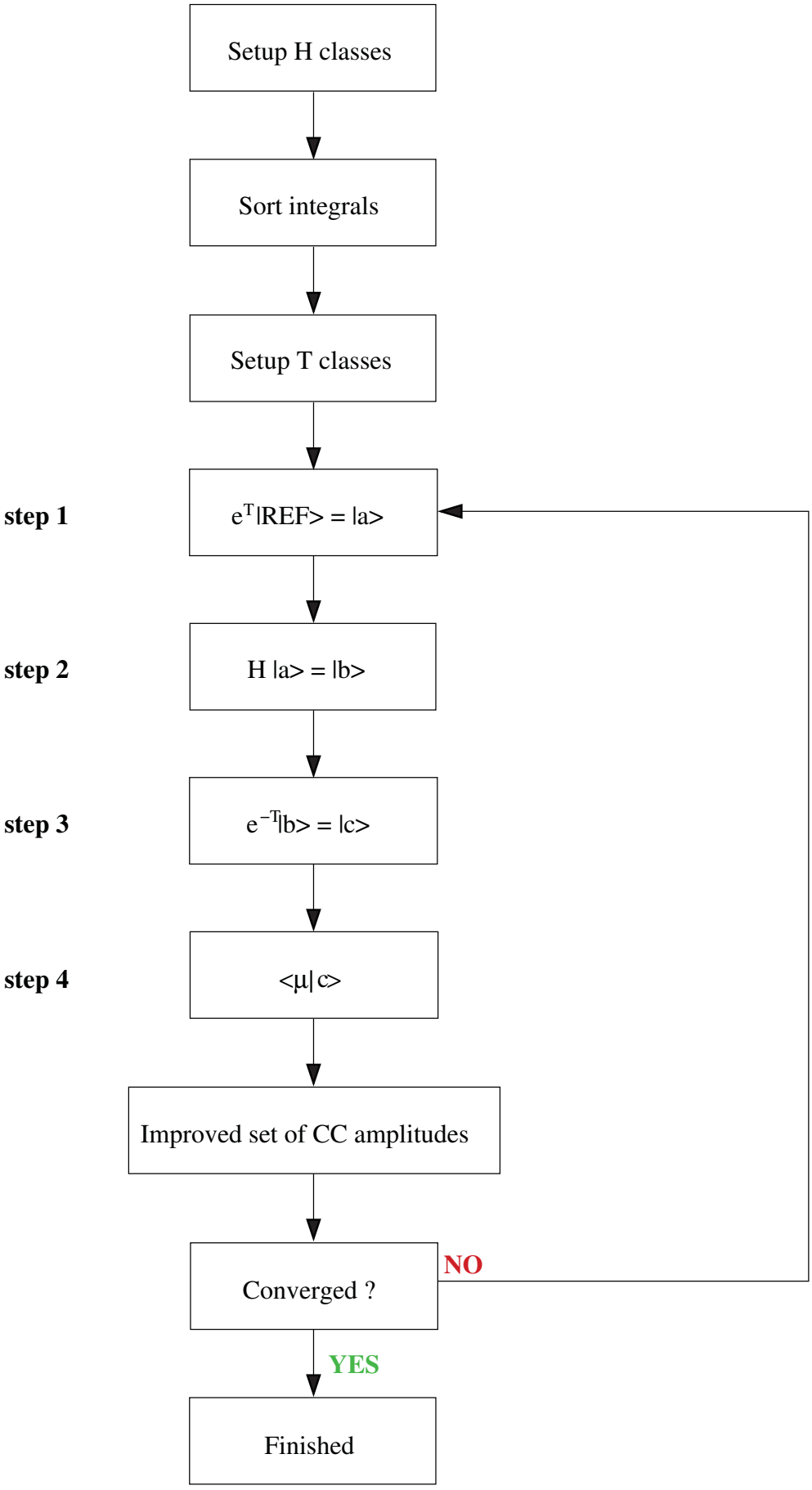

The expansion is carried out by invoking the routines for calculating a CI sigma vector repeatedly, i.e. once for each term $\hat{T}$ working on a vector. The loop structure of this routine then becomes

COPY |Ref⟩ TO |a⟩, |Temp1⟩
loop $\{N = 1, 4\}$
$\frac{1}{N}$ $\hat{T}$|Temp1⟩= |Temp2⟩
ADD |Temp2⟩ TO |a⟩
COPY |Temp2⟩ TO |Temp1⟩
end loop[N]

where the successive building up of the coupled-cluster wave function in |a⟩ with the help of two additional vectors is seen. Since these vectors are also stored in core this algorithm requires additional memory to be allocated. In each of these steps, the contraction is not performed with integrals, however, but with the CC amplitudes of the current iteration. Since the CI sigma vector previously only used the Hamiltonian operator classes this has been extended to also use the cluster operator classes of different sizes with corresponding amplitudes. This means a looping over more than $|\Delta M_K| > 2$ in the sigma vector call as for the Hamiltonian but up to the maximum excitation level M

$$\sigma = \sum_{\Delta M_K=-M}^{\Delta M_K=+M} \sigma^{\Delta M_K} \tag{6.3}$$

The expansion in step 1 is otherwise truncated when the highest excitation level has been reached which may couple to the excitation manifold, in line with the arguments in the above discussion (Section 6.2.1). This first step is the most expensive one in the algorithm due to the use of the extended cluster operator. The input for the extended cluster operator is given in the third space under the keyword .GASSPC (see Section 6.4).

Step 2:

$|b\rangle = \hat{H}\,|a\rangle$: linear transformation of the expanded reference vector.

This step again corresponds to the calculation of a linear transformation (CI sigma vector) of the expanded reference vector $|a\rangle$. The contraction is now carried out with integrals over Kramers-paired spinors which are classified according to main operator classes and the associated change of the auxiliary quantum number M_K. The excitation class formalism does not only define the structure of the Hamiltonian operator (with a

ΔM_K range of $\{+2,\ldots,-2\}$) but is also used in the definition of the cluster excitation operators in Eq. 2.70.

A relativistic sigma vector therefore consists of a sum of five contributions according to

$$\sigma = \sum_{\Delta M_K=-2}^{\Delta M_K=+2} \sigma^{\Delta M_K} \tag{6.4}$$

with a sample contribution corresponding to the partition $\Delta M_K = +1$ decomposed into 1- and 2-electrons parts

$$\begin{aligned}
\sigma^{+1}(\mathcal{T}^\dagger, \overline{\mathcal{T}^\dagger}) &= \sum_{ij}\sum_{\mathcal{S}} \left\langle \mathcal{T}^\dagger | a_i^\dagger | \mathcal{S}^\dagger \right\rangle \sum_{\overline{\mathcal{S}}} \left\langle \overline{\mathcal{T}}^\dagger | a_{\bar{j}} | \overline{\mathcal{S}}^\dagger \right\rangle \\
&\qquad \cdot h_{i\bar{j}} \cdot C_{\mathcal{S},\overline{\mathcal{S}}} \\
&+ \sum_{\substack{i\geq k \\ \bar{l}\bar{j}}}\sum_{\mathcal{S}} \left\langle \mathcal{T}^\dagger | a_i^\dagger a_k^\dagger a_l | \mathcal{S}^\dagger \right\rangle \sum_{\overline{\mathcal{S}}} \left\langle \overline{\mathcal{T}}^\dagger | a_{\bar{j}} | \overline{\mathcal{S}}^\dagger \right\rangle \\
&\qquad \cdot \left[(i\bar{j}|kl) - (k\bar{j}|il) \right] \cdot C_{\mathcal{S},\overline{\mathcal{S}}} \\
&+ \sum_{\substack{ik \\ \bar{l}\geq j}}\sum_{\mathcal{S}} \left\langle \mathcal{T}^\dagger | a_i^\dagger | \mathcal{S}^\dagger \right\rangle \sum_{\overline{\mathcal{S}}} \left\langle \overline{\mathcal{T}}^\dagger | a_{\bar{k}}^\dagger a_{\bar{l}} a_{\bar{j}} | \overline{\mathcal{S}}^\dagger \right\rangle \\
&\qquad \cdot \left[(l\bar{i}|jk) - (j\bar{i}|lk) \right] \cdot C_{\mathcal{S},\overline{\mathcal{S}}}
\end{aligned} \tag{6.5}$$

where $\mathcal{S}^\dagger$ denotes a string of unbarred creation operators. A full account of the sigma vector partitions is given in reference [71]. We here notice that the CI-coefficients $C_{\mathcal{S},\overline{\mathcal{S}}}$ are in fact a linear combination of the amplitudes found in step 1.

As discussed above, the vector $\hat{H}e^{\hat{T}}\,|Ref\rangle$ should be in the space of at most n-fold excitations whereas $e^{\hat{T}}\,|Ref\rangle$ may be in the space of $n+2$-fold excitations. The operation count of this step thus scales as $O^{n+2}V^{n+2}$ like in step 1.

The efficiency of the direct CI steps in terms of required computer memory benefits from the batching of coefficients in the linear transformation steps. In terms of speed, the string-based CI algorithm [73, 129] allows for the treatment of large expansions as no explicit comparison of configurations/occupations is carried out and higher than double excitations are treated on the same footing as double excitations.

Step 3:

$|c\rangle = e^{-\hat{T}}\,|b\rangle$, expansion of the transformed reference vector.

$$\begin{aligned}
|c\rangle &= \left(\sum_{n=0} \frac{(-1)^n}{n!}\hat{T}^n \right) |b\rangle \\
&= |b\rangle - \hat{T}\,|b\rangle + \frac{1}{2!}\hat{T}\left\{\hat{T}\,|b\rangle\right\} - \frac{1}{3!}\ldots
\end{aligned} \tag{6.6}$$

The expansion is carried out in complete analogy with step 1. It is assured that the expansion is restricted to the excitation manifold $\langle\mu|$ and will therefore have the regular scaling of O^nV^{n+2}.

Step 4:

$\Omega_\mu = \langle\mu|c\rangle$, evaluation of transition density matrix elements.

$$\Omega_\mu = \left\langle \mathrm{Ref} \left| \hat{\tau}_\mu^\dagger \right| c \right\rangle$$

The projection of the excitation manifold $\langle\mu|$ against the expanded transformed reference vector $|c\rangle$ corresponds to the calculation of transition density matrix elements and yields the CC vector function. Employing the concise implementation described in references [72] and [73] the evaluation becomes equivalent to the calculation of CI sigma vectors, where instead of a contraction with integrals a contraction with expansion coefficients is performed. For the present case, the left-hand vector of expansion coefficients is a unit vector. As this step is carried out in the space of at most n-fold excitations, it scales as O^nV^{n+2} and is therefore significantly faster than step 1 and 2.

6.2.2 The Unlinked Coupled-Cluster formalism for the CI-based Coupled-Cluster

Looking at the four steps for the implementation in Section 6.2.1 of the CI-driven generalized active space coupled cluster it is seen that if the third step is left out we end in the unlinked coupled-cluster formalism. The vector function generated in this way is shown in Eq. 3.19 where we see that $\exp(-\hat{T})$ is not present. While it in principle should be straight forward to omit step 3 and then evaluate the transition density matrix element $\Omega_\mu = \langle\mu|b\rangle$ this, however, has other consequences. The most important consequence is that the loop structure in step 1 does not truncate after four but after $M + 2$ where M is the highest excitation in the actual calculation space since only in this way can we be sure to have included all possible connections to the projection manifold[4]. When doing state-selective multireference coupled-cluster calculations we will often include higher restricted excitations than doubles meaning the truncation of the loop in step one would come much later. Since step 1 is the costly step this would mean a slowdown of the code if an unlinked approach was attempted which is why it has not been pursued.

[4]Of course in the limit of FCC this will also be M.

6.3 Documentation of the Commutator-Based Coupled-Cluster Code

The documentation of the commutator-based coupled-cluster code will mainly focus on the algorithm itself. In many steps it will not be evident from the documentation what changes has been needed in the individual subroutines since this would be much too technical and unmanageable to present without showing many of the subroutines explicitly themselves. This also applies to many of the setup routines where the additional new Hamiltonian and cluster operator classes are being constructed and the more technical routines for input/common block transfer for the getting the correct information from the other `DIRAC` modules. A complete overview of the commutator-driven coupled-cluster code is shown in Figure 6.3. It is here noted that the external setup routines are in parts different from those used in the CI-driven coupled-cluster code (see Figure 6.2) since there is no doubling of certain main operator classes for the Hamiltonian here. The major new routines like the integral fetcher and the handling of these will, however, be presented in some detail since a completely new routine was here needed and because it can be presented in a standalone way. Furthermore, an example of optimization of the code will be given where it is shown in Section 6.3.1 how to eliminate overhead in the setup of the equations. Further optimization like a reduction of the memory requirement to around one third was done but will also be too technical to show even if this was the step that enabled the code to be used in large-scale calculations ($+500 \times 10^6$ amplitudes) on standard Linux machines. Further options for memory reduction, besides batching, are also presented in Section 6.3.1.

The solution of the coupled-cluster equations is most effectively realized by using iterative algorithms that rely on repeated evaluations of the coupled-cluster vector function for given coupled-cluster operators $\hat{T}$

$$\Omega_\mu = \langle HF|\hat{\tau}_\mu^\dagger \exp(-\hat{T})\hat{H}\exp(\hat{T})|HF\rangle \tag{6.7}$$

The relativistic Hamiltonian contains at most two-body operators and has therefore at most four elementary operators that may be contracted with the $\hat{T}$-operator. The Baker-Cambell-Hausdorff expansion of the similarity transformed Hamiltonian $\exp(-\hat{T})\hat{H}\exp(\hat{T})$

terminates therefore after four commutators and so we have

$$\Omega_\mu = \langle HF|\hat{\tau}_\mu^\dagger(\hat{H} + [\hat{H},\hat{T}] + \frac{1}{2}[[\hat{H},\hat{T}],\hat{T}] + \frac{1}{6}[[[\hat{H},\hat{T}],\hat{T}],\hat{T}] + \frac{1}{24}[[[[\hat{H},\hat{T}],\hat{T}],\hat{T}],\hat{T}])|HF\rangle \tag{6.8}$$

A central part of the development of coupled-cluster programs is the development of efficient algorithms for the evaluation of the coupled-cluster vector function. We will now sketch our implementation of this evaluation for the general Kramers-restricted relativistic coupled-cluster method. A central feature of our code is the use of general algorithms that allows arbitrary excitation levels and subdivisions of the spaces of occupied and unoccupied spinors. Furthermore, the use of algorithms that exhibits optimal scaling with respect to the number of occupied and virtual orbitals and that relies on matrix multiplications for the innermost loops, produces an efficient code that allows the calculations combining large excitation levels and spinor bases. The current relativistic code is in this way in line with the recent developments of general coupled-cluster methods. Although the scalings of the various terms are identical to the optimal scalings, the prefactors of the various terms are currently not optimal, as the various terms are not collected in the optimal way.

Another central feature of the code is the use of second-quantized operators and their commutation relationship. In the outer loops, this is used to find the possible contractions between classes of the Hamiltonian and classes of one or several T-operators and to reduce these connections to the smallest possible number. In the inner loops, second quantization is used to re-express the various terms in a form that allows the use of matrix multiplication to evaluate these terms.

A sign of the generality of the code is that no significant changes in the loop structure were needed for adapting the non-relativistic code [99] to the relativistic framework, only extra classes of operators and coupled-cluster amplitudes needed to be added to the arrays describing these terms. However, considerable work was required to adapt for the occurrence of complex rather than real algebra, the use of double group rather than point group symmetry as well as to interface to another program for generating integrals and for fetching of these sorted integrals in an efficient way. Minor changes were necessary in many subroutines for including double group symmetry and the additional classes while

some subroutines needed an almost complete rewrite. It was, however, here realized that no explicit looping over vectors of different M_k for the ΔM_k flipping was needed as it is done in the CI codes [71, 72]. Instead, the Hamiltonian and cluster operator classes with $\Delta M_k \neq 0$ are directly included in the contraction scheme from the non-relativistic code like any operator class with $\Delta M_k = 0$ and therefore no further loop structure was needed.

The algorithm relies on the division of the Hamiltonian and coupled-cluster operator into different classes. So, the highest level of the program consists of loops over such classes and all terms belonging to given classes of these operators are treated simultaneously. Neglecting all the logistics related to ensuring that the right data are in memory when needed, the overall structure of the program is

loop {Classes of H}
  Rank H → Min,Max ncomm
  loop {Number of commutators: ncomm}
    loop {ncomm classes of T}
      Find all possible contractions of the current classes of H and ncomm T operators
      loop {Contractions}
        Get optimal order of parts of contraction, reorder operators
        loop {Parts of contraction}
          Perform part of contraction
        end loop[Parts of contraction]
      end loop[Contractions]
    end loop[ncomm classes of T classes]
  end loop[Number of commutators]
end loop[Classes of H]

This loop structure can be divided into three parts: The setup of equations for given classes of operators, optimum solution of equations and calculation of vector functions. These three parts along with a schematical overview of the code is seen in Figure 6.3. The external setup of the classes works as described in Sections 2.2.1 and 5.1.2. The sorting of the integrals according to the Hamiltonian classes is the same as in the CI codes, the fetching of these integrals for the construction of the inactive Fock matrix and for the Hamiltonian is for the two electron integrals the same and described in more details in Section 6.3.2. The equation setup along with the optimum solution to these along with

Figure 6.3: Overview of the commutator-driven coupled-cluster code.

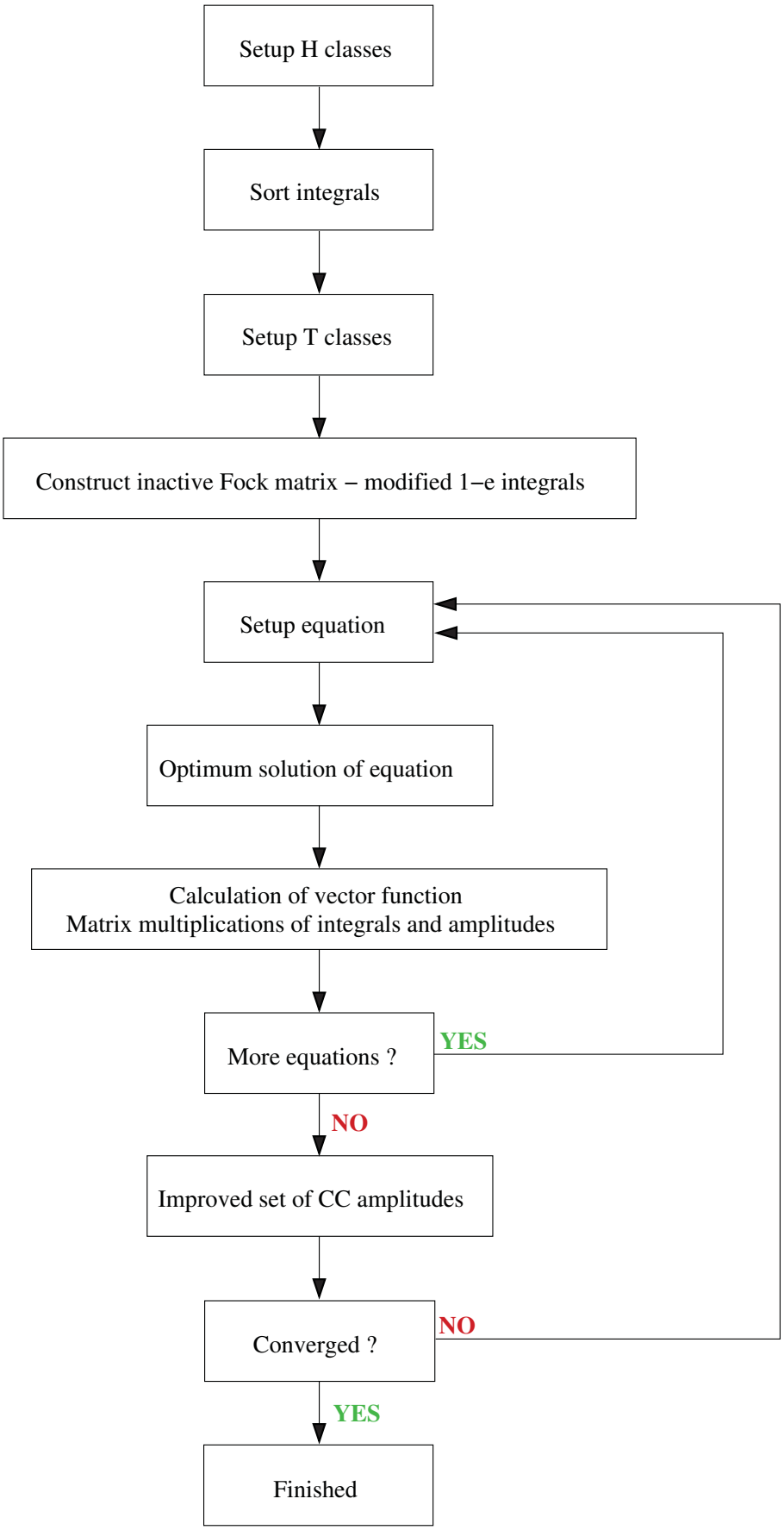

the execution of the solution will in the following be discussed as it has been used in the applications presented in Section 9.2. In Section 6.3.1 another way to setup the equation to avoid bottlenecks in this region will be presented.

The largest number of non-vanishing commutators associated with a given class of the Hamiltonian is twice the down-rank of this class of operators, so only operators with down rank 2 gives rise to non-vanishing four-fold commutators. All commutators are formally projected by a determinant $\langle HF|\hat{\tau}_{\mu i}$. Therefore, in addition to ensuring that a given combination of Hamiltonian class and classes of T-operators is non-vanishing, only such combinations that lead to operators within the operator manifold of $\hat{T}$ are evaluated.

Assume now that we have a class of the Hamiltonian $\hat{H}_c$ and M classes of $\hat{T}$, $\hat{T}_{i_1}, \ldots, T_{i_M}$ that produce a non-vanishing M-fold nested commutator $[\ldots, [\hat{H}_C, \hat{T}_{i_1}] \ldots, \hat{T}_{i_M}]$. Non-vanishing terms in the nested commutator occur only from the match of down-operators, i.e. creation of occupied spinors and annihilation of unoccupied spinors in the Hamiltonian, with up-operators, i.e. annihilation of occupied spinors and creation of unoccupied spinors, in the coupled-cluster wave operator. Furthermore, as the operator defined by the nested commutator acts on the reference state, all down-operators in the Hamiltonian must be matched by up-operators in the cluster operators. Finally, to ensure that all of the commutators in the nested commutator are non vanishing, each cluster operator must have at least one elementary operator matched by an operator in the Hamiltonian. A nested commutator may thus be evaluated by taking all possible matches between the elementary operators in the Hamiltonian and the wave operator. Borrowing from the language of many-body physics, a match of down-operators (creation of occupied spinors and annihilation of unoccupied spinors) with the corresponding up-operators (annihilation of occupied spinors and creation of unoccupied spinors) is called a contraction and we will denote such a contraction of operators A, B as $\overbrace{AB}$. Note that we have not discussed any signs connected with the transposition of the elementary operators, but we will return to this. As an example of the evaluation of a nested commutator we consider the commutator of the Hamiltonian main operator class ($\hat{H}_{2,0,2}$) containing four unbarred virtual indices

$$\hat{H}_{4v} = \frac{1}{2} \sum_{abcd} (ad|bc) a_a^\dagger a_b^\dagger a_c a_d \tag{6.9}$$

and two double excitations of unbarred spinors

$$\hat{T}_{i_1} = \hat{T}_{i_2} = \frac{1}{4} \sum_{ijab} t_{ij}^{ab} a_a^\dagger a_b^\dagger a_i a_j \tag{6.10}$$

The commutator $[[\hat{H}_{4v}, \hat{T}_{i_1}], \hat{T}_{i_2}]$ may then be written as the sum of all possible combinations of connections

$$\begin{aligned}
&[[\hat{H}_{4v}, \hat{T}_{i_1}], \hat{T}_{i_2}] \\
&= \frac{1}{32} \sum_{abcd,i'j'a'b',i''j''a''b''} (ad|bc) t_{i'j'}^{a'b'} t_{i''j''}^{a''b''} [a_a^\dagger a_b^\dagger a_c a_d, a_{a'}^\dagger a_{b'}^\dagger a_{i'} a_{j'}], a_{a''}^\dagger a_{b''}^\dagger a_{i''} a_{j''}] \\
&= \frac{1}{32} \sum_{abcd,i'j'a'b',i''j''a''b''} (ad|bc) t_{i'j'}^{a'b'} t_{i''j''}^{a''b''} a_a^\dagger a_b^\dagger a_c a_d a_{a'}^\dagger a_{b'}^\dagger a_{i'} a_{j'} a_{a''}^\dagger a_{b''}^\dagger a_{i''} a_{j''} \\
&+ \frac{1}{32} \sum_{abcd,i'j'a'b',i''j''a''b''} (ad|bc) t_{i'j'}^{a'b'} t_{i''j''}^{a''b''} a_a^\dagger a_b^\dagger a_c a_d a_{a'}^\dagger a_{b'}^\dagger a_{i'} a_{j'} a_{a''}^\dagger a_{b''}^\dagger a_{i''} a_{j''} \\
&+ \frac{1}{32} \sum_{abcd,i'j'a'b',i''j''a''b''} (ad|bc) t_{i'j'}^{a'b'} t_{i''j''}^{a''b''} a_a^\dagger a_b^\dagger a_c a_d a_{a'}^\dagger a_{b'}^\dagger a_{i'} a_{j'} a_{a''}^\dagger a_{b''}^\dagger a_{i''} a_{j''} \\
&+ \frac{1}{32} \sum_{abcd,i'j'a'b',i''j''a''b''} (ad|bc) t_{i'j'}^{a'b'} t_{i''j''}^{a''b''} a_a^\dagger a_b^\dagger a_c a_d a_{a'}^\dagger a_{b'}^\dagger a_{i'} a_{j'} a_{a''}^\dagger a_{b''}^\dagger a_{i''} a_{j''} \\
&+ \frac{1}{32} \sum_{abcd,i'j'a'b',i''j''a''b''} (ad|bc) t_{i'j'}^{a'b'} t_{i''j''}^{a''b''} a_a^\dagger a_b^\dagger a_c a_d a_{a'}^\dagger a_{b'}^\dagger a_{i'} a_{j'} a_{a''}^\dagger a_{b''}^\dagger a_{i''} a_{j''} \\
&+ \frac{1}{32} \sum_{abcd,i'j'a'b',i''j''a''b''} (ad|bc) t_{i'j'}^{a'b'} t_{i''j''}^{a''b''} a_a^\dagger a_b^\dagger a_c a_d a_{a'}^\dagger a_{b'}^\dagger a_{i'} a_{j'} a_{a''}^\dagger a_{b''}^\dagger a_{i''} a_{j''} \\
&+ \frac{1}{32} \sum_{abcd,i'j'a'b',i''j''a''b''} (ad|bc) t_{i'j'}^{a'b'} t_{i''j''}^{a''b''} a_a^\dagger a_b^\dagger a_c a_d a_{a'}^\dagger a_{b'}^\dagger a_{i'} a_{j'} a_{a''}^\dagger a_{b''}^\dagger a_{i''} a_{j''} \\
&+ \frac{1}{32} \sum_{abcd,i'j'a'b',i''j''a''b''} (ad|bc) t_{i'j'}^{a'b'} t_{i''j''}^{a''b''} a_a^\dagger a_b^\dagger a_c a_d a_{a'}^\dagger a_{b'}^\dagger a_{i'} a_{j'} a_{a''}^\dagger a_{b''}^\dagger a_{i''} a_{j''}
\end{aligned} \tag{6.11}$$

The above eight terms are not independent. By using the anti-commutation relations of the elementary operators and the antisymmetry of the coupled-cluster amplitudes under the permutation of indices, it is straightforward to show that the nested commutator of Eq. 6.11 reduces to a single term

$$\begin{aligned}
&[[\hat{H}_{4v}, \hat{T}_{i_1}], \hat{T}_{i_2}] \\
&= \frac{1}{4} \sum_{abcd,i'j'a'b',i''j''a''b''} (ad|bc) t_{i'j'}^{a'b'} t_{i''j''}^{a''b''} a_a^\dagger a_b^\dagger a_c a_d a_{a'}^\dagger a_{b'}^\dagger a_{i'} a_{j'} a_{a''}^\dagger a_{b''}^\dagger a_{i''} a_{j''}
\end{aligned} \tag{6.12}$$

To evaluate the nested commutator, we then calculate the number of transpositions of elementary operators required to bring the operators to be contracted next to each

other, and use the parity of this permutation as the overall sign. In Eq. 6.12 there are three elementary operators between the operators to be contracted giving an overall sign of minus 1. The nested commutator is finally evaluated by removing the contracted operators and replacing the pair of indices by a common index for each match. The nested commutator of Eq. 6.12 therefore becomes

$$\begin{aligned}&[[\hat{H}_{4v},\hat{T}_{i_1}],\hat{T}_{i_2}]\\&=\frac{1}{4}\sum_{ab,i'j'b',i''j''b''}(\sum_{cd}(ad|bc)t^{db'}_{i'j'}t^{cb''}_{i''j''})a^\dagger_a a^\dagger_b a^\dagger_{b'}a_{i'}a_{j'}a^\dagger_{b''}a_{i''}a_{j''}\end{aligned}\tag{6.13}$$

The nested commutator $[[\hat{H}_{4v},\hat{T}_{i_1}],\hat{T}_{i_2}]$ is a four-body operator with the factors determined by a matrix multiplication of Hamiltonian integrals and T-amplitudes. Note, however, that both the creation or the annihilation indices occur as free summations, although the operators may be required—and are stored—as matrices with ascending indices. In Eq. 6.13, the indices corresponding to occupied spinors are not included in the matrix operations, and it is therefore trivial to impose an ascending order of these

$$\begin{aligned}&[[\hat{H}_{4v},\hat{T}_{i_1}],\hat{T}_{i_2}]\\&=\sum_{ab'b'',i'<j',i''<j''}(\sum_{cd}(ad|bc)t^{db'}_{i'j'}t^{cb''}_{i''j''})a^\dagger_a a^\dagger_b a^\dagger_{b'}a_{i'}a_{j'}a^\dagger_{b''}a_{i''}a_{j''}\end{aligned}\tag{6.14}$$

giving a matrix multiplication of integrals and amplitudes as stored in the code.

Above we have considered the two identical cluster operators as can also be seen from Eq. 6.10. In case of non-identical cluster operators, the ordering of the contraction of the operators will be changed if this reduces the operational count. The ordering of the operators will then be chosen such that the inner most contraction contains the most elements.

These three steps where an equation is set up, arranged and solved is then done for every possible fully connected combination of Hamiltonian and cluster operator classes. Since the form of the equations is not fixed, like in a regular CCSD code where the matrix elements are explicitly programmed, this allows for an easy implementation of truncation schemes since one here only needs to define the cluster operator classes in the external setup. Here in the internal part we will just try to find the possible equations and calculate these. The approach to finding these is described in more detail in Section 6.3.1 where it is seen that all combinations are tried. Thus all possible equations are included regardless

of the structure of the cluster operator. Since the number of possible equations always match the number of amplitudes regardless of how the cluster operator is truncated this ensures that the equation system will always be fully determined.

6.3.1 Solution to a Bottleneck in the Equation Setup

As mentioned in Section 6.3, all possible combinations of the Hamiltonian and cluster operator classes are tried in the setup for the vector function. We will here examine the scaling, if we do an elementary search for the vector function, with respect to the number of GAS in the non-relativistic and fully relativistic case for the real groups. Since the number of combinations is the largest for the four-fold commutators we will focus on these. The loop structure originally suggested is as displayed below where the first part with the equation setup is shown in more details and the rest suppressed.

loop {DO IH=1,NHTP ← H classes}
  Lower Commutators
  IF RANK(IH)=2
  loop {DO IT1=1,NTTP ← T classes}
    [IH,IT1]=O1 ← Contraction
    loop {DO IT2=IT1,NTTP ← T classes}
      [O1,IT2]=O2 ← Contraction
      loop {DO IT3=IT2,NTTP ← T classes}
        [O2,IT3]=O3 ← Contraction
        loop {DO IT4=IT3,NTTP ← T classes}
          [O3,IT4]=O4 ← Contraction
          IF O4 $\in \mu \rightarrow$ Check if Fully Connected
          IF Fully Connected → Calculate contribution
        end loop[IT4]
      end loop[IT3]
    end loop[IT2]
  end loop[IT1]
end loop[IH]

We here simply loop over all classes of the Hamiltonian and the cluster operators and if the resultant class belongs inside the projection manifold and is fully connected it is calculated. In this way we have guaranteed that all possible equations will be searched and only the needed calculated. The problem is, however, we here try all combinations of equations where, in fact, only few of these are needed.

As we see from Figure 6.3 this set up of equations is done in each iteration. The equations from one iteration to the next of course do not change so this is in principle a redundant step to repeat in every iteration. This however is not a problem as long as the number of classes remain small. When one attempts to do a state-selective multireference coupled-cluster calculation this, however, will not be the case. This is due to the increased number of generalized active spaces and excitation level as can be seen in Table 6.1 and is discussed in Section 5.1.2. We here find that the number of classes grows dramatically and can give large overheads that are independent of calculation size, but depend just on calculation type.

Table 6.1: Number of Hamiltonian and cluster operator classes in the non-relativistic and fully relativistic case for various types of calculations and generalized active spaces. For the T classes the maximum number is here listed.

		# H classes	# T classes	# H classes rel	# T classes rel
Method	NGAS	NHTP	NTTP	NHTP	NTTP
CCSD	2	42	5	68	13
CCSDT	2	42	9	68	29
CC(6_2)	4	488	398	720	1848
CC(6_2)	5	1125	942	1625	4256
CCSDTQ	5	1125	492	1625	2244

From the loop structure of the equation setup we see that the number of contractions between the operator strings representing the classes to be performed is NHTP$\times$NTTP^4/8 which then has to be compared against NTTP to see if the resultant contraction is inside the projection manifold. Let us start with the evaluation of the non-relativistic case and

the CC(6_2) method with four GAS. As we see from Table 6.1, we will then have 1.5×10^{12} number of contractions which then has to be compared against the 398 cluster operator classes which is still possible in a reasonable amount of time. In the relativistic case we here find 1×10^{15} number of contractions which has to be compared against 1848 cluster operator classes. From this we clearly see that if we want to fully exploit the GAS concept and use many GAS with higher excitations we need to find a way to setup the equations significantly faster since the CC(6_2) with 5 GAS is completely out of reach with 6.7×10^{16} possible contractions which should be compared against 4256 cluster operator classes[5].

A fast equations setup along with the removal of the equation setup in the iterative procedure has been programmed. Inside the iterative procedure the needed equations are now just read in, arranged and calculated. The fast equation setup relies on a systematic generation of the nested commutator and on the generation of the cluster operator classes. The new algorithm for this is presented below:

Find Rank H
Find and Store Connection for Rank Zero H
Find All Rank Reducing T's for given H
loop {DO IH=1,NHTP ← H classes}
  IF RANK(IH)=1
  loop {DO IT1=1,NTTP ← T classes}
    [IH,IT1]=O1 ← Contraction
    IF RANK(O1) = 0 ← Store Connections for One Commutator
  end loop[IT1]
  IF RANK(IH)>1
  loop {DO IT1=1,NTTP_{con} ← Only Rank Reducing T classes}
    [IH,IT1]=O1 ← Contraction
    IF RANK(O1) = 0 ← Store Connections for One Commutator
    Find Excitation level of O1
    If Second Contraction Possible ← Store operator O1
  end loop[IT1]

[5]From Section 5.1.2 we see that with increased number of GASs the length of the string representing a class grows, thereby giving an additional slowdown for more GASs. Hence, double the number of GAS doubles the length of the string representing a class.

end loop[IH]
loop {DO IH=1,NHTP ← H classes}
IF RANK(IH)=2
loop {DO IT2=IT1,NTTP$_{con}$ ← Only Rank Reducing T classes}
[O1,IT2]=O2 ← Contraction
IF RANK(O2) = 0 ← Store Connections for Two Commutators
end loop[IT2]
IF RANK(IH)>2
loop {DO IT2=IT1,NTTP$_{con}$ ← Only Rank Reducing T classes}
[O1,IT2]=O2 ← Contraction
IF RANK(O2) = 0 ← Store Connections for Two Commutators
Find Excitation level of O2
If Third Contraction Possible ← Store operator O2
end loop[IT2]
end loop[IH]
loop {DO IH=1,NHTP ← H classes}
IF RANK(IH)=3
loop {DO IT3=IT2,NTTP$_{con}$ ← Only Rank Reducing T classes}
[O2,IT3]=O3 ← Contraction
IF RANK(O3) = 0 ← Store Connections for Three Commutators
end loop[IT3]
IF RANK(IH)>3
loop {DO IT3=IT2,NTTP$_{con}$ ← Only Rank Reducing T classes}
[O2,IT3]=O3 ← Contraction
IF RANK(O3) = 0 ← Store Connections for Three Commutators
Find Excitation level of O3
If Fourth Contraction Possible ← Store operator O3
end loop[IT3]
end loop[IH]
loop {DO IH=1,NHTP ← H classes}
IF RANK(IH)=4
loop {DO IT4=IT3,NTTP$_{con}$ ← Only Rank Reducing T classes}

[O3,IT4]=O4 ← Contraction
IF RANK(O4) = 0 ← Store Connections for Four Commutators
end loop[IT3]
end loop[IH]

From the algorithm above we see we build the commutators successively by transferring the possible operators over to the next contraction. While it may look similar to the algorithm for the four-fold nested commutators there are here many reductions in the building of further commutators being made, i.e. eliminating contracted operators where further contractions will not be inside the projection manifold or completely reduce the rank. The reductions come about in only looping over rank-reducing cluster operators classes for a given Hamiltonian class which also includes already contracted Hamiltonian classes. This furthermore also ensures that all stored operators with up to two commutators will be fully connected. We here also note that the more GASs included the more cluster operator classes can reduce the rank of a given Hamiltonian class but since the number of zeros/small numbers increase the percentage of rank-reducing operators will go down, i.e. giving greater savings with more GASs. The insistence on a continual rank reduction helps to ensure that the resultant operator will be fully connected for up to two commutators. Furthermore the sorting of the cluster operator in excitation level and Kramers flip is used to reduce comparison in the projection manifold by only comparing against same excitation level and Kramers flip[6] and to eliminate intermediate operator classes (O1-3) which cannot stay inside the projection manifold since the following cluster operator classes will take it outside. Large reductions were here also introduced by performing contractions of the string representation in a different fashion where no negative number can appear. With all the equations known these can be taken outside the iterative procedure of the code to give the code structure shown in Figure 6.4 where also the number of equations passed down to the optimum solution step has been significantly reduced. This has made it possible to find the equations for all the GAS setups shown in Table 6.1 in a reasonable amount of time.

[6]Hence the same elementary operator class (see Section 2.2.1.2).

Figure 6.4: Overview of the commutator-driven coupled-cluster code with an efficient equation generation.

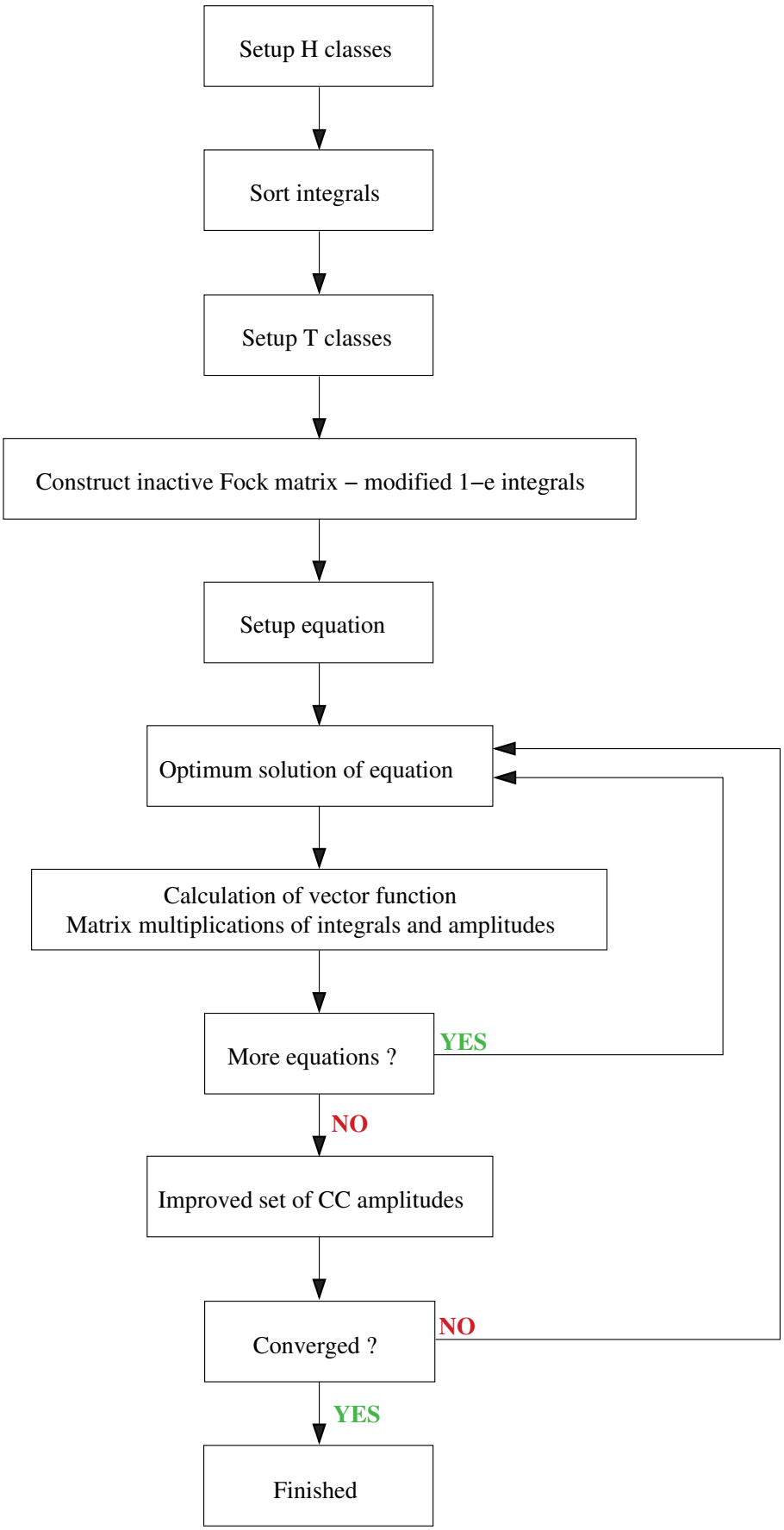

6.3.2 Integral Handling

After the integral transformation step where the integrals have been transformed from the AO to the MO basis (see Section 4.3.2) these are written to disk in an i,j,k,l sorting fashion. While this sorting is easy to deal with it is not practical for the codes used here since it is difficult to get a reduction in the number of integrals stored in core and a resorting of the integrals is therefore needed. In section 2.2.1 it was shown how an operator can be divided into the main operator class form and later in Section 5.1.2 this division was extended to the classes. Since only integrals belonging to a given Hamiltonian class will appear when this Hamiltonian class is being calculated this can be used to have a sorted list of integrals and to reduce the number of integrals stored in core.

At the moment the sorting of integrals is proceeding in the same fashion as the one developed for the GASCI routines. An algorithm for this sorting is shown in [72]. This means the two fully relativistic coupled-cluster codes share this sorting despite the fact that the commutator-driven coupled-cluster code has a different treatment of the $\hat{H}_{2,0,1}$ main operator class. In the Hamiltonian main operator classes $\hat{H}_{2,0,0}$ and $\hat{H}_{2,0,2}$ where there are either four unbarred or barred indices, the integrals are stored as Coulomb minus exchange while the other classes are stored separately. This also includes $\hat{H}_{2,0,1}$ which is why in the commutator-driven coupled-cluster code two integrals are fetched instead of one for this class. In this way the $\hat{H}_{2,0,1}$ main operator class is also fetched as Coulomb minus exchange just from two different CI-Hamiltonian classes. The sorting in the $\hat{H}_{2,0,0}$, $\hat{H}_{2,0,2}$, $\hat{H}_{2,2,0}$ and $\hat{H}_{2,-2,0}$ classes is such that so we here have indices l>j and k>i while this is not the case for the $\hat{H}_{2,0,1}$ class meaning a different fetching of these is necessary and described in the algorithm below. Since the particle-hole formalism is used we here work with modified one-electron integrals. These are instead the elements of the inactive Fock matrix and, as seen in Figure 6.4, generated in the external setup. The construction of the inactive Fock matrix uses the new integral fetcher and is stored in memory throughout[7]. As can be seen from the loop structure for the equation generation in Section 6.3.1, the outer loop is always over the Hamiltonian classes. With the sorting of the integrals one can therefore significantly reduce the number of integrals stored in core by storing all the integrals on disk and then just reading in the class of integrals needed for a given

[7]This could also be written to disk and just read in when the one-electron Hamiltonian classes are looped over.

Hamiltonian class. This way one would never need to store more integrals in core than needed for the largest Hamiltonian class. For this to work a new sorting of the $\hat{H}_{2,0,1}$ main operator class would be needed, so these would also be stored as Coulomb minus exchange, to make the reduction in the number of integrals and an easier readin. Because this is not yet implemented all integrals are at the moment stored in core.

The integral fetching at the moment includes a few redundant steps although these do not significantly influence the performance. The fetching of two-electron integrals is performed as shown in the algorithm below where the only information needed are the indices of the integral and the number of bars. The one-electron integrals are just taken from the inactive Fock matrix. Due to the different sorting of some of the classes, differences in the fetching of these was necessary.

Map indices to GAS
Reorder indices (except for $\hat{H}_{2,0,1}$)
Calculate class and offset
Calculate offset in class and absolute offset
Fetch integral

For the mapping of the orbital indices to a GAS a loop over the number of GAS is performed for the mapping. This is the only loop structure in the integral fetcher. Everything else follows from one-line formulas with the use of arrays set up in the integral sorting step and from the input. The reordering of indices is done since integrals for these classes are stored as Coulomb minus exchange only once, i.e. not with the indices switched, and a sign is therefore also introduced. A correct ordering to the sorting is needed to be able to identify the integral in the calculation of the class. Here the class is calculated again depending on the sorting. For the $\hat{H}_{2,0,1}$ class both types for a Coulomb minus exchange fetching is identified. The offset is calculated via an array setup in the integral sorting step. An offset inside a class is calculated and an absolute offset is found by adding the offset from the class. With the absolute offset we have the position of the integral(s) on the array and can find this/these. What is not seen from the algorithm above is that the way to calculate classes and offset is quite different for the different sorting. This means the integral fetcher is in fact more like a combination of two fetchers with the same overall structure but for differently sorted integrals. An added complication

is the fact that trivially zero integrals[8] are not stored giving a slightly different fetching depending on indices being equal or not. Despite a fast integral fetching this could be improved by a better integral sorting.

Since a simple reading in of integrals for a given class could be done in the first loop of the code, only these integrals would be needed in core. A step like this would free up a lot of memory from the integrals. With a sorting of the integrals as done for the $\hat{H}_{2,0,1}$ just as Coulomb minus exchange the fetching of the integrals could be done in a much simpler and faster way which would improve the overall performance of the code since this is a time consuming due to the many integrals required in large scale calculations.

6.4 Documentation of the Usage of ARDUCCA Module

Since the spin-free and the fully relativistic codes are two separate entities[9] they require separate input. These inputs will be described in the following sections.

6.4.1 Documentation of Input of the Spin-Free ARDUCCA Module

The ARDUCCA module in DIRAC[10] is called in the wave function section as

```
**WAVE FUNCTION
.ARDUCCA
```

and all ARDUCCA specific input are under

```
*ARDUCCA
```

[8] From Coulomb minus exchange

[9] They do of course share some routines but never ones with any common blocks.

[10] For a complete input description of the visit the DIRAC wiki page at http://wiki.chem.vu.nl/dirac/index.php/

The inputs will be divided into essential and optional but only those needed for the coupled-cluster runs are here included. The input is often followed by a specification of the keyword. Certain inputs will have to be specified before others which will be clear from the loop structure. The essential inputs are:

.INIWFC

WFTYP

WFTYP options are DHFSCF for closed shell reference and OSHSCF for open shell.

.CITYPE

GASCI

GASCI is for general expansion. Here standard blackbox CCSD input could be explicitly programmed.

.NACTEL

NELEC

NELEC is the number of electrons in the correlation step.

.MULTIP

MS2

MS2 is the spin multiplicity times two of the wave function.

.GASSHE

NGAS

loop {1,NGAS}
A,B, . . . , NIRREP
end loop[NGAS]

NGAS is the number of generalized active spaces. A,B, ..., NIRREP is the number of orbitals in each symmetry (separated by comma) of each GAS (one GAS per line). Notice the order of the irreps is determined by the generator input for the point group in the .MOL file (see http://wiki.chem.vu.nl/dirac/index.php/)

.GASSPC

NSEQCALC

loop {1,NSEQCALC}
  loop {1,NGAS}
    MINOCC MAXOCC
  end loop[NGAS]
end loop[NSEQCALC]

NSEQCALC is the number of sequential calculations. For coupled-cluster calculations this is a minimum of two for the commutator driven and three for the CI-driven coupled-cluster code. MINOCC and MAXOCC is the minimum and maximum accumulated occupation in each GAS for each calculation. For any coupled-cluster calculation the first one must be a single determinant. For the CI-driven coupled-cluster code the second calculation is the extended space while the third is the actual space, see Section 6.2.1 for more details on this.

.SEQUEN

loop {1,NSEQCALC}
  loop {1,NCALC}
    CALCTYP,NITER,TDEF
  end loop[NCALC]
end loop[NSEQCALC]

NCALC is the number of calculations with the given accumulated occupation in the sequential calculation. CALCTYP is the type of calculation, options are CI or GEN_CC for a GASCI or GASCC type of calculations, respectively. NITER is the maximum number of iterations and TDEF is the T defining space for the cluster operator. In normal calculations TDEF equals two. Notice in the CI-driven this will be different to the actual space.

.NEWCCV

Is an optional keyword and will start the commutator driven coupled-cluster code. The default in the spin-free case is the CI-driven. To reach the last type of general-order coupled-cluster code one has to hardwire it in the code.

.CCLR

NROOT_A,NROOT_B,. . . ,NROOT_NIRREP

Activates the linear response module. This works with the CI-driven coupled-cluster code. NROOT_X specifies the number of roots in a given irrep X.

6.4.2 Documentation of Input of the Fully Relativistic ARDUCCA Module

The fully relativistic coupled-cluster codes is currently residing behind the MCSCF module [130] together with the LUCIAREL module [71–73]. Because of this the input for the coupled-cluster codes is in the wave function section

**WAVE FUNCTIONS

.KRMCSCF

All coupled-cluster inputs are under the MCSCF input so we have

*KRMCSCF

The input will resemble the ones shown in Section 6.4.1 for the spin-free case since the fully relativistic codes are adaptations of the spin-free codes. The inputs from the spin-free case will therefore in large parts be the same in the relativistic case and I will therefore restrict the documentation of keywords to new or changed keywords from the spin-free case. As some might notice there is no restart keyword this is because I have made an automated restart that commences if the file CCAMP is present. The inputs are:

.CI PROGRAM

CIMOD

The options for CIMOD are LUCIAREL and GOSCI where LUCIAREL is the option to choose for the coupled-cluster runs.

.INACTIVE

NINAC

where NINAC is the number of occupied Kramers pairs not to be taken into account in the correlation treatment. This keyword replaces .NACTEL in the spin-free case. Further replacement is done with .GASSH which replaces .GASSHE but the structure of this input is otherwise preserved.

.MK2REF

IMK2

.MK2REF replaces .MULTIP and IMK2 is two times the Kramers projection of the reference.

.MK2DEL

DELMK2

DELMK2 denotes the maximal flipping of the Kramers projection. This gives the possibility of doing approximation in the Kramers flip as described in Section 8.1.

.CCONCI

.CCONCI replaces .NEWCCV in the spin-free case. Notice the default in the fully relativistic case is the commutator-driven coupled-cluster code and .CCONCI will start the CI-driven coupled-cluster code.

.SYMMETRY

IIRREP

IIRREP specifies the symmetry.

.MAX MACRO

NMACRO

NMACRO specifies the number of macro iteration done in a calculation. Notice this is only in conjunction with the MCSCF module itself i.e. this has been zero throughout this thesis.

.CIONLY

give the possibility to skip the integral sorting step performed before every run[11]. This is mostly used for different types of calculations at a given internuclear distance or for restarted calculations.

.INOCOVA

INUM

INUM determines the number mixing of the active and inactive hole indices as described in Section 8.3.

.CCEX_E

NROOT_A,NROOT_B,...,NROOT_NIRREP

.CCEX_E activates the linear response module. This module is implemented but not debugged.

6.4.3 Sample Input

This section will be concerned with giving a realistic sample input for the fully relativistic generalized active space coupled-cluster method from the keywords shown in Section 6.4. I will here also briefly comment on how to use two of the approximations presented in Section 8. The input will be restricted to only *KRMCSCF and the commutator driven coupled-cluster code.

[11]It is the same for all types of calculations since they use the same Hamiltonian.

The example chosen is a state-selective multireference coupled-cluster setup for the BiH molecule in a cc-pVTZ basis with a truncation of the virtual space of 5.6 E_h. The inactive holes are the $5d$ electrons on Bi and the active holes consist of the occupied $6s6p$ on Bi and $1s$ on H. For the active particles the unoccupied $6p$ on Bi is chosen. This then makes it a CC(6_2) calculation[12].

*KRMCSCF

.CI PROGRAM

LUCIAREL

States modules to use.

.INACTIVE

34

The KR-MCSCF module calls the MOLTRA module (see Section 4.3.2) which freezes 34 Kramers pairs.

.GASSH

4

5

3

2

54

Four GA spaces with 5 Kramers pairs in the first space ($5d$ on Bi), three in the second (occupied $6s6p$ on Bi and $1s$ on H), two in the third (unoccupied $6p$ on Bi) and 54 Kramers pairs in the last space.

.GASSPC

[12]Notice no higher than hextuple excitations can be present due to the number of active particles.

2

10 10

16 16

16 16

16 16

8 10

10 16

14 16

16 16

Two calculations with minimum and maximum occupation in each GA space. First calculation defines reference determinant second the calculation the type. For the calculation up to two holes are allowed among the inactive holes (8 10), six holes/particles among the active holes and particles(10 16) and two particles among the inactive particles (14 16). The last line (16 16) ensures that all electrons are limited to the given Kramers pairs.

.SEQUEN

1

CI,50

1

GEN_CC,70,2

The sequential execution of the calculations. 1 CI calculation with a maximum of 50 iterations in the first GA space. 1 coupled-cluster calculation with a maximum of 70 iterations where the defining space for the cluster operator is the second GAS.

.MK2REF

0

Kramers projection of the reference.

.MK2DEL

6

Maximal Kramers flip equals highest included excitation.

.SYMMETRY

1

In symmetry one.

.MAX MACRO

0

Do not do MCSCF.

To make approximations in the Kramers flip the value for .MK2DEL would be reduced and all cluster operators with a higher Kramers flip would be discarded.

The CC(n_m) approximation can be invoked by increasing the accumulated occupation for .GASSPC. For a CC(4_2) one would then have

.GASSPC

2

10 10

16 16

16 16

16 16

8 10

12 16

14 16

16 16

where (10 16) is replaced by (12 16).

Chapter 7

Relativistic vs. Non-Relativistic Coupled Cluster

The coupled-cluster method being the most successful method for accurate *ab initio* calculations in quantum chemistry to date has seen surprisingly little adaptation from the non-relativistic to the relativistic framework. This in particular since the need for methods which can handle open-shell systems with large static and dynamic correlation is there in many cases needed, like in the actinides and lanthanides. Like with many other methods the adaptation to the relativistic framework, i.e. the inclusion of spin-orbit interaction is often done *a posteriori* with an effective spin-orbit operator. This means diagonalizing an effective operator in a set of spin-free states. While this way has the advantage of lower computational costs, accurate calculations can be difficult to perform when the spin-orbit splitting is large or when there is a significant difference in the charge distribution of the various components split by the spin-orbit interaction. As is evident from Section 2.2.2 the costly part in including relativistic effects is the inclusion of the spin-orbit operator. The effect on the coupled-cluster equations will in this section be discussed to show the additional cost involved in running calculations where spin-orbit is included *a priori*. In Section 2.2.2 it was shown that the number of main operator classes increased quadratically instead of linearly in the cluster hierarchy when including the spin-orbit interaction. The discussion will be more qualitative and not focused on exact scaling and prefactors for higher order coupled cluster but more on the processes leading to higher prefactors. This will be kept in the context of a Kramers restricted coupled-cluster formalism as presented in Section 2.2.2.

7.1 Theory and Application

In a paper by Visscher *et al.* [74] it was shown that for a Kramers restricted CCSD where time reversal symmetry of the amplitudes was used (see Eq. 2.74) the floating point operation was increased by a maximum of 32 in comparison to a spin-free CCSD provided there existed at least one two-fold element of symmetry like C_2. Having such an element it would mean we would be in the real and complex groups (see Section 2.2.3). For the real groups the complex algebra could be omitted giving a reduction of 4 and thereby only being 8 times more expensive. For the quaternion groups the expense would be significantly higher since here we would also have an odd Kramers flip which was omitted in the above analysis. As outlined below higher order coupled cluster would be expected to have an even higher increase in the floating points operations since we would there have many more connections between Hamiltonian and cluster operator classes not present in the non-relativistic framework. This implies that the ratio between the prefactors of a spin-free and spin-dependent coupled cluster would increase with increasing excitation level.

From Section 2.2.1.3 we have seen that the number of main operator classes increase quadratic with the excitation level in the fully relativistic case while only linear in the non-relativistic case. From this we clearly see that the number of amplitudes increase at a greater rate with every increase in the coupled-cluster hierarchy since the difference in the number of main operator classes increases. We see that for the $\hat{T}_1$ operator the number of amplitudes are doubled in comparison to the non-relativistic case while for the $\hat{T}_2$ there is a more than fourfold increase in the number of amplitudes. A second bottleneck with the introduction of these many additional classes of amplitudes is the number of connections in Eq. 7.1 since there is a large increase in the number of possible contractions due to the Kramers flips of the cluster operators.

$$\langle \mu | \exp(-\hat{T}) \hat{H} \exp(\hat{T}) | HF \rangle \tag{7.1}$$

The problem of connections can be viewed as an combinatorial problem where the number of combinations increase with the excitation level of the cluster operator. This increase comes from the fact that more combinations of lower order main operator classes will appear in the highest main operator class with each increase in excitation level. Thus giving a larger vector function.

Both of these problems becomes very evident when a state-selective multireference coupled-cluster [115, 116] as described in Section 3.1.5 with higher internal excitations is performed and shown in Table 9.2. Here the problems is more the number of connections than the number of amplitudes since up to 6 fold internal excitations has here been included. These problems are similar to what has also been observed for CI when going from the non-relativistic framework to the relativistic one namely that the CI matrix is no longer as sparse as in the non-relativistic case since no block diagonalization after M_K can be performed like M_S in the non-relativistic case. In coupled-cluster we here observe a large increase in the equation length per amplitude from both higher excitations and the Kramers flip which is seen by a larger vector function. This means for a given element in μ in the projection manifold the number of non-zero terms in Eq. 7.1 will be increased since there is an increased number of excitation operators and these can be combined with different Kramers flip. Therefore one needs to consider not only the number of amplitudes but also the excitation levels and the Kramers flip when trying to assess the computational timings. This need for selected higher excitations in the state-selective multireference coupled-cluster is a severe bottleneck from an application viewpoint since the number of contractions needed increase dramatically with the size of the formal model space and is a problem that is made significantly worse in the fully relativistic regime. A number of approximation schemes has therefore been suggested to reduce the highest excitation levels in the model space but still trying to retain the accuracy. These different methods are presented in Section 8.

Chapter 8

Approximation Schemes

The development of efficient algorithms for accurate calculations along with sensible approximations is really the center of all many-body theories and a balance between the effort of performing the calculation and the accuracy has to be found. Systematic approximations are therefore essential not only to see if the approximation is good but also to have the exact value as the limit. The approximation schemes proposed here is an alternative to the state-selective multireference coupled-cluster method and can be used as standalone approximation or combined in any way desired. In Sections 7 and 2.2.2 we found that extending the generalized active space coupled-cluster method to the fully relativistic framework has increased the computational cost of running calculations with this method significantly. To extend the applicability of the method to larger systems a sensible set of approximations to reduce the cost of calculations without compromising the accuracy has been introduced, although not yet numerically tested. The aim here has been to utilize the generalized active space concept to reduce the number of high excitation operators in the cluster operator, to include the expensive of spin-orbit as efficient as possible and going to more than one heavy center. The methods will here only be discussed since no numerical investigation of these has so far been undertaken.

8.1 Restriction of Kramers Flip

The inclusion of spin-orbit in a rigorous fashion has lead to a cluster operator which does a flipping of the Kramers projection as shown in Section 2.2.2. This has greatly

increased the number of amplitudes but also the equation length of the coupled cluster amplitude equations discussed in Section 7. Since the cluster operators with $\Delta M_k \neq 0$ is introduced to describe the spin-orbit coupling an approximation in the truncation of the cluster operator not only in the regular excitation hierarchy but also in the Kramers flip so

$$|\Delta M_k| < M \tag{8.1}$$

where M is the truncation in the cluster hierarchy is here proposed. A reduced coupling scheme for the spin-orbit contribution where the maximum Kramers flip is reduced would eliminate the higher excitation operator with large Kramers flip that appears in the state-selective multireference coupled-cluster method. One would here then still retain the most important amplitudes but get a significant reduction in the number of amplitudes and connections and the simultaneous truncation in the projection manifold. This could appear to be a promising way to go since in CC theory we do not get the exact amplitudes until the limit of FCC is reached and the change in the remaining amplitudes introduced by the operators with the very high Kramers flip is expected to be very small. At $\pm\Delta M_k = 2$ the most important one- and two-electron spin-orbit contributions will be in. From Eq. 2.74 we see that truncation the cluster operator at $\pm\Delta M_k < M$ we conserve the time reversal properties of the coupled-cluster wave function since an eliminated amplitude and its time reversed conjugate is simultaneously removed. This type of approximation is implemented but not yet explored. An input example can be found in Section 6.4.3 of this approximation.

8.2 CC(n_m)

The starting point for the GAS is the single-reference coupled-cluster theory which divides the spin-orbital space into a hole- and a particle-space where the cluster operator creates holes in the former and particles in the latter. These spaces we will abridge to HS for hole space and PS for particle space.

The HS and PS may now in the GAS approach be further subdivided as shown in Figure 8.1. Here the most physically intuitive division has been shown where the orbitals

has been divided into 6 subspaces but where only 4 of these are included in the correlation step[1]. It is in this division made possible to exclude the inner core and the very high-lying virtual Kramers pairs which is something that is usually done in at least heavy element calculations. The active holes are here denoted HS-1 and inactive HS-2. HS-1 will then typically contain Kramers pairs which contributes most to the non-dynamical correlation like the valence electrons (or at least part of them) and HS-2 will then contain the outer-core/inner-valence electrons where static correlation is of less importance. The particle space is likewise divided into an active particle space PS-1 and an inactive particle space PS-2. PS-1 will then contain the unoccupied Kramers pairs which gives the strongest correlation effect for HS-1 and PS-2 will then contain the remaining inactive virtuals.

The cluster operator and thereby also the projection manifold may now be truncated by setting restrictions on the minimum and maximum accumulated number of holes and particles created in each subspace. For an example of such truncations of the cluster operator one could imagine using the following restrictions: HS-2 a maximum of two holes, HS-1 a maximum of 6 holes, PS-1 a maximum of 6 particles and PS-2 a maximum of 2 particles. This would following the CC(n_m) notation be a CC(8_2) calculation where n is the maximum number of hole indices[2] and m is the maximum number of inactive particle indices. This notation work fine as long as the number of active/inactive indices are the same for the hole- and particle spaces. Since there will not be discussed any calculations here where this is not the case the author will refrain for trying to find a general notation for all GAS setups.

Doing a CAS calculation with two external indices i.e. a state-selective multireference coupled-cluster single doubles for the system shown in Figure 8.1 the restrictions would be as follows: HS-2 a maximum of two holes, HS-1 a maximum of 10 holes, PS-1 a maximum of 10 particles and PS-2 a maximum of 2 particles. This would then be a CC(12_2) calculation. Instead of doing a complete expansion in the active space an incomplete expansion like the CC(8_2) could then be employed instead. Making an incomplete expansion of the formal modelspace is exactly what the CC(n_m) approximation aims at doing. The advantage of the CC(n_m) approach is that it eliminates the highest excitations

[1]Notice this elimination of inner core and high-lying virtuals is in fact done in the integral transformation step. These are here only included to show that we do not correlate all electrons for heavy elements.

[2]Equal to the maximum excitation level.

Figure 8.1: Example of a division of the hole and particle space into active and inactive hole and particle spaces for the generalized active space coupled cluster

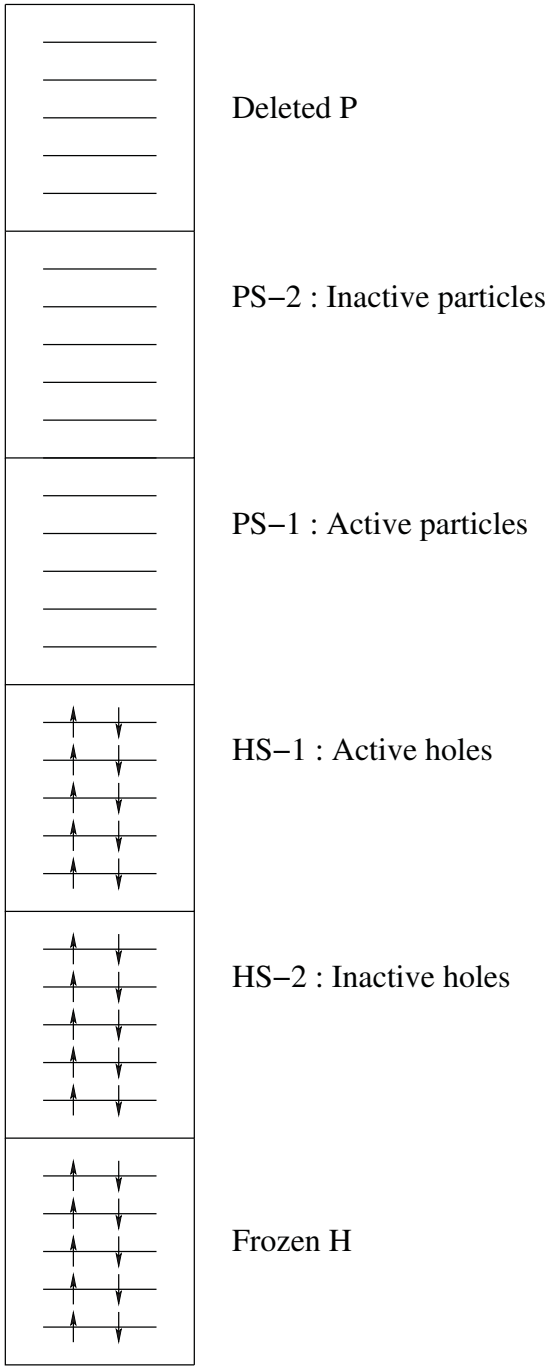

in the cluster operator thereby significantly reducing the number of amplitudes but also reducing the size of the vector function associated with increases in the excitation level. This type of approximation has in the non-relativistic framework shown to be very good and to come close to the state-selective multireference coupled-cluster method for both ground and excited states [5,118] and is therefore expected to carry over to the relativistic framework.

The CC(n_m) approximation is immediately available for a generalized active space coupled-cluster program, just like the state-selective multireference coupled-cluster method, since the division of holes and particle spaces and arbitrary excitations between them is possible. Further approximations like dividing the active hole and particle space into two and having different number of holes and particles in these could be another way to eliminate most of the highest excitations in both the CC(n_m) approximation and in the state-selective multireference coupled-cluster method. Another variant where only one hole is allowed in the inactive hole space and two particle in the inactive particle space has been used in the MRCI calculations for RbYb and $(RbBa)^+$ calculations shown in Sections 9.4 and 9.5, respectively. In this way one get the polarization of the outer-core (inactive holes) and correlation of the valence electrons (active holes). Due to the great flexibility of the generalized active space approach many more divisions of suborbital spaces could be envisaged which could be directly aimed at a specific system. The numerical experience with many of these setups still remain largely unexplored and larger systematic studies of this would in the future be necessary.

8.3 Mixed Core-Valence Correlation Approximations for Generalized Active Space Coupled-Cluster Method

I will now discuss approximation is primarily aimed at multiple heavy center calculations where there are many electrons in the inner-valence/outer-core and at the same time a need for a multireference expansion of the valence electrons. It can however just as well be used in somewhat larger molecules where one would also have many core electrons which would have to be correlated to achieve highly accurate results.

The approximation stems from the realization that for accurate spectroscopic values

the outer-core electrons will have to be correlated as shown for LiCs and BiH in Sections 9.3 and 9.2, respectively. The outer-core correlation, however, rarely needs a higher than doubles for the error to be smaller than the error remaining from the basis set or correlation of the valence electrons, see Section 9.6 for the importance of outer-core correlation. This combined with the fact that the Kramers pairs included in the first particle space (PS-1) is usually the most important correlating orbitals for the first hole space (HS-1) but not for the second hole space (HS-2) and higher combined excitations of (HS-1) and (HS-2) is also small. What this approximation seeks to do is eliminate combined high excitation from the first and second hole space to the first and second particle space since these will grow dramatically if one has a large HS-2 and at the same time many orbitals in PS-1 and PS-2. This is a case one will often encounter in heavy element calculations with multiple heavy centers and half filled shells. With this approximation it should be possible to get the outer-core contribution without having to truncate the higher excitations for the valence electrons in HS-1 and compromising on the accuracy. In case double excitations from the core should not suffice the approximation is implemented in a systematic way so higher excitations from HS-2 can the be included.

While the CC(n_m) approximation truncates not only the higher excitations of the outer-core electrons but also the much more important valence electrons and still retains many of the combined high excitations from HS-1 and HS-2 to PS-1 and PS-2 this approximations seeks to eliminate the latter while still having higher excitations in the valence space. This means a step away from the input based on the accumulated number of electrons to a post selection of cluster operators. The approximation presented here these combined excitations between hole and particle spaces can also be eliminated for the CC(n_m) approximation.

An example for such an approximation could be done for the Bi dimer where it would be expected that for an accurate description one would put the $5d$ in HS-2 and the occupied $6s6p$ in HS-1 and the unoccupied $6p$ in PS-1. With this division it is seen that a state-selective multireference single doubles would correspond to a CC(8_2). While with a CC(n_m) approximation this could be reduced to a CC(7_2) to a CC(3_2) the question of whether it is sensible to reduce the higher excitations in the formal incomplete model space remains. The problem with the CC(n_m) approximation is that the important higher excitations in the valence space are being truncated and the highest excitations will still

contain double excitations from the outer-core. These will only give a minor contribution but will dominate the calculation time since the number of electrons in the outer-core is large and many virtuals will have to be included in PS-2. These higher excitations where there are double excitations from the outer-core therefore need to be eliminated to make calculations like these tractable. The higher excitations in the formal model space (complete or incomplete) will however be sought to be retained. This will be done by setting a limit on how high an excitation a HS-2 index can occur. By setting this at $R < 8$ then the highest excitations with mixed core-valence indices in the CC(8_2) will disappear and thereby significantly reduce the number of amplitudes and contractions. In this way we can retain the high excitations in the formal model space and at the same time eliminate the highest excitations without much loss on accuracy. This approximation is then equal to neglecting core-valence correlation of the highest excited configurations of the formal model space which is expected not to significantly influence all other well separated configurations in the formal model space. Since we would rarely try to calculate many excited states in the formal model space the restriction R would then likely most often be set to four since at least all doubly excited configurations in the formal model space would then have core-valence correlation included.

8.4 Summary and Outlook

In this chapter three separate approximations have been presented. The reduction in the Kramers flip of the cluster operator, the incomplete formal model space approach (CC(n_m)) and an approximation for the core-valence correlation in the model space. The three approximations is programmed so they can be used in combination or as standalone approximations and will all have a different way of eliminating cluster operator with a high excitation level. Elimination after ΔM_k will be suitable of if spin-orbit is small while the CC(n_m) approximation will be important if we are dealing with a large formal model space and reduction in the core-valence correlation will be essential for multiple heavy centers or larger systems.

Chapter 9

Calculations

The implemented generalized active space coupled-cluster method presented over various chapters in this thesis have been applied to a variety of dimers. The objective has been to determine spectroscopic and electric properties of the ground state and to provide benchmark data for more approximate methods such as MRCI. While the applications can be grouped into two namely the *p*-block elements, as presented in Sections 9.1 and 9.2, and ultracold molecules, shown in Sections 9.3, 9.4 and 9.5, the methods used for these have varied a great deal. I have here decided to group the sections after molecule and not after method used. The methods used will become clear in the individual sections where the discussion will also contain performance of methods but not the methods themselves. All methods implemented in Sections 6.1, 6.2 and 6.3 are employed in the calculations. For the RbYb and $(RbBa)^+$ molecules the parallel MRCI code [131] in `DIRAC` [57] has been used for the excited states.

The performance of the spin-free generalized active space coupled-cluster method is presented along with the LiCs calculations in Section 9.3. Coupled cluster based on configuration interaction expansions is shown together with result on HBr in Section 9.1 and the commutator driven coupled-cluster calculations has been performed on BiH in Section 9.2. The calculations on RbYb (Section 9.4) and $(RbBa)^+$ (Section 9.5) the calculations have been carried out using the parallel MRCI code LUCIAREL [72, 73, 131] and the RELCCSD code [74,125] and been pure application projects. The final application in Section 9.6 is an examination of the importance of including lowerlying electrons in the correlation calculation and the basis set requirements that follows from it.

9.1 HBr

We presented the initial implementation of a determinant-based general-order coupled-cluster method which fully accounts for relativistic effects within the four-component framework in Section 6.2. The method opens the way for the treatment of multireference problems through a state-selective expansion of the model space. The evaluation of the coupled-cluster vector function is carried out via relativistic configuration interaction expansions. The implementation is based on a large-scale configuration interaction technique, which may efficiently treat long determinant expansions of more than 10^8 terms. We demonstrate the capabilities of the new method in calculations of complete potential energy curves of the HBr molecule. The inclusion of spin-orbit interaction and higher excitations than coupled cluster double excitations, either by multireference model spaces or the inclusion of full iterative triple excitations, lead to highly accurate results for spectral constants of HBr.

9.1.1 Introduction

In this section, we present the first relativistic general-order coupled cluster method which moreover is capable of treating multireference problems and molecules with an arbitrary number of unpaired electrons. The essential idea is to generalize a non-relativistic variant of state-specific MRCC to the relativistic formalism, which retains the advantages of the single-reference approach and which allows for a flexible definition and robust treatment of MR expansions.

In the Section 3.1.5 we have reviewed this state-selective multireference approach and in Section 2 the underlying relativistic theory of our implementation. Sections 2.1.3 and 6.1 give a detailed account on the implementation of the method, and in Section 9.1.2 we present an initial application. We unfold some of the capabilities of the new method in this application. Some aspects, however, like the treatment of a large number of unpaired electrons in the reference state, have been demonstrated successfully with the non-relativistic precursor method [4] and for the relativistic case will be left for future work.

9.1.2 Application to the HBr Molecule

To demonstrate that our newly implemented method is operational and to outline its potential we discuss an initial application to a diatomic molecule and calculate full potential energy curves of the ground state at various levels of theory and computational demand. This investigation therefore does not aim at highest precision for the obtained quantities.

9.1.2.1 Objective and Setup

The spectroscopic properties of the HBr molecule are significantly influenced by relativistic effects and electron correlation. Furthermore, this molecule is heavy enough to elucidate these effects and small enough to keep the computational demand of this pilot study limited. In particular, we investigate the importance of spin-orbit interaction by comparing with the 4-component spin-orbit free formalism of Dyall [64]. In work published [30, 132] we have interfaced the original non-relativistic CC program to this 4-component spin-orbit free formalism. Here, the transformed molecular integrals are structurally equivalent to a set of integrals in a scalar relativistic (one-component) framework such as the Douglas-Kroll-Hess formulation [133–135], but the Hamiltonian for obtaining the integrals remains 4-component. The corresponding CC calculations are thus based on non-relativistic point-group symmetry. Moreover, a proper description of the dissociation of the molecule requires the inclusion of higher excitations, which are studied also by exploiting multireference approaches. We finally compare our results to MRCI calculations carried out with the spin-orbit free program `LUCITA` [66] and the fully relativistic program `LUCIAREL` [72, 73] where the same basis sets and active orbital spaces are used as in the corresponding CC calculations.

We use two different uncontracted basis sets, in the following denoted as DZ and TZ. The smaller set DZ consists of the sp-pvdz set from the MOLFDIR suite in the DIRAC program package [136] for Br ($15s12p6d$) and H ($4s1p$). The larger set TZ is the relativistic finite nucleus optimized triple zeta basis set including valence-correlating functions for Br ($23s16p10d1f$) and the cc-pVTZ of the `MOLCAS5` package [137] for H ($5s2p1d$). Virtual orbitals beyond an energy of 10 a.u. are discarded which does not comprise a mentionable approximation here. All calculations are performed with the Dirac-Coulomb Hamiltonian, i.e., without two-electron contributions of spin-other-orbit

type (Gaunt term). As Visscher et al. [138] have shown for HBr, the influence of these lacking terms on the properties studied here is at least one order of magnitude smaller than the errors we will discuss.

We correlate 6 and 8 electrons occupying $\sigma_{1/2}$, a $\pi_{1/2}$, and a $\pi_{3/2}$ orbital formed from the atomic valence orbitals of Br ($4p$) and H ($1s$), and in addition Br ($4s$) in the case of 8 electrons, respectively, in the reference state. A spin-orbit free benchmark calculation including the Br d electrons (18 electrons in total) and full triple excitations is also carried out to elucidate the effect of core-electron correlation. A fully relativistic CCSDT with 18 correlated electrons is feasible in principle with our current implementation, but has not been carried out due to extensive memory and computing time requirements. We perform single-reference (SR) and multireference calculations, where the latter are defined by a Complete Active Space (CAS) expansion with 6 (8) electrons in 4 (5) orbitals. The correlating orbital is the antibonding $\sigma^*_{1/2}$ with bromine and hydrogen contributions. All calculations are performed in the (double) point group $C^{(*)}_{2v}$.

9.1.2.2 Results and Discussion

The results for the equilibrium bond length, the harmonic vibrational frequency, and the dissociation energy for various CC models and Hamiltonians are compiled in Table 9.1. The molecular bond is well described at all computational levels with very small deviations from experiment. For both basis sets the multireference treatment stretches the bond as does the inclusion of higher excitations in the calculation including full iterative triples (CCSDT) and MR models (MRCCSD). The same stretching is observed when spin-orbit interaction is included which is due to a weakening of the bond by a reduced σ-bonding character of the bonding valence p orbital on bromine. Increasing the basis set from DZ to TZ reduces the bond length and brings it closer to the experimental value. Correlating the $4s$ electrons results in a slight stretching of the bond which is compensated when the Br d electrons are included (CCSDT (18)). The bond contraction is caused by allowing for excitations out of the diffuse Br d orbitals. Spin-orbit coupling will lead to a bond elongation which almost exactly compensates for the final minute deviation of -0.0002 Å from the experimental value. However, we expect that the error from basis set incompleteness or the basis set superposition error (BSSE) with the TZ set are in the same order of magnitude.

Table 9.1: Spectral constants of HBr using various CC models and the corresponding CI models with (SO) and without (SOF) spin-orbit interaction, single-reference and multireference (MR), and correlating (n) electrons.

Method	R_e [Å]	ω_e [cm^{-1}]	D_e [eV]
DZ SOF CCSD (6)	1.4148	2705.7	4.19
DZ SOF MRCISD (6)	1.4164	2693.7	3.86
DZ SOF MRCCSD (6)	1.4162	2691.1	3.88
DZ SO CCSD (6)	1.4153	2697.8	4.05
DZ SO CCSDT (6)	1.4159	2690.8	3.74
DZ SO MRCISD (6)	1.4173	2678.7	3.72
DZ SO MRCCSD (6)	1.4173	2685.2	3.73
TZ SOF MRCISD (6)	1.4145	2675.1	4.04
TZ SOF MRCCSD (6)	1.4148	2675.1	4.05
TZ SO MRCISD (6)	1.4151	2668.4	3.90
TZ SO MRCCSD (6)	1.4154	2668.0	3.90
TZ SOF MRCISD (8)	1.4180	2641.4	3.90
TZ SOF MRCCSD (8)	1.4192	2637.1	3.90
TZ SOF CCSDT (8)	1.4178	2647.3	3.96
TZ SO MRCISD (8)	1.4187	2634.9	3.77
TZ SO MRCCSD (8)	1.4193	2630.6	3.76
TZ SOF CCSDT (18)	1.4142	2663.9	4.01
TZ SOF CCSDT (18) $+\Delta_{SO}$	1.4143	2657.4	3.77
Exp. [139]	1.41444	2648.975	3.92
apVTZ SO CCSD(T) (26) [140]	1.408	2706	3.92

For most of the calculations, an elongation of the bond is accompanied by a reduction of the harmonic frequency. The multireference methods produce in general somewhat lower harmonic frequencies than the corresponding single-reference method. Spin-orbit coupling reduces the harmonic frequency by 7 cm^{-1} in the TZ basis and by 6 cm^{-1} in the DZ basis. In the strive for harmonic frequencies with an accuracy of a few cm^{-1}, spin-orbit coupling is thus required even for a closed-shell molecule like HBr.

Whereas the difference between MRCI and MRCC calculations is negligible for the small number of 6 correlated electrons, it becomes more pronounced when 8 electrons are correlated, and here the harmonic frequency is the property which is most affected (-4 cm^{-1}). The error of 15 cm^{-1} observed for the SOF CCSDT (18) calculation is explained to a large part by the neglect of spin-orbit interaction, and finally also by basis set incompleteness or the BSSE which increases the harmonic frequency.

The largest differences between the various calculations are observed for the dissociation energy. Clearly, single-reference CCSD treatments do not yield satisfactory results as they give too high energies for the separated atoms. The multireference calculations decrease the dissociation energy significantly. We illustrate the effect of the multirefer-

Figure 9.1: Potential curves of the ground state of HBr neglecting (SOF) and including (SO) spin-orbit interaction. The energy offset is -2605 E_H.

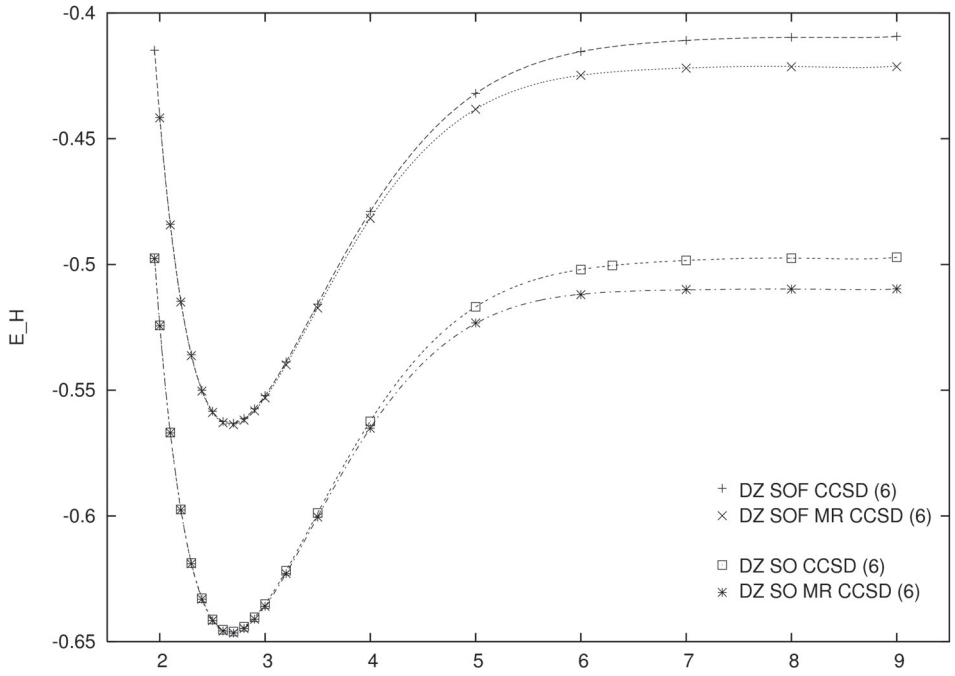

ence treatment on full potential curves in Figure 9.1 where the difference between the single- and multireference methods becomes obvious. The inclusion of higher excitations can of course also be achieved by increasing the general excitation level to full triples, as shown in Table 9.1. This calculation is more expensive computationally, though, than the MRCCSD run and does not give a higher accuracy. Addressing spin-orbit interaction, the decrease in dissociation energy has two sources: First, as already mentioned, there is a bond weakening due to the increased π character of the bonding spinor, and second, the spin-orbit splitting lowers the energy of the bromine ground state in the atomic limit. The latter effect is the dominating.

The dissociation energy varies strongly with the extent of the basis set and the number of correlated electrons. Clearly, for obtaining the right answer for the right reason, a large basis set has to be used and at least 18 electrons have to be correlated. The dissociation energy resulting from the TZ SOF CCSDT (18) calculation is too high by roughly 0.1 eV. The increase of the dissociation energy through core-electron correlation is also found by Styszyński [140] at the CCSD(T) level (see also Table 9.1 for one reference calculation). However, spin-orbit interaction (as reported here) and a counterpoise correction [138] decrease the dissociation energy in this order of magnitude.

For a final comparison with experiment, we add a spin-orbit shift ($+\Delta_{\mathrm{SO}}$) to the properties obtained with the TZ SOF CCSDT (18) model which is the difference between the values with and without spin-orbit interaction at TZ MRCCSD(8) level. The bond length and vibrational frequency are now in excellent agreement with experiment, but the dissociation energy is slightly too low most likely due to remaining correlation (number of electrons) and basis set errors.

All of the calculations have been performed in serial on a Linux cluster equipped with Pentium IV Xeon 2.4 GHz processors, except for TZ SO MRCCSD(8) for which we required a machine with more core memory (IBM Regatta Power 4+). A single-point calculation at TZ SO MRCCSD(6) level which included about 36×10^6 terms in the extended CI space finished in one to two days with an allocation of roughly 3 GB of core memory. The spin-orbit free calculations TZ SOF CCSDT(18) were slightly less demanding, computationally. When correlating 8 electrons including spin-orbit interaction (TZ SO MRCCSD(8), 224×10^6 terms in the extended space) the demand increased to 1 week runtime and roughly 12 GB of allocated core memory.

9.1.3 Conclusions and Outlook

We present the initial implementation of a fully relativistic CC method which allows for multireference expansions and higher than CC double excitations. The current version is very general with respect to the definition of multireference spaces by means of the GAS technique, but it lacks optimal efficiency due to the CI-driven CC vector function evaluation. In a showcase application we demonstrate its applicability in the dissociation problem of the HBr molecule. Here, we show the effect of including spin-orbit interaction and higher excitations in calculations of full potential energy curves of the electronic ground state. When using multireference expansions and a basis set of triple-zeta quality, the final results for spectral properties of the molecule are in close agreement with experiment. The method is prepared for the application to heavy-element systems with a large number of open shells such as small actinide molecules.

For the treatment of systems where a large number of electrons needs to be correlated, i.e. exceeding about 10 to 12, the efficiency bottleneck forces us to alter the algorithm for evaluating the CC vector function. In current work, we are generalizing a commutator-driven evaluation of the CC vector function as implemented for the non-relativistic case by Olsen [99] to the relativistic framework. This method will exhibit the optimal scaling of $O^n\,V^{n+2}$ as do conventional CC implementations and will open for the more accurate treatment of heavy-element compounds with a large number of correlated electrons and extensive basis sets.

The Kramers-restricted approach pursued here does not account for the time-reversal symmetry relations between CC amplitudes. We are currently exploring the implementation of various schemes for accounting for time-reversal symmetry at the many-particle level in general open-shell CC theory. A fully Kramers-symmetry adapted formulation entails a non-commuting CC formalism and will be implemented for a newly-developed suite of general contraction methods [99] including CC models.

We are furthermore exploring the calculation of excited states of different double group symmetry representation than the ground state, where a re-definition of the Fermi vacuum via relativistic MCSCF calculations yields the desired reference state. For the calculation of excited states of the same symmetry as the ground state, we are considering an initial implementation of linear response theory as it is utilized in the `DIRAC` program

package for Hartree-Fock and MCSCF wave functions.

9.2 BiH

In this section we present the initial calculations of a string-based general-order coupled-cluster method which fully accounts for relativistic effects within the four-component framework. This method opens the way for the treatment of multireference problems through a state-selective expansion of the model space as described in Section 3.1.5. The evaluation of the coupled-cluster vector function is done by considering contractions of elementary second quantized operators, see Section 6.3. The capabilities of the new commutator-driven coupled-cluster method is demonstrated on BiH where the effects of multireference expansions with both doubles and triples excitations into the virtuals plus the regular coupled-cluster hierarchy up to full quadruples are compared. The importance of core-correlation is shown for accurate calculations.

To demonstrate our newly implemented correctly scaling coupled-cluster code we have chosen the BiH molecule. In a Russel-Saunders coupling picture the electronic ground state is the 0^+ component of a $^3\Sigma^-$ state with $\sigma^2\sigma^2\pi^2$. Since Bi is a heavy element, a $j-j$ coupling scheme might be more appropriate where the lowest occupation would correspond to a $\sigma^2_{1/2}\sigma^2_{1/2}\pi^2_{1/2}$ configuration, but also smaller contributions from $\sigma^2_{1/2}\sigma^2_{1/2}\pi^2_{3/2}$ and $\sigma^2_{1/2}\pi^2_{1/2}\pi^2_{3/2}$ are to be expected. Here we will show that we can calculate with various GAS setups but also can go beyond the first reported CI-driven coupled-cluster method in [70] and Section 9.1 to real production calculation with many electrons and large basis sets for heavy elements.

9.2.1 Objective and Computational Details

The spectroscopic properties of BiH are influenced by both relativity and electron correlation. As will be seen, the number of electrons correlated is also of significant importance. Additionally one would expect that a multireference expansion which includes the remaining unoccupied $6p$-orbitals on BiH would give a better description along the potential curve. This indicates that BiH would be a good candidate for a show case calculation where significantly higher accuracy than previously possible can be achieved. The aim,

however, has not been to go to maximal accuracy but still to demonstrate a significantly improvement in the correlation step in comparison to previous codes [70].

We have throughout used an uncontracted cc-pVTZ from the MOLCAS6 package [46] for H ($5s2p1d$) and an uncontracted cc-pCVTZ from [141,142] for Bi ($30s26p17d13f1g$). The truncation of the virtual spinors has in one set of calculations been set at 5.6 E_h and another higher one at 27 E_h, where in the latter all correlating functions for the ($5d$) on Bi have been taken into account in the correlation step. All spinors beyond these cutoffs are discarded in the correlation step since these will primarily be core correlating. All calculations presented have been performed with the Dirac-Coulomb Hamiltonian and all correlation calculations have been started from a closed-shell Dirac-Fock calculation.

We performed calculations in which either 6 or 16 electrons were correlated. In the former the 6 electrons occupying a $\sigma_{1/2}$, a $\sigma_{1/2}$ and a $\pi_{1/2}$ orbital formed from the atomic valence orbitals of Bi ($6s, 6p$) and H ($1s$) are correlated. In the calculations correlating 16 electrons the ($5d$) on Bi has also been included. Both single-reference and multireference calculations were carried out where in the latter a Complete Active Space (CAS) CC expansion with 6 electrons in 5 Kramers pairs ($\sigma_{1/2}\sigma_{1/2}\pi_{1/2}\pi^2_{3/2}\pi^2_{3/2}$) was performed. In principle the same approximative scheme to the full CAS as shown in [118] with the CC(n_m) approximations (see Section 8.2) could be used. This type of approximations would, however, go beyond the scope of an initial application. In the 16 electron case the calculations have been restricted to singe-reference calculations but the full iterative triples have been included for a CCSDT calculation.

9.2.2 Results and Discussion

The results for the equilibrium bond length and the harmonic frequency for the various CC models and number of electrons are compiled in Table 9.2. It is seen that for both 6 and 16 electrons correlated the effect of increasing the correlation level is smaller than expected with only a change in the bond distance in the third digit after the comma. The change in harmonic frequency is around 13 cm^{-1} going from CCSD to CCSDTQ with 6 electrons correlated. For 16 electrons correlated the change is slightly larger with 17 cm^{-1} from the CCSD to the CCSDT model for both levels of truncation of the spinors in the virtual space. The usual trends for a covalent bond is observed, in the regular CC

hierarchy, in the 6 electrons case with the slight increase in bond length with increased correlation and the simultaneous decrease in harmonic frequency due to the better long range description. In the 16 electrons case a similar trend is found when comparing CCSD and CCSD(T)/CCSDT results, however, when going from CCSD(T) to CCSDT only a minimal difference in the spectroscopic values is observed.

Going from single-reference to the state selective multireference model one observes the expected trend with a longer bond length and lower harmonic frequency. The difference is here larger when going from CCSD to the MRCCSD(6in5) than going from CCSDT to MRCCSDT(6in5) which is to be expected. The MRCCSD(6in5) seems to overestimate the importance of the unoccupied p-orbitals and thereby produce a too long bond and too low in frequency. Something that is corrected by the MRCCSDT(6in5) or the CCSDT which yields results that are almost identical to the CCSDTQ result despite only have one fourth or one-twentieth of the amplitudes, see Table 9.3.

The most noticeable change in the spectroscopic values occurs when going from 6 to 16 electrons correlated. Here we observe a large contraction of the bond of around 0.03Å and an increase of about 25 to 30 cm^{-1} in the harmonic frequency depending on the model chosen for the low cutoff of the virtual spinors. In the 6 electrons case we find that the harmonic frequency is a little too low whereas it is slightly too high when correlating 16 electrons with the low cutoff if the experimental value is taken to be 1699 cm^{-1} [155] (see Table 9.2). Increasing the number of correlated electrons the bond length at the same time goes from being 0.01Å longer than the experimental ones of around 1.81Å to being 0.02Å shorter. The problem here is likely due to the $5d$ electrons on Bi which can cause larger bond contractions even if the used basis sets are of the same quality (see Sections 9.6 and 9.3). The outcome from this is a noticeable BSSE when correlating the lowerlying d electrons on Bi. This would in parts explain the large contraction of the bond and the increased harmonic frequency with the low cutoff. This imbalance is expected to diminish with increased basis set size and, as can be seen, a higher truncation of virtuals which includes all correlating functions for the $5d$ electrons on Bi. With the higher truncation of the virtual spinors we see the bond length increases by around 0.01Å and the harmonic frequency decreases by around 10 cm^{-1}. The correction here is in the same direction as a counterpoise correction would be and thereby showing the need to include higher lying spinors. The inclusion of these additional spinors, however, comes at a steep price. When

Table 9.2: Spectroscopic properties of the BiH molecule with different approaches and various excitation levels in coupled-cluster treatments using the uncontracted cc-pCVTZ basis set [141, 142] for Bi and an uncontracted cc-pVTZ [46] for H. For the calculations marked with * the truncation of the virtual spectrum has been performed at 27 E_h and the rest at 5.6 E_h. The second column (corr. el.) denotes the number of explicitly correlated electrons.

Method	corr. el.	R_e[Å]	ω_e [cm^{-1}]
CCSD	6	1.8225	1691.2
CCSD(T)	6	1.8241	1681.9
CCSDT	6	1.8245	1678.7
CCSDTQ	6	1.8246	1678.1
MRCCSD(6in5)	6	1.8261	1673.5
MRCCSDT(6in5)	6	1.8247	1677.8
CCSD	16	1.7919	1721.7
CCSD(T)	16	1.7934	1704.6
CCSDT	16	1.7932	1704.3
CCSD*	16	1.8004	1713.2
CCSD(T)*	16	1.8030	1694.6
CCSDT*	16	1.8028	1694.2
CCSD(T)/MRCIS [143]	24/6	1.800	1716
CISD [144, 145]	6	1.90	1619
MRD-CI [146]	6	1.867	1632
SICCI [147]	6	1.868	1584
EXP. [148]			1635.73
EXP. [149]		1.811	1699.5
EXP. [150]		1.818	1677
EXP. [151]		1.819	1656.93
EXP. [152]			1699.517
EXP. [153]			1699.521
EXP. [154]		1.80867	1697.62
EXP. [155]		1.809	1698.9

Table 9.3: Number of amplitudes for a given calculation. For the calculations marked with * the truncation of the virtual spectrum has been performed at 27 E_h and the rest at 5.6 E_h. The second column (corr. el.) denotes the number of explicitly correlated electrons.

Method	corr. el.	Amplitudes
CCSD	6	47040
CCSDT	6	2326240
CCSDTQ	6	48909700
MRCCSD(6in5)	6	620677
MRCCSDT(6in5)	6	12870037
CCSD	16	374080
CCSDT	16	64191680
CCSDT*	16	259716240

looking at Table 9.3 we see the number of amplitudes for the CCSDT is four times larger for the high cutoff compared to the low cutoff of the virtual spinors. From large scale CI calculations it is known that increasing the basis set from TZ to the QZ can increase the bond length up to 0.01Å [131]. These calculation are, however, not directly transferable since these do not include all correlating functions for the 5d electrons on Bi but a small increase is, however, to be expected also for the coupled-cluster calculations. Although the primary goal of this study has not been to achieve highly accurate spectroscopic values we do see that including all correlating functions and increasing the excitation level we have obtained spectroscopic results that are in very good agreement with experiment.

9.2.3 Summary and Prospects

We present calculations from a newly implemented correctly scaling fully relativistic general-order CC method which also allows for doing state-selective multireference coupled-cluster expansion (see Section 6.3). The current version is completely general with the definition of the multireference expansion due to the GAS setup. Although the code can be used for production calculations it however still need optimization to be very efficient,

this goes in particularly when extending the number of GASs. This is, however, a significant step in comparison to the previously reported CI-driven CC method in [70] since both the number of correlated electrons and the basis set size can be significantly increased. At the present state with this new code it should be possible to routinely do calculations with more than 100 million amplitudes. Larger calculations with +500 million has also shown to be feasible on standard Linux clusters.

At the moment work is being done on extending the code to include also the complex groups so systems with lower symmetry can be handled. The possibility to start from a MCSCF [130] instead of a HF reference is also pursued since both options are included in the `DIRAC` [57] program package. This would be very significant when tackling more complex system like the actinides or other systems with open shell where a good reference is needed.

Calculations with the approximations such as a reduced coupling scheme for the Kramers flip and the CC(n_m) scheme of GAS setups are being investigated along with other approximation schemes to reduce the number of amplitudes and connections without compromising the accuracy.

9.3 LiCs

Aimed at obtaining complete and highly accurate potential energy surfaces for molecules containing heavy elements we present calculations from the general-order spin-free coupled-cluster method (see Section 3.1.5) which can be applied in the framework of the spin-free Dirac formalism presented in Section 2.1.3. As an initial application we present a systematic study of electron correlation and relativistic effects on spectroscopic and electric properties of the LiCs molecule in its electronic ground state. In particular, we closely investigate the importance of excitations higher than coupled cluster doubles, spin-free and spin-dependent relativistic effects, and the correlation of outer-core electrons on the equilibrium bond length, the harmonic vibrational frequency, the dissociation energy, the dipole moment and the static electric dipole polarizability. We demonstrate that our implementation shown in Section 6.1 allows for highly accurate calculations not only in the bonding region but also along the complete potential curve. The quality of our results is demonstrated by a vibrational analysis where an almost complete set of vibrational levels

has been calculated accurately.

9.3.1 Introduction

Research in the field of cold and ultracold molecules is currently exhibiting rapid progress and expansion [14]. Beyond groundbreaking applications as the production of Bose-Einstein Condensates (BEC) [156], the investigation of collision processes of atoms and molecules at ultracold temperatures is of key importance for the development of controlled reactions [16] and for the possibility of testing fundamental symmetries in nature, e.g. through measurements of the electron's postulated electric dipole moment (EDM) [17,18]. Heteronuclear alkali diatomics such as LiCs, KCs, NaCs, BaLi and selected molecules formed from alkali and lanthanide atoms (e.g. RbYb [11,157]) appear to be particularly suited for the study of dipole-dipole interactions and electric-field control [158] in the ultracold regime, since they exhibit large molecular electric dipole moments. Among these molecules, the largest dipole moment has been predicted for the LiCs molecule [159] with a value of around 5.5 D for the $^1\Sigma^+$ electronic ground state. Recently, ultracold LiCs molecules have been produced in the electronic ground state through photoassociation in a two-species magneto-optical trap [160]. Since then it has also been shown that it was possible to produce LiCs in the rovibrational ground state [161] and to perform spectroscopy on the excited states [162].

The understanding of collision processes requires the knowledge of accurate short-range (molecular) potential-energy curves. In a recent high-resolution Fourier-transform spectroscopical investigation [163], short-range potentials for the LiCs singlet and triplet ground states have been derived from experimental data and compared to the most recent ab-initio calculations [159] using configuration interaction (CI) theory. These calculations has been made with a large core pseudopotential. Therefore, the accuracy of the obtained spectral constants for the electronic states should be tested against high-level quantum-chemical calculations. Today, such high-accuracy electronic potentials for heavy-element molecules can be obtained by coupled cluster theory in fully relativistic all-electron calculations [70, 108].

Diatomic molecules formed from group 1 and group 2 atoms are characterized by electronic ground states with very small contributions from spin-orbit interaction. For

these Σ states, the dominating relativistic effects are instead scalar-relativistic contributions such as the mass-velocity and Darwin terms as also discussed in Section 1.2.1. These scalar relativistic effects are important for determining the shape and spatial extent of the orbitals and thereby the molecular bonding, and must therefore also be included for accurate descriptions of potential curves.

In this section, we present ground-state potential energy curves and molecular electric properties of the LiCs molecule by applying a relativistic general-order coupled cluster approach. The method [3, 4] has been interfaced to a local version of the relativistic 4-component program package `DIRAC` [57]. It is capable of treating scalar-relativistic effects on the basis of the 4-component spin-free Dirac equation through an exact separation of spin-free and spin-orbit contributions [64]. The spin-free formalism which we denote SFDC (Spin-Free Dirac-Coulomb) has previously been interfaced to CI approaches [27, 66] and is similar to scalar-relativistic methods like the Douglas-Kroll-Hess (DKH) approach [134,135] taken to the infinite order in its expansion parameter. Electron correlation can be treated at very high accuracy by the general-order CC implementation, and we report calculations up to the level of full iterative Triple (T) excitations, i.e. with the coupled cluster model CCSDT. Moreover, the implementation allows for simulating multireference expansions by including higher excitations within a selected internal one-particle space which lead to further improvements in the obtainable accuracy of the spectroscopic properties.

The work presented in this section covers the following aspects:

- We show that spin-orbit interaction is negligible in the ground-state properties of LiCs, and we discuss scalar-relativistic contributions to the bonding by comparing the calculated properties with a Lévy-Leblond (LL) Hamiltonian [33] to the spin-free Hamiltonian results.

- We study contributions from higher-order excitations systematically both in spin-free and spin-dependent calculations. The inclusion of the full iterative triples is discussed in spin-free applications. We furthermore discuss the influence of the number of correlated electrons and the counterpoise (CP) correction to correct for the basis set superposition error (BSSE).

- With an accurate potential curve obtained at the CCSDT level we perform a vibrational analysis and present the vibrational states. This is also compared with the vibrational states obtained from a CCSD(T) curve.

- Last, we calculate the ground-state dipole moment function and the static electric dipole polarizability and show the necessity of including higher-order excitations in the wave operator.

Particular emphasis in this section put on the CC determination of molecular properties for which accurate complete potential energy curves are required. The sections are structured as follows: In the following section, we describe the computational details of our study and refers to Sections 2 and 6.1 for theoretical and implementational aspects, respectively . We continue with the application section and finally conclude on the most important findings of this investigation.

9.3.2 Methodological and Computational Details

The type of CC implementation discussed here is described in detail in references [3, 4] for the non-relativistic case. The implementation supports arbitrary excitation levels up to Full CC expansions. The MR approach is based on the idea of retaining particle and hole spaces in the active one-particle space (State-Selective approach, see also [115] and Section 3.1.5). If we consider for example the multireference space which is important in the current context: three configurations which are obtained by exciting 0,1,2 electrons from a bonding orbital to an antibonding orbital. An active space is defined containing the bonding orbital as the occupied active space and the antibonding orbital as the unoccupied space. The dynamic correlation from the configuration with two electrons in the antibonding orbital is then included as fourfold excitations combining the double excitation from the bonding to the antibonding active orbitals with a general double excitation. In this fashion, a commutative operator manifold is retained leading to the simplifications of standard single-reference coupled cluster methods.

The current implementation evaluates the CC vector function using an approach based on string-manipulations [99] that is significantly more efficient than the one based on CI expansions (in [3, 4]) .

The CC vector function

$$f_\mu = \left\langle \mu \left| e^{-\hat{T}} \hat{H} e^{\hat{T}} \right| \mathrm{REF} \right\rangle$$

with μ the excitation manifold and $|\mathrm{REF}\rangle$ the reference state is determined by considering the joint evaluation of the Hamiltonian and the CC exponential on the reference state

$$\hat{H} e^{\hat{T}} |\mathrm{REF}\rangle .$$

This step can be carried out without resorting to excitation spaces beyond that of the excitation manifold of $\hat{T}$. This procedure leads to the same scaling of CC implementations as the traditional approaches containing explicit code for each excitation level.

The multireference coupled cluster presented here does not exploit the full potential of the implemented approach. The commutator-driven coupled-cluster presented in Section 6.3 can perform CC expansions which are based on ambiguous numbers of active spaces and their occupations. This allows for more general and elaborate correlation treatments, e.g. performing restricted instead of complete valence space multireference expansions.

9.3.2.1 Computational Details

A series of calculations using our new implementation within the `DIRAC` program package [57] has been performed to assess the contribution of scalar relativistic effects, spin-orbit coupling, and electron correlation on the bond distance, harmonic frequency, dissociation energy, permanent electric dipole moment and static electric dipole polarizability of the LiCs molecule. For the assessment of spin-orbit contributions we compare with results obtained with the `DIRAC` module `RELCCSD` [74, 125]. Restricted DCHF calculations, either in LL- or SF- approximation or without approximation, were used for the complete potential curves.

We employ an uncontracted ANO-RCC basis set from the *MOLCAS* [46] package containing {26s22p15d4f} functions on Cs and {14s9p4d3f1g} functions on Li for the large component. This basis set was chosen since it not only contains functions for an accurate correlation description but also diffuse functions to give accurate dipole moments with several exponents ranging from to 10^{-1} to 10^{-2} on both Cs and Li. Small component functions are obtained within the restricted kinetic balance prescription [77, 81]. The

effect of the small component is approximated by including Coulombic interaction of atomic small component densities [164]. The calculations are carried out by truncating the virtual orbital space at 17 au. unless stated otherwise. Orbitals above this threshold can be considered core correlating and therefore will only give a relative energy shift if the Cs atomic core electrons were correlated, but will have very little influence on the shape of the potential curves. The cutoff has been tested at the CCSD and MRCCSD level with 22 electrons correlated and found to be of sufficient accuracy. We correct for the basis set superposition error (BSSE) by applying a counterpoise (CP) correction [165]. The dissociation energies were obtained as the difference between the energy of the molecule and the energies of the isolated atoms, and the harmonic frequencies were obtained by numerical differentiation. The reduced mass has been calculated from the standard atomic weights.

The ground-state dipole moment was calculated by applying a finite electric field (see Appendix A) of varying strength along the bond axis (chosen as z). The field strengths chosen here were ± 0.001, ± 0.002, ± 0.004 au. From the seven points a polynomial fit to the total field-dependent energy was made to find the dipole moment at a given internuclear distance. All coupled cluster energies were converged to residual errors smaller by at least five orders of magnitude than the energy changes due to the external field. The static electric dipole polarizability was calculated along the bond $\alpha_{\parallel}$ in a similar fashion because in the case of LiCs the polarizability tensor is diagonal due to the high symmetry of the system. Being the second derivative of the applied electric field the accuracy of the polarizability is therefore lower than that of the dipole moment, but even more so because additional diffuse functions would have to be added to the basis set to obtain highly accurate values for this property. Since the static polarizability is only calculated along the bond the need for diffuse functions is diminished due to a sharing of the basis functions of the two atoms which would not be the case perpendicular to the bond. We therefore consider these accurate calculations of the parallel polarizability component $\alpha_{\parallel}$.

9.3.3 Results

9.3.3.1 Spectroscopic Properties

The chemical bond of the LiCs molecule can be described qualitatively by considering only the σ bond formed from the 6s orbital on Cs and the 2s on Li, resulting in a $^1\Sigma^+$ ground state. Correlation of the energetically close-lying Cs 5p and 5s electrons (10 electrons in total) will give a significant improvement on the description of the bond. Further improvement is expected when correlating the 1s electrons of Li (12 electrons in total) and for very accurate calculations also the outer-core 4d electrons of Cs (22 electrons in total) and including higher excitations in the wave function. The results are compiled in Table 9.4 and we will now discuss these in detail.

Table 9.4: Spectroscopic properties of the LiCs molecule with different approaches and various excitation levels in coupled cluster treatments using the uncontracted ANO-RCC basis set. LL denotes Lévy-Leblond, SF spin-free and no label denotes the fully relativistic Dirac-Coulomb Hamiltonian which includes spin-orbit interaction. cp- designates counterpoise corrected values. The second column (corr. el.) denotes the number of explicitly correlated electrons.

Method	corr. el.	R_e[Å]	ω_e [cm^{-1}]	D_e [eV]
DCHF-LL	0	3.9872	167.506	
DCHF-SF	0	3.9247	170.303	
DCHF	0	3.9244	171.084	
CCSD-LL	2	3.9017	189.197	0.8042
CCSD-SF	2	3.8548	175.169	0.7664
CCSD	2	3.8538	175.256	0.7667
CCSD-LL	10	3.7707	182.339	0.7150
CCSD-SF	10	3.7191	183.953	0.6822
CCSD	10	3.7180	184.183	0.6828
cp-CCSD	10	3.7300	183.593	0.6741
MRCCSD(10in6)-SF	10	3.7245	182.459	0.6910

Continued on next page

Table 9.4 – continued from previous page

Method	corr. el.	R_e[Å]	ω_e [cm^{-1}]	D_e [eV]
CCSD(T)-SF	10	3.6937	183.349	0.7188
CCSD(T)	10	3.6926	183.577	0.7194
cp-CCSD(T)	10	3.7063	182.923	0.7097
CCSDT-SF	10	3.6963	182.908	0.7200
CCSD-LL	12	3.7606	183.226	0.7111
CCSD-SF	12	3.7087	184.893	0.6781
CCSD	12	3.7075	185.004	0.6785
cp-CCSD	12	3.7199	184.550	0.6694
CCSD(T)-SF	12	3.6823	184.219	0.7217
CCSD(T)	12	3.6810	184.334	0.7222
cp-CCSD(T)	12	3.6952	183.810	0.7120
CCSDT-SF	12	3.6848	183.676	0.7235
CCSD-LL	22	3.7487	183.616	0.7217
CCSD-SF	22	3.6949	185.425	0.6896
CCSD	22	3.6937	185.549	0.6901
cp-CCSD	22	3.7174	184.659	0.6663
MRCCSD(22in12)-SF	22	3.6997	184.147	0.6988
CCSD(T)-SF	22	3.6667	184.787	0.7364
CCSD(T)	22	3.6655	184.917	0.7369
cp-CCSD(T)	22	3.6916	183.859	0.7115
CCSD+2g[1]	22	3.6925	185.914	
CCSD(T)+2g	22	3.6622	185.561	
Exp. [163]		3.6681		0.728
CIPSI [166]		3.615	187.1	
CIPSI [159]		3.604		0.717
MELD [167]		3.65	183	0.72

[1]Cs augmented with 2g functions with exponents of 0.555649375 and 0.28536000

9.3.3.1.1 Effects of number of correlated electrons The most striking trend in the system is the large bond contraction upon correlating the electrons. The trend shows up already including two electrons so we have studied this by using a low cutoff value for the virtual orbitals, employing a more elaborate correlation scheme allowed by the GAS setup, and a Mulliken population analysis, see Table 9.5. Our finding is that this decrease in bond length stems from moving density from predominantly the delocalized bonding orbital into the more diffuse and localized low-lying $3p_x$ and $3p_y$ orbitals on Li but not the $3p_z$ thereby making the molecule more ionic. Including all virtuals in the two-electron calculation however gives a too long bond and an overbinding which shows the need for core-polarization or correlation for accurate spectroscopic values as seen in Table 9.4.

While it appears to be relatively easy to obtain a qualitatively correct picture it is however significantly more difficult to get an accurate picture. In Table 9.4 the demand for correlating the energetically underlying electrons is evident due to the large contraction of the bond and change in harmonic frequency. By correlating 10 electrons the overbinding observed for the correlation of 2 electrons has disappeared. Correlating the 1s on Li has a smaller but still very significant effect.

The effect of outer-core correlation in general is small compared to the correlation effect as such though not negligible and about one tenth of scalar-relativistic contributions. At a first glance the correlation of the 4d on Cs seems more important than inclusion of the 1s on Li. However, after correcting for the BSSE it is found to be only up to one third

Table 9.5: Analysis of the decreasing bond distance and harmonic frequency from correlating 2 electrons.

Method	virtual space	R_e[Å]	ω_e [cm^{-1}]	D_e [eV]
CCSD-SF	σ^*	4.02	145.2	0.092
CCSD-SF	$\sigma^* 2p(Li)$	3.98	149.4	0.186
CCSD-SF	$\sigma^* 2p(Li) 3p(Li)$	3.77	181.5	0.548
CCSD-SF	$\sigma^* 2p(Li) 3p_x 3p_y(Li)$	3.73	184.7	0.439
CCSD-SF	$\sigma^* 2p(Li) 3p_x(Li)$	3.84	168.2	0.266
CCSD-SF	$\sigma^* 2p(Li) 3p_z(Li)$	4.01	152.5	0.226

Figure 9.2: Comparison of 10 and 22 electrons correlated at CCSD level. The shifted energies are given as $(total\ energy) + 7793.0\ E_h$ (CCSD 10) and $(total\ energy) + 7793.2025\ E_h$ (CCSD 22), respectively.

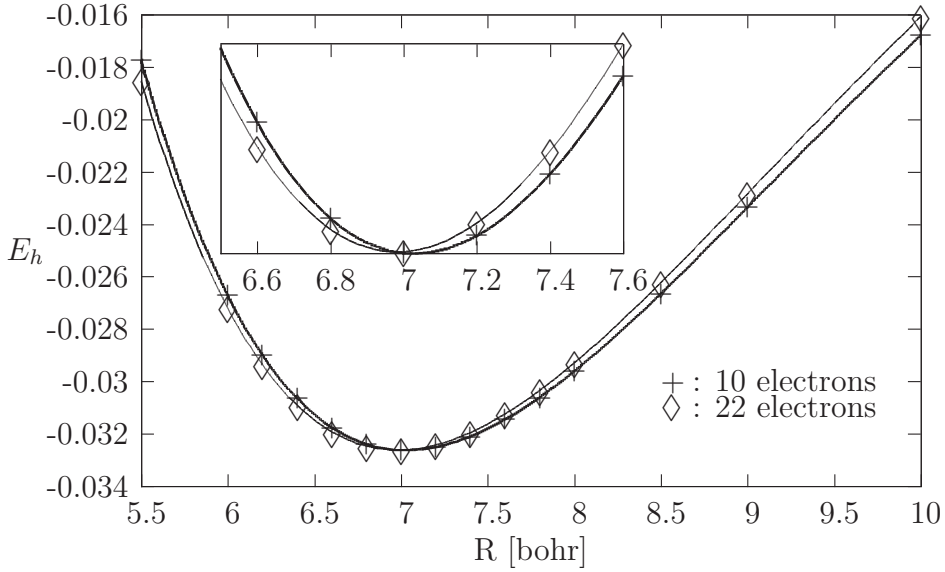

of the latter. Augmenting the basis set on Cs with 2 additional g functions does not seem to alleviate this rather large CP correction which primarily stems from the lack of core-correlating functions. The importance and saturation of the outer-core correlation on Cs is currently under investigation [168] and preliminary results are presented in Section 9.6. The effect, before a CP correction, on the shape of the potential curves and therefore also the harmonic frequency, is rather small around equilibrium but gives sizeable contributions at longer range, giving corrections of 1.3 cm^{-1}. This change is consistent with a slight increase in steepness of the potential curve when dissociating (see Figure 9.2). With the CP correction this visible difference disappears.

Had the dissociation energy been calculated by separating the atoms this overbinding for the 2 electrons case would not have been visible. We would then see an increase in the dissociation energy which can be explained by the better description of the system near the equilibrium bond distance compared to the separated atoms, an inequality which is engrained in any single-reference method, especially when it as here is based on a restricted DCHF determinant. Whereas the restricted DCHF determinant is the dominant part of the wave function at equilibrium, it is at dissociation only about 50 % of the wave function consisting of the two doublet atomic states coupled to singlet spin. This would make higher excitations very important not just for obtaining highly accurate complete potential curves but also for accurate dissociation energies. As the dissociation energies

are obtained from molecular energies at the equilibrium and the atomic energies, these are not affected by the erroneous dissociation of the restricted DCHF calculations. In fact, the atomic energies are in general more accurate than the molecular energies so the dissociation energies are in general expected to converge from below. The dissociation energy is, however, still strongly influenced by the level of correlation

and the CP correction. The trend in the dissociation energy with increased correlation level is here opposite of what is seen when calculating it from a curve since here the atomic calculations are better than the molecular ones, an artifact that diminishes with an improving description of electron correlation.

9.3.3.1.2 Relativistic effects in LiCs To assess and compare the magnitude of relativistic effects in LiCs three different approaches have been used. First, in order to find the non-relativistic energy a correlation treatment at the CCSD level using the Lévy-Leblond Hamiltonian has been carried out. For determining the scalar-relativistic contribution a spin-free calculation has been performed at the same correlation level. The effects of spin-orbit coupling have been investigated by comparing with corresponding results from `RELCCSD`. We report all these calculations correlating 10, 12, and 22 electrons in Table 9.4, so the importance of outer-core correlation can also be evaluated.

As expected, the bond is contracted considerably when including scalar-relativistic effects since the predominantly bonding 6s orbital on the Cs atom is contracted. At the non-relativistic level the potential curves are wider due to the larger spatial extent of the 6s on Cs. Hence, the harmonic frequencies are reduced by almost 2 cm^{-1} (see Figure 9.3). The dissociation energy is around 0.02 eV larger for the non-relativistic case than for the spin-free case. This is consistent with a Mulliken population analysis which shows an increase in the population of the 6s on Cs and subsequently a decrease of the 2s population on Li in the bonding orbital, and opposite for the antibonding, when going from the non-relativistic to the spin-free method around the equilibrium bond distance. The difference in dissociation energy then comes from the fact that the 2s on Li is lower in energy than the 6s on Cs. The inclusion of spin-orbit coupling on the other hand has, as expected, only little effect on any of the properties in question here which is clearly visible by comparing CCSD-SF and CCSD calculations from Figure 9.3 where the two curves are just horizontally linear displacements of each other. The very good agreement between

Figure 9.3: Comparison of the non-relativistic, the spin-free and the full relativistic curves at CCSD level with 10 electrons correlated. The shifted energies are given as (*total energy*) + 7561.623 E_h (CCSD-LL 10), (*total energy*) + 7793.0 E_h (CCSD-SF 10) and (*total energy*) + 7794.849 E_h (CCSD 10), respectively.

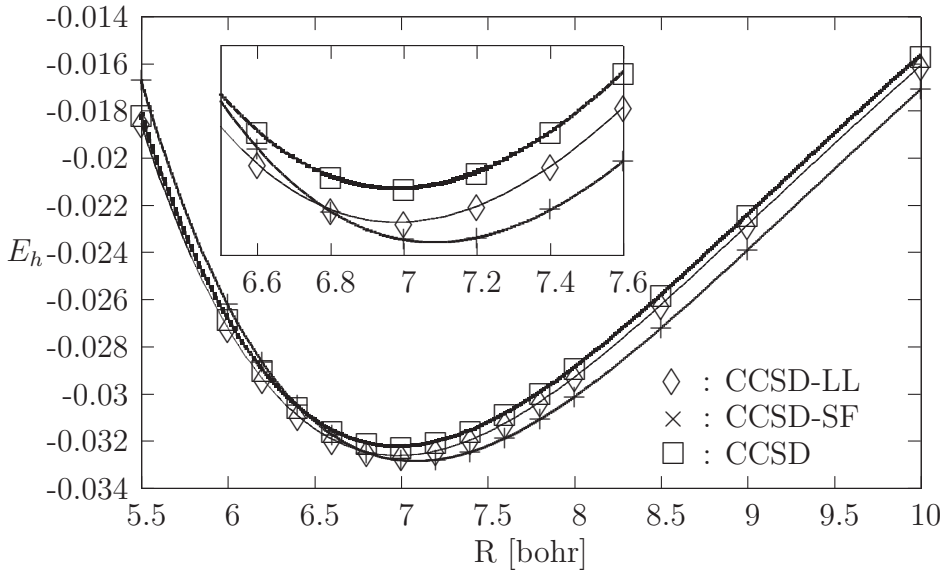

CCSD-SF and CCSD is explained since in the sense of perturbation theory, spin-orbit contributions only enter to second order by coupling of the $^1\Sigma_0^+$ ground state to excited triplet states.

9.3.3.1.3 Effect of higher correlation treatment The effect of more extensive correlation treatment will be examined under several aspects. First, the effect of increasing the excitation level from doubles (CCSD) to perturbative triples (CCSD(T)) and to the full iterative triples (CCSDT) is studied. All comparisons have been carried out at the levels of correlating 10, 12, and 22 electrons and neglecting spin-orbit contributions. In addition, we investigate the effect of going from a single-reference to a multireference CC expansion though only at the 10 and 22 electrons level.

Due to the relatively weak bond in the system an extensive correlation treatment is needed. This is evident from the results in Table 9.4 where it can be seen that there still are sizeable differences of −0.02 to −0.03 Å in the bond length, 0.04 eV in dissociation energy but only −0.5 to −1.0 cm^{-1} in harmonic frequency between the CCSD and the perturbative and full iterative triples for 10, 12, and 22 electrons. The sign of these results is consistent with our above statements that the bond is contracted with increased correlation. The potential curve is slightly widened since the better correla-

Figure 9.4: Comparison of the spin-free correlation methods for 10 electrons. The shifted energies are given as (*total energy*) + 7792.997 E_h (CCSD), (*total energy*) + 7792.996 E_h (MRCCSD) and (*total energy*) + 7794.65 E_h (CCSD(T)), respectively.

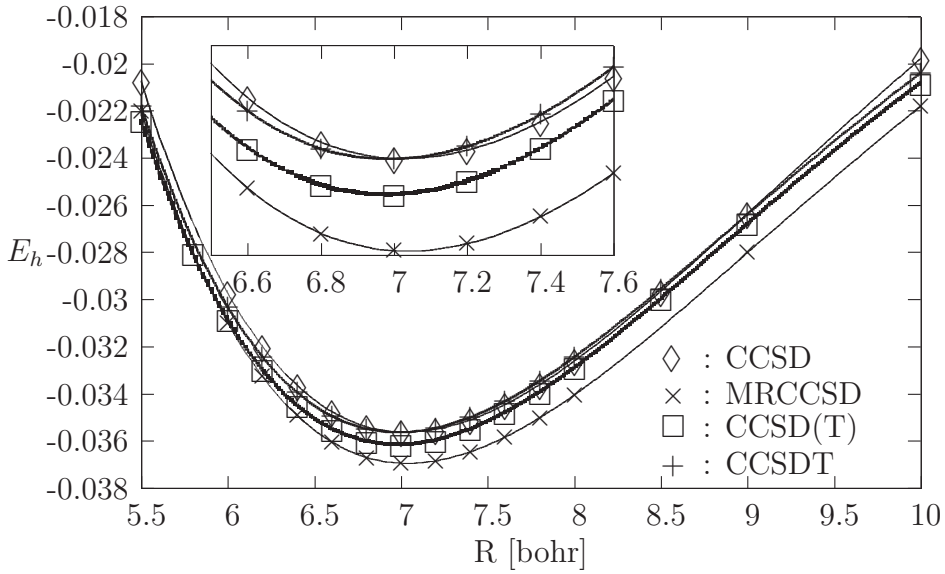

tion description decreases the unphysical hump observed in the bondbreaking region for single-reference methods and thereby yields a more balanced description on the whole curve. The CCSD(T) seems to perform very well in and around the equilibrium region and there gives results that are significantly better than CCSD and comparable with the full iterative triples values. But when dissociating the CCSD(T) shows unphysical behavior due to the breakdown of the perturbative estimate of the triples. This deficiency also becomes evident in the later vibrational analysis where only few vibrational states can be calculated accurately. The dissociation energy can, however, also here be calculated from atomic energies for both CCSD(T) and cp-CCSD(T) calculations, see Table 9.4. When extending the single-reference CCSD to the minimal CAS-space MRCCSD(10in6) for 10 electrons the small increase in correlation hardly changes the bond length, but the curve is slightly widened in the bondbreaking region (Figure 9.4) due the inclusion of the most dominant excitations for a correct dissociation. This extension in terms also results in an increase of the dissociation energy due to the balanced description the MRCCSD provides for the whole curve when the most important configurations are included in the CAS space. The same trend is also observed for the 22 electrons case.

9.3.3.1.4 Vibrational analysis With accurate potential curves it is possible to achieve not only precise harmonic frequencies and thereby accurate zero-point vibrational energies but also to do a further analysis of the excited vibrational states. For this analysis we have used version 8.0 of the program LEVEL [28]. Since we wanted to obtain many vibrational states of the electronic potential we have based the analysis on the CCSDT-SF 10 and CCSDT-SF 12 curves as these curves yield accurate values for all spectroscopic properties, in particular because the dissociation energy only shows minor changes when calculated from the atoms in comparison to a stretching of the bond. If the dissociation energy is calculated from stretching the bond we find a dissociation energy in eV of 0.7344 and 0.7394 of the CCSDT-SF 10 and CCSDT-SF 12 which is comparable to the values in Table 9.4 of 0.7200 and 0.7235 respectively. The inclusion of full iterative triple excitations is important for a balanced description of the system along the entire potential curve, especially the bond-breaking region and further out.

Figure 9.5: Change in relative spacing, shown in Table 9.6, defined as $\Delta^2 G_{\nu+1} = G(\nu+3/2) - G(\nu+1/2)$.

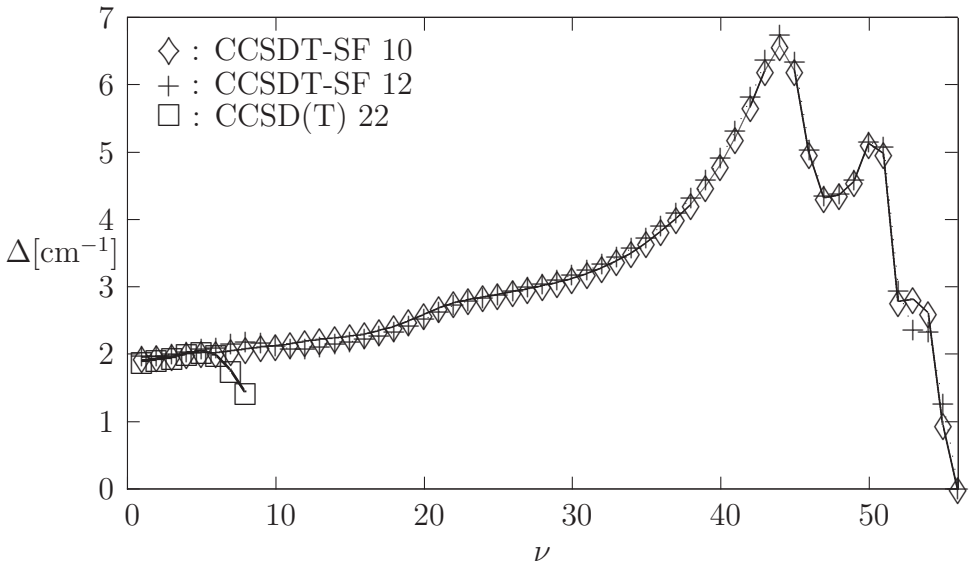

The vibrational states from the CCSDT-SF 10 and CCSDT-SF 12 curves are presented in Table 9.6. These are seen to be slightly lower, like the harmonic frequency, than the corresponding states from CCSD(T) 22 also in Table 9.6, for which only the first few states are reproduced reliably. We observe the expected trend of a decreasing separation of vibrational states with vibrational quantum number which is shown in Figure 9.5. However, only for the CCSDT curves do we continue to see the separation decreasing all

Table 9.6: Relative spacing of vibrational states calculated with *LEVEL*8.0 [28] from respectively the CCSDT-SF 10, CCSDT-SF 12, and CCSD(T) 22 potential curves. At $\nu = 0$ the zero-point energy is given. The relative spacing is defined as $\Delta G_{\nu+1/2}$ = G($\nu + 1$) - G(ν) and given in cm^{-1}

ν	CCSDT-SF 10	CCSDT-SF 12	CCSD(T) 22	ν	CCSDT-SF 10	CCSDT-SF 12
0	90.694	91.088	91.699	29	113.522	114.862
1	180.020	180.813	182.046	30	110.450	111.758
2	178.059	178.851	180.142	31	107.320	108.588
3	176.090	176.874	178.214	32	104.119	105.339
4	174.104	174.872	176.255	33	100.832	102.005
5	172.090	172.835	174.244	34	97.445	98.561
6	170.070	170.764	172.197	35	93.936	94.989
7	168.047	168.661	170.201	36	90.279	91.264
8	166.001	166.518	168.431	37	86.451	87.364
9	163.917	164.343	166.996	38	82.437	83.269
10	161.806	162.177		39	78.207	78.951
11	159.675	160.062		40	73.716	74.367
12	157.517	157.983		41	68.907	69.453
13	155.320	155.907		42	63.705	64.136
14	153.094	153.795		43	58.027	58.327
15	150.851	151.647		44	51.815	51.964
16	148.584	149.459		45	45.234	45.219
17	146.285	147.232		46	39.025	38.884
18	143.933	144.963		47	34.052	33.861
19	141.522	142.632		48	29.734	29.519
20	139.028	140.217		49	25.362	25.139
21	136.438	137.698		50	20.789	20.565
22	133.753	135.064		51	15.659	15.420
23	130.988	132.335		52	10.686	10.351
24	128.173	129.543		53	7.900	7.415
25	125.326	126.711		54	5.078	5.058
26	122.440	123.831		55	2.468	2.727
27	119.508	120.896		56	1.516	1.464
28	116.538	117.908				

the way up to $\nu = 44$ where the decrease of separation is 12.7% of the relative distance between $\nu = 44$ and $\nu = 43$. For CCSD(T) this already happens at $\nu = 5$. Higher-lying vibrational states from the CCSD(T) 22 curve are moreover very sensitive to the input parameters of the fitting program since no complete curve could be calculated.

To obtain many reliable vibrational states it is necessary to have an accurate and balanced potential energy curve which only comes about from the CCSDT level or higher. The small difference between the CCSDT-SF 10 and CCSDT-SF 12 vibrational states suggests that including the $1s$ electrons on Li in the correlation treatment only has a minor effect on the vibrational levels even though the effect on the bond length is significant.

Figure 9.5 reproduces the expected trend from a molecular potential very well up to $\nu = 47$. Beyond this some unsystematic behavior is observed. $\Delta^2G_{\nu+1}$, defined as $(\Delta G(\nu+3/2) - \Delta G(\nu+1/2)$, is dominated by the first anharmonicity up to around $\nu = 30$. Here at around $1.6 * R_e$ the bond-breaking region is entered and therefore large changes in the electronic wave function as well as in the potential energy surface are observed. In this region $\Delta^2G_{\nu+1}$ grows rapidly and higher anharmonicities dominate. This growth continues until $\Delta^2G_{\nu+1}$ is comparable to the relative distance of the vibrational states ($\Delta G_{\nu+1/2}$ defined as G($\nu + 1$) - G(ν)) thereafter it rapidly decreases again, as expected. To eliminate the remaining unsystematic behavior one would have to increase the number of points at very long range since small changes in the potential energy curve will here cause large changes in $\Delta^2G_{\nu+1}$.

To come even closer to a complete curve with reliable high vibrational levels one would also require a CCSDTQ treatment or a multireference treatment with at least full iterative triples included. This would reduce the non-parallelity error and lead to a further reduction of the difference in dissociation energies calculated from the supermolecular and the atomic approach.

9.3.3.2 Electric Properties

The final results for the electric properties have been obtained at the CCSDT level correlating 10 electrons since this was found to give the desired accuracy.

9.3.3.2.1 Dipole Moment Function At and below equilibrium distance (6.0 bohr and 7.0 bohr) there is no significant difference in the dipole moment at the CCSD level for

Figure 9.6: CCSDT-SF 10 dipole moment curve in Debye. Also shown are results from CCSD-SF 10, CCSD-SF 22, and CCSD(T)-SF 10 calculations

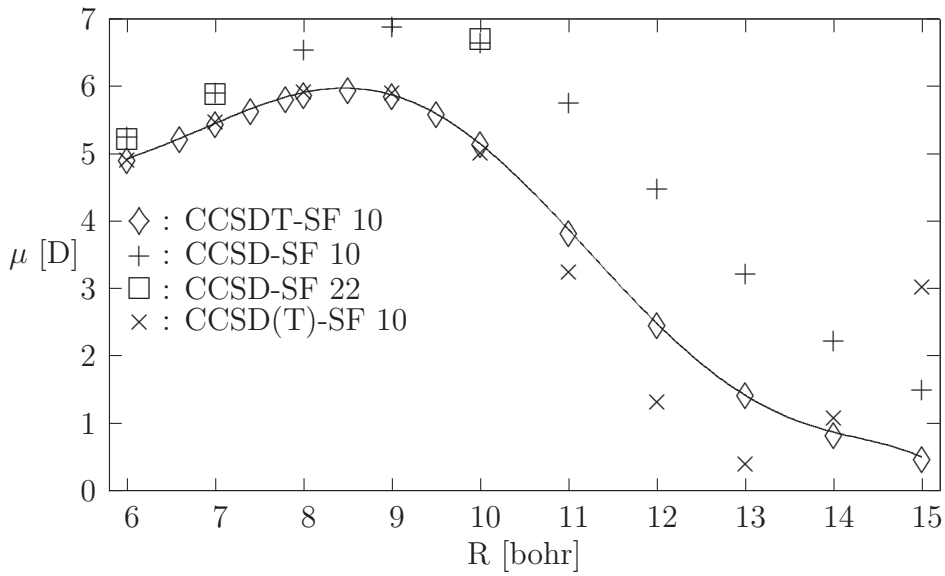

correlating 10 or 22 electrons (roughly 0.1% difference), see Figure 9.6. At longer distance (10 bohr) the difference increases to 1% which is still smaller than the expected residual errors in our calculations. A significantly larger contribution was found by going from CCSD to CCSDT which is consistent with the general knowledge about dipole moments in other molecules [169]: In addition to the excitations required to describe electron correlation, combined excitations for describing the relaxation of the wave function to the external field are needed, emphasizing the importance of the full triple excitations. At the CCSDT level and at a distance of 6.0 bohr the difference amounts to 6.8% which increases slightly to 7.6% at 7.0 bohr. In the bondbreaking region CCSD significantly overshoots the dipole moment giving a difference of 28.8% at 10 bohr, which is attributed to the poor description CCSD gives in the bondbreaking region. The maximum absolute value of the dipole moment function is found at 8.504 bohr for CCSDT-SF 10 with a strength of 5.969 Debye. The CCSD(T) model, also pictured in Figure 9.6, does well until the bondbreaking region where the description of the potential energy curve also deteriorates. Unlike CCSD and CCSDT, the CCSD(T) model does not provide a qualitatively correct complete curve which is inferred from the increasing dipole moment at 14 bohr.

9.3.3.2.2 Static electric dipole polarizability As mentioned in Section 9.3.2.1 the static electric dipole polarizability is significantly more difficult to calculate accurately

Figure 9.7: CCSDT-SF 10 parallel static electric dipole polarizability curve in Atomic units. Also shown are results from CCSD-SF 10, CCSD-SF 22, and CCSD(T)-SF 10 calculations

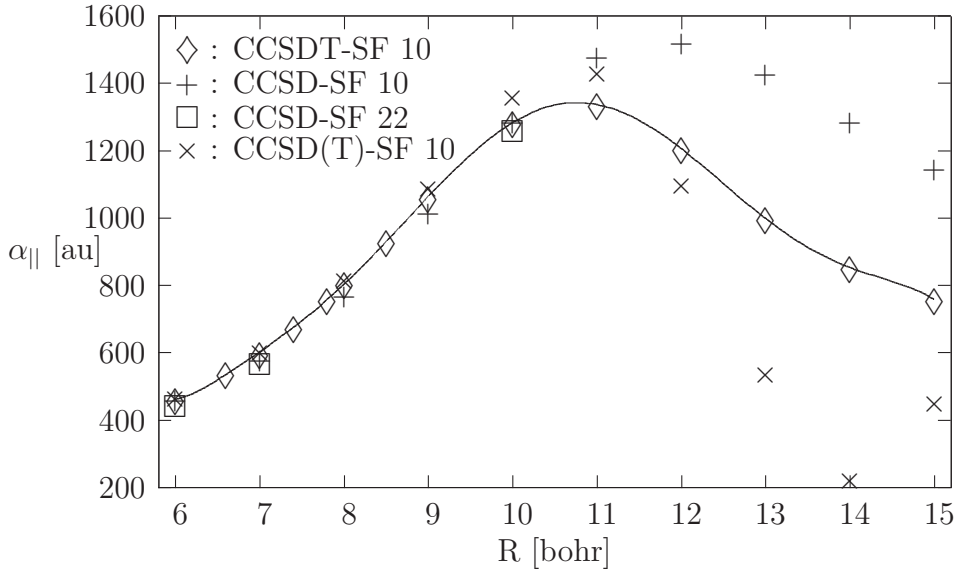

than the dipole moment since the property is more sensitive to the basis set used. With an improving correlation treatment the static electric dipole polarizability will usually increase but the effect of increased correlation is often difficult to assess because of the interplay with the basis set. Here we will, however, only improve the correlation level since the parallel component $\alpha_{\|}$ is already available when the polynomial fit to the dipole moment has been made and because we do not calculate the static electric dipole polarizability perpendicular to the bond $\alpha_{\perp}$. The perpendicular polarizability is not calculated since the basis set used is only suited for the parallel component.

If we again compare the CCSD and CCSD(T) with the CCSDT value in Figure 9.7 at short range we find there is only little dependence on the correlation level for $\alpha_{\|}$ and the number of electrons correlated. The difference is only $1-4\%$ between CCSD and CCSDT and the core electrons only play a minor role of around 1% so we expect that additional correlation will not change the static electric dipole polarizability anymore. The CCSD(T) values around equilibrium differ by less than 1 a.u. from the CCSDT values. This difference, however, increases to 73 a.u. at a distance of 10 bohr, and at longer range the CCSD(T) curve again shows unphysical behavior. A polynomial fit of the calculated points reveals a maximum of 1344 a.u. at 10.76 bohr and a value of 598 a.u. at the equilibrium bond distance for the model CCSDT-SF 10.

9.3.3.3 Comparison with Literature Values

Comparing what we consider the most reliable result for bond length and harmonic frequency, namely the cp-CCSD(T) 12 result, with previously calculated results (see Table 9.4) we observe that the calculated bond distance of 3.6952 Å is about 0.08 Å longer than the latest reported results [166] and [159] whereas the earlier value in [167] is closer at around 0.04 Å. Those results were all obtained using atomic pseudopotentials and Configuration Interaction (CI) techniques for correlating two valence electrons whereas we have employed all-electron calculations and coupled-cluster for correlation. This has opened for the possibility to not only explore effects of relativity and higher excitations but also the core-valence correlation in a systematic way. Due to this series of coupled-cluster calculations we believe to have achieved a significantly higher accuracy on the spectroscopic properties examined than previously reported from theory. Our present results are closer to a recent experimental result [163] of 3.6681 Å from laser-induced fluorescence Fourier-transform spectroscopy. The remaining difference between the calculated bond distance and the experimental one is primarily due to basis set insufficiency. The calculated bond distance will approach the experimental when the size of the basis set is increased and a higher truncation value for the virtual space is used [168].

For the harmonic frequency the differences between most recent theoretical results [166] and our cp-CCSD(T) 12 value of 183.8 cm^{-1} amount to roughly 3 cm^{-1}. This difference is rather small but still appears to be larger than the corrections that would be expected from higher correlation treatment and larger basis sets [168]. We therefore consider our cp-CCSD(T) 12 value an accurate prediction for the vibrational frequency which is not reported in the experimental work in reference [163]. The harmonic frequency can to a large extent be reproduced from a two-electron correlated calculation as shown in Table 9.5. Since the harmonic frequency is only very little influenced by the excitation level in the cluster model or the number of electrons correlated it is not surprising that the difference in the vibrational analysis between CCSDT-SF 10 and CCSDT-SF 12 is minor.

The dissociation energies from [159] and [167] of 0.717 eV and 0.72 eV respectively both lie close to the experimental value in [163] of 0.728 eV, and [167] is in perfect agreement with the value 0.72 eV cited in [170]. These values are also in very good agreement with the dissociation energy D_e in Table 9.4 found in this work where the

counterpoise corrected CCSD(T) with 12 electrons of 0.712 eV would be considered the best value we found due to the lack of correlating functions for the 4d electrons on Cs.

From Table 9.4 it is also evident that higher excitations play a significant role in obtaining a correct dissociation energy. Inclusion of full iterative triples increases the dissociation energy D_e to around the experimental value but it is expected that full iterative quadruples will be necessary to come to a more definite conclusion.

The absolute maximum value for the dipole found here at a nuclear displacement of 8.504 bohr is slightly longer than the 8.33 bohr found in reference [159] but with almost exactly the same strength. Since the CCSD model predicts an absolute maximum both larger and at longer bond length than the CCSDT model we expect that the CISD model would exhibit a similar behavior if more than the absolute minimum number of electrons were correlated. The dipole moment at the equilibrium distance is found to be 5.447 Debye (CCSDT-SF 10) which is also in good agreement with the results of both reference [159] of 5.462 Debye and reference [167] of 5.48 Debye. The vibrationally averaged dipole moment of 5.440 Debye is found to be close to the value at the equilibrium bond distance since the rovibronic wave function for the ground state is coinciding with a linear part of the dipole moment curve. The calculated static electric dipole polarizability also agrees with other recently calculated results in reference [171] of 597 a.u. both with respect to the internuclear distance and the maximum property value where we find the polarizability to be 598 a.u. both at the equilibrium bond distance as well for vibrationally averaged polarizability with the CCSDT-SF 10 model.

9.3.4 Conclusion and Outlook

In this study of the ground-state properties of the LiCs molecule we demonstrate the capability of our relativistic all-electron quantum-chemical methodology to yield highly accurate complete potential energy curves. We therefore go beyond other approaches applied to cold and ultracold molecules which typically employ small numbers of explicitly correlated electrons and effective core potentials.

In particular, we report on the implementation of a GAS coupled cluster in the spin-free Dirac formalism for large-scale electron correlation calculations on molecular ground states. It is demonstrated that the spin-free Dirac framework gives significant im-

provements over non-relativistic approaches for certain types of molecules, where electron correlation effects by far outweigh spin-orbit contributions. As in the present case, we obtain results of high accuracy.

In order to obtain accurate spectroscopic properties of LiCs the level of correlation treatment exceeds Coupled Cluster Singles and Doubles. In the case of the harmonic frequency and the equilibrium bond distance the CCSD(T) model suffices if no further vibrational analysis is needed. However, due to the breakdown of the perturbative triples correction in the bond-breaking region CCSD(T) cannot yield a full potential curve. Here we demonstrate that the full iterative triple excitations or a multireference approach yield a balanced description. The various trends in the correlation treatment like the contraction of the bond with a shift from delocalized to more localized bond, the change in dissociation energy with increased correlation treatment and, moreover, small variations in the harmonic frequency have been explained. Besides this a thorough comparison between results obtained in the non-relativistic, the spin-free and the fully relativistic regime has been made.

We demonstrate a greater accuracy on the entire potential energy curve in comparison to other methods for both spectroscopic and electric properties. This is corroborated by obtaining proper atomic limits for the electric properties upon dissociating the molecule. The dipole moment tends to zero and the polarizability goes towards the sum of the atomic polarizabilities of 401 au. for Cs [172] and 164 au. for Li [173, 174]. The quality of the potential curve is in addition confirmed by a complete vibrational analysis.

The importance of an extensive correlation treatment is also demonstrated for the dipole moment, where CCSD gives a very poor description in the region of the maximum dipole moment. The parallel component $\alpha_{\|}$ of the static electric dipole polarizability, however, turns out to be much less sensitive to electron correlation with this basis set.

Besides having accurate potential surfaces for electronic ground states there would be a great interest in having these also for excited states. This is currently under development using linear response theory. For molecules with large spin-orbit contributions a fully relativistic version of the CI-driven spin-free code has been implemented [70] and a more efficient commutator-driven implementation is under development [68].

9.4 RbYb

We present high-level four-component coupled cluster and multireference configuration interaction calculations of potential energy curves, dipole moment, Franck-Condon factors and spectroscopic constants of the newly formed RbYb molecule. From finite-field calculations we obtain an electric dipole moment for RbYb of almost 1 Debye. In combination with its magnetic dipole moment this makes RbYb an excellent candidate for trapping and for studying dipolar interaction in the ultracold regime. Significant Franck-Condon factors are found between the rovibronic ground state and the lowest rovibrational levels of the first excited $^2\Sigma^+_{1/2}$ state but also between a broad range of rovibrational levels of the $^2\Pi_{1/2}$ and $^2\Pi_{3/2}$ states. This allows for several two-step approaches to reach the rovibronic ground state after initial photoassociation.

9.4.1 Introduction

A number of groundbreaking achievements has been reported from the field of cold and ultracold molecules, and ongoing investigations bear the potential for yet further findings of fundamental importance [14]. These range from the production of Bose-Einstein condensates (BECs) [15] to the striving for a controlled chemistry at the quantum level [16] and the possibility of testing, e.g., fundamental symmetries in nature through measurements of a postulated electric dipole moment (EDM) of an electron [17, 18] or the space-time variation of fundamental constants such as the fine-structure constant α [19, 20]. The experimental work for producing (ultra-)cold molecules has to the date been conducted in a variety of ways, such as photoassociation (PA) [21], buffer gas cooling (sympathetic cooling) [22], Stark deceleration of polar molecules via time-modulated electric fields [23] and magnetically tunable Feshbach resonances [24].

Theoretical contributions to the field of (ultra-)cold molecules are of value in many different respects. Among the most important is the determination of accurate molecular potential energy curves (PECs) of ground and relevant electronically excited states. These potentials are often required to be known both at short and long range [21]. At long range, atom-atom interactions are typically evaluated by perturbation theory, whereas at short range advanced methods of molecular electronic structure theory come into play. In

addition to the spectral constants which may be extracted directly from the short-range potentials (equilibrium bond lengths, harmonic vibrational

frequencies, dissociation and excitation energies) [25–27], vibrational states and Franck-Condon factors (FCFs) [28], molecule formation rates [29], and electric properties such as permanent EDM [30,31], transition dipole moments [32], and static polarizabilities are of interest and have been determined by theoretical methods.

A large fraction of investigated systems in the (ultra-)cold molecular sciences is comprised by alkali metal diatomics. The RbYb molecule belongs to a new class of heteronuclear diatomics that due to their unpaired electron(s) may be trapped and manipulated using magnetic fields [11]. They are, for example, promising candidates for an experimental search for a permanent electric dipole moment of the electron or for producing lattice-spin models [12] for quantum computing. Recently, the thermalization of various bosonic and fermionic Yb isotopes through collisions with ultracold Rb has been shown, giving first insights into the long-range behavior of the RbYb potential [175]. Based on this work, the controlled production of electronically excited RbYb* molecules by single-photon photoassociation techniques has been demonstrated [11], and continued efforts include the conservative trapping of the Rb-Yb mixture. Ultimately, the investigations aim at a molecular BEC with adjustable dipolar interaction and a new approach to measuring the electron EDM. The prospects have motivated us to explore the electronic structure of the RbYb molecule with reliable and accurate relativistic electronic structure methods.

In this section we present, to the best of our knowledge, the first theoretical investigation of the RbYb molecule. The focus of this investigation has been on a simultaneously accurate description of the ground and lowest electronically excited states and to propose possible ways for a photoassociation process leading to the rovibronic ground state. Since two heavy atoms are involved we apply quantum-chemical methods which treat electron correlation and relativistic effects on the same footing. Relativistic coupled cluster and configuration interaction approaches are used in a complementary fashion, the details of which are described in the following section. In the main body of the section (Section 9.4.3) we outline a way of achieving high accuracy by first a systematic study of the ground and excited states of the atoms and, in addition, of the electronic ground state of the molecule. Based on these results, a final multireference (MR) CI model expansion

is chosen which can deliver accurate spectroscopic values for the states in question. We present and discuss electronic molecular potentials obtained with this MRCI model and point to possible pathways to the rovibronic ground state based on the derived FCFs. We furthermore present the computed dipole moment function of the ground state showing that RbYb also possesses a substantial electric dipole moment along with a magnetic dipole moment due to the unpaired electron. In the final section we summarize and draw conclusions.

9.4.2 Theory and Computational Details

9.4.2.1 Hamiltonian Operators

The spectroscopic properties of RbYb are expected to be significantly influenced by relativistic effects and electron correlation. For the ground state $^2\Sigma^+_{1/2}$ scalar-relativistic effects cause a large contraction and stabilization of the 6s spinors on Yb and a smaller one of the 5s spinors on Rb. For the lowest excited states we expect a significant spin-orbit splitting for $\mathrm{Rb}_{5p^1}(^2P_{3/2,1/2})$ and a large spin-orbit coupling (SOC) for $\mathrm{Yb}_{6s^16p^1}(^3P_{2,1,0})$ and $\mathrm{Yb}_{6s^16p^1}(^1P_1)$. We have therefore decided to carry out this theoretical investigation in the more rigorous 4-component framework using the Dirac-Coulomb (DC) Hamiltonian for calculations including excited states and Dyall's spin-free Hamiltonian [64] for ground-state-only calculations. To correctly describe the SOC of the excited states the DC Hamiltonian suffices since it contains the leading spin-orbit terms for heavy elements, namely the one-electron spin-orbit and the two-electron spin-same-orbit terms. The effect of the spin-other-orbit term which is derived from the Gaunt operator and is therefore not included in the DC Hamiltonian has been examined at the SCF level. It was found that the change in the splitting of the $\mathrm{Rb}_{5p}(P_{3/2,1/2})$ and $\mathrm{Yb}_{6p}(P_{3/2,1/2})$ levels decreased by 0.72 and 19.8 cm^{-1}, respectively. This reduction amounts to a change for $\mathrm{Rb}_{5p}(P_{3/2,1/2})$ of 1.7% and $\mathrm{Yb}_{6p}(P_{3/2,1/2})$ of 1% which is still below the accuracy we can typically achieve for relative energies. Including the full Breit interaction has been shown to have only little influence on the excitation energies of Yb [176] and on the alkali metal atoms in general. [177]

9.4.2.2 Correlation Methods and Setup

For the study of ground-state spectroscopic and electric properties we employed the RELCCSD module [74, 125] in the DIRAC quantum chemistry program package [57] which can perform CCSD and CCSD(T) calculations. The dominant relativistic contributions to the ground state are scalar relativistic. We therefore applied Dyall's spin-free Hamiltonian [64] in the coupled cluster calculations. Dirac-Coulomb Hartree-Fock (DCHF) calculations were performed with an averaging of three electrons in two Kramers pairs (3in2) consisting of the Rb 5s and Yb 6s spinors. Additional test calculations were carried out in a spin-dependent framework employing either a (3in2) or (3in5) averaging. In the latter DCHF setup three electrons were distributed among five Kramers pairs consisting of the Rb 5s and Yb 6s6p spinors. These ground-state coupled cluster calculations served as a benchmark for the corresponding MRCI calculations.

The calculation of excited-state wave functions and vertical as well as adiabatic excitation energies has been performed with the relativistic large-scale MRCI program LUCIAREL [71–73]. Like in the CIDBG [50] and SOCI [51] in the COLUMBUS code, double group symmetry is used. The recent parallel implementation [131] of LUCIAREL has opened for the possibility to treat larger CI expansions ($> 10^8$ determinants) within a reasonable time frame on standard Linux-based clusters which has also been demonstrated for the SOCI program. [178]

The CI program LUCIAREL operates on the basis of a fully variational treatment of any spin-dependent two- or four-component Hamiltonian that is available in the present developer version of the DIRAC package [57]. It furthermore takes advantage of the concept of generalized active spaces (GAS) [71] to define suitable orbital spaces thereby allowing for arbitrary occupation constraints. Molecular spinors based on a true two- or four-component framework can be obtained from either all-electron self-consistent field (SCF), Kramers-restricted multi-configurational self-consistent field (KR-MCSCF) [130] or natural MP2 spinor [179] calculations. The string-driven MRCI [71–73, 127] as well as the MRCC [3, 5, 30, 68, 70] methods are an alternative to the Tensor Contraction Engine [180] in generation of higher-order methods or code for more complex calculations.

To obtain accurate excitation energies the initial DCHF step was performed with a (3in5) averaging of states. A (3in8) averaging, where the Rb 5p spinors are included,

was not possible along the entire potential energy curve due to strong mixing with the Yb 5*d* spinors. The Rb 5*p* spinors were, however, included in the correlation step in a (3in8) MRCI excitation scheme that is in the following dubbed as S6_(3in8)_SD. Our notation follows the scheme "GAS I_(GAS II)_GAS III" and is most easily explained by an example: "S6_(3in8)_SD" means that at most 1 hole among the 6 electrons in 3 Kramers pairs (in this case: Rb 4*p* spinors) is allowed, 3 electrons are distributed in 8 Kramers pairs in all possible ways (plus of course excitations from GAS I to GAS II), and finally that all possible single and double excitations into GAS III Kramers pairs are generated from the reference configurations obeying the constraints put on GAS I and GAS II. As discussed in more detail in Section 9.4.3.1, the inclusion of the Rb 4*p* spinors is required in the correlation step to obtain a good description of the lowest three atomic channels.

In addition to our thorough investigation of the four lowest molecular electronic states of RbYb, we show in Figure 9.8 a qualitative picture of the low-lying molecular elec-

Figure 9.8: Sørensen et al. JPCA 2009; Qualitative picture of the potential energy curves of the molecular electronic states constituting the lower electronic spectrum of RbYb. Correlating atomic dissociation channels for the states are labeled. The computational level is CI SDT3 (see text for more details).

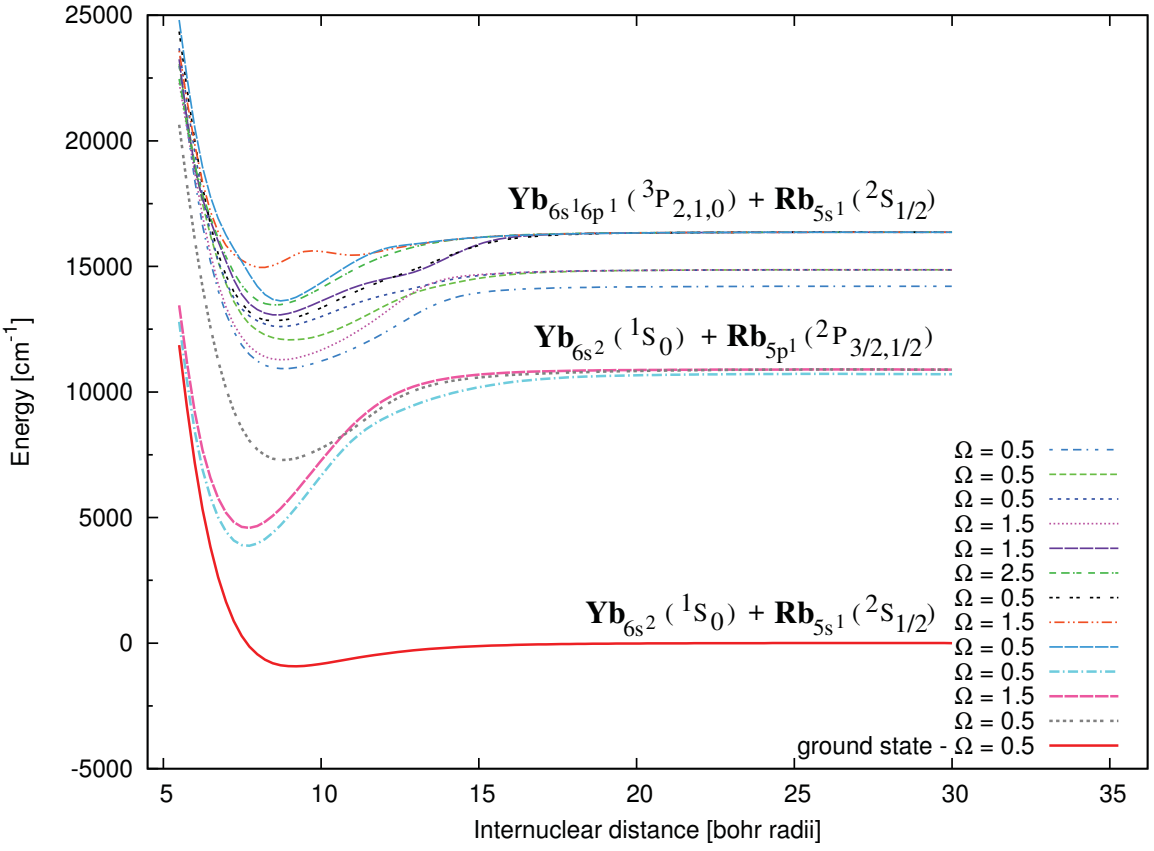

tronic spectrum including respective atomic dissociation channels. In these calculations, denoted as SDT3 which corresponds to a Full CI calculation with three electrons, we truncated the space of virtual spinors at 2.0 E_h. It should be noted that the $Rb_{4d^1}(^2D_{5/2,3/2})$ states should be below the $Yb_{6s^1 6p^1}(^3P_2)$ states in the atomic limit which is not the case here due to the choice of DCHF averaging.

As full linear symmetry is not available yet in the present `LUCIAREL` implementation the calculations have been carried out in the Abelian sub double group C_2^*. The assignment of the Ω quantum number for each individual electronic state has been accomplished by means of calculating the expectation value for the one-electron operator $\hat{j}_z = \hat{l}_z + \hat{s}_z$. This option has become available with the very recent implementation of a general CI property module [181] capable of treating basically any one-electron operator that is implemented in the `DIRAC` program package [57].

9.4.2.3 Basis Sets and Number of Correlated Electrons

All calculations were performed using uncontracted basis sets. For the ground-state coupled cluster calculations the aug-cc-pVTZ basis set for Yb ($30s24p16d13f4g2h$) [182] from Gomes and Dyall was chosen. It includes correlating functions for outer- and inner-valence shells down to the Yb $4f$ and polarizing functions for these. For Rb ($29s21p15d2f$) [183] Dyall's aug-cc-pVTZ basis set which includes correlating and polarizing functions down to Rb $4s4p$ was used. For a description of the general procedure of how to derive these functions see for example Ref. [184]. In the following this basis set will be referred to as (*ext_bas*).

The effect of changing the number of correlated electrons has been examined at the CCSD and CCSD(T) levels. Either nine electrons from the Rb $4p5s$ and Yb $6s$ spinors were treated explicitly in the correlation step or 23 electrons where the Yb $4f$ spinors were then included in addition. As shown in Sections 9.4.3.1 and 9.4.3.2, the differential effects of correlating the Yb $4f$ electrons were found to be minor. In contrast, the correlation of the Rb $4p$ electrons had significant impact on the energy separation of the atomic levels and on the equilibrium distance of the molecular ground state. We therefore decided to correlate nine electrons (Rb $4p5s$ and Yb $6s$) in the MRCI calculations.

For the MRCI calculations the core-polarizing functions for both atoms were omitted since no electric properties were calculated. This reduced the size of the basis set (*min_bas*)

to $(30s24p16d13f3g1h)$ for Yb and $(28s20p14d1f)$ for Rb. The truncation value for the virtual spinors in all correlated calculations was kept at 7.8 E_h since this threshold includes all polarizing functions and, on the other hand, was still tractable for the MRCI calculations. Spinors above this threshold are primarily core-correlating and will therefore only give minor contributions to valence spectroscopic values and electric properties.

9.4.2.4 Dipole Moment

The ground-state dipole moment was calculated by applying a finite electric field of varying strength along the bond axis (chosen as z). The field strengths considered here were ± 0.0001, ± 0.0002, ± 0.0004 $E_h e^{-1} bohr^{-1}$. From these seven points a polynomial fit to the total field-dependent energy was made to find the numerical derivative and thereby also the dipole moment at a given internuclear distance. This was done at the CCSD and CCSD(T) levels of theory with 23 explicitly correlated electrons.

9.4.2.5 Spectroscopic Values and Franck-Condon Factors

A polynomial fitting procedure with exponents ranging from -1 to +4 was used to fit the electronic ground- and excited-state potentials around their respective minima. Spectroscopic constants have then been determined by solving a one-dimensional Schrödinger equation of nuclear motion using a reduced mass calculated from isotopic abundance [185]. The harmonic frequency has been calculated from the second derivative at the minimum. Vibrational wave function, eigenvalues and FCFs have been computed with the program `LEVEL` 8.0 by LeRoy [28].

9.4.2.6 Counterpoise Correction

As RbYb is a van der Waals complex and therefore the ground state is very weakly bound by dispersion forces, the basis set superposition error (BSSE) may play a significant role in determining spectroscopic values even in large and balanced basis sets [89, 186] due to the slow convergence towards basis set saturation. This artifact has been examined by a counterpoise (CP) correction as suggested by Boys and Bernardi [165] for both ground and excited states which is the correct way of evaluating differential quantities [89, 187, 188].

The BSSE is defined in the usual manner

$$BSSE(R) = E^{A(AB)}(R) + E^{B(AB)}(R) - E^{A} - E^{B} \tag{9.1}$$

where $E^{A(AB)}(R)$ and $E^{B(AB)}(R)$ are the monomer energies obtained in the full dimer basis (AB) at a given distance (R) and E^{A} and E^{B} are the monomer energies in their respective basis. Every point on the potential energy curve is thereby CP corrected. The CP correction has been shown to be a very good estimate for the BSSE in medium to large basis sets and to provide a smooth convergence of properties to the complete basis set limit [189,190]. Despite the apparent ease to eliminate a basis set incompleteness artifact one should, however, be careful in relying on this form of error compensation since a CP correction will not improve the overall basis.

9.4.3 Results and Discussion

9.4.3.1 Qualitative Molecular Electronic Spectrum and Atomic Calculations

Table 9.7 gives an overview over the atomic configurations and terms as well as the associated molecular states in the $\Lambda - S$ coupling picture that are expected to form the lower part of the electronic spectrum of RbYb. The energetically close-lying valence-electronic Yb $6s$ and $6p$ shells as well as the valence-electronic Rb $5s$ and low-lying Rb $5p$, $4d$, $6s$ and $6p$ shells suggest a large variety of excited states with angular momentum projection greater than zero within an energetic range of ≈ 25000 cm^{-1}. As these states are affected by spin-orbit interaction to first order in a perturbation theory sense and as ytterbium is a heavy atom, the corresponding splittings and mixings are expected to be sizeable. We provide in Figure 9.8 a qualitative survey of all molecular states correlating to the three lowest atomic channels listed in Table 9.7. Comparing the atomic-like excitation energies, computed at the CI SDT3 level of theory with the experimentally available data we find a large deviation of $\approx 2000 - 3000$ cm^{-1} for the lowest P channels of both Rb and Yb. In contrast, the splitting among the various J-states is reproduced rather well. These results indicate that spin-dependent effects are taken into account properly whereas significant parts of the differential electron correlation are missing at this level of calculation. As we in the present study turn our main attention to the ground and three lowest excited states of RbYb which are of particular importance for the experimental PA

Table 9.7: A selection of molecular electronic states in the $\Lambda - S$ coupling picture and associated atomic dissociation channels in an energy range of $\approx$ 25000 cm^{-1}. Molecular electronic states correlating to atomic channels with intra-atomic Yb $f - d$ excitations, e.g. $Yb_{4f^{13}5d^16s^2}$ are not considered.

Atomic $^{(2S+1)}L_J$	Molecular $^{(2S+1)}\Lambda_\Omega$
$Rb_{5s^1}(^2S_{1/2}) + Yb_{6s^2}(^1S_0)$	$^2\Sigma^+_{1/2}$
$Rb_{5p^1}(^2P_{3/2,1/2}) + Yb_{6s^2}(^1S_0)$	$^2\Pi_{3/2,1/2}$, $^2\Sigma^+_{1/2}$
$Rb_{5s^1}(^2S_{1/2}) + Yb_{6s^16p^1}(^3P_{2,1,0})$	$^4\Pi_{5/2,3/2,1/2,-1/2}$, $^2\Pi_{3/2,1/2}$, $^4\Sigma^+_{3/2,1/2}$, $^2\Sigma^+_{1/2}$
$Rb_{4d^1}(^2D_{5/2,3/2}) + Yb_{6s^2}(^1S_0)$	$^2\Delta_{5/2,3/2}$, $^2\Pi_{3/2,1/2}$, $^2\Sigma^+_{1/2}$
$Rb_{6s^1}(^2S_{1/2}) + Yb_{6s^2}(^1S_0)$	$^2\Sigma^+_{1/2}$
$Rb_{5s^1}(^2S_{1/2}) + Yb_{6s^15d^1}(^3D_{3,2,1})$	$^4\Delta_{7/2,5/2,3/2,1/2}$, $^2\Delta_{5/2,3/2}$, $^4\Pi_{5/2,3/2,1/2,-1/2}$, $^2\Pi_{3/2,1/2}$
	$^4\Sigma^+_{3/2,1/2}$, $^2\Sigma^+_{1/2}$
$Rb_{6p^1}(^2P_{3/2,1/2}) + Yb_{6s^2}(^1S_0)$	$^2\Pi_{3/2,1/2}$, $^2\Sigma^+_{1/2}$
$Rb_{5s^1}(^2S_{1/2}) + Yb_{6s^16p^1}(^1P_1)$	$^2\Pi_{3/2,1/2}$, $^2\Sigma^+_{1/2}$

process, [11] we further investigated the effect of correlating the outer-core Rb $4p$ shell on the excitation energies. Since alkali atoms are known to have easily polarizable cores we expect a considerable influence here.

Our calculated atomic and atomic-like excitation energies T_e for the lowest Rb $5s-5p$ transitions are compiled in Table 9.8 and atomic Yb $6s - 6p$ transitions in Table 9.9. If core-valence polarization from the Rb $4p$ shell is neglected in the calculation of the lowest Rb $5s - 5p$ transition, not only a considerable underestimation of the excitation energies of almost 2000 cm^{-1} is found as indicated in Table 9.8 for the atomic S1 (one electron CI) and quasi-molecular SDT3 calculations. It also yields a too small fine-structure splitting of the $(^2P_{3/2,1/2})$ state of 183(2) cm^{-1} in comparison with the measured splitting of 237.6 cm^{-1}. However, taking into account single excitations from the outer-core Rb $4p$ shell (S6_(1in4)_SD) results in a significant improvement towards the experimental values. Excitation energies and the fine-structure splitting differ from the experimental data by about 40 - 60 cm^{-1}and 15 cm^{-1}, respectively.

Table 9.8: Atomic and atomic-like (values taken at R = 30 bohr) excitation energies T_e in cm^{-1} for the lowest $Rb_{5s^1}(^2S_{1/2}) \rightarrow Rb_{5p^1}(^2P_{3/2,1/2})$ transitions calculated at the MRCI S1, S6_(1in4)_SD, SDT3, and S6_(3in8)_SD levels, respectively. Details on the computational levels are given in the text.

	J = 0.5	J = 0.5	J = 1.5	
Method / T_e [cm^{-1}]	$\Omega = 0.5$	$\Omega = 0.5$	$\Omega = 1.5$	$\Omega = 0.5$
S1	0	10692	10875	10875
S6_(1in4)_SD	0	12636	12857	12857
SDT3	0	10708	10890	10892
S6_(3in8)_SD	0	12662	12879	12883
experiment [191]	0	12578.95	12816.55	12816.55

What about T_e for the Rb $5p$ excitation computed at the quasi-atomic limit (R= 30 bohr) applying our MRCI S6_(3in8)_SD model? It can be seen from Table 9.8 that in the atomic limit the excitation energies are slightly shifted to higher energies by about 22-26 cm^{-1} yet yielding an excellent spin-orbit splitting of 218 cm^{-1}. The excitation energies are in very good agreement with the experimental data exhibiting a maximum deviation of 83 cm^{-1} for the lower 2 0.5 state and compare well to the two-component MRCI results of Lim *et al.* [192] using energy-consistent pseudopotentials. Furthermore, the energetic difference of only 4 cm^{-1} between the sublevels of the $J = 1.5$ atomic channel indicates that we are almost in the atomic limit at an internuclear distance of 30 bohr.

As a prospect for future studies on this system we show our atomic MRCI calculations on the Yb atom where we studied the relevance of taking into account core-valence polarization from the Yb $4f$ and $5p$ shells. If only the two Yb $6s$ valence electrons are correlated (denoted as S2) transition energies for the respective Yb $6s - 6p$ excitation are consistently too low by around 18%. The inclusion of the Yb $4f$ electrons in the correlation step (S14_(2in4)_SD) yields some improvement. However, only upon explicitly treating core-valence polarization from the Yb $5p$ shell (S20_(2in4)_SD) we obtain excitation energies which are in good agreement with the experimental data. A further improvement is achieved by extending the active space to comprise the Yb $6s$, $6p$ and $5d$

shells (S20_(2in9)_SD). In this case, the deviations from the experimental values are less than 60 cm^{-1}, and the fine-structure splitting is very well reproduced.

Summarizing, the SDT3 level is insufficient for an accurate description even of the four lowest-lying dissociation channels (Rb $5s^1$ + Yb $6s^2$ and Rb $5p^1$ + Yb $6s^2$). It may thus be used only for obtaining a qualitative overview. In contrast, the S6_(3in8)_SD scheme reproduces the energetic splitting of these levels very well. Yb excitations do not play a major role in the atomic channels that correlate with the four lowest-lying molecular states relevant for the PA process. We thus conclude that our chosen MRCI S6_(3in8)_SD model should provide a reliable description of the long-range behavior of these states in the RbYb molecule.

Table 9.9: Atomic excitation energies T_e in cm^{-1} for the lowest $Yb_{6s^2}(^0S_0) \rightarrow Yb_{6s^1 6p^1}(^3P_{2,1,0})$ transitions calculated at the MRCI S2, S14_(2in4)_SD, S20_(2in4)_SD and S20_(2in9)_SD levels, respectively. Details on the computational levels are given in the text.

Method / T_e [cm^{-1}]	J = 0	J = 0	J = 1	J = 2
S2	0	14209	14865	16362
S14_(2in4)_SD	0	15497	16164	17734
S20_(2in4)_SD	0	17233	17931	19611
S20_(2in9)_SD	0	17346	18034	19722
experiment [191]	0	17288.44	17992.01	19710.39

9.4.3.2 Ground State Potential

The electronic ground state of RbYb exhibits a shallow potential shape (see Figure 9.9) that is a characteristic feature of a van der Waals molecule. Since the ground state is very sensitive to the DCHF averaging of the spinors and to the level of electron correlation, the simultaneously correct description of both ground and excited states becomes a complicated matter. Changes in the DCHF averaging or the correlation treatment can lead to large variations of the spectroscopic constants, here in particular the equilibrium bond

Figure 9.9: Sørensen et al. JPCA 2009; Potential energy curves of the four lowest-lying molecular electronic states of RbYb. Atomic dissociation channels for the states are shown. The computational level is S6_(3in8)_SD (see text for more details).

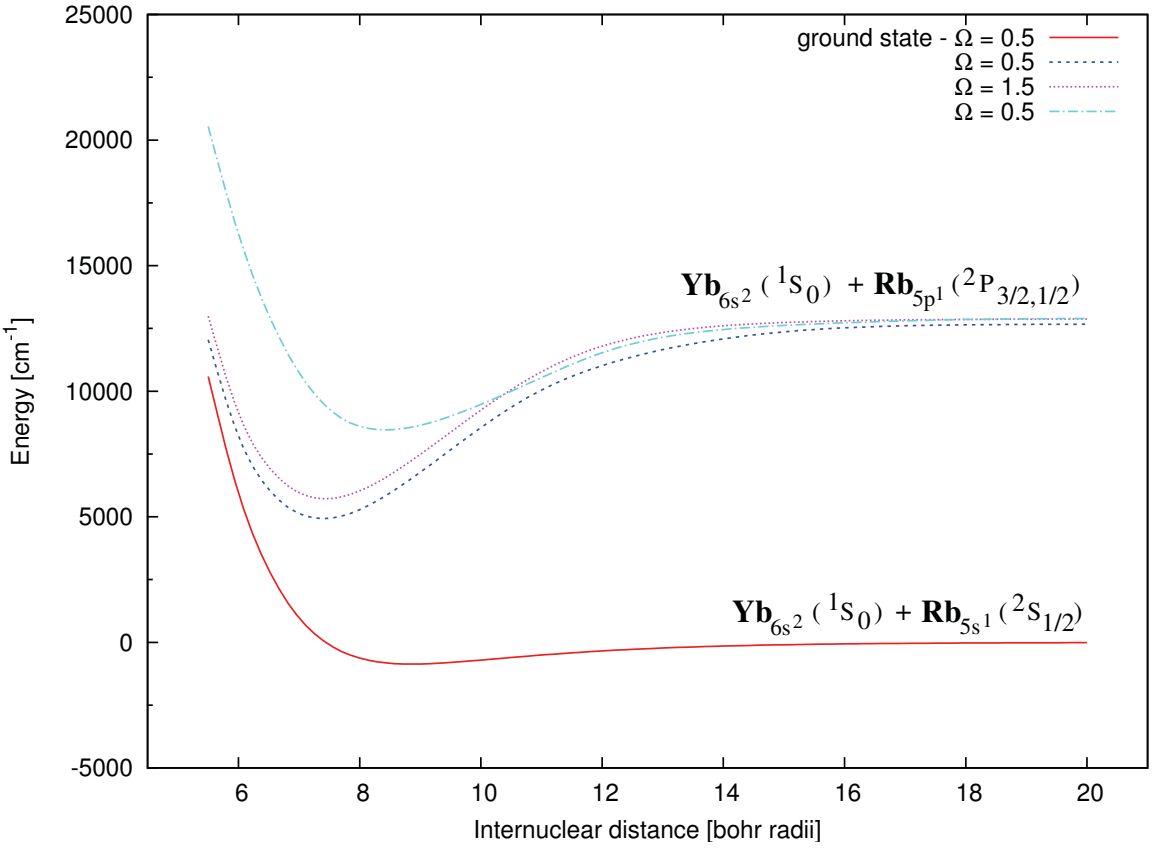

distance. These differences may result in a substantial change of FCFs between ground and excited states.

We therefore first examined the ground state of RbYb with the coupled-cluster method to provide a benchmark for the MRCI calculations. The aim here was to find the effect of outer-core polarization/correlation of the Yb $4f$ and Rb $4p$. This has been done by varying the number of explicitly correlated electrons from three to nine and to 23. Results of these calibration calculations are compiled in Table 9.10. Comparing those results it becomes evident that after a CP correction the effect of including the Rb $4p$ electrons on the bond length is more than one magnitude larger than including Yb $4f$ as the bond contracts from 9.18 bohr (CP-CCSD(T), three electrons correlated) to 8.94 bohr (CP-CCSD(T), nine electrons correlated) and 8.93 bohr (CP-CCSD(T), 23 electrons correlated). The correlation of the Yb $4f$ electrons does, nevertheless, have an effect comparable to the inclusion of the Rb $4p$ electrons on the harmonic frequency and

Table 9.10: Spectroscopic values for the 1 0.5 ground state calculated at the CCSD and CCSD(T) level with three, nine and 23 explicitly correlated electrons and with CP corrected values.

Method	corr. el.	R_e[bohr]	ω_e [cm^{-1}]	D_e [cm^{-1}]
CCSD-SF	3	9.30	26.278	606
CP-CCSD-SF	3	9.30	26.257	605
CCSD(T)-SF	3	9.18	28.941	818
CP-CCSD(T)-SF	3	9.18	28.923	816
CCSD-SF	9	9.20	24.814	600
CP-CCSD-SF	9	9.22	24.554	588
CCSD(T)-SF	9	8.93	29.724	820
CP-CCSD(T)-SF	9	8.94	29.462	804
CCSD-SF	23	9.15	24.186	742
CP-CCSD-SF	23	9.23	22.882	674
CCSD(T)-SF	23	8.86	28.990	870
CP-CCSD(T)-SF	23	8.93	28.196	749

the dissociation energy in reducing both. These changes are, however, of little importance for the present investigation and, furthermore, the polarization of Yb $4f$ plays a minor role in the lowest-lying excited states for the molecule (see Section 9.4.3.1). Therefore, we decided not to include the Yb $4f$ in the MRCI calculations. Another reason to omit the Yb $4f$ is the large CP correction which shows that with this particular basis set and truncation of virtuals we did not yet come close enough to basis set saturation for the Yb $4f$ shell. The otherwise minor CP correction for the three and nine electron CCSD and CCSD(T) calculations indicates that we have a balanced basis set.

The perturbative triples, on the other hand, have a substantial impact on the spectroscopic parameters. We therefore restrict the following discussion to results obtained at the CCSD(T) level. A comparison of the spin-free CCSD(T) correlating nine electrons with corresponding calculations including SOC (Table 9.11) shows that spin-dependent terms are of minor importance for the ground-state spectroscopic parameters. In contrast,

Table 9.11: Spectroscopic values for the 1 0.5 ground state calculated at the CCSD and CCSD(T) level with nine explicitly correlated electrons and including SOC. The spinor basis was derived from average-of-configurations DCHF calculations, distributing either three electrons in two Kramers pairs (3in2) or three electrons in five Kramers pairs (3in5). A CP-correction was not applied.

Method	basis set (av. in DCHF)	corr. el.	R_e[bohr]	ω_e [cm^{-1}]	D_e [cm^{-1}]
CCSD-SOC	*min_bas* (3in2)	9	9.25	24.073	591
CCSD(T)-SOC	*min_bas* (3in2)	9	8.98	28.620	795
CCSD-SOC	*min_bas* (3in5)	9	9.15	25.572	654
CCSD(T)-SOC	*min_bas* (3in5)	9	8.89	30.214	828
CCSD-SOC	*ext_bas* (3in2)	9	9.17	24.969	603
CCSD(T)-SOC	*ext_bas* (3in2)	9	8.90	29.888	826
CCSD-SOC	*ext_bas* (3in5)	9	9.08	26.443	670
CCSD(T)-SOC	*ext_bas* (3in5)	9	8.82	31.321	868

both the choice of the basis set and one-particle spinor basis have a significant effect on the equilibrium distance and dissociation energy. Augmentation of the basis set by polarization functions on both atoms (*ext_bas*) leads to a bond contraction as well as to a bond strengthening. Similar trends are found when the Yb 6*p* shell is included in the spinor optimization step. Although the CCSD(T) calculations based on a (3in5) averaged spinor basis yield the most attractive potential, the results need to be regarded with caution because of the use of a single-reference method. This choice of one-particle basis is more appropriate for a multireference correlation approach.

The MRCI results for the ground state (Table 9.12) reproduce very well the spectroscopic values derived from the CCSD(T) calculations. We find a slightly shorter bond and a higher dissociation energy of 844 cm^{-1} in relation to the CP-CCSD(T)-SF value of 804 cm^{-1}(Table 9.10). Typically, CCSD(T) is expected to result in larger binding energies than CI. A thorough analysis of the MRCI wave function reveals, however, substantial multi-configurational character. The leading configuration consists of a doubly occupied Yb 6*s* Kramers pair and a bonding orbital composed of Rb 5*s* and Yb $6p_{1/2}$. In addi-

Table 9.12: Spectroscopic constants for the ground and three lowest excited states (Ω designation) of RbYb calculated at the MRCI S6_(3in8)_SD level with nine explicitly correlated electrons. CP corrected values are given in the lower part of the table.

state	$\Lambda-\Sigma^a$	R_e[bohr]	ω_e [cm^{-1}]	D_e [cm^{-1}]	T_v [cm^{-1}]	T_e [cm^{-1}]
1 0.5	$^2\Sigma^+$	8.85	29.751	865	0	0
2 0.5	$^2\Pi$	7.40	69.294	7735	7387	5794
1 1.5	$^2\Pi$	7.43	69.322	7164	8104	6581
3 0.5	$^2\Sigma^+$	8.43	52.789	4423	9431	9326
1 0.5 (CP)	$^2\Sigma^+$	8.88	29.458	844	0	0
2 0.5 (CP)	$^2\Pi$	7.40	69.441	7688	7441	5819
1 1.5 (CP)	$^2\Pi$	7.44	69.181	7131	8153	6592
3 0.5 (CP)	$^2\Sigma^+$	8.44	52.284	4388	9451	9339

[a] leading $\Lambda-\Sigma$ configuration

tion, large coefficients are found for single excitations from the bonding orbital as well as double excitations from the Yb 6*s* shell. The simultaneous occurrence of polarizing and correlating excitations are indicative of the importance of triples as observed in the CC calculations.

From the benchmark calculations on the molecular ground state in connection with a balanced description of the atomic limit (see Table 9.8) we conclude that with the chosen MRCI setup high accuracy can be achieved both for ground and low-lying excited states.

9.4.3.3 Excited State Potentials

We now discuss in more detail the lower part of the electronic excitation spectrum of the RbYb molecule. Figure 9.9 displays the calculated potential energy curves for the three lowest excited states corresponding to the atomic Rb $5p_{3/2,1/2}$ and Yb $6s^2_{1/2}$ dissociation channels. The results for the spectroscopic constants of these states are compiled in Table 9.12 where data is listed with and without a CP correction, respectively.

The three electronically excited states can be divided into two classes as illustrated in Figure 9.9. The second state with Ω quantum number 0.5 (denoted in the following by 2 0.5) and the lowest state with $\Omega = 1.5$ (1 1.5) display a similar shape with pronounced potential wells centered around 7.40 bohr (2 0.5) and 7.44 bohr (1 1.5), respectively, and a harmonic frequency ω_e of ca. 69 cm^{-1} derived from the CP-corrected data. Both states are deeply bound with a D_e of 7688 cm^{-1} and 7131 cm^{-1}, respectively, whereas the 3 0.5 excited state has a considerably lower binding energy of 4388 cm^{-1}. We find for the latter excited state an equilibrium bond length R_e of 8.44 bohr that is significantly longer compared to the excited states mentioned afore but much closer to the minimum internuclear distance of the ground state. This geometric shift is furthermore in agreement with a small difference of ≈ 112 cm^{-1} between the vertical T_v and adiabatic T_e excitation energies compared to the much larger difference for the other two states.

Comparison of the CP-corrected excited-state spectroscopic constants with their uncorrected counterparts in Table 9.12 reveals that the excited-state bond distances are less sensitive to basis set superposition errors than the ground-state bond distance. The RbYb bond in the ground state, e.g., decontracts by ≈ 0.03 bohr upon CP correction whereas the largest shift for an excited state is found to be around 0.01 bohr. Moreover, the adiabatic transition energies T_e are hardly affected by the CP correction with changes of the order of $10 - 20$ cm^{-1}.

9.4.3.4 Vibrational Overlaps

Nemitz proposed a two-step mechanism for the production of ultracold RbYb molecules in the rovibronic ground state [193]. Initially, the molecule is prepared in a highly excited rovibrational level close to the dissociation limit of the electronic ground state. Interaction of the molecule with laser light of two different wavelengths promotes RbYb in a first step to some vibrational level of an electronically excited state correlating with the Rb(^2P) + Yb(^1S) atomic levels from which the population is pumped down in a second step to the rovibronic ground state of the molecule. For experimental realization of this scheme, knowledge of the vibrational overlaps between the electronically excited- and ground-state potential wells is of utmost importance. We expect that the dominating difference for a transition probability will be the FCF since all transitions are dipole allowed. We have therefore computed FCFs between vibrational wave functions of the

Figure 9.10: Sørensen et al. JPCA 2009; The highest and lowest vibrational states for the electronic ground state.

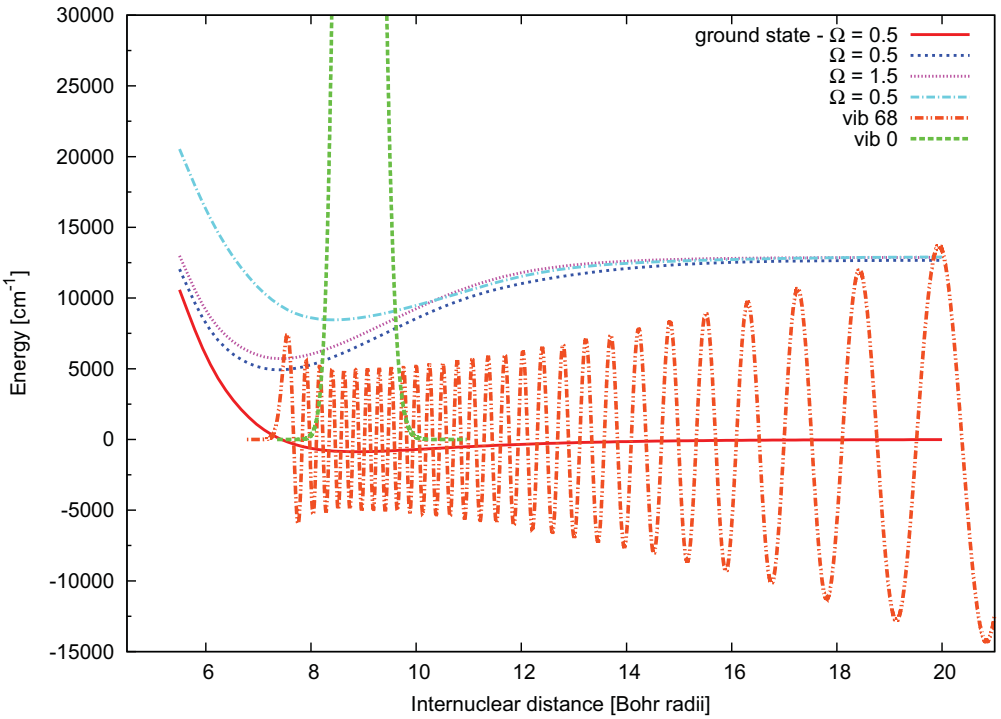

electronic ground state and those of the three lowest electronically excited states. These calculations were performed for the ^{87}Rb and ^{176}Yb isotopes since these are favorably employed in experiment [11].

In Table 9.13 selected FCFs between the rovibronic ground state (1 0.5, $v = 0$) and vibrational levels of the electronically excited states are listed. (Complete tables of the FCFs are available upon request.) As may be expected from the small geometrical shift between the 1 0.5 and 3 0.5 potential energy wells (see Section 9.4.3.3), large Franck-Condon overlaps for the lowest vibrational levels of the 3 0.5 state are obtained. For the first excited 2 0.5 as well as the 1 1.5 state significant FCFs are observed for a wide range of vibrational states due to the large spatial extent of the electronic ground state as the maximum amplitude of the $v = 0$ wave function coincides approximately with the outer turning points of these excited-state vibrational wave functions.

FCFs between the calculated highest vibrational state ($v = 69$) of the electronic

Table 9.13: Selected Franck-Condon factors between the rovibronic ground state and vibrationally excited states (v) of the electronically excited states of $^{87}Rb^{176}Yb$.

State	v	Δ E [cm^{-1}]	FC factor
1 0.5 – 2 0.5	0	5839	3.4D-11
1 0.5 – 2 0.5	1	5908	7.8D-10
1 0.5 – 2 0.5	2	5976	8.9D-09
1 0.5 – 2 0.5	14	6777	7.1D-03
1 0.5 – 2 0.5	15	6842	1.1D-02
1 0.5 – 2 0.5	16	6907	1.7D-02
1 0.5 – 2 0.5	23	7357	7.5D-02
1 0.5 – 2 0.5	24	7421	7.8D-02
1 0.5 – 2 0.5	25	7484	7.7D-02
1 0.5 – 2 0.5	35	8105	1.2D-02
1 0.5 – 2 0.5	36	8165	8.1D-03
1 0.5 – 2 0.5	37	8226	5.6D-03
1 0.5 – 1 1.5	0	6612	1.0D-10
1 0.5 – 1 1.5	1	6681	2.2D-09
1 0.5 – 1 1.5	2	6749	2.4D-08
1 0.5 – 1 1.5	13	7483	6.4D-03
1 0.5 – 1 1.5	14	7549	1.1D-02
1 0.5 – 1 1.5	15	7614	1.6D-02
1 0.5 – 1 1.5	22	8063	7.6D-02
1 0.5 – 1 1.5	23	8127	7.9D-02
1 0.5 – 1 1.5	24	8190	7.8D-02
1 0.5 – 1 1.5	34	8810	1.2D-02
1 0.5 – 1 1.5	35	8870	8.1D-03
1 0.5 – 1 1.5	36	8931	5.5D-03
1 0.5 – 3 0.5	0	9350	1.5D-01
1 0.5 – 3 0.5	1	9403	2.3D-01
1 0.5 – 3 0.5	2	9454	2.3D-01
1 0.5 – 3 0.5	3	9506	1.7D-01
1 0.5 – 3 0.5	4	9557	1.0D-01
1 0.5 – 3 0.5	12	9964	1.2D-04
1 0.5 – 3 0.5	13	10014	3.9D-05
1 0.5 – 3 0.5	14	10064	1.3D-05
1 0.5 – 3 0.5	20	10359	8.0D-09
1 0.5 – 3 0.5	21	10407	2.2D-09
1 0.5 – 3 0.5	22	10456	5.7D-10

Table 9.14: Selected Franck-Condon factors between the highest excited vibrational state ($v = 69$) of the electronic ground state and vibrationally excited states (v) of the electronically excited states of $^{87}Rb^{176}Yb$.

State	v	Δ E [cm^{-1}]	FC factor
1 0.5 – 2 0.5	0	5007	1.7D-04
1 0.5 – 2 0.5	1	5076	4.9D-05
1 0.5 – 2 0.5	2	5144	3.1D-05
1 0.5 – 2 0.5	14	5945	1.2D-05
1 0.5 – 2 0.5	15	6010	1.5D-05
1 0.5 – 2 0.5	16	6075	4.3D-05
1 0.5 – 2 0.5	37	7394	3.4D-05
1 0.5 – 2 0.5	38	7454	3.5D-06
1 0.5 – 2 0.5	39	7515	1.4D-05
1 0.5 – 1 1.5	0	5780	1.9D-04
1 0.5 – 1 1.5	1	5848	1.5D-05
1 0.5 – 1 1.5	2	5917	7.1D-05
1 0.5 – 1 1.5	13	6651	2.8D-05
1 0.5 – 1 1.5	14	6716	4.1D-06
1 0.5 – 1 1.5	15	6782	4.5D-05
1 0.5 – 1 1.5	37	8159	3.4D-06
1 0.5 – 1 1.5	38	8219	1.4D-05
1 0.5 – 1 1.5	39	8279	3.7D-05
1 0.5 – 3 0.5	0	8518	9.6D-15
1 0.5 – 3 0.5	1	8570	5.8D-14
1 0.5 – 3 0.5	2	8622	5.1D-16
1 0.5 – 3 0.5	12	9132	2.7D-05
1 0.5 – 3 0.5	13	9182	3.3D-05
1 0.5 – 3 0.5	14	9231	7.9D-06
1 0.5 – 3 0.5	20	9527	1.4D-04
1 0.5 – 3 0.5	21	9575	2.0D-05
1 0.5 – 3 0.5	22	9623	6.3D-05

Figure 9.11: Sørensen et al. JPCA 2009; CCSD(T) and CCSD dipole moment curve in Debye with 23 explicitly correlated electrons. The vibrationally averaged dipole moment for CCSD and CCSD(T) is found to be 0.761 and 0.985 Debye, respectively.

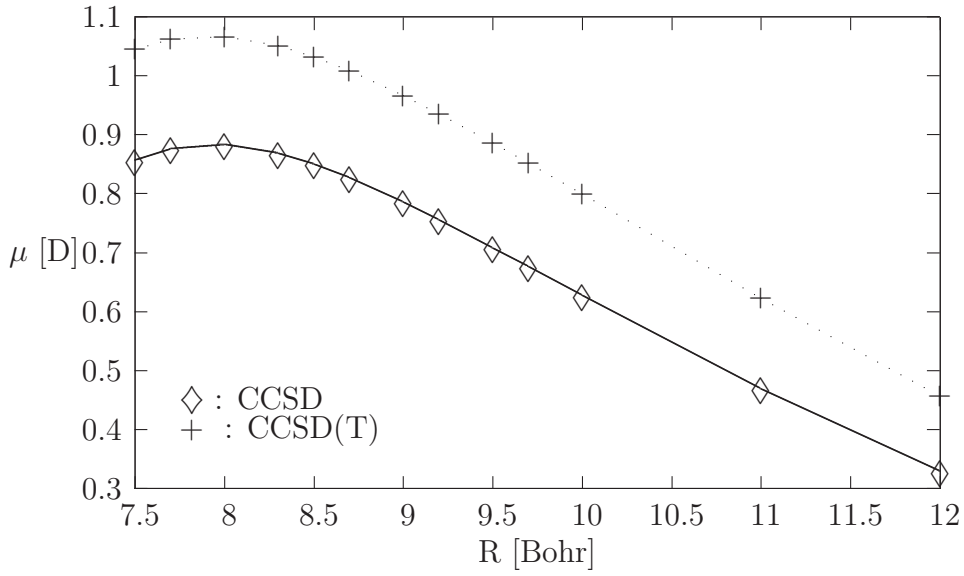

ground state were found to be on the order of 10^{-4} to 10^{-6} for the 2 0.5 , 1 1.5 , and 3 0.5 electronic states as shown in Table 9.14. Contrary to the situation for the 2 0.5 and 1 1.5 states, none of the vibrational levels of the 3 0.5 state has non-negligible FCFs with the $v = 0$ and $v = 69$ levels of the electronic ground state at the same time. This is, however, a requirement for an effective experimental excitation/deexcitation process. The difficulty in determining which state will have the largest combined Franck-Condon overlap with both the highest and lowest vibrational state of the electronic ground state is demonstrated in Figure 9.10 where the difference in these two vibrational states are clearly visible.

Our findings thus support a postulated two-step scheme mentioned afore aiming at reaching the lowest rovibrational level of the electronic ground state [193]. However, we propose to use either the 2 0.5 or 1 1.5 state as intermediate for this process.

9.4.3.5 Dipole Moment

Besides having a magnetic dipole moment from an unpaired electron, RbYb also exhibits an electric dipole moment of around 1 Debye as illustrated in Figure 9.11. A fit of the CCSD and CCSD(T) dipole moment curves results in an electric dipole moment of

0.763 and 0.987 Debye, respectively, at the equilibrium bond distance. A slight decrease of around 0.01 Debye is observed if the CP correction is added to the ground state as reported in Table 9.15. It should be noted that in these cases the dipole moment has not been CP-corrected but has been evaluated at the CP-corrected equilibrium bond distance. In Table 9.15 we have also listed the vibrationally averaged dipole moment which is only slightly lower despite the large variation shown by the dipole moment across the rovibrational ground state.

Table 9.15: Dipole moments at R_e (μ_e) and the vibrationally averaged dipole moment μ_v for the CCSD and CCSD(T) levels of theory with 23 explicitly correlated electrons and with CP corrected values.

Method	μ_e [D]	μ_v [D]
CCSD-SF	0.763	0.761
CP-CCSD-SF	0.751	0.747
CCSD(T)-SF	0.987	0.985
CP-CCSD(T)-SF	0.977	0.974

9.4.4 Summary and Conclusions

In this study we demonstrate the capability of our relativistic all-electron quantum-chemical methodology to yield accurate ground and excited states on this new and challenging system by approaching the problem in a systematic way. We show that with our chosen MRCI model we are not only able to obtain excellent atomic data but we are also able to get close to the accurate CCSD(T) data around the equilibrium bond distance of the ground state. We furthermore report spectroscopic constants and Franck-Condon factors for ground and excited states.

Our coupled cluster calculations indicate that RbYb possesses a substantial dipole moment of almost 1 Debye thus making it an excellent candidate for the study of dipole-dipole interactions and considering its magnetic dipole moment making it accessible to magneto-optical trapping. Strongest candidates for reaching the rovibronic ground state via a two-step procedure (after the initial photoassociation), judging from the determined

Franck-Condon factors, appear to be the two lowest excited electronic states. For these two states we find reasonable Franck-Condon factors both for the absorption and for the emission simultaneously. We therefore propose the following two-color process. The longer wavelength laser should excite the molecule to levels with vibrational quantum numbers in the range of $v = 15 - 35$ in either the 2 0.5 or 1 1.5 potential wells followed by stimulated emission to the rovibronic ground state. This mechanism will give the largest combined Franck-Condon overlap. This picture can, however, change depending on how well the ground state is determined. For example, a shorter equilibrium bond distance for the ground state would favor the first two excited states whereas a longer would favor the third excited state. We have therefore performed high-level coupled cluster benchmark studies using a varying number of correlated electrons to calibrate our results.

The inclusion of higher excited states in this molecule necessitates core polarization from Yb $4f5p$ as these correlate to the atomic $\mathrm{Yb}_{6s^16p^1}(^3P_{2,1,0})$ channels thereby dramatically increasing the computational demand of the problem. Moreover, an accurate description of the $\mathrm{Rb}_{4d^1}(^2D_{5/2,3/2})$ atomic limit which will lie in between the $\mathrm{Yb}_{6s^16p^1}(^3P_{1,0})$ and $\mathrm{Yb}_{6s^16p^1}(^3P_2)$ channels would require additional higher angular momentum functions to be included in the basis set on Rb. Furthermore, Yb $4f - 5d$ excitations need to be taken into account which are extremely difficult to compute properly. From the methodological aspect one would here also come to the limit of CI because with 31 explicitly correlated electrons size-extensivity errors would likely become sizeable. A change to a size-extensive method would then be desirable. Such an approach is currently being investigated by extending the newly implemented general-order four-component multireference coupled cluster [68] to allow for the treatment of excited states.

9.5 $(\mathrm{RbBa})^+$

Collisions of ultracold Ba^+ ions on a Rb Bose-Einstein condensate have been suggested as a possible benchmark system for ultracold ion-neutral collision experiments, however, *a priori* knowledge of the possible processes is desirable. For this purpose we here present high-level four-component coupled-cluster and multireference configuration interaction calculations of potential energy curves, dipole moment, and spectroscopic constants of the experimentally interesting low-lying electronic states of the $(\mathrm{RbBa})^+$ molecule. Our

results show significant avoided crossings between the $^3\Sigma^+_{1,0^-}$ Rb + Ba^+ entrance channels and low-lying charge transfer $^3\Pi_{1,0^-}$ states of the Rb^+ and $Ba_{6s^15d^1}(^3D)$ atomic channels, indicating that a fast non-radiative charge transfer could be possible. For the ground state population analysis shows that the ground state deviates significantly from a pure Rb^+ + Ba interaction but instead a partially covalent polar bond is formed. This finding is corroborated by the electric dipole moment which is found only to be 4.5 D at the equilibrium bond distance, compared with the 14 D for a pure Rb^+ + Ba interaction, thereby supporting the view of a partial charge transfer between the two atoms.

9.5.1 Introduction

The study of reactive collisions at very low temperatures is a promising new direction in the field of cold and ultracold quantum matter. This temperature regime comprises a unique environment to investigate, *i.a.*, the quantum mechanical details of chemical reactions, ultimately aiming at a controlled chemistry at the quantum level [16]. Other interesting prospects concern the possibility of testing fundamental symmetries in nature [17, 18] or the space-time independence of electron and nuclear masses [20].

Ion-neutral interactions are distinguished from neutral-neutral collisions in that the interaction of the former is long-range, in general leading to large collision cross Sections [194] and entailing the possibility of charge transfer between the collision partners [195]. Quite a number of experimental and theoretical studies of ion-neutral reactions exist, but the low-energy regime has only been addressed recently, *e.g.* in references [194, 196, 197]. Due to the complexity of the level of ab-initio electronic-structure calculations needed for determining the accurate short-range potentials, most of these studies considered few-electron systems. The limited number of investigations on many-electron systems involving a cationic reaction partner, such as the studies on $(NaNa)^+$ and $(NaCa)^+$ [195, 198], employ rather approximate potentials involving parameters taken from experiment.

Also other aspects of ion-neutral collisions beside the charge-transfer processes have received attention. The formation of a postulated mesoscopic molecular bound state arising from a single trapped ion in a sea of ultracold atoms [199] comprises an intriguing finding. In this context, the collision kinetics and electronic potential energy curves of the molecular benchmark system $(RbBa)^+$, starting from a Ba^+ ion that interacts with a

Bose-Einstein condensate of neutral Rb atoms, are of great interest [200]. The $(RbBa)^+$ system is valence isoelectronic with the $(MgK)^+$, $(MgCs)^+$, and $(NaCa)^+$ systems which have been considered in earlier experiments [198, 201, 202]. The associated theoretical investigations were mainly carried out using large-core pseudopotentials and neglecting spin-orbit coupling. In these systems, the lowest-lying electronic states are characterized as Σ states, which is also true for the $(RbBa)^+$ molecular ion [27] and most likely also for another heavier species of interest, $(MgCs)^+$. The neglect of spin-orbit interaction is reasonable in the determination of such Σ states, since it affects these states only through higher-order couplings to excited states of different angular momentum projection onto the internuclear axis. For the $(RbBa)^+$ molecular ion, however, electronic states of projection $\Lambda > 0$ play a role for the lowest dissociation channels to the different atomic fragments [27]. An understanding of experiments involving the lower dissociation channels of $(RbBa)^+$ which come to lie in an energy window of about 2 eV, therefore necessitates inclusion of spin-orbit interaction in the electronic-structure calculations.

The objective of this study has been to investigate the electronic excited states lying close to the Rb + Ba^+ entrance channel and expected to have a complicated distance dependence, to form a firm basis for design of ultracold collision experiments for this system. One aim here was the search for possible charge transfer mechanism from Rb to Ba^+ by a characterization of the excited states. Another closely related aim was the search for metastable excited states which could be used for creating a mesoscopic molecular bound state with the Rb Bose-Einstein condensate. To obtain this objective we extend an earlier

scalar relativistic study [27] to also include the spin-orbit interaction, which we will show to be imperative for an understanding of the charge transfer mechanisms in $(RbBa)^+$ at ultracold experimental conditions.

Since two heavy atoms are involved we apply quantum-chemical methods which treat electron correlation and relativistic effects on the same footing. Relativistic coupled-cluster and configuration interaction approaches are used in a complementary fashion, the details of which are described in the following section. In the main body of the section (Section 9.5.3) we achieve high accuracy by first a systematic study of the ground and excited states of the atoms and, in addition, of the electronic ground state of the molecule. Based on these results, a final multireference configuration interaction (MRCI)

model expansion is chosen which can deliver accurate spectroscopic values for the states in question and describe well the relevant avoided crossings of the potential curves. We present and discuss electronic molecular potentials obtained with the MRCI model and point to possible radiative as well as non-radiative charge transfer processes which can occur. We also investigate the ground state dipole moment as a function of distance to visualize effects of any covalent character in the ground state. In the final section we summarize and draw conclusions.

9.5.2 Theory and Computational Details

9.5.2.1 Hamiltonian Operator

Atomic excitation energies along with ionization potentials suggest a rich manifold of low-lying excited states with angular momentum projection greater than zero in the region around the Rb_{5s^1} + $Ba^+_{6s^1}$ entrance channel. This was confirmed by the calculations in a previous study [27] where the nine lowest-lying molecular electronic states of the $(RbBa)^+$ ion were calculated employing a spin-free Hamiltonian. These spin-free states will split into their Ω components upon taking into consideration spin-orbit coupling. Since these high angular momentum states are possible candidates for a charge transfer from Ba^+ to Rb, which could be lead to a transition to the electronic ground state, it is therefore essential to account properly for the various Ω components of these higher angular momentum states to aid the interpretation of ongoing experiments [200]. We therefore here extend the spin-free investigation to account for spin-orbit interactions in the rigorous four-component Dirac-Coulomb framework. All classes of two-electron integrals were included, also the integrals involving four small-component indices and spin-orbit, except where otherwise noted.

9.5.2.2 Correlation Methods and Setup

In the study of the ground state properties we used the `RELCCSD` module [74,125] which can perform coupled-cluster single doubles (CCSD) and perturbative triples (CCSD(T)) calculations and is available in the `DIRAC08` quantum chemistry program package [57]. Since the dominant relativistic contribution for the ground state of $(RbBa)^+$ is scalar relativistic we employed the computationally cheaper spin-free Dirac-Coulomb Hamiltonian by

Table 9.16: Spectroscopic values for the $\Omega = 0^+$ ground state calculated at the spin-dependent MRCI S12_(2in13)_SD level in comparison to CC results, both at the spin-free (SF) and spin-dependent levels, and results from earlier spin-free MRCI SF-SD16_(2in7)_SD where an ANO-RCC basis was used and with a truncation of the virtual space at 5 E_h. Counterpoise corrections ("cp-" prefix) have also been tested.

Method	R_e[bohr]	ω_e [cm^{-1}]	D_e [cm^{-1}]
SF-SD16_(2in7)_SD [27]	8.75	54.327	5509
S12_(2in13)_SD	8.72	51.773	5055
SF-CCSD	8.80	52.171	4887
CCSD	8.80	52.187	4886
SF-CCSD(T)	8.75	52.785	5035
CCSD(T)	8.75	52.799	5034
cp-SF-CCSD	8.81	52.145	4877
cp-CCSD	8.80	52.161	4876
cp-SF-CCSD(T)	8.76	52.755	5023
cp-CCSD(T)	8.76	52.768	5022

Dyall [64] in the ground-state calculations. This was checked against the Dirac-Coulomb (DC) Hamiltonian as shown in Table 9.16, and the spin-orbit effect on the ground state potential was found to be well within the expected error bounds for the spectroscopic properties. We therefore consistently used the spin-free Hamiltonian for the ground-state calculations since the time consuming part in the CCSD and CCSD(T) with the DC Hamiltonian is the flipping of the Kramers projection to describe the in this case negligible spin-orbit contribution to the electronic potential. Along the entire potential energy curve we used closed-shell spin-free Dirac-Coulomb Hartree Fock (SF-DCHF) for the generation of molecular spinors. This was employed since the ground state is dominated by a single determinant. The CCSD(T) furthermore served to validate the quality of the MRCI calculations.

In the coupled-cluster and MRCI treatments we decided to correlate the valence and outer core electrons, i.e. the $4p$ shell on Rb^+ and the $5p$ and $6s$ shells on Ba. Recent studies on LiCs [30] (see also Sections 9.3 and 9.6) showed that the correlation of the core $4d$ shell on Cs had very little impact on the spectroscopic values, and this would then be expected also to be the case for the $3d$ shell on Rb and the $4d$ shell on Ba. The LiCs

study also showed that the energetically lower-lying $5s$ outer core on Cs contracted the bond by about 0.02 bohr which is expected to carry over for the outer core $4s$ Rb and $5s$ Ba.

Ground- and excited-state wave functions along with vertical and adiabatic excitation energies have been calculated with the recently parallelized [131] relativistic double group large-scale MRCI program `LUCIAREL` [71–73]. This code is able to routinely handle large CI expansions ($> 10^9$ determinants) on standard Linux-based clusters. This CI program will be made available in the forthcoming release of the `DIRAC` program package. By exploiting the generalized active space (GAS) concept in the CI, a flexible correlation treatment is possible. The orbital space can be divided into any number of sub-orbital spaces and any restrictions can be imposed on the allowed excitations between these sub-orbital spaces. The molecular spinors can in the developers version of `DIRAC` be obtained from either DCHF, Kramers-restricted multi-configurational self-consistent-field (KR-MCSCF), [130] or natural MP2 spinors [179]. We found that the best way to obtain accurate excitation energies in this case was to start from a closed-shell DCHF. The Ω quantum number for a given electronic state has been assigned by calculating the expectation value for the $\hat{j}_z$ operator [203].

In the MRCI calculations we included the Rb $5s5p$ and the Ba $5d6s6p$ spinors (of which only Ba $6s$ is formally occupied in the ground state) in the active space, yielding a distribution of two valence electrons in 13 Kramers pairs. Single holes in the Rb $4p$ and Ba $5p$ shells were included to describe outer-core polarization, and single and doubles into the energy selected virtual spinors (see Section 9.5.2.3) were included to account for dynamic correlation. In our notation we dub this computational scheme S12_(2in13)_SD which follows the notation of GAS1_(GAS2)_GAS3 laid out in earlier publications [204].

9.5.2.3 Basis Sets and Basis Set Superposition Error

All calculations were performed using uncontracted scalar Gaussian type orbitals (GTO) large component basis sets. The small component basis functions were generated by restricted kinetic balance condition [205]. For all the ground-state coupled cluster calculations we used extended TZ basis sets by Dyall [206]. For Rb the $(29s21p15d2f)$ basis set is his TZ basis set extended with his correlating and polarizing functions for the valence and the $4s4p$ shells, since this choice of basis set has been shown to perform well in a

recently published paper on RbYb [204]. For Ba we added Dyall's correlating and polarizing functions for the valence and the $5s5p$ shells to form an $(31s25p18d3f)$ extended TZ basis set. The polarizing functions were added to ensure accurate dipole moments for the electronic ground state.

For the MRCI calculations, where the focus was on proper treatment of all low-lying excited states, we followed the scheme in Ref. [207], and the Ba basis set was further augmented with one diffuse d, f, and g function with exponents of 0.036645714, 0.3000341, and 0.76354824, respectively, in the MRCI treatment. This was done in order to properly describe excitations to the Ba $5d$ shell which plays a crucial role in the charge transfer from Rb to Ba^+ and could enable a transition to electronic ground state. The polarizing functions were, on the other hand, not included since no electric properties were calculated with the MRCI. This setup results in a total of $(28s20p14d1f)$ for Rb and $(30s24p18d3f1g)$ for Ba. This basis set has been used in all MRCI calculations.

Table 9.17: Spectroscopic values for the $\Omega = 0^+$ ground state calculated with the spin-free (SF) CCSD and CCSD(T) methods, with an energy truncation threshold for active virtual spinors at 18 and 42 Hartree, and using the Visscher small component approximation [164].

Method	Virtuals truncation	R_e[bohr]	ω_e [cm^{-1}]
SF-CCSD	18	8.8027	52.179
SF-CCSD	42	8.8025	52.179
SF-CCSD(T)	18	8.7528	52.794
SF-CCSD(T)	42	8.7526	52.795

The threshold for the truncation of the virtual spinors in all the correlated calculations was set at 18 Hartree. The validity of this choice was checked for the ground state at the CCSD and CCSD(T) levels using the approximation to the small-component density by Visscher [164]. To this end, complete potential energy curves with a truncation of the virtuals at 42 Hartree were also constructed. As seen from the results in Table 9.17 the truncation errors in the spectroscopic parameters derived from these calculations are more than a factor of 100 smaller than the difference between CCSD and CCSD(T).

Table 9.18: A selection of molecular electronic states in the $\Lambda - S$ coupling picture and associated atomic dissociation channels in an energy range of up to ≈ 14000 cm^{-1}.

Atomic $^{(2S+1)}L_J$	Molecular $^{(2S+1)}\Lambda_\Omega$
$Rb^+_{5s^0}$ $(^1S_0)$ + Ba_{6s^2} $(^1S_0)$	$^1\Sigma^+_{0^+}$
Rb_{5s^1} $(^2S_{1/2})$ + $Ba^+_{6s^1}$ $(^2S_{1/2})$	$^3\Sigma^+_{1,0^-}$, $^1\Sigma^+_{0^+}$
$Rb^+_{5s^0}$ $(^1S_0)$ + $Ba_{6s^15d^1}$ $(^3D_{1,2,3})$	$^3\Delta_{3,2,1}$, $^3\Pi_{2,1,0^+,0^-}$, $^3\Sigma^+_{1,0^-}$
$Rb^+_{5s^0}$ $(^1S_0)$ + $Ba_{6s^15d^1}$ $(^1D_2)$	$^1\Delta_2$, $^1\Pi_1$, $^1\Sigma^+_{0^+}$
$Rb^+_{5s^0}$ $(^1S_0)$ + $Ba_{6s^16p^1}$ $(^3P_{0,1,2})$	$^3\Pi_{2,1,0^+,0^-}$, $^3\Sigma^+_{1,0^-}$

The basis set superposition error (BSSE) in the electronic ground state was accounted for by applying the counterpoise (CP) correction as suggested by Boys and Bernardi [165] (see also Section 9.4.2.6).

9.5.2.4 Dipole Moments

Dipole moments along the ground state potential energy curve were calculated using the finite-field technique where we varied the electric field along the bond axis (chosen as z). For the dipole moment a seven-point numerical derivative has in previous publications [30, 204] been shown not to be the limiting factor for the accuracy of the dipole moment and will therefore also be used here. The field strengths used were ± 0.0001, ± 0.0002, and ± 0.0004 $E_h\, e^{-1}\, bohr^{-1}$ to form the numerical derivative of the energy with respect to electric field taken at zero field strength. The origin of the molecular coordinate system was chosen to lie in the center of mass. In this way we could calculate the dipole moment at different internuclear distances with the WFFIT program from Sadlej [208], and this has been done at the CCSD and CCSD(T) levels of theory for the ground state.

9.5.3 Results

Table 9.18 compiles the atomic configurations and terms as well as their corresponding molecular states that form the lower part of the electronic spectrum of the $(RbBa)^+$ molecular ion up to $\approx$ 14000 cm^{-1} above the ground state. These molecular states include also the Σ states correlated with the entrance channel for the envisaged collision

experiments involving an ultracold ionized trapped barium atom and a Bose-Einstein condensate of neutral rubidium atoms. In the following we shall elaborate on our results for all the molecular states located below the entrance channel plus d channels associated with the $Rb^+_{5s^0}(^1S_0)$ + $Ba_{6s^1 5d^1}(^3D_{1,2,3}$; $^1D_2)$ atomic limits listed in Table 9.18. As our results discussed in Section 9.5.3.3 show, notable interactions between electronic states of the same Ω quantum number are observed for the molecular states correlating with these channels. It is therefore anticipated that radiative as well as non-radiative transitions will play a crucial role in the charge transfer process from Rb + Ba^+ to Rb^+ + Ba and of the life time of the different states in the excited state manifold.

9.5.3.1 Atomic Calculations and Ionization Potentials

Table 9.19 compiles our results of atomic and atomic-like excitation energies of the lowest Ba atomic transitions as well as previous theoretical work and experimental data. Comparisons of our atomic MRCI S6_(2in9)_SD and the atomic-like molecular MRCI S12_(2in13)_SD results show that the dissociation limit is reached at an internuclear separation of 50 bohr. From previous studies on transition metals it is known that ns^2(n-1)d^m $\rightarrow$ ns^1(n-1)d^{m+1} excitations are difficult to describe in general within an MRCI approach because of the slow convergence of the dynamical electron correlation contributions [209]. Multireference CC approaches, such as for example the Fock-space CCSD (FSCCSD) or the intermediate Hamiltonian IHFSCCSD methods [108, 210, 211], are better at describing dynamical electron correlation energies. They are therefore expected to yield closer agreement with experiments, as the results in Table 9.19 confirm. In view of these difficulties for MRCI the deviations of our computed ^{3}D and ^{1}D excitation energies from the experimental values on the order of a few 100 cm^{-1} are satisfactory. The fine-structure splittings of these terms are even reproduced within a few tens of cm^{-1}(see Table 9.19). Furthermore, the good agreement of our calculated $Ba_{6s^1 6p^1}(^3P)$ energies to experiments shows that the chosen basis set and correlation treatment are adequate.

In addition to the energetic location of the low-lying neutral Ba channels, the differential ionization potential of Rb and Ba is of vital importance for an unbiased description of the $(RbBa)^+$ molecular states. Our computed ΔIP (IP(Ba)-IP(Rb)) value of 8454 cm^{-1} is in excellent agreement with experiment (8344 cm^{-1}) [213]. This ΔIP was calculated as the excitation energy in the atomic-like limit at 50 bohr of a molecular calculation.

The Ba^+ + Rb entrance channel is thus placed only slightly below the $Ba_{6s^15p^1}(^3D_1)$ + $Rb^+_{5s^0}$ atomic channel. This is in contrast to the lighter homologs $(NaCa)^+$, $(MgK)^+$ and $(MgCs)^+$ where the corresponding energy gap is much larger.

9.5.3.2 Ground State Potential

In Table 9.16 we report our calculated MRCI spectroscopic constants for the $^1\Sigma^+_{0^+}$ ground state of $(RbBa)^+$ and compare with values derived from our four-component CCSD and CCSD(T) calculations. In agreement with the findings of an earlier study on RbYb [204], counterpoise correction has only a minor effect on the spectroscopic constants of the ground state. Inspecting Table 9.16, it is comforting that the present spin-dependent MRCI S12_(2in13)_SD approach compares favorably to the more sophisticated CCSD(T) method. The deviation of 0.03 bohr in the equilibrium bond distance R_e is small for such

Table 9.19: Excitation energies T in cm^{-1} for the lowest $Ba_{6s^2}(^1S_0) \rightarrow Ba_{6s^15d^1}(^3D_{1,2,3})$, $Ba_{6s^2}(^1S_0) \rightarrow Ba_{6s^15d^1}(^1D_2)$ and $Ba_{6s^2}(^1S_0) \rightarrow Ba_{6s^16p^1}(^3P_{0,1,2})$, electronic transitions calculated at the atomic MRCI S6_(2in9)_SD and atomic-like S12_(2in13)_SD (molecular calculation; values taken at $R = 50$ bohr) levels. The active space in the atomic calculation includes the same Ba shells and the same truncation threshold for the virtual spinors as in the molecular case. Details on the molecular computational level are given in the text. The MRCI results are compared to previous theoretical and experimental data. In the atomic-like "J states" (Ω) the individual M_j components are almost degenerate at $R = 50$ bohr with deviations on the order of $4 - 8$ cm^{-1} from the lowest to highest M_j component. We here show the energies of the lowest M_j values in the table.

	$^1S_0$	$^3D_{1,2,3}$			$^1D_2$	$^3P_{0,1,2}$		
Method	$J = 0$	$J = 1$	$J = 2$	$J = 3$	$J = 2$	$J = 0$	$J = 1$	$J = 2$
Experiment [212]	0	9034	9216	9597	11395	12266	12637	13515
Atomic calculations								
S6_(2in9)_SD	0	8627	8809	9175	11197	12732	13091	13944
FSCCSD [210]	0	9075	9260	9639	11621	12423	12802	13793
IHFSCCSD [210]	0	9117	9296	9677	11426	12397	12728	13610
Molecular calculation at $R = 50$ bohr								
S12_(2in13)_SD	0	8619	8812	9174	11198	12736	13109	13936

a weakly-bound molecular ion with $R_e = 8.75$ bohr. Moreover, the harmonic frequency ω_e as well as the dissociation energy D_e agree perfectly with the CCSD(T) values. The differences between the spin-free and spin-dependent MRCI results are mainly attributed to AO basis set effects since in the spin-free case an ANO-RCC basis set with a truncation of the virtual space at 5 E_h was used. As could be expected for a "Σ" state, spin-orbit coupling hardly affects the calculated spectroscopic parameters as seen for the coupled cluster calculations. In contrast we see a substantial contraction of the equilibrium distance and an increase of the dissociation energy by about 150 cm^{-1} when triple excitations are included perturbatively in the coupled cluster treatment. This finding is in line with what has also been observed for other weakly bound systems like LiCs [30] and RbYb [204] (see also Sections 9.3 and 9.4, respectively) where a CCSD treatment was also found to be insufficient.

In the MRCI expansion the ground state is dominated by the reference determinant which has a CI coefficient of 0.94 around equilibrium. A Mulliken population analysis of the underlying DCHF wave function reveals that the highest occupied molecular orbital (HOMO) is not a purely atomic Ba 6s Kramers pair, the Ba 6s spinors are populated by 1.5 electrons. Roughly 0.4 electrons have been transferred to a Rb σ-type orbital. The remaining 0.1 electrons reside in the Ba $5d_\sigma$ that is also involved in the binding. The second largest CI coefficient of about -0.1 is found for the double excitation to the lowest unoccupied molecular orbital (LUMO), which the Mulliken population analysis again reveals to be significantly mixed. The LUMO is composed of Rb 5s(0.613), Ba $6p_z$(0.209), 6s(0.150), and $5d_{xx}$, $5d_{yy}$(0.011). We furthermore see many single and double excitations to molecular spinors which are made up of Rb 5s and 5p and Ba 6s, 6p, and 5d atomic spinors. This large mixing of the atomic spinors is what leads to the choice of including all these spinors in the active space of the MRCI calculations and why we are confident that the MRCI with this active space performs well for the low-lying states. Upon dissociation we observe that the HOMO becomes more and more atomic and localizes on Ba.

The mixing with the Rb 5s and 5p in HOMO also means that the ground-state potential cannot be considered to be just a charge – induced dipole $1/R^4$ interaction between Rb^+ and Ba but that there is a significant amount of the valence electron density residing on the Rb atom. The charge transfer is perhaps not so large that one would talk

about a bond in a chemical sense but we find that the bond is significantly stronger than what would be expected from a charge-induced dipole interaction. With a dissociation energy of around 5000 cm^{-1} (see Table 9.16) this is in fact directly comparable to the dissociation energy of the LiCs alkali dimer where D_e is measured to 5875.455 cm^{-1} [163]. The picture of a partially covalent polar bond is also confirmed by the dipole moment which is significantly influenced by the charge distribution in the molecule (see Section 9.5.3.4).

9.5.3.3 Excited State Potentials

In contrast to the ground state, accounting for spin-orbit coupling in the excited states clearly yields a more complex picture for the potential energy curves of the electronic excited states of the molecular ion $(RbBa)^+$ compared to the spin-free calculations [27]. The avoided crossings between the $^3\Sigma^+_{0^-}$-$^3\Pi_{0^-}$ states and the $^3\Sigma^+_1$-$^3\Pi_1$ states are easily discernible in Figure 9.12 and in the enlargement of the critical region in Figure 9.13. Of course, in the spin-free calculations all these curves cross, and it is thus evident that proper treatment of spin-orbit coupling is mandatory for explanation and prediction of outcomes of ultracold reactive collisions of Ba^+ on a Rb Bose-Einstein condensate. An even more pronounced avoided crossing between the $^1\Sigma^+$ of the entrance channel and the $^1\Sigma^+$ of the $Ba_{6s^15d^1}(^1D)$ channel is also visually identifiable in Figure 9.12. Unlike the above mentioned avoided crossings this one would also be present in a non-relativistic or scalar relativistic calculation. The spin-orbit splitting of the calculated scalar-relativistic states is sizeable, in particular for the $^3\Delta$ and $^3\Pi$ states which are split into their $\Omega = 1, 2, 3$ and $\Omega = 0^+, 0^-, 1, 2$ components (see Figure 9.12 and Table 9.20). This splitting of the $^3\Delta$ and $^3\Pi$ into their Ω components is of 250 and 80 cm^{-1}, respectively, at the ground state equilibrium bond distance. While some of the Ω components are degenerate in the atomic limit because they belong to the same atomic J level, the molecular field gives a spin-orbit splitting also of these components. The $^3\Sigma^+$ state originating from the $Ba_{6s^15d^1}(^3D)$ channel exhibits very irregular behavior due to avoided crossings, and it is therefore not meaningful to give an estimate of the molecular spin-orbit splitting of this state.

Most of the electronically excited states exhibit strong multi-configurational character and are thus more difficult to describe in a molecular orbital picture. We will therefore discuss their electronic structure in a more qualitative way. The lowest excited $\Omega = 0^-$

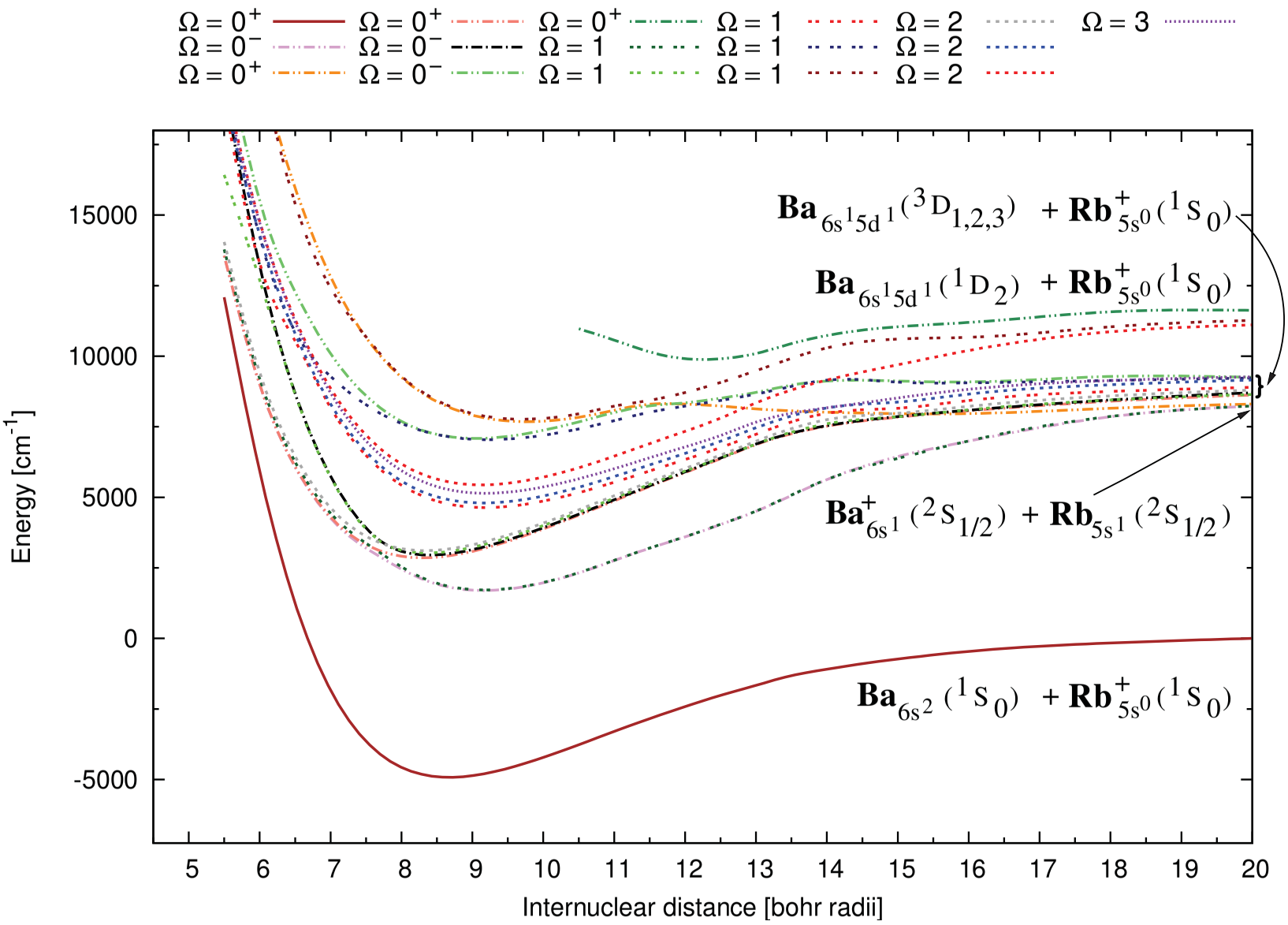

Figure 9.12: Potential energy curves of the ground and low-lying states (Ω designation) of $(RbBa)^+$ computed at the four-component MRCI S12_(2in13)_SD level (see text for more details). Atomic dissociation channels for the states are indicated in the picture (see Table 9.18 for details).

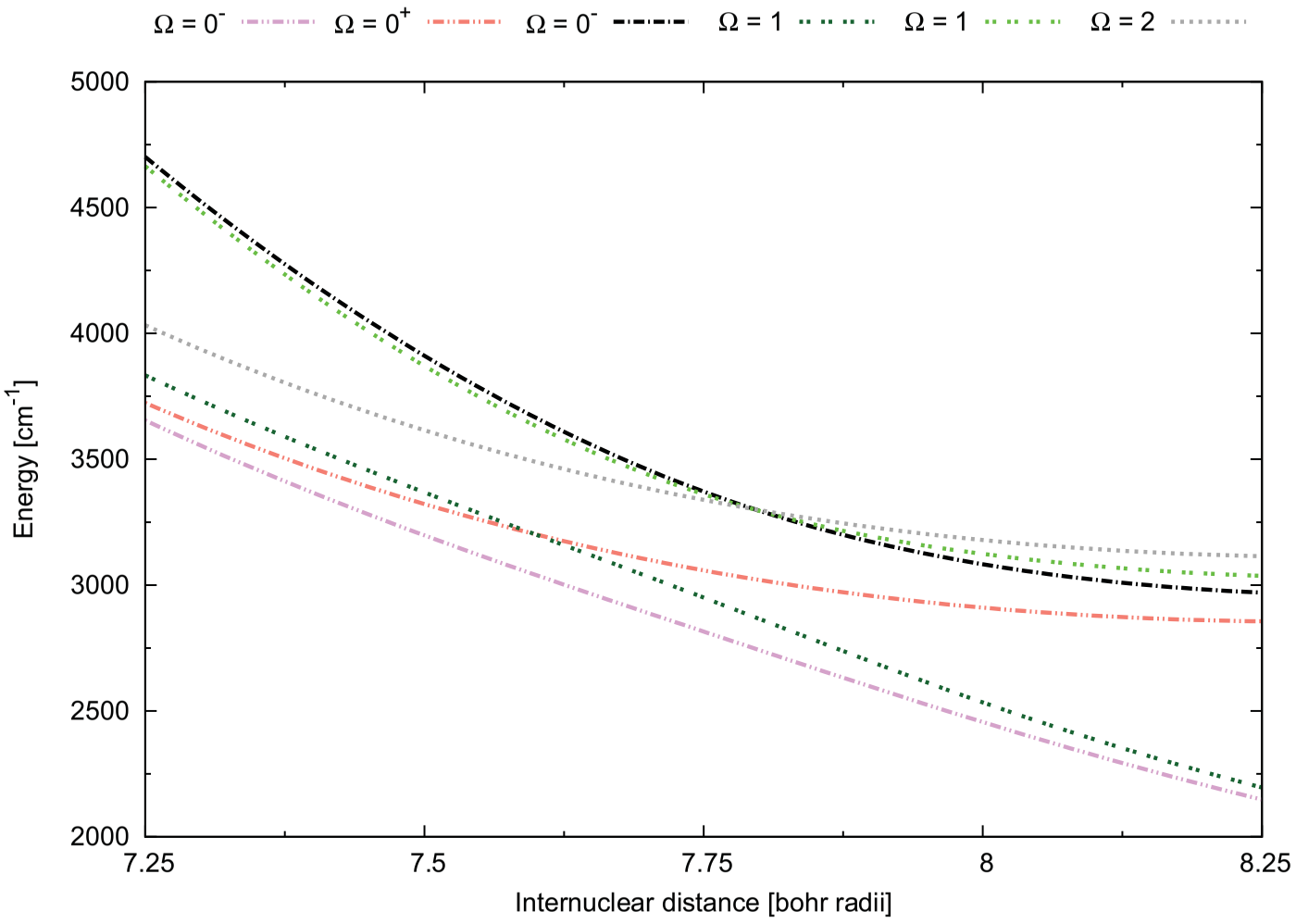

]

Figure 9.13: Close up of the avoided crossings between the $^3\Sigma^+_{1,0^-}$ Rb + Ba^+ entrance channels and and low-lying charge transfer $^3\Pi_{1,0^-}$ states of the Rb^+ and $Ba_{6s^1 5d^1}$ (^{3}D) atomic channels.

Table 9.20: Spectroscopic constants for the ground and lowest excited states (Ω designation) of $(RbBa)^+$ calculated at the MRCI S12_(2in13)_SD level with 14 explicitly correlated electrons.

State	Ω	$\Lambda - S^a$	R_e [bohr]	ω_e [cm^{-1}]	D_e [cm^{-1}]	T_v [cm^{-1}]	T_e [cm^{-1}]
1	0^+	$^1\Sigma^+$	8.72	52	5055	0	0
2	0^-	$^3\Sigma^+$	9.22	45	6889	6711	6621
3	1	$^3\Sigma^+$	9.22	45	6871	6737	6638
4	0^+	$^3\Pi$	8.28	52	5899	7865	7775
5	0^-	$^3\Pi$	8.40	53	5980	7939	7878
6	1	$^3\Pi$	8.28	56	5742	8022	7932
7	2	$^3\Pi$	8.28	52	6702	8109	7156
8	1	$^3\Delta$	9.22	43	4302	9653	9556
9	2	$^3\Delta$	9.22	43	4500	9809	9721
10	3	$^3\Delta$	9.22	43	4157	10165	10064
11	2	$^1\Delta$	9.22	43	5887	10440	10365
12	1	$^3\Sigma^+$	9.22	37	2258	12047	11963
13	0^-	$^3\Sigma^+$	9.03	44	2216	12053	12005
14	0^+	$^1\Sigma^+$	9.77	39	-	13030	12601
15	1	$^1\Pi$	9.72	40	3566	13112	12687

[a] leading $\Lambda - S$ projection

and $\Omega = 1$ states all correlate to a $^3\Sigma^+$ state in the Λ-S representation (see Table 9.18). In the dissociation limit their electronic structure corresponds to $Ba^+ + Rb$. At shorter nuclear distances more and more $Ba_{6s^1 5d^1_\sigma}(^3D)$ character is mixed in. In the Franck-Condon region the wave function has nearly equal contributions from these two configurations. At about 7.75 bohr the $^3\Sigma^+$ components undergo an avoided crossing with the $\Omega = 0^-$ and $\Omega = 1$ of a $^3\Pi$ state (see Figure 9.13). The $^3\Pi$ state has a significantly shorter equilibrium distance than the other states originating from the $Ba_{6s^1 5d^1}(^3D) + Rb^+$ channel (see Table 9.20). This can be traced back to the strong admixture of Ba $6p_\pi$ and Rb $5p_\pi$ character into the Ba $5d_\pi$ spinor.

The non-adiabatic interaction between the $^3\Sigma^+$ and $^3\Pi$ states is anticipated to have significant impact on the charge-transfer process. In the entrance channel the system

is prepared initially in a highly excited vibrational level of the $^3\Sigma^+$ potential. At short internuclear separation the non-adiabatic interaction yields a finite probability for a non-radiative transition to the $^3\Pi$ potential which in turn can relax to the electronic ground state by emission of a photon.

At an internuclear distance of 15 to 16 bohr we see the $^1\Sigma^+$ of the entrance channel crossing the $\Omega = 0^+$ of a $^3\Pi$ state (see Figure 9.12). While formally it would not be allowed for two $\Omega = 0^+$ state to cross it appears that for this charge transfer process the non-adiabatic coupling matrix element or off diagonal element between the two states is so small we cannot visibly see any effect of it. A clear avoided crossing in the 12 to 13 bohr range between the $^1\Sigma^+$ and the higher lying $\Omega = 0^+$ of a $^1\Sigma^+$ from the $Ba_{6s^15d^1}(^1D)$ but also $\Omega = 0^+$ of a $^3\Pi$ of the $Ba_{6s^16p^1}(^3P)$ is observed. These avoided crossing help making the $^1\Sigma^+$ of the entrance channel a metastable state which is in contrast to what is observed in the lighter homologs where this is a dissociative state.

The remaining states correlating with the ^3D channel are dominated by configurations in which the Ba $6d_\sigma$ spinor is singly occupied. As seen from Table 9.20 the Ω components of the $^3\Delta$ state are markedly split by spin-orbit, but exhibit equal equilibrium distances, indicating no differential spin-orbit coupling to other $^s\Lambda$ states.

9.5.3.4 Dipole Moment

Finally, we show in Figure 9.14 the dipole moment curve of the molecular ground state of $(RbBa)^+$ calculated at the four-component CCSD(T) level with origin at the center of mass. The corresponding curve at the CCSD level (not shown) is almost identical, supporting that the CCSD(T) curve is converged. For a charge distribution corresponding purely to Rb^+ and Ba a dipole moment of around 14 Debye could be expected at an internuclear separation of 8.75 bohr (see Fig. 9.14). Due to a partial electron transfer from Ba to Rb^+ (*cf.* discussion in Section 9.5.3.2), the dipole moment of the electronic ground state is significantly lower at the equilibrium distance. As seen in Table 9.21 we find a vibrationally averaged dipole moment of 4.53 Debye at the counterpoise corrected CCSD(T) level. Since the dipole moment function is almost linear around the rovibrational ground state we only see a minor difference between the vibrationally averaged dipole moment and the dipole moment taken at the electronic equilibrium distance as

Figure 9.14: Four-component CCSD(T) dipole moment curve (in Debye) of the molecular ground state with calculated with 14 explicitly correlated electrons. The straight line (blue) indicates the asymptotic limit of the dipole moment μ for a charged system in the center-of-mass coordinates.

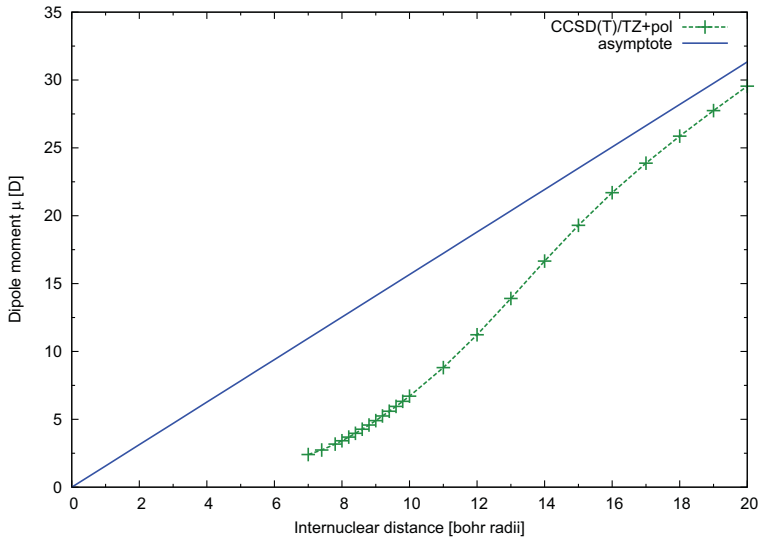

shown in Table 9.21. It should be noted that in perfect agreement with the theory, an asymptotic behavior of the dipole moment is obtained for large internuclear distances.

9.5.4 Summary and Prospects

In an earlier study on the valence isoelectronic system $(NaCa)^+$ of $(RbBa)^+$, a radiative lifetime of charge transfer in the order of 10^4 s to 10^6 s for the $A\ ^1\Sigma^+$ to the $X\ ^1\Sigma^+$ is found by Makarov *et. al* [198]. The $A\ ^1\Sigma^+$ (and most likely also the $a\ ^3\Sigma^+$) electronic states of $(NaCa)^+$ are thus very long-lived metastable species. This occurs since there is no close lying P states mixing into the excited Σ states, making both radiative transitions electric dipole forbidden and for the $a\ ^3\Sigma^+$ also spin forbidden. This is in great contrast to what is observed in $(RbBa)^+$. The non-adiabatic interaction in the short range of the potential (see Figure 9.13) between the $^3\Sigma^+_{1,0^-}$ and $^3\Pi_{1,0^-}$ states is expected to lead to a non-radiative charge transfer from the $^3\Sigma^+_{1,0^-}$ entrance channel to the $^3\Pi_{1,0^-}$ states. While transition from the $^3\Pi_{1,0^-}$ states to the ground state in $(RbBa)^+$ is also in a scalar-relativistic approximation electric dipole and spin forbidden, the large mixing of the Ba $5d_\pi$ with the close lying Ba $6p_\pi$ and Rb $5p_\pi$ spinors induced by spin-orbit coupling will greatly decrease the radiative lifetime.

Table 9.21: Dipole moments at R_e (μ_e) and the vibrationally averaged dipole moment μ_v for the CCSD and CCSD(T) levels of theory and with counterpoise (cp) corrected values.

Method	μ_e [D]	μ_v [D]
SF-CCSD	4.528	4.550
cp-SF-CCSD	4.533	4.556
SF-CCSD(T)	4.507	4.528
cp-SF-CCSD(T)	4.514	4.534

The expected fast non-radiative charge transfer to the $^3\Pi_{1,0^-}$ states may not be experimentally desirable since it will irreversibly 'destroy' the Ba ion. Furthermore the shorter lifetime of the $^3\Pi_{1,0^-}$ states may not be long enough to consider the states metastable for all experiments in question [200]. With the transition dipole moments it would be possible to go from the present qualitative analysis to more quantitative predictions of life times. This is clearly of interest, and this has prompted us to start the development of a MRCI transition dipole moment module [181]. Since Ba is a special case among the alkaline earth metals with its low lying D shell it presents a unique opportunity to study non-radiative charge transfer processes in the excited state manifold thereby making $(RbBa)^+$ experimentally very interesting.

The $(RbBa)^+$ ground state is found to form a partially covalent polar bond stronger than expected. While the dissociation energy is comparable to the LiCs alkali dimer the harmonic frequency is only one third of the LiCs value, showing that the two bonds are significantly different. The broader $(RbBa)^+$ potential shows the longer ranging charge induced dipole interaction against the neutral dissociation of LiCs. We furthermore show that the electronic ground state possesses a dipole moment significantly smaller than what a charge-dipole interaction would lead one to expect. We attribute this finding to a partial charge transfer from Ba to Rb^+.

In this study we demonstrate the capability of our relativistic all-electron quantum-chemical methodology to yield accurate ground and excited states. We show that these methods are capable of handling both neutral and complex ionized systems from the atomic limit all the way in the short range potential. This is seen from the accurate

differential ionization potential ΔIP, atomic excitation energies and fine structure splitting but it is primarily the ability to handle the complicated excited state potentials of highly multi-configurational character. We show that with our chosen MRCI model we can handle the above along with reproducing the accurate CCSD(T) data for the spectroscopic properties of the ground state.

9.6 HBr and LiCs

Although HBr and LiCs have been examined extensively in Sections 9.3 and 9.1 there however appeared for the author unanswered questions on how to systematically approach the exact result for a given Hamiltonian with the usual approximations done for calculations on heavy elements. The author therefore undertook the task of examining what kind of accuracy should be expected with a given basis set, truncation of virtual space, correlation level and how the interplay between these and the number of correlated electrons in two very different systems containing a heavy element. LiCs with a large bond length and dipole moment and low harmonic frequency and dissociation energy and HBr with a small bond length and dipole moment but high harmonic frequency and dissociation energy. Since the largest counterpoise correction is on the heavy atom these systems also differ in that Cs becomes the positive part of the dipole while Br becomes the negative part. This has meant some spectroscopic properties can be calculated with a higher accuracy on one molecule compared to the other and the other way around. The calculations presented in this section are all unpublished calculations. All comparisons have been performed at the CCSD(T) level of theory since the trend of the correlation methods are the same and CCSD(T) is the most accurate method used in this section.

9.6.1 Introduction

The development of algorithms for accurate and efficient description of both relativistic effects and correlation has received large attention over the past decades. The need for robust and simultaneous treatment of both spin-orbit and correlation effects has been nowhere more evident than in the actinides. However, the need for highly accurate potential of simpler heavy dimers in the expanding field of ultra cold molecules has also created a demand for methods which can perform an extensive correlation treatment.

In the non-relativistic framework extensive work has been done in finding the estimation of error bars from systematic calculations on small closed-shell dimers [67, 87, 90]. The studies have been carried out by systematically extending the basis set and the level of correlation for a test set of molecules thereby enabling a statistical investigation of the performance of a correlation method and basis set. For the lightest elements a comprehensive review of this can be found in [67] where all standard *ab initio* methods and basis sets have been examined. In this systematic investigation it is clearly seen that the most efficient many-body theory in electronic structure theory today is the coupled-cluster (CC) model. It has, in combination with extensive large one-particle basis sets [87,90], for the light elements shown to give and unprecedented accuracy. Here smaller relativistic effects has become the dominant error. This has been further carried over to the second row [98] where, however, it was significantly more difficult to achieve the same kind of accuracy since core-correlation become important and the one-particle and N-particle sectors needed to be increased. A trend that would be expected to carry on to the rows below thus making highly accurate calculations on heavy elements extremely expensive.

The aim of this study is to systematically investigate two known systems (HBr and LiCs) to make an estimate of the performance of the correlation treatment, the basis set and the additional approximations used in the calculation of heavy elements like the truncation of the virtual space and outer-core correlation. This will be done for the ground state of these molecules where the number of electrons, the basis set, truncation of virtual space and correlation level will be varied. In this way a systematic examination of the interplay between the basis set, truncation of virtual space and the number of correlated electrons is particularly sought for since it was observed for LiCs in Section 9.3.3.1.1 that a large basis set superposition error (BSSE) was introduced when correlating the outer core electrons. What will be attempted is to establish a systematic way to improve the calculated results within the usual approximations done for calculations and to examine where the truncation of the virtual space should be performed for a balanced description in a given basis set.

9.6.2 Computational Details

For the study of ground-state spectroscopic properties we employed the `RELCCSD` module [74, 125] in the `DIRAC` quantum chemistry program package [57] which can perform

CCSD and CCSD(T) calculations. Although the dominant relativistic contributions to the ground state are scalar relativistic, the full Dirac-Coulomb Hamiltonian has been used throughout since the dissociation energy of HBr is very dependent on spin-orbit effects as previously discussed (see Table 9.1).

In the calculation of the LiCs molecule in Section 9.3 it was seen that correlating up to 12 electrons the BSSE remains small. Including the lowerlying $4d$ electrons in the correlation step to a total of 22 electrons the BSSE rises dramatically and becomes comparable to correlation and relativistic effects. The BSSE in the 22 electron case becomes so large that without a counterpoise correction [165] (cp) the result is far of the experimental one [163]. The 12 electron LiCs calculation will hereafter be called the valence calculation and the 22 electron core-valence calculation. The question then arises whether core-valence calculations can be made without having to resort a CP-correction giving corrections one- to two magnitudes larger than what appears to be the effect of correlating the $4d$ electrons. For HBr the result of including the lowerlying $3d$ electrons on the other hand appears to bring an improvement of the result as seen in Table 9.1. The BSSE was, however, not examined in that case but will be here. In the HBr case it has therefore been chosen to correlate 8 and 18 electrons which will also here be called valence and core-valence correlation, respectively.

All calculations were performed using uncontracted basis sets. For the ground-state coupled-cluster calculations the cc-pVXZ and aug-cc-pVXZ (X=D-Q) basis sets have been used for all valence correlation calculations where the Br basis was taken from [141, 142], Cs [206] and H and Li both from [91]. For the core-valence correlation calculations the correlating functions for the lowerlying d electrons were included creating the cc-pCVXZ and aug-cc-pCVXZ (X=D-Q) basis sets. The small-component basis functions were generated by restricted kinetic balance condition [205] and the approximate small-component density according to Visscher [164] was employed. In the following, the aug-cc-pVXZ will be abbreviated as XZ and the aug-cc-pVXZ basis sets as AXZ.

The counterpoise correction has been performed in the same fashion shown in Section 9.4.2.6 where special care has been taken to include all virtuals on the ghost atom also present in the molecular calculation. Performing the counterpoise correction in this way helps to ensure a balanced description when a truncation in the virtual space is performed. The truncation (in E_h) of the virtual space can therefore differ slightly between molecular

Table 9.22: Values of the truncation threshold of the virtual space in E_h with all correlating functions for HBr and LiCs in a given basis set. The augmented basis sets was truncated at the same level as the regular basis set since the augmenting functions were all below the correlating functions. The value given is the energy of the highest (min) included and the lowest (max) not included orbital. Due to gaps in the virtual space for small basis sets this is not completely systematic.

	LiCs		HBr	
Basis	min	max	min	max
DZ	12.7	19.3	30.1	48.9
TZ	10.5	15.2	34.2	36.6
QZ	24.5	29.4	65.6	76.5

and atom with ghost basis since orbitals can move in the virtual spectrum depending on them being for an atom or a ghost. The total number of occupied plus unoccupied spinors has therefore been sought to remain constant for molecular and atom plus ghost calculations. This means including also the previously occupied virtuals on the ghost atom and still eliminating the not included virtuals from the molecular calculation.

For the study of the truncation of the virtuals space two sets of calculations have been conducted in each basis set and separately counterpoise corrected with atomic and atomic plus ghost calculations. One set of calculations has been performed with a fixed truncation of the virtual space for both the valence and the core-valence calculations. This fixed truncation has been the lowest one used in all calculations which for HBr was set at 14.5 E_h and for LiCs at 13.2 E_h which is still significantly larger than most calculations presented but, as we will see, not sufficient when including core-valence correlation. The higher truncation was set so that all correlating functions for the core-valence calculation would be included. As is seen from Table 9.22 the level where the virtual space is truncated increases significantly with the size of the basis set. A set of calculations for the valence and the core-valence have been performed at this level.

9.6.3 Results

The investigation will proceed along three lines. First, the counterpoise correction will be examined as a function of the basis set and truncation of the virtual space for the

spectroscopic values. Second, the outer-core contribution will be scrutinized and, finally, the difference to experiment for the various calculations will be looked at. All calculations along with the spectroscopic data for LiCs is presented in the Tables 9.23, 9.24 ,9.25 and 9.26 and for HBr in Tables 9.27, 9.28, 9.29 and 9.30. The tables are arranged after, first, the truncation of the virtual space and, second, the number of correlated electrons.

9.6.3.1 Effect of Counterpoise Correction

To examine the effect of the BSSE all curves have been counterpoise corrected. The effect of the counterpoise correction on the various spectroscopic properties presented in the previous tables will here be compared. The comparison is throughout this section made at the CCSD(T) level and presented as uncorrected data minus counterpoise corrected data (CCSD(T) - cp-CCSD(T)). We note here that the curves with the high and low cutoff of the virtual space for LiCs will always coincide for the basis sets DZ to ATZ since this is the same set of data because only one set of calculations has been performed. This was done because the low truncation of the virtual space here included all correlating functions for the $4d$ electrons.

In Figures 9.15 and 9.16 the effect of the counterpoise correction on the equilibrium bond distance is shown for LiCs and HBr, respectively. In the two figures we see the expected trend that fewer correlated electrons with the same truncation of the virtual space gives a smaller counterpoise correction. For LiCs the difference in counterpoise correction on the equilibrium bond distance for the valence and core-valence correlation calculations is seen to increase as the basis set increases until ATZ. At QZ we see a that the calculations with a high virtual cutoff approach each other and ΔR_e tends to zero. For the low cutoff the valence calculation remains more or less constant whereas the core-valence calculation has an increased counterpoise correction. For HBr we see the opposite trend with a slight decrease in the difference between the valence and core-valence calculations as the basis set increases. While for the smaller basis sets the difference between the high and low cutoff is very small here and remains so for the valence calculations it increases again for the large QZ basis set and above for the core-valence calculations. Another noticeable trend is the counterpoise correction with respect to adding polarizing functions. We here see an opposite effect for LiCs and HBr. For LiCs the added polarizing functions significantly decrease the counterpoise correction while for HBr a small increase

Table 9.23: LiCs with 12 correlated electrons and low truncation of the virtual space with and without counterpoise correction.

Method	Basis	corr. el.	R_e [Å]	ω_e [cm^{-1}]	D_e [eV]
CCSD	DZ	12	3.7111	180.915	0.630391
CCSD(T)	DZ	12	3.7000	179.566	0.659989
cp-CCSD	DZ	12	3.7440	178.321	0.608658
cp-CCSD(T)	DZ	12	3.7367	176.613	0.636326
CCSD	ADZ	12	3.7299	182.247	0.641527
CCSD(T)	ADZ	12	3.7172	180.504	0.675867
cp-CCSD	ADZ	12	3.7397	182.235	0.634362
cp-CCSD(T)	ADZ	12	3.7287	180.464	0.667736
CCSD	TZ	12	3.7136	182.462	0.665653
CCSD(T)	TZ	12	3.6905	181.275	0.703407
cp-CCSD	TZ	12	3.7271	182.261	0.656290
cp-CCSD(T)	TZ	12	3.7068	180.974	0.692386
CCSD	ATZ	12	3.7134	183.879	0.670428
CCSD(T)	ATZ	12	3.6887	183.039	0.711259
cp-CCSD	ATZ	12	3.7211	184.136	0.664992
cp-CCSD(T)	ATZ	12	3.6974	183.301	0.705242
CCSD	QZ	12	3.7093	183.923	0.675220
CCSD(T)	QZ	12	3.6806	183.524	0.717607
cp-CCSD	QZ	12	3.7182	184.006	0.669693
cp-CCSD(T)	QZ	12	3.6909	183.591	0.711228
CCSD	AQZ	12	3.7074	184.457	0.677612
CCSD(T)	AQZ	12	3.6787	184.181	0.722920
cp-CCSD	AQZ	12	3.7169	184.860	0.672148
cp-CCSD(T)	AQZ	12	3.6890	184.502	0.716030

Table 9.24: LiCs with 22 correlated electrons and a low truncation of the virtual space with and without counterpoise correction.

Method	Basis	corr. el.	R_e [Å]	ω_e [cm^{-1}]	D_e [eV]
CCSD	DZ	22	3.7083	181.164	0.6270767
CCSD(T)	DZ	22	3.6950	179.766	0.6607280
cp-CCSD	DZ	22	3.7411	178.646	0.6055171
cp-CCSD(T)	DZ	22	3.7324	176.815	0.6368037
CCSD	ADZ	22	3.7270	182.420	0.6393937
CCSD(T)	ADZ	22	3.7124	180.617	0.6769989
cp-CCSD	ADZ	22	3.7376	182.420	0.6314317
cp-CCSD(T)	ADZ	22	3.7249	180.582	0.6679756
CCSD	TZ	22	3.7045	182.922	0.6627914
CCSD(T)	TZ	22	3.6785	181.698	0.7055677
cp-CCSD	TZ	22	3.7214	182.686	0.6516538
cp-CCSD(T)	TZ	22	3.6987	181.320	0.6925008
CCSD	ATZ	22	3.7051	184.534	0.6690328
CCSD(T)	ATZ	22	3.6777	183.680	0.7149266
cp-CCSD	ATZ	22	3.7160	184.523	0.6602190
cp-CCSD(T)	ATZ	22	3.6899	183.633	0.7052394
CCSD	QZ	22	3.6960	184.153	0.6747570
CCSD(T)	QZ	22	3.6639	183.829	0.7225186
cp-CCSD	QZ	22	3.7122	184.492	0.6649228
cp-CCSD(T)	QZ	22	3.6825	183.967	0.7114463
CCSD	AQZ	22	3.6942	185.797	0.6809440
CCSD(T)	AQZ	22	3.6625	185.583	0.7316544
cp-CCSD	AQZ	22	3.7111	185.189	0.6672104
cp-CCSD(T)	AQZ	22	3.6809	184.797	0.7168895

Table 9.25: LiCs with 12 correlated electrons and a high truncation of the virtual space with and without counterpoise correction. For the DZ to ATZ basis sets the high and low truncation of the virtual space is the same. The DZ to ATZ results are presented in Table 9.23

Method	Basis	corr. el.	R_e [Å]	ω_e [cm^{-1}]	D_e [eV]
CCSD	QZ	12	3.7094	184.453	0.6737991
CCSD(T)	QZ	12	3.6811	184.012	0.7165511
cp-CCSD	QZ	12	3.7154	184.242	0.6700085
cp-CCSD(T)	QZ	12	3.6883	183.702	0.7120068
CCSD	AQZ	12	3.7114	185.048	0.6743941
CCSD(T)	AQZ	12	3.6833	184.655	0.7199434
cp-CCSD	AQZ	12	3.7140	185.119	0.6724648
cp-CCSD(T)	AQZ	12	3.6864	184.727	0.7167787

Table 9.26: LiCs with 22 correlated electrons and a high truncation of the virtual space with and without counterpoise correction. For the DZ to ATZ basis sets the high and low truncation of the virtual space is the same. The DZ to ATZ results are presented in Table 9.24

Method	Basis	corr. el.	R_e [Å]	ω_e [cm^{-1}]	D_e [eV]
CCSD	QZ	22	3.7021	184.903	0.6694411
CCSD(T)	QZ	22	3.6709	184.476	0.7174802
cp-CCSD	QZ	22	3.7089	184.761	0.6651172
cp-CCSD(T)	QZ	22	3.6791	184.218	0.7123373
CCSD	AQZ	22	3.7040	185.562	0.6708654
CCSD(T)	AQZ	22	3.6731	185.162	0.7215820
cp-CCSD	AQZ	22	3.7079	185.479	0.6674069
cp-CCSD(T)	AQZ	22	3.6777	185.067	0.7177452

Table 9.27: HBr with 8 correlated electrons and a low truncation of the virtual space with and without counterpoise correction.

Method	Basis	corr. el.	R_e [Å]	ω_e [cm^{-1}]	D_e [eV]
CCSD	DZ	8	1.4159	2690.099	3.6009407
CCSD(T)	DZ	8	1.4170	2677.282	3.6435767
CP-CCSD	DZ	8	1.4237	2651.521	3.4993334
CP-CCSD(T)	DZ	8	1.4255	2635.273	3.5259419
CCSD	ADZ	8	1.4193	2670.590	3.6887266
CCSD(T)	ADZ	8	1.4210	2654.731	3.7351609
CP-CCSD	ADZ	8	1.4290	2621.656	3.5669283
CP-CCSD(T)	ADZ	8	1.4315	2601.303	3.5981243
CCSD	TZ	8	1.4156	2663.658	3.7424313
CCSD(T)	TZ	8	1.4175	2646.030	3.7960169
CP-CCSD	TZ	8	1.4189	2655.761	3.6959814
CP-CCSD(T)	TZ	8	1.4211	2636.330	3.7394716
CCSD	ATZ	8	1.4166	2662.994	3.7736408
CCSD(T)	ATZ	8	1.4189	2643.204	3.8280453
CP-CCSD	ATZ	8	1.4209	2640.843	3.7093131
CP-CCSD(T)	ATZ	8	1.4235	2619.205	3.7512819
CCSD	QZ	8	1.4163	2667.558	3.7947671
CCSD(T)	QZ	8	1.4186	2647.598	3.8535865
CP-CCSD	QZ	8	1.4181	2659.449	3.7789573
CP-CCSD(T)	QZ	8	1.4206	2638.769	3.8211233
CCSD	AQZ	8	1.4168	2664.722	3.8137377
CCSD(T)	AQZ	8	1.4193	2643.724	3.8934783
CP-CCSD	AQZ	8	1.4185	2656.193	3.7901999
CP-CCSD(T)	AQZ	8	1.4212	2634.442	3.8335860

Table 9.28: HBr with 18 correlated electrons and a low truncation of the virtual space with and without counterpoise correction.

Method	Basis	corr. el.	R_e [Å]	ω_e [cm^{-1}]	D_e [eV]
CCSD	DZ	18	1.4123	2697.133	3.620734
CCSD(T)	DZ	18	1.4135	2682.940	3.659243
CP-CCSD	DZ	18	1.4218	2656.543	3.503317
CP-CCSD(T)	DZ	18	1.4237	2638.621	3.532030
CCSD	ADZ	18	1.4154	2681.066	3.709291
CCSD(T)	ADZ	18	1.4171	2663.829	3.761653
CP-CCSD	ADZ	18	1.4270	2626.857	3.572145
CP-CCSD(T)	ADZ	18	1.4297	2604.778	3.605242
CCSD	TZ	18	1.4101	2681.894	3.783206
CCSD(T)	TZ	18	1.4123	2660.259	3.851281
CP-CCSD	TZ	18	1.4138	2666.594	3.707477
CP-CCSD(T)	TZ	18	1.4165	2642.382	3.755416
CCSD	ATZ	18	1.4108	2688.696	3.816584
CCSD(T)	ATZ	18	1.4134	2664.950	3.884838
CP-CCSD	ATZ	18	1.4158	2655.098	3.721208
CP-CCSD(T)	ATZ	18	1.4188	2628.323	3.767230
CCSD	QZ	18	1.4080	2706.805	3.877238
CCSD(T)	QZ	18	1.4106	2682.957	3.938597
CP-CCSD	QZ	18	1.4122	2680.170	3.792638
CP-CCSD(T)	QZ	18	1.4151	2655.494	3.846258
CCSD	AQZ	18	1.4077	2715.914	3.890690
CCSD(T)	AQZ	18	1.4105	2691.333	3.972083
CP-CCSD	AQZ	18	1.4132	2665.160	3.803505
CP-CCSD(T)	AQZ	18	1.4163	2642.570	3.850965

Table 9.29: HBr with 8 correlated electrons and a high truncation of the virtual space with and without counterpoise correction.

Method	Basis	corr. el.	R_e [Å]	ω_e [cm^{-1}]	D_e [eV]
CCSD	DZ	8	1.4157	2690.596	3.6019945
CCSD(T)	DZ	8	1.4169	2677.726	3.6446836
CP-CCSD	DZ	8	1.4236	2651.993	3.5003872
CP-CCSD(T)	DZ	8	1.4253	2635.681	3.5270487
CCSD	ADZ	8	1.4191	2670.963	3.6895759
CCSD(T)	ADZ	8	1.4208	2655.018	3.7360886
CP-CCSD	ADZ	8	1.4288	2622.005	3.5678049
CP-CCSD(T)	ADZ	8	1.4313	2601.591	3.5991064
CCSD	TZ	8	1.4155	2664.127	3.7428765
CCSD(T)	TZ	8	1.4174	2646.449	3.7964947
CP-CCSD	TZ	8	1.4181	2583.882	3.6959912
CP-CCSD(T)	TZ	8	1.4210	2636.739	3.7401127
CCSD	ATZ	8	1.4165	2663.180	3.7739378
CCSD(T)	ATZ	8	1.4188	2643.337	3.8283480
CP-CCSD	ATZ	8	1.4208	2641.113	3.7097733
CP-CCSD(T)	ATZ	8	1.4234	2619.411	3.7518568
CCSD	QZ	8	1.4162	2667.995	3.7951229
CCSD(T)	QZ	8	1.4185	2647.983	3.8540764
CP-CCSD	QZ	8	1.4181	2659.427	3.7647821
CP-CCSD(T)	QZ	8	1.4204	2639.128	3.8217221
CCSD	AQZ	8	1.4167	2670.027	3.81386118
CCSD(T)	AQZ	8	1.4193	2653.310	3.86654158
CP-CCSD	AQZ	8	1.4184	2655.876	3.79072061
CP-CCSD(T)	AQZ	8	1.4211	2634.034	3.83417363

Table 9.30: HBr with 18 correlated electrons and a high truncation of the virtual space with and without counterpoise correction.

Method	Basis	corr. el.	R_e [Å]	ω_e [cm^{-1}]	D_e [eV]
CCSD	DZ	18	1.4108	2702.511	3.6110
CCSD(T)	DZ	18	1.4122	2686.047	3.6523
CP-CCSD	DZ	18	1.4204	2660.875	3.5020
CP-CCSD(T)	DZ	18	1.4226	2640.528	3.5331
CCSD	ADZ	18	1.4140	2684.633	3.6999
CCSD(T)	ADZ	18	1.4159	2665.000	3.7556
CP-CCSD	ADZ	18	1.4256	2631.347	3.5711
CP-CCSD(T)	ADZ	18	1.4285	2606.710	3.6063
CCSD	TZ	18	1.4093	2680.702	3.7621
CCSD(T)	TZ	18	1.4116	2658.044	3.8310
CP-CCSD	TZ	18	1.4135	2664.575	3.7065
CP-CCSD(T)	TZ	18	1.4162	2639.857	3.7554
CCSD	ATZ	18	1.4103	2680.281	3.7921
CCSD(T)	ATZ	18	1.4130	2655.373	3.8613
CP-CCSD	ATZ	18	1.4154	2654.576	3.7207
CP-CCSD(T)	ATZ	18	1.4185	2627.327	3.7675
CCSD	QZ	18	1.4094	2685.136	3.8226
CCSD(T)	QZ	18	1.4121	2659.579	3.8849
CP-CCSD	QZ	18	1.4118	2676.364	3.7927
CP-CCSD(T)	QZ	18	1.4148	2650.017	3.8475
CCSD	AQZ	18	1.4100	2682.994	3.8252
CCSD(T)	AQZ	18	1.4129	2656.461	3.9078
CP-CCSD	AQZ	18	1.4122	2670.425	3.8038
CP-CCSD(T)	AQZ	18	1.4154	2646.197	3.8525

Figure 9.15: The effect of a counterpoise correction on the bond length as a function of the basis set size for LiCs with 12 and 22 electrons explicitly correlated and a high and low truncation of the virtual space. The comparison has been made at the CCSD(T) level and performed as uncorrected data minus counterpoise corrected data (CCSD(T) - cp-CCSD(T)).

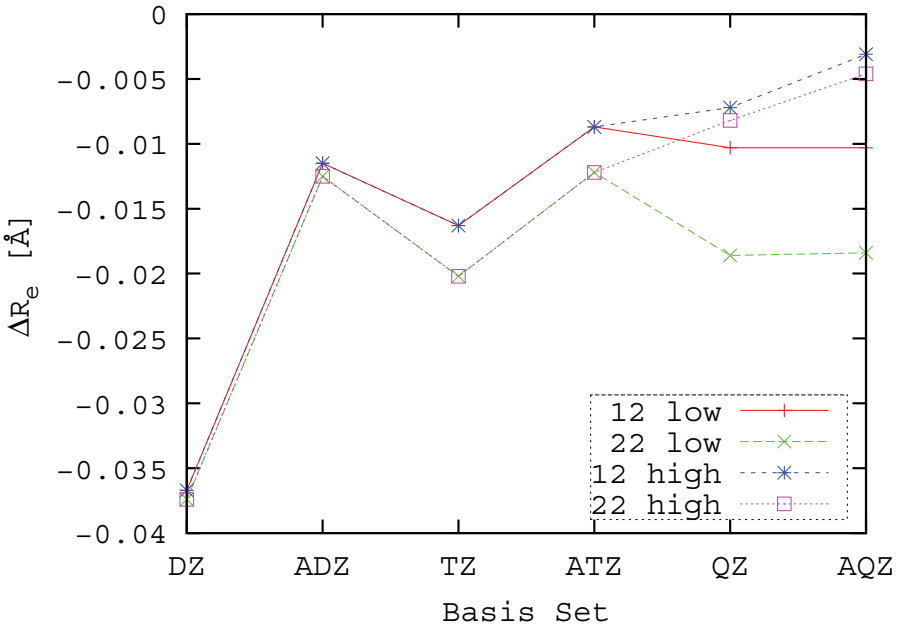

Figure 9.16: The effect of a counterpoise correction on the bond length as a function of the basis set size for HBr with 8 and 18 electrons explicitly correlated and a high and low truncation of the virtual space. The comparison has been made at the CCSD(T) level and performed as uncorrected data minus counterpoise corrected data (CCSD(T) - cp-CCSD(T)).

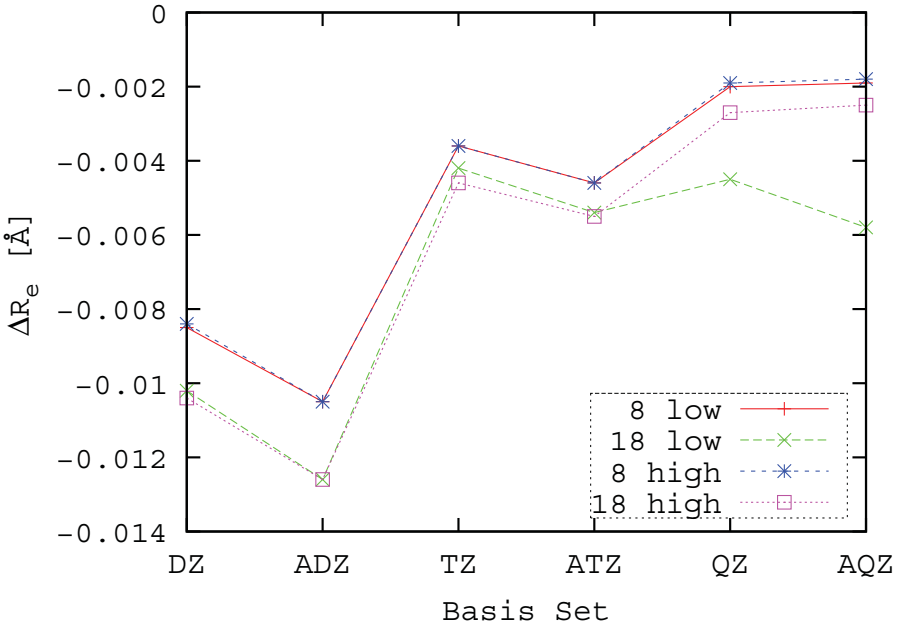

is observed. This opposite trend is expected to be caused by the significant difference in bondlength between LiCs and HBr. The polarizing functions stabilizes both the atomic and molecular calculations and would normally give an increase in the counterpoise correction, as seen for HBr, since these additional polarizing functions on the ghost atom would help to reduce the energy of the other atom. In LiCs the opposite is observed where the counterpoise correction decreases with the inclusion of augmenting functions. This decrease in counterpoise correction is due to the large bond length in LiCs where the polarizing function has stabilized the atom and the ghost atom is too far away for the ghost polarizing functions to have a significant effect on the stabilized atom.

The Figures 9.17 and 9.18 show the effect of the counterpoise correction on the harmonic frequency. For LiCs we see that this correction is less than 0.5 cm^{-1} except for the DZ basis set where it amounts to 3 cm^{-1} and for the core-valence correlation calculation in the AQZ basis set with the low cutoff. It is again here seen that correlating the outer-core with fixed cutoff of the virtual space will lead to larger BSSE errors for larger basis sets. As is seen from Figure 9.29 the difference between the calculated harmonic frequency in the various basis sets is for LiCs small and the counterpoise correction could therefore also be expected to be small. The counterpoise correction of the harmonic frequency for HBr is around one magnitude larger than for LiCs. For HBr it is again seen that including polarizing functions increases the counterpoise correction which otherwise decrease with increasing cardinal number for the basis set. For the valence correlation calculation there is not any noticeable difference in the counterpoise correction except for the AQZ basis set. For the core-valence correlation calculation the difference between the high and the low cutoff becomes noticeable at the ATZ level and increases with basis set size. The counterpoise correction at the AQZ level for the low cutoff is in fact larger than in the DZ basis set. The core-valence calculation with the high cutoff instead approach the counterpoise correction for the valence correlation calculations.

The dissociation energy is a direct measure for the size of the counterpoise correction since the change here is identical to the size of the counterpoise correction on the energy when neglecting the differential change in the counterpoise correction on the bond length. For LiCs we see in Figure 9.19 the same pattern as before where the counterpoise correction for the calculation with the high truncation of the virtual space decreases when including polarizing functions and with increasing basis set size. Again the valence and core-valence

Figure 9.17: The effect of a counterpoise correction on the harmonic frequency as a function of the basis set size for LiCs with 12 and 22 electrons explicitly correlated and a high and low truncation of the virtual space. The comparison has been made at the CCSD(T) level and performed as uncorrected data minus counterpoise corrected data (CCSD(T) - cp-CCSD(T)).

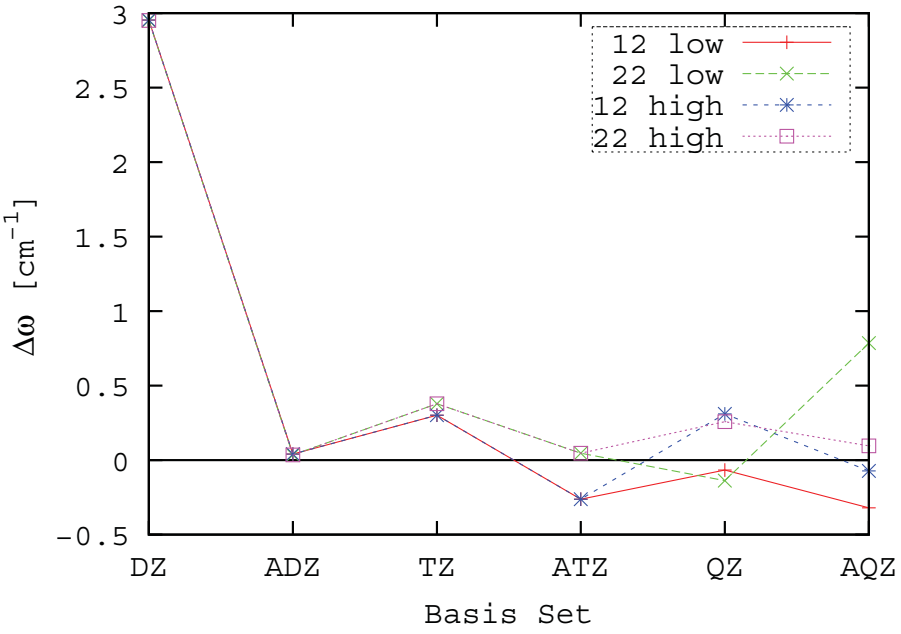

Figure 9.18: The effect of a counterpoise correction on the harmonic frequency as a function of the basis set size for HBr with 8 and 18 electrons explicitly correlated and a high and low truncation of the virtual space. The comparison has been made at the CCSD(T) level and performed as uncorrected data minus counterpoise corrected data (CCSD(T) - cp-CCSD(T)).

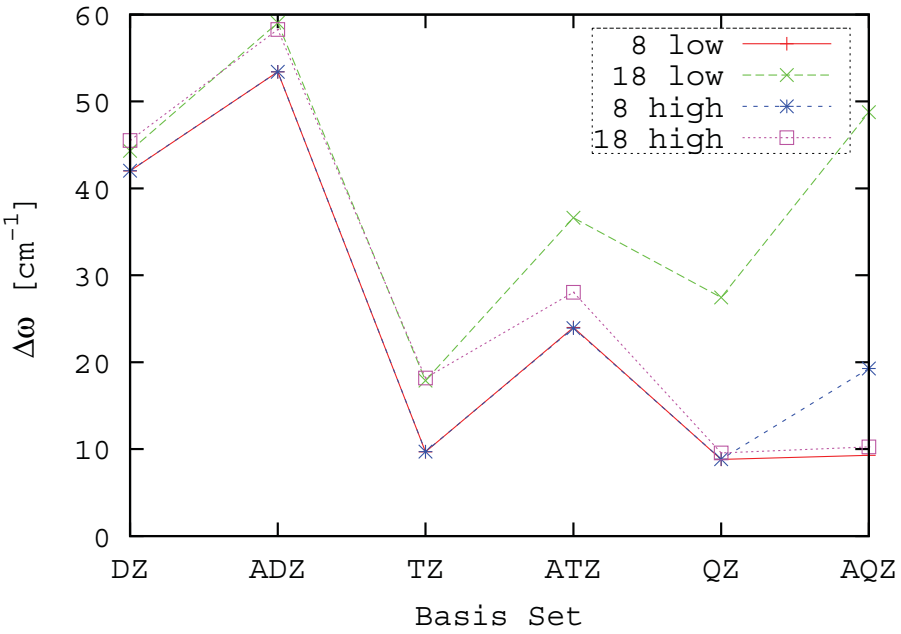

Figure 9.19: The effect of a counterpoise correction on the dissociation energy as a function of the basis set size for LiCs with 12 and 22 electrons explicitly correlated and a high and low truncation of the virtual space. The comparison has been made at the CCSD(T) level and performed as uncorrected data minus counterpoise corrected data (CCSD(T) - cp-CCSD(T)).

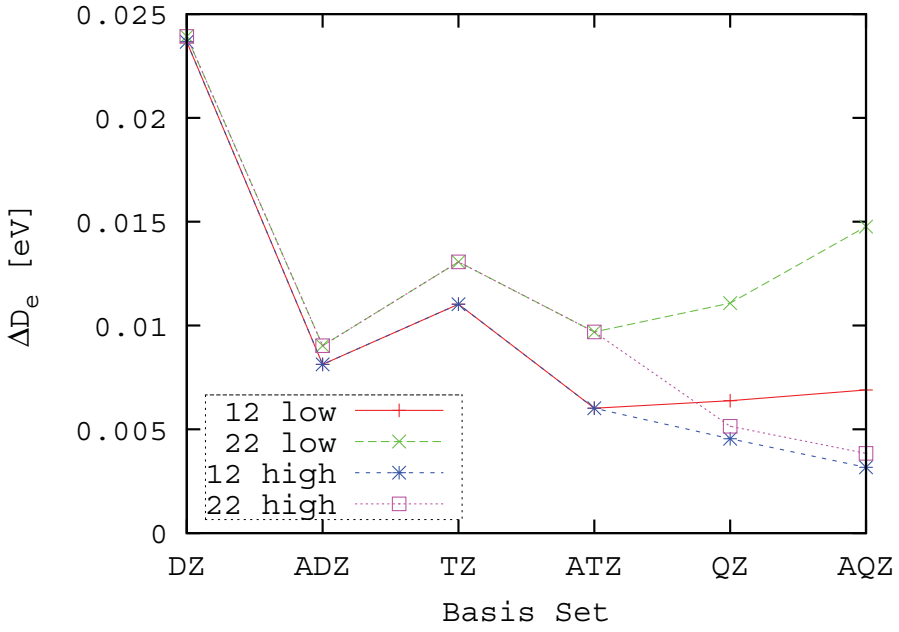

Figure 9.20: The effect of a counterpoise correction on the dissociation energy as a function of the basis set size for HBr with 8 and 18 electrons explicitly correlated and a high and low truncation of the virtual space. The comparison has been made at the CCSD(T) level and performed as uncorrected data minus counterpoise corrected data (CCSD(T) - cp-CCSD(T)).

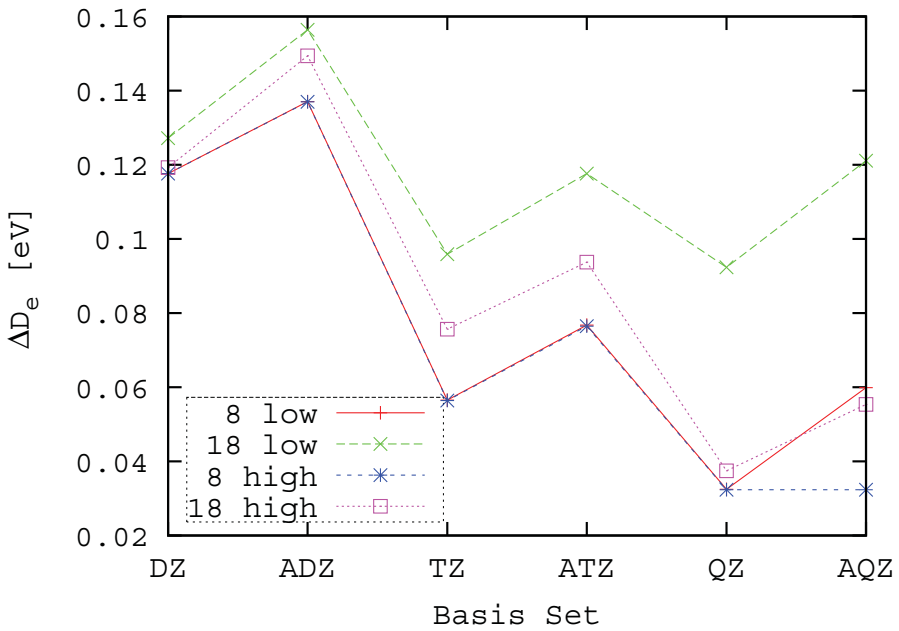

calculations with the high cutoff approach each other with increasing basis set size. For the calculations with the low cutoff we clearly see that increasing the basis set above ATZ does not diminish the counterpoise correction. For the core-valence calculations with the low cutoff the counterpoise correction again increases with the larger basis sets, which is in line with what has also been observed for the other spectroscopic properties. For HBr we see by comparing Figures 9.19 and 9.20 that the counterpoise correction is around one magnitude larger than for LiCs which is due to the significantly shorter bond of the HBr molecule. This is due to the counterpoise correction being dependant on distance. The counterpoise correction is observed to be decreasing with the distance since the basis functions on the ghost atom will at greater distance no longer be able help better the description of the atom. HBr shows the same trend for the dissociation energy as also seen for the bond distance and harmonic frequency where the polarizing functions increase the counterpoise correction and the core-valence correlation calculation with the low cutoff shows large corrections also for the large basis sets.

9.6.3.2 Core Contribution

In the first calculations with the spin-free coupled-cluster method carried out by the author [132] it was, to the author's surprise, seen that the contribution on the spectroscopic properties from the lowerlying $4d$ shell on Cs was very large. These calculations, however, showed unsystematic behavior with respect to increased correlation since the basis set used was simply insufficient. Later in [30] and also shown in Table 9.4 it was seen that this large contribution from the $4d$ shell on Cs in fact comes from the BSSE and would disappear when including a counterpoise correction. On the other hand, analyzing the results for HBr presented in [70] and Table 9.1 it is not offhand noticed whether the contribution from the $3d$ electrons on Br is overestimated. This could be the case since the truncation of the virtual space was there set at 10 E_h, so lower than the low truncation of the virtual space presented here and therefore the correlating functions for Br would not be included.

In Section 9.6.3.1 it was seen that including these lowerlying d electrons created a larger counterpoise correction and these could only be safely included when also increasing the cutoff of the virtual space. The objective here has been to determine the contribution of the d electrons are on the spectroscopic properties. In the figures in this section this

Figure 9.21: The effect of outer-core correlation on the bond length as a function of the basis set size for LiCs with (cp) and without a counterpoise correction and a high and low truncation of the virtual space. The comparison has been made at the CCSD(T) level and performed by subtracting the core-valence calculation results from the same type of valence calculations which then gives the effect of correlating the *d* electrons.

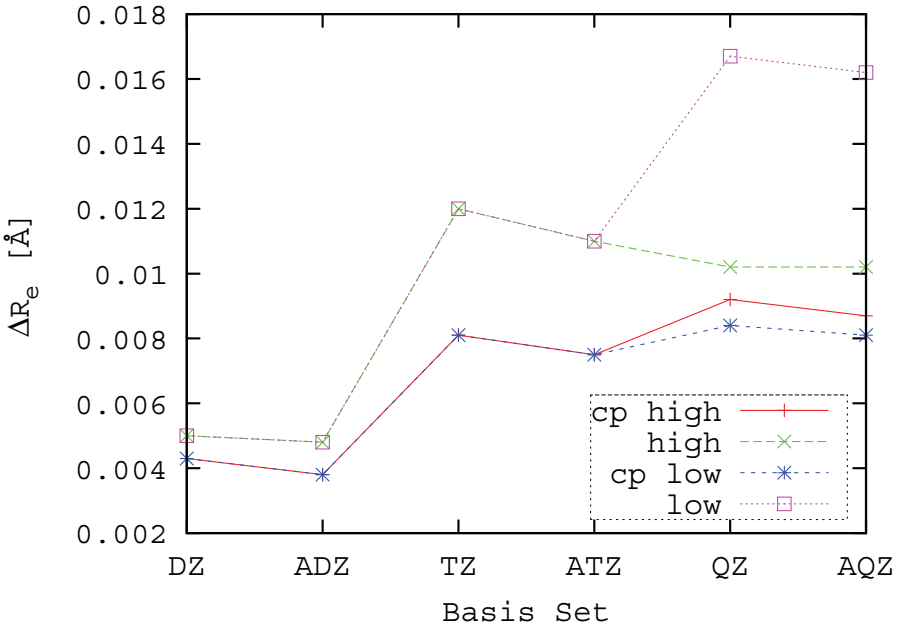

Figure 9.22: The effect of outer-core correlation on the bond length as a function of the basis set size for HBr with (cp) and without a counterpoise correction and a high and low truncation of the virtual space. The comparison has been made at the CCSD(T) level and performed by subtracting the core-valence calculation results from the same type of valence calculations which then gives the effect of correlating the *d* electrons.

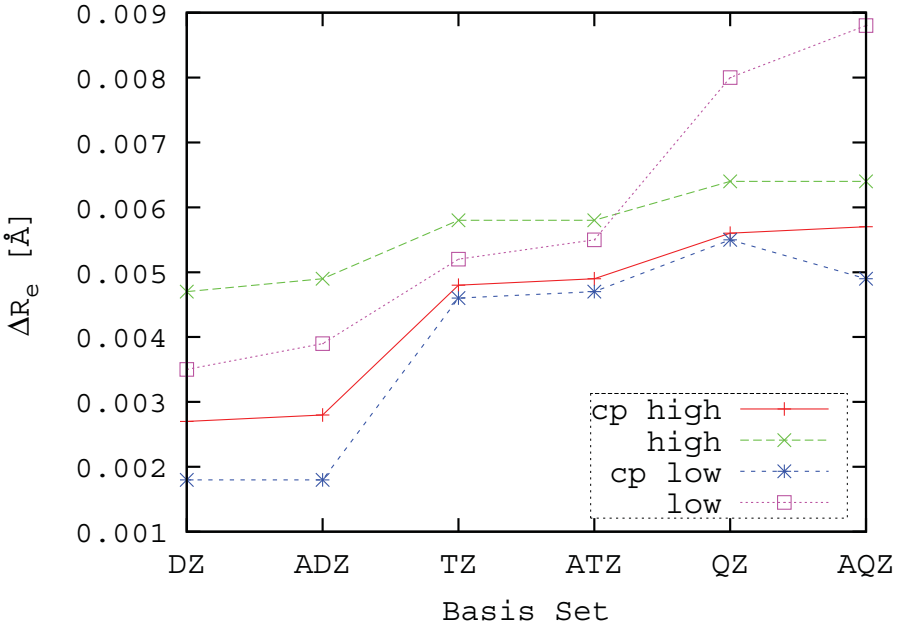

will be examined by subtracting core-valence calculation results from the same type of valence calculations to find the effect of correlating the d electrons has on the spectroscopic properties. This has been done both for the calculations with and without counterpoise correction. The influence of the lowerlying d electrons on the bond length for LiCs and HBr is presented in Figures 9.21 and 9.22, respectively. We here see that the influence from the d electrons increases with increased basis set and that the contribution is always reduced by a counterpoise correction. It is also noticeable how close the counterpoise corrected curves are despite the different truncation of the virtual orbitals for both LiCs and HBr. For both LiCs and HBr it is seen that the difference between the counterpoise corrected curve and the not counterpoise corrected curve increases with the basis set size for the low cutoff while for the high cutoff they again approach each other. It is also noted that the contribution from the d electrons on LiCs is about twice that for HBr and that the polarization functions only play a minor role unlike for the BSSE.

The changes in the harmonic frequency from including core-correlation is displayed in Figures 9.23 and 9.24. For LiCs, when including the counterpoise correction, this correction is, as expected, small and is stable around -0.3 to -0.4 cm^{-1} for the basis sets larger than TZ. It is again here seen that low truncation of the virtual space in the AQZ basis causes a larger shift in the harmonic frequency. For HBr the influence of the $3d$ electrons is around 10 cm^{-1} but but not completely converged with respect to basis set size. The low cutoff of the virtual space is for HBr giving an increasing exaggerated influence of the $3d$ electrons to the harmonic frequency when the basis set is increased.

From Figure 9.25 we see that with the low cutoff of the virtual space the importance of the outer-core correlation on the dissociation energy increases with increased basis set size. From the counterpoise corrected values we, however, see that this is due to an increased BSSE and with a counterpoise correction the importance of outer-core correlation drops around one magnitude in size. As could be expected we here also see a large discrepancy between the high and the low cutoff of the virtual for the calculations without a counterpoise correction. The counterpoise correction, however, seems to recover the importance of the outer-core correlation regardless of the truncation of the virtual space. For HBr in Figure 9.26 the trend is very similar to LiCs where the calculation with the low cutoff of the virtual space sees an increase in the importance of outer-core correlation with increasing basis set size. This effect of outer-core correlation is also seen for the

Figure 9.23: The effect of outer-core correlation on the harmonic frequency as a function of the basis set size for LiCs with (cp) and without a counterpoise correction and a high and low truncation of the virtual space. The comparison has been made at the CCSD(T) level and performed by subtracting the core-valence calculation results from the same type of valence calculations which then gives the effect of correlating the *d* electrons.

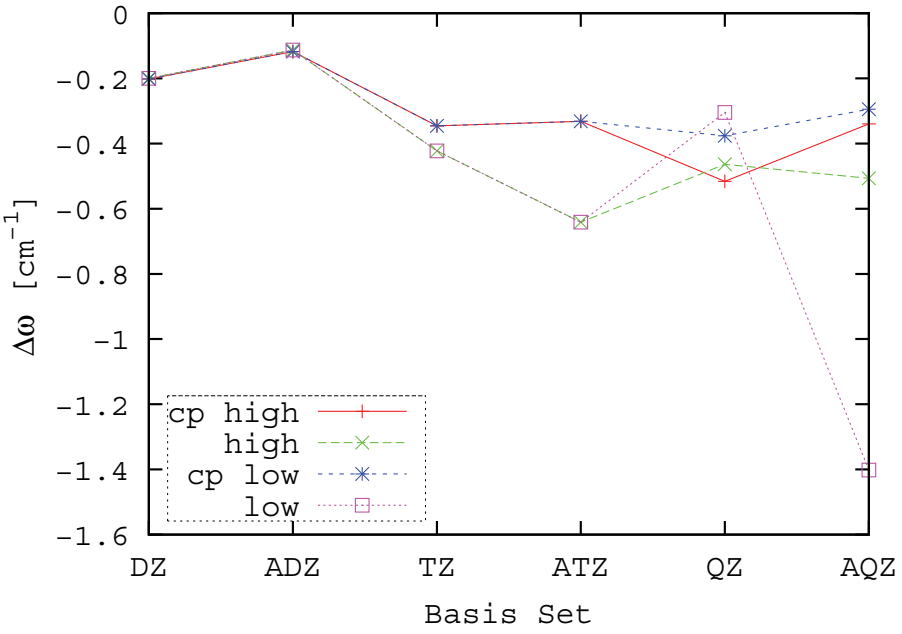

Figure 9.24: The effect of outer-core correlation on the harmonic frequency as a function of the basis set size for HBr with (cp) and without a counterpoise correction and a high and low truncation of the virtual space. The comparison has been made at the CCSD(T) level and performed by subtracting the core-valence calculation results from the same type of valence calculations which then gives the effect of correlating the *d* electrons.

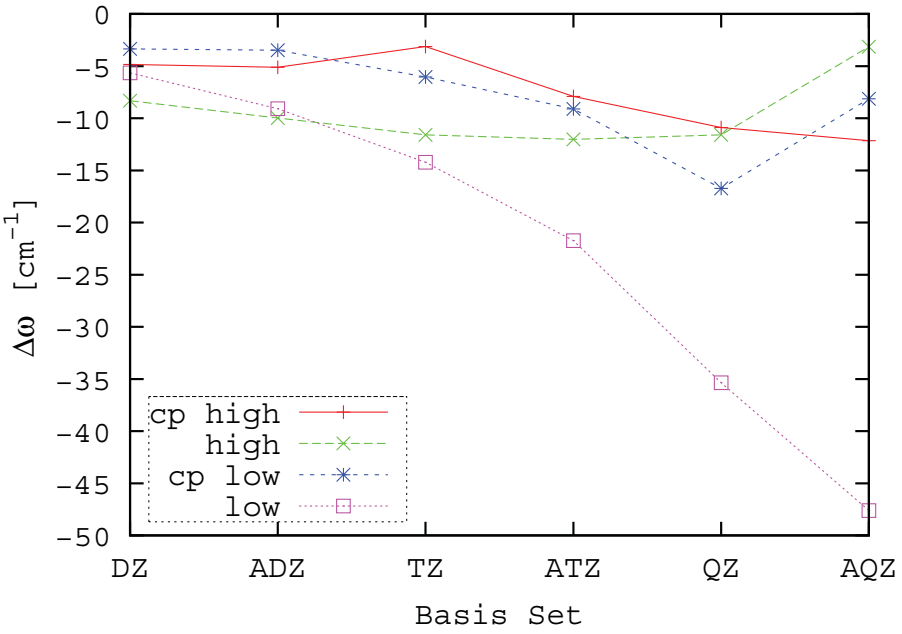

Figure 9.25: The effect of outer-core correlation on the dissociation energy as a function of the basis set size for LiCs with (cp) and without a counterpoise correction and a high and low truncation of the virtual space. The comparison has been made at the CCSD(T) level and performed by subtracting the core-valence calculation results from the same type of valence calculations which then gives the effect of correlating the *d* electrons.

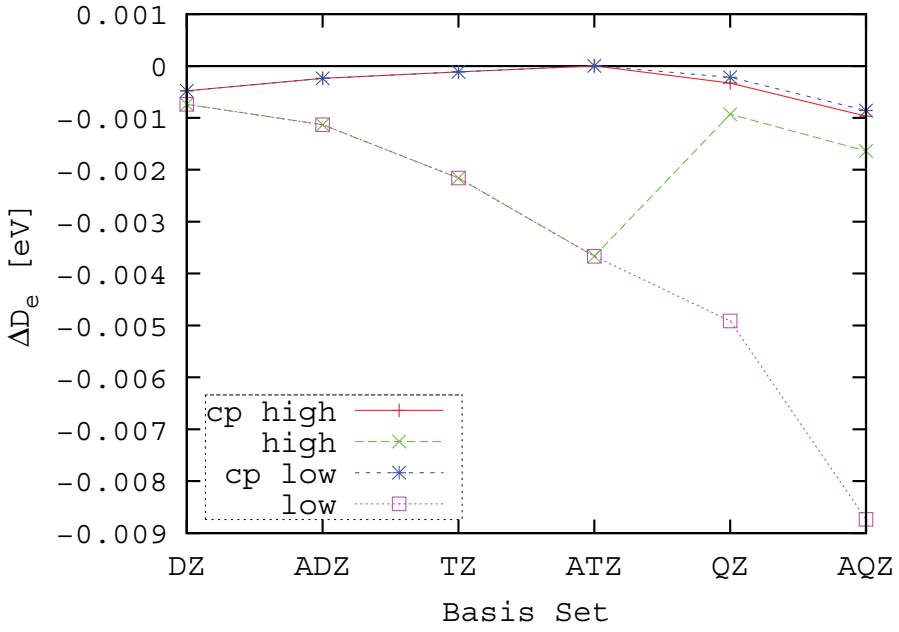

Figure 9.26: The effect of outer-core correlation on the dissociation energy as a function of the basis set size for HBr with (cp) and without a counterpoise correction and a high and low truncation of the virtual space. The comparison has been made at the CCSD(T) level and performed by subtracting the core-valence calculation results from the same type of valence calculations which then gives the effect of correlating the *d* electrons.

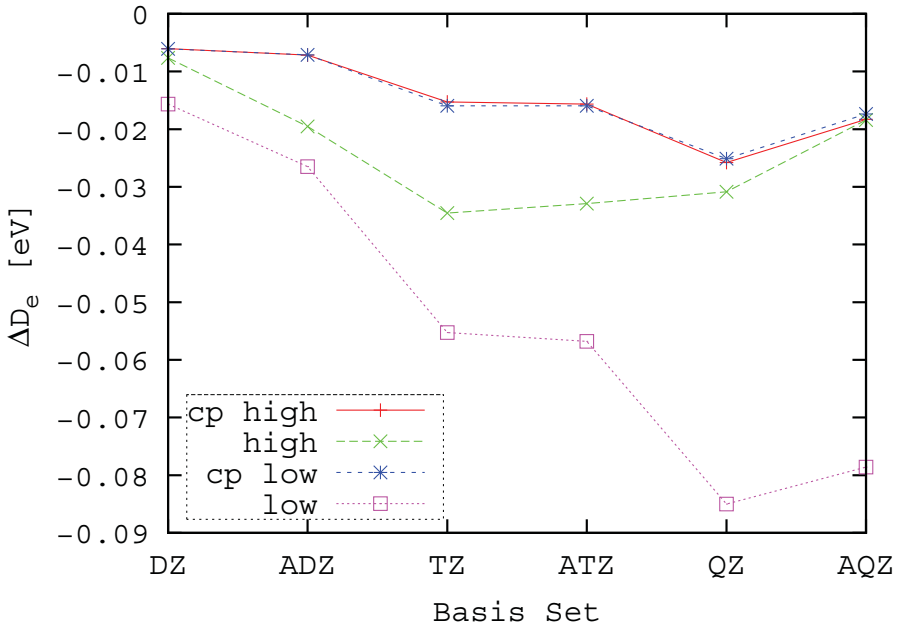

counterpoise corrected values though much smaller but still around one magnitude larger than for LiCs.

9.6.3.3 Comparison to Experiment

Although the aim of this study is not to provide accurate spectroscopic data from theory, but rather how data can be produced, it is of large interest to compare the various calculations to the experimental values to see how the CCSD(T) method converges with respect to basis set size, truncation of the virtual space and number of correlated electrons. The difference to experiment will be given as calculated minus experimental value.

In Figure 9.27, where the difference to experiment for the bond length is displayed for LiCs, we see that we approach the experimental value from the top when increasing the basis set except for the core-valence correlation calculation with the low cutoff. To obtain a very accurate bond length with errors below 0.01Å many variables have to be considered. For the calculations with the high cutoff it is seen that the counterpoise correction can be reduced to an error below 0.01Å when the largest basis sets are used. The inclusion of the $4d$ electrons in the correlation treatment is absolutely essential since the contribution from these are around 0.01Å. To reduce the residual error below 0.01Å one must consider an even larger basis[1] with an even higher cutoff of the virtuals along with a higher truncation in the coupled-cluster hierarchy and correlation of the $4d$ electrons. Here correlation will most likely give the largest contribution based on the large difference between the CCSD and the CCSD(T) results. For HBr the determination of the bond length with an error bar below 0.01Å is significantly easier and clearly demonstrated in Figure 9.28. In Figure 9.28 we see little variation with respect to basis set size, however, significant improvement can be made by including the $3d$ electrons into the correlation treatment where the error bars can be reduced below 0.005Å. While the absolute error in the bond length for HBr is significantly smaller than in LiCs the relative error is around the same size.

Since there is no experimental harmonic frequency available the harmonic frequency for LiCs has been plotted without subtracting these. A clear trend where the harmonic frequency is increasing with the size of the basis set is observed though the spread between the calculations also increases when neglecting the large spread at the DZ basis set level.

[1] These are not available.

Figure 9.27: The difference to experiment on the bond length as a function of the basis set size for LiCs with and without a counterpoise correction and a high (h) and low (l) truncation of the virtual space for 12 and 22 electrons correlated. The comparison has been made at the CCSD(T) level and performed by subtracting the experimental value from the calculated.

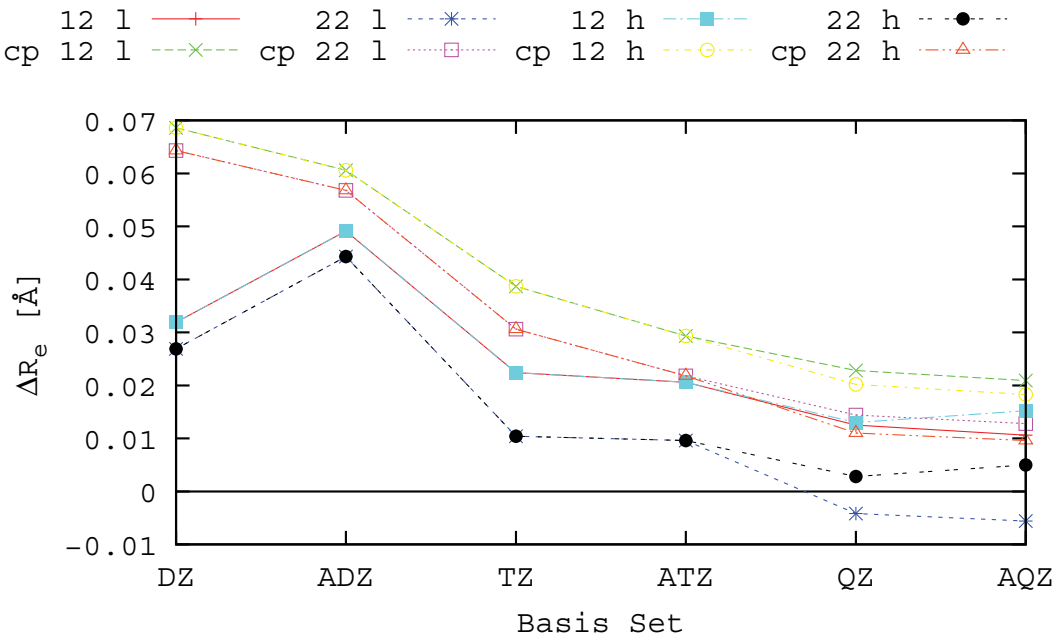

Figure 9.28: The difference to experiment on the bond length as a function of the basis set size for HBr with and without a counterpoise correction and a high (h) and low (l) truncation of the virtual space for 8 and 18 electrons correlated. The comparison has been made at the CCSD(T) level and performed by subtracting the experimental value from the calculated.

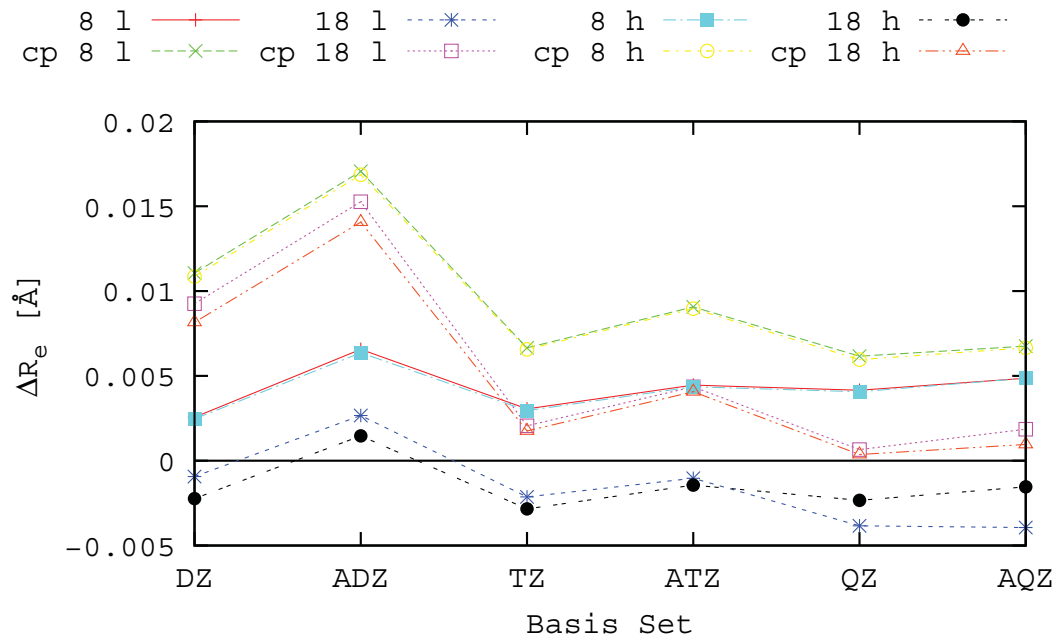

Figure 9.29: The harmonic frequency as a function of the basis set size for LiCs with and without a counterpoise correction and a high (h) and low (l) truncation of the virtual space for 12 and 22 electrons correlated performed at the CCSD(T) level of theory. No comparison to experiment has been made since no experimental value is known.

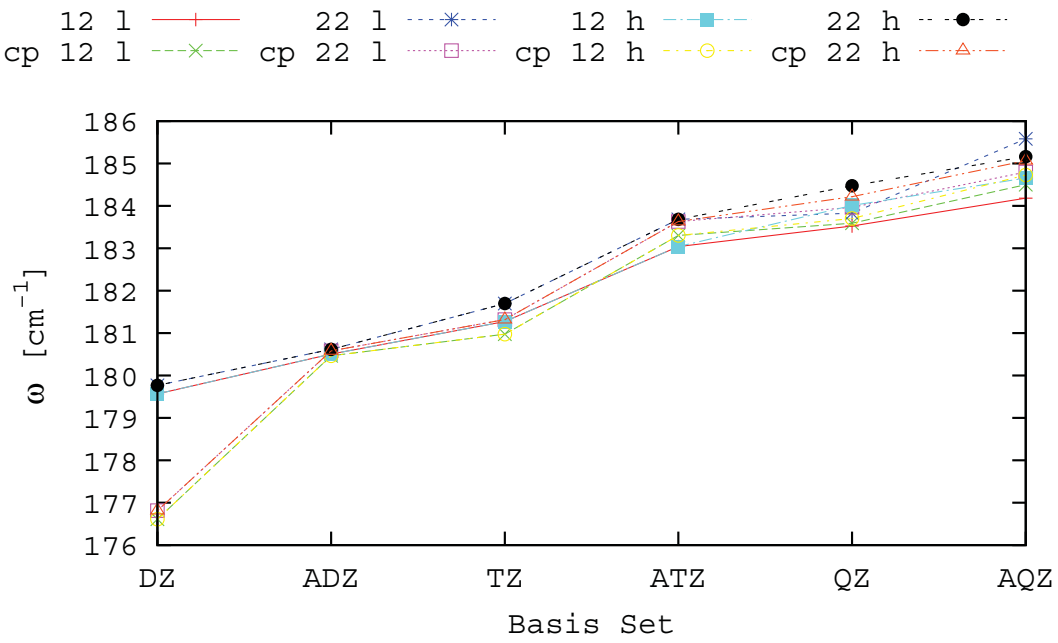

Figure 9.30: The difference to experiment on the harmonic frequency as a function of the basis set size for HBr with and without a counterpoise correction and a high (h) and low (l) truncation of the virtual space for 8 and 18 electrons correlated. The comparison has been made at the CCSD(T) level and performed by subtracting the experimental value from the calculated.

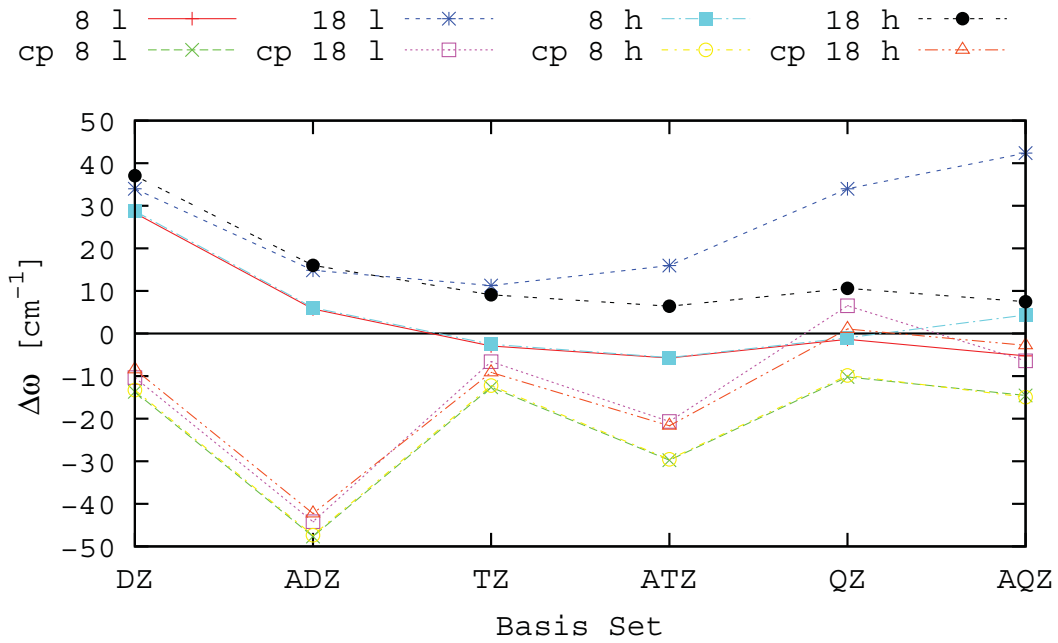

This is the opposite trend of what is seen when increasing the cluster hierarchy, see Tables 9.23, 9.24 ,9.25 and 9.26. The only type of calculation to show some irregular behavior is the core-valence calculation with the low cutoff of the virtual space which is not surprising since these calculations clearly overestimate the contribution from the $4d$ electrons as seen in Sections 9.6.3.1 and 9.6.3.2. The accuracy in the determination of the harmonic frequency for HBr is around one magnitude lower than that of LiCs as seen in Figure 9.30. It is clearly seen from Figure 9.30 that the counterpoise correction reduces the harmonic frequency and even for the large basis sets gives a contribution of around 10 cm^{-1} for the calculations with the high cutoff. For the valence correlation calculations no noticeable difference is observed between the high and low cutoff of the virtual space while the opposite is observed for the core-valence calculations.

The dissociation energy of LiCs is displayed in Figure 9.31 where we clearly see that the difference to the experimental value decreases with increasing basis set size. Again it is seen that the core-valence calculation with the low cutoff overshoots the dissociation energy but this is recovered well by the counterpoise correction. Here only minor differences are observed between the valence- and core-valence calculations with the high cutoff. For HBr we, one the other hand, see larger contributions from outer-core correlation as observed in Figure 9.32. Again the counterpoise correction has a very significant influence on the dissociation energy which, however, diminishes with increasing basis set size for the calculations with the high cutoff. Again it is seen that there is hardly any difference observed between the counterpoise correction from the high and low truncation of the virtual space.

9.6.4 Conclusion and Outlook

In this study the interplay between basis set, truncation of virtual space and number of correlated electrons has been examined in a systematic fashion on two very different molecules LiCs and HBr. It is shown that the errors in the calculations can be controlled when extending the basis set size of the calculation but that these extension errors are closely related to the truncation of the virtual space in particular when core-valence correlation is taken into consideration.

Figure 9.31: The difference to experiment on the dissociation energy as a function of the basis set size for LiCs with and without a counterpoise correction and a high (h) and low (l) truncation of the virtual space for 12 and 22 electrons correlated. The comparison has been made at the CCSD(T) level and performed by subtracting the experimental value from the calculated.

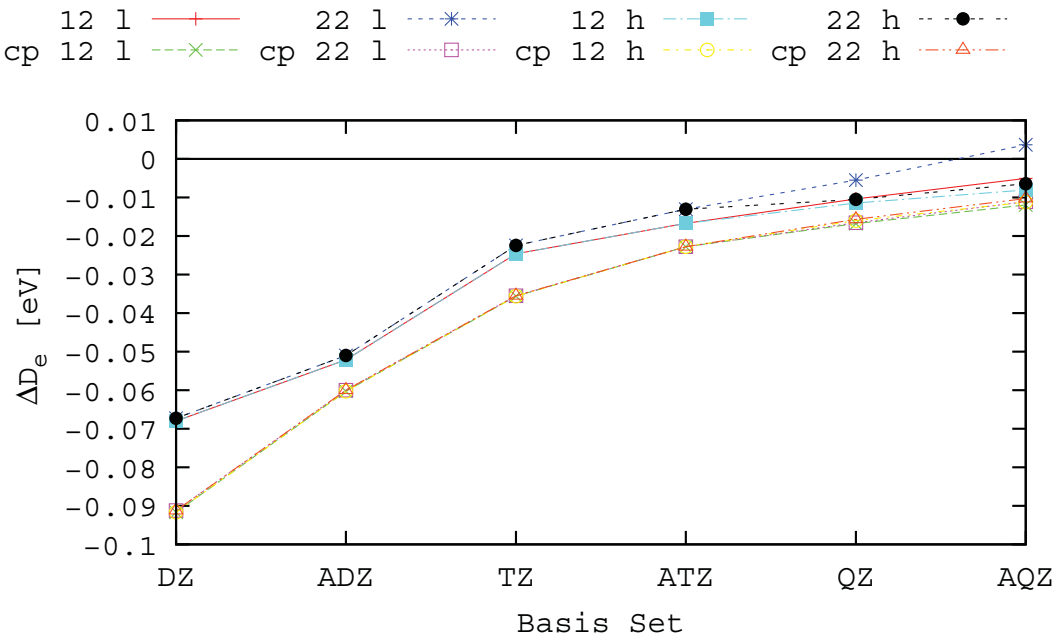

Figure 9.32: The difference to experiment on the dissociation energy as a function of the basis set size for HBr with and without a counterpoise correction and a high (h) and low (l) truncation of the virtual space for 8 and 18 electrons correlated. The comparison has been made at the CCSD(T) level and performed by subtracting the experimental value from the calculated.

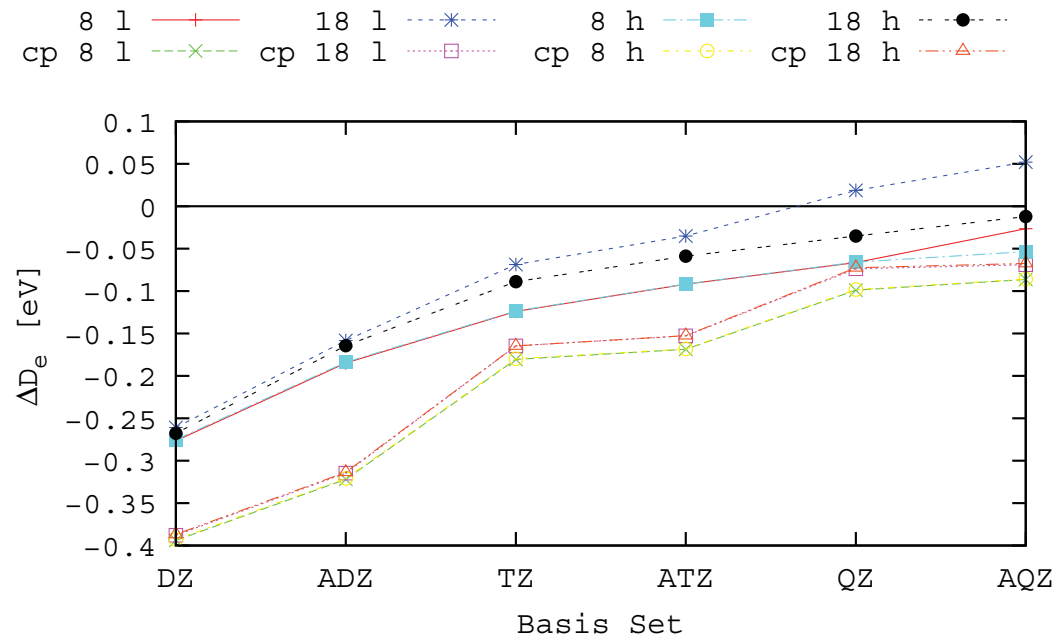

The BSSE is shown to be a persistent problem in performing accurate calculations. It increases with the number of correlated electrons. Increasing the cardinal number of the basis set without also increasing the truncation of the virtual space appears to be viable when only correlating the valence electrons provided that the truncation of the virtual space is set high enough[2]. When including core-valence correlation the BSSE can in the large basis (AQZ) in fact be larger than in the small basis sets. An improvement can only be achieved when the cardinal number of the basis set along with the truncation of the virtual space is increased. The augmentation of the basis set with polarizing functions can both increase or diminish the BSSE depending on the system. Since the by far largest counterpoise correction happens on the heavy center an augmentation of the basis set can the reduce the BSSE provided the bond distance to the heavy center is large. This is a case often seen in weakly bound systems. The BSSE, however, is visibly reduced when increasing the cardinal number of the basis set along with an increase in the truncation of the virtual space.

The outer-core contribution to the spectroscopic properties have proven very difficult, but not impossible, to capture. It is clearly demonstrated that when including lowerlying d electrons the truncation of the virtual space will have to be significantly increased in comparison to a valence only calculation. Furthermore all core-correlating functions should be included in the correlation treatment otherwise the importance of the outer-core will be grossly overestimated. While the contribution from the outer-core is small it is clearly essential to include when trying to achieve high accuracy though the cost in calculation time of doing so will dramatically increase.

Throughout a counterpoise correction has been made for all calculations at their given level of theory, basis set, truncation of virtual space and number of correlated electrons. What is very notable is how well this correction is capable of recovering the large BSSE that occurs for the core-valence calculation with the low cutoff so that the spectroscopic properties that can be directly derived from the shape of the potential energy curve. There do, however, appear to be limits for how much can be recovered which is seen in the difference between the counterpoise corrected core-valence calculations with

[2]This is a little vague formulation since even lower truncation of the virtual space, which is often seen in the literature, would have to be performed to see how accurate this statement is. It is definitely possible that the same behavior as for the core-valence calculations with the low cutoff would be observed if the truncation of the virtual space would be lower than what is used here.

the high and low cutoff. This difference is, nevertheless, smaller than the counterpoise correction itself even for the high cutoff. While the counterpoise correction works very well for the spectroscopic properties depending on the shape of the potential energy surface it should not be relied on to correct for basis set insufficiencies since it will not improve the wave function and any properties derived from it.

In the comparison to experiment for the CCSD(T) method it is clear that there still remains a difference to experiment larger than what is seen for the light elements. This difference is expected to be primarily from correlation and to a lesser extent finite basis set differences and approximations from the Hamiltonian since the difference between CCSD(T) and CCSD is large in these systems. Increasing the correlation level would be an enormous undertaking considering the scaling of the coupled-cluster hierarchy of O^nV^{n+2} and the many virtual spinors that need to be included for a balanced and guarantied better description than the CCSD(T) model. In the largest calculations performed here for HBr a total of 398 virtual spinors was included in the correlation step and another 174 virtuals still were left out from the truncation of the virtual space. For the LiCs the one-particle basis was even larger, namely 514 included virtual spinors and another 266 virtual spinors left out. Including this many virtual spinors and at the same time increasing the correlation level would be extremely time consuming task. Therefore a better selection of the virtual spinors than just the elementary cutoff at a energy threshold should be sought after to reduce the size of the calculation and still retain the accuracy provided by the basis set since brute force does not appear to be feasible. That not all virtuals give any significant contribution has already been seen in Table 9.17 for the $(RbBa)^+$ molecule where it was seen that including more virtuals did not give any significant change to the spectroscopic properties. A way to select virtuals has already been presented in the non-relativistic framework. There the virtuals were selected from an MP2 natural orbital (NO) occupation number calculation [214]. Recently this approach was implemented in the fully relativistic framework [179] in `DIRAC`. This way of selecting is expected also to work for core-valence correlation calculations since the correlation of the outer-core would also show up in the MP2 NO. The truncation of the virtual space would then follow from the magnitude of the MP2 NO's.

Summary and Outlook

Summarizing, this work combines the development of new codes with potential of providing results with unprecedented accuracy and precision, approximation methods to reduce the computational costs and a numerical investigation that will help guide the direction of highly accurate calculations towards a systematic improvement. Several examples of application have been shown on a large variety of molecular heavy-element compounds in their ground state. Although the implementation was the central goal from the onset further method development was achieved along with large scale applications.

The major achievements of this work is the implementation of the commutator-driven coupled-cluster code in the fully relativistic framework since this code has pushed the boundaries of the accuracy of correlation codes significantly further. This has been demonstrated in large-scale calculations even without having to push the code to the hardware limit of standard Linux clusters. Optimization of the code to reduce certain bottlenecks has given significant speed up and reduction in memory requirement. The implementation of the CI-driven coupled-cluster code has provided a simple and flexible test program for further developments of other approximations to the usual coupled-cluster hierarchy or the state-selective multireference coupled-cluster method. The spin-free programs have proven to be a valuable tool for an accurate determination of spectroscopic values for species with a Σ ground state.

Finding a way to systematically improve the result is essential when dealing with general-order codes since the pitfalls are plentiful and high accuracy and precision can only be achieved by knowing the errors in the calculation and knowing in which direction to go to improve these. The demonstration on how to reduce errors, their interplay and the magnitude of these is the cornerstone for a better employment of the developed codes.

Knowing the errors in the basis set, truncation of the virtual space and core cor-

relation, improvements in the correlation treatment can be addressed. Several schemes for approximations which can be used alone or in conjunction with others have been proposed and implemented. These approximations are expected to be a regular part of future applications once a numerical testing has been performed.

Interesting side projects in applications in the field of ultracold molecules have been performed. Here a way of reaching the rovibronic ground state via a two-step procedure was proposed for RbYb after an initial photoassociation. A non-radiative charge-transfer mechanism in the collision process of a Ba^+ ion and a Rb atom at very low temperatures yielding a Ba atom and a Rb^+ ion has been outlined qualitatively on the basis of the computed electronic excitation spectrum of the $(RbBa)^+$ molecular ion.

What remains to be done is further optimization of the commutator-driven coupled-cluster code. Here the collection of terms will need improvement for a more efficient code and along with a new sorting of integrals the memory demands would be significantly reduced.

A numerical investigation of the various approximation methods and for which classes of molecules these approximations can give significant reduction in computational timings without compromising the accuracy.

What will be in store for the future is the possibility to achieve higher accuracy in the calculation of properties on molecules containing heavy elements. Knowing the limitations of the approximations schemes and having a systematic way of ensuring an improved result will greatly enhance the predicative powers of the method. By extending the Dirac-Coulomb Hamiltonian with the Breit term along with a linear response module this accuracy and predicative power could also encompass the excited states.

Appendix A

Finite-Field Dipole Moment

The response of a molecular system to a weak external electric field ϵ can be treated as a perturbation to the field-free case. If the energy is expanded in a Taylor series around the field-free case

$$E(\epsilon) = E(\epsilon = 0) + \left.\frac{dE}{d\epsilon}\right|_{\epsilon=0} \epsilon + \frac{1}{2} \left.\frac{d^2E}{d\epsilon^2}\right|_{\epsilon=0} \epsilon^2 + \dots \ , \tag{A.1}$$

the first derivative of the energy E with respect to the external electric field ϵ taken at $\epsilon = 0$ is the static dipole moment of the molecule. Likewise can the second derivative be related to the static polarizability and higher derivatives to higher-order (hyper-)polarizabilities.

With the finite-field technique these analytical derivatives are approximated by a numerical derivative. To this end a small external electric field of varying field strength is applied and then a series of energy calculations is performed with these fields. By applying fields in various directions higher-order numerical derivatives can also be determined though these are not as accurate as the analytical ones.

The advantage of the derivative technique is that it holds also for approximate wavefunctions, which are typically dealt with in quantum chemistry, unlike the evaluation of properties by calculating expectation values in the Hellmann-Feynman theorem which differ from the correct value by the *wave function force*. [215]

List of Tables

List of Figures

Bibliography

[1] W. Greiner. *Relativistic Quantum Mechanics*. Springer, Berlin [et. al], 2000.

[2] P A M Dirac. The Quantum Theory of the Electron. *Proc. Roy. Soc.* **117**, 610 (1928).

[3] J Olsen. The initial implementation and applications of a general active space coupled cluster method. *J. Chem. Phys.* **113**, 7140 (2000).

[4] J W Krogh and J Olsen. A general coupled cluster study of the N_2 molecule. *Chem. Phys. Lett.* **344**, 578 (2001).

[5] M Kállay and P Surján. Higher excitations in coupled-cluster theory. *J. Chem. Phys.* **115**, 2945 (2001).

[6] M Kállay, P Szalay, and P Surján. A general state-selective multireference coupled-cluster algorithm. *J. Chem. Phys.* **117**, 980 (2002).

[7] K. G. Dyall and K. Fægri, Jr. *Introduction to Relativistic Quantum Chemistry*. Oxford University Press, New York [et. al], 2007.

[8] R E Moss. *Advanced Molecular Quantum Mechanics*. Chapman and Hall, London, 1973.

[9] P Pyykkö. Relativistic effects in structural chemistry. *Chem. Rev.* **88**, 563 (1988).

[10] M. Reiher and A. Wolf. *Relativistic Quantum Chemistry: The Fundamental Theory of Molecular Science*. Wiley-VCH, Weinheim, 2009.

[11] N Nemitz, F Baumer, F Münchow, S Tassy, and A Görlitz. Production of heteronuclear molecules in an electronically excited state by photoassociation in a mixture of ultracold yb and rb. *Phys. Rev. A* **79**, 061403 (2009).

[12] A Micheli, G K Brennen, and P Zoller. A toolbox for lattice-spin models with polar molecules. *Nature* **2**, 341 (2006).

[13] R Côté, V Kharchenko, and M D Lukin. Mesoscopic Molecular Ions in Bose-Einstein Condensates. *Phys. Rev. Lett.* **89**, 093001 (2002).

[14] O Dulieu, M Raoult, and E Tiemann. Cold Molecules; a chemistry kitchen for physicists? *J. Phys. B* **39 (19)** (2006).

[15] E A Cornell and C E Wieman. Bose-Einstein Condensation in a Dilute Gas: The First 70 Years and some Recent Experiments (Nobel Lecture). *Comp. Phys. Commun.* **3**, 476 (2002).

[16] J Doyle, B Friedrich, R V Krems, and F Masnou-Seeuws. Quo vadis, cold molecules? *Eur. Phys. J. D* **31**, 149 (2004).

[17] J J Hudson, B E Sauer, M R Tarbutt, and E A Hinds. Measurement of the Electron Electric Dipole Moment Using YbF Molecules. *Phys. Rev. Lett.* **89**, 023003 (2002).

[18] B C Regan, E D Commins, C J Schmidt, and D DeMille. New Limit on the Electron Electric Dipole Moment. *Phys. Rev. Lett.* **88**, 071805 (2002).

[19] T Zelevinsky, S Kotochigova, and J Ye. Precision Test of mass-Ratio Variations with Lattice-Confined Ultracold Molecules. *Phys. Rev. Lett.* **100**, 043201 (2008).

[20] S Schiller and V Korobov. Tests of time independence of the electron and nuclear masses with ultracold molecules. *Phys. Rev. A* **71**, 032505 (2005).

[21] W C Stwalley and H Wang. Photoassociation of Ultracold Atoms: A New Spectroscopic Technique. *J. Mol. Spectrosc.* **195**, 194 (1999).

[22] J D Weinstein, R deCarvalho, T Guillet, B Friedrich, and J M Doyle. Magnetic trapping of calcium monohydride molecules at millikelvin temperatures. *Nature* **395**, 148 (1998).

[23] H L Bethlem, G Berden, and G Meijer. Decelerating Neutral Dipolar Molecules. *Phys. Rev. Lett.* **83**, 1558 (1999).

[24] T Köhler, K Góral, and P S Julienne. Production of cold molecules via magnetically tunable Feshbach resonances. *Rev. Mod. Phys.* **78**, 1311 (2006).

[25] M Korek, A R Allouche, K Fakhreddine, and A Chaalan. Theoretical study of the electronic structure of LiCs, NaCs, and KCs molecules. *Can. J. Phys.* **78**, 977 (2000).

[26] D Edvardsson, S Lunell, and C M Marian. Calculation of potential energy curves for Rb_2 including relativistic effects. *Mol. Phys.* **101**, 2381 (2003).

[27] S Knecht, H J Aa Jensen, and T Fleig. Large-scale parallel configuration interaction. I. Non-relativistic and scalar-relativistic general active space implementation with application to $(Rb\text{-}Ba)^+$. *J. Chem. Phys.* **128**, 014108 (2008).

[28] R. J. Le Roy, LEVEL 8.0: *A Computer Program for Solving the Radial Schrödinger Equation for Bound and Quasibound Levels, University of Waterloo Chemical Physics Research Report CP-663 (2007); see http://leroy.uwaterloo.ca/programs/* . .

[29] S Azizi, M Aymar, and O Dulieu. Prospects for the formation of ultracold ground state polar molecules from mixed alkali atom pairs. *Eur. Phys. J. D* **31**, 195 (2004).

[30] L K Sørensen, T Fleig, and J Olsen. Spectroscopic and electric properties of the LiCs molecule. A coupled cluster study including higher excitations. *J. Phys. B* **42**, 165102 (2009).

[31] M Aymar and O Dulieu. Calculation of accurate permanent dipole moments of the lowest $^{1,3}\Sigma^+$ states of heteronuclear alkali dimers using extended basis sets. *J. Chem. Phys.* **122**, 204302 (2005).

[32] M Aymar, O Dulieu, and F Spiegelman. Electronic properties of francium diatomic compounds and prospects for cold molecule formation. *J. Phys. B* **39**, S905 (2006).

[33] Jean-Marc Lévy-Leblond. Nonrelativistic Particles and Wave Equations. *Commun. math. Phys.* **6**, 286 (1967).

[34] E J Baerends, W H E Schwarz, P Schwerdtfeger, and J G Snijders. Relativistic atomic orbital contractions and expansions: magnitudes and explanations. *J. Phys. B: At. Mol. Opt. Phys.* **23**, 3225 (1990).

[35] W H E Schwarz, E M van Wezenbeek, E J Baerends, and J G Snijders. The origin of relativistic effects of atomic orbitals. *J. Phys. B: At. Mol. Opt. Phys.* **22**, 1515 (1989).

[36] W H E Schwarz. Relativistic calculations of molecules; relativity and bond lengths. *Phys. Scr.* **36**, 403 (1987).

[37] Snijders and P Pyykkö. Is the relativistic contraction of bond lengths an orbital-contraction effect? *Chem. Phys. Lett.* **75**, 5 (1980).

[38] B A Heß, C M Marian, and S D Peyerimhoff. Ab initio calculation of spin-orbit effects in molecules including electron correlation. In *Modern Electronic Structure Theory, Part I*, edited by D R Yarkony, volume 2, page 152, World Scientific Publishing Co. Pte. Ltd., Singapur, 1995.

[39] A Messiah. In *Quantum Mechanics*, Dover, 1999.

[40] S. S. Schweber. *An Introduction to Relativistic Quantum Field Theory.* Dover, New York, 2005.

[41] P. Schwerdtfeger. *Relativistic Electronic Structure Theory Part 1. Fundamentals.* Elsevier, Amsterdam, 2002.

[42] C D Anderson. *Phys. Rev.* **41**, 405 (1932).

[43] K Pitzer. Relativistic effects on chemistry properties. *Acc. Chem. Res.* **12**, 271 (1979).

[44] J P Desclaux. Relativistic Dirac-Fock Expectation Values for Atoms with Z=1 to Z=120. *Atomic Data and Nuclear Data Tables* **12**, 311 (1973).

[45] L Visscher, O Visser, P J C Aerts, H Merenga, and W C Nieuwpoort. MOLFDIR, A relativistic Dirac-Fock-CI program package developed at the University of Groningen, http://hydra.chem.rug.nl/ broer/molfdir/molfdir.html. *Comp. Phys. Commun.* **81**, 120 (1994).

[46] G Karlström, R Lindh, P-Å Malmqvist, B O Roos, U Ryde, V Veryazov, P-O Widmark, M Cossi, B Schimmelpfennig, P Neogrády, and L Seijo. MOLCAS: a program package for computational chemistry. *Comp. Mater. Scien.* **28**, 222 (2003).

[47] M Kleinschmidt, J Tatchen, and C M Marian. Spin-Orbit Coupling of DFT/MRCI Wavefunctions: Method, Test Calculations, and Application to Thiophene. *J. Comput. Chem.* **23**, 824 (2002).

[48] M Kleinschmidt and C M Marian. Efficient generation of matrix elements for one–electron spin–orbit operators. *Chem. Phys.* **311**, 71–79 (2005).

[49] R Ahlrichs, M Bär, M Häser, H Horn, and C Kölmel. Electronic structure calculations on workstation computers: The program system turbomole. *Chem. Phys. Lett* **162**, 165–169 (1989).

[50] R M Pitzer and N W Winter. Electronic-structure methods for heavy-atom molecules. *J. Phys. Chem.* **92**, 3061 (1988).

[51] S Yabushita, Z Zhang, and R M Pitzer. Spin-orbit configuration interaction using the graphical unitary group approach and relativistic core potential and spin-orbit operators. *J. Phys. Chem.* **103**, 5791 (1999).

[52] MAGIC, a relativistic density functional quantum chemistry code, written by A Simper, A Willetts, A Ioannou, S Spencer, C Skylaris, L Gagliardi, University of Cambridge, UK (1998).

[53] ACES II, a CC and an MBPT suite of codes by J F Stanton, J Gauss, J D Watts, W J Lauderdale, and R J Bartlett, *Intern. J. Quantum Chem. Symp.***26**, 879 (1992), with contributions by J Almløf and P R Taylor (MOLECULE), T Helgaker, H J Jensen, P Jørgensen, J Olsen, P R Taylor (ABACUS), and D Bernholdt.

[54] M.W.Schmidt, K.K.Baldridge, J.A.Boatz, S.T.Elbert, M.S.Gordon, J.H.Jensen, S.Koseki, N.Matsunaga, K.A.Nguyen, S.Su, T.L.Windus, M.Dupuis, and J.A.Montgomery. General atomic and molecular electronic structure system. *J. Comput. Chem.* **14**, 1347 (1993).

[55] M.S.Gordon and M.W.Schmidt. Advances in electronic structure theory: Gamess a decade later. *Theory and Applications of Computational Chemistry: the first forty years* .

[56] B. Huron, J.-P. Malrieu, and P. Rancurel. *J. Chem. Phys.* **58**, 5745 (1973).

[57] DIRAC, a relativistic ab initio electronic structure program, Release DIRAC08 (2008), written by L. Visscher, H. J. Aa. Jensen, and T. Saue, with new contributions from R. Bast, S. Dubillard, K. G. Dyall, U. Ekström, E. Eliav, T. Fleig, A. S. P. Gomes, T. U. Helgaker, J. Henriksson, M. Iliaš, Ch. R. Jacob, S. Knecht, P. Norman, J. Olsen, M. Pernpointner, K. Ruud, P. Sałek, and J. Sikkema (see http://dirac.chem.sdu.dk).

[58] J Sucher. Foundations of the relativistic theory of many-electron atoms. *Phys. Rev. A* **22**, 348 (1980).

[59] G. E. Brown and D. G. Ravenhall. On the interaction of two electrons. *Proc. Roy. Soc.* **208**, 552–559 (1951).

[60] G Breit. The Effect of Retardation on the Interaction of Two Electrons. *Phys. Rev.* **34**, 553 (1929).

[61] J A Gaunt. The triplets of helium. *Proc. Roy. Soc.* **A122**, 513 (1929).

[62] T. Saue. Spin-interactions and the non-relativistic limit of electrodynamics'. *Adv. Quant. Chem.* **48**, 383 (2005).

[63] W. Kutzelnigg. Basis set expansion of the dirac operator without variatinal collapse. *Int. J. Quantum Chem.* **25**, 107 (1984).

[64] K G Dyall. An exact separation of the spin-free and spin-dependent terms of the Dirac-Coulomb-Breit Hamiltonian. *J. Chem. Phys.* **100**, 2118 (1994).

[65] L Visscher and E van Lenthe. On the distinction between scalar and spin–orbit relativistic effects. *Chem. Phys. Lett.* **306**, 357 (1999).

[66] T Fleig and L Visscher. Large-Scale Electron Correlation Calculations in Framework of the Spin-Free Dirac Formalism. The Au_2 Molecule Revisited. *Chem. Phys.* **311**, 113 (2005).

[67] T. Helgaker, P. Jørgensen, and J. Olsen. *Molecular Electronic-Structure Theory.* John Wiley & Sons, Ltd, Chichester [et al.], 2000.

[68] L. K. Sørensen, J. Olsen, and T. Fleig. 2- and 4-component relativistic generalized active space coupled-cluster. Implementation and application on BiH.

[69] H. A. Kramers. Théorie générale de la rotation paramagnétique dans les cristaux. *Proc. R. Acad. Amsterdam* **33**, 959–972 (1930).

[70] T Fleig, L K Sørensen, and J Olsen. A relativistic 4-component general-order multi-reference coupled cluster method: Initial implementation and application to HBr. *Theoret. Chem. Acc.* **118**, 347 (2007). DOI: 10.1007/s00214-007-0265-y.

[71] T Fleig, J Olsen, and C M Marian. The generalized active space concept for the relativistic treatment of electron correlation. I. Kramers-restricted two-component configuration interaction. *J. Chem. Phys.* **114**, 4775 (2001).

[72] T Fleig, J Olsen, and L Visscher. The generalized active space concept for the relativistic treatment of electron correlation. II: Large-scale configuration interaction implementation based on relativistic 2- and 4-spinors and its application. *J. Chem. Phys.* **119**, 2963 (2003).

[73] T Fleig, H J Aa Jensen, J Olsen, and L Visscher. The generalized active space concept for the relativistic treatment of electron correlation. III: Large-scale configuration interaction and multi-configuration self-consistent-field four-component methods with application to UO_2. *J. Chem. Phys.* **124**, 104106 (2006).

[74] L Visscher, K G Dyall, and T J Lee. Kramers-restricted closed-shell CCSD theory. *Int. J. Quantum Chem.: Quantum Chem. Symp.* **29**, 411 (1995).

[75] P Schwerdtfeger, editor. *Relativistic Electronic Structure Theory*, volume 1 : Fundamentals, chapter 6, page 291. Elsevier, Amsterdam, 2002. L Visscher, Post Dirac-Hartree-Fock methods - Electron Correlation.

[76] P Schwerdtfeger, editor. *Relativistic Electronic Structure Theory*, volume 1 : Fundamentals, chapter 5, page 259. Elsevier, Amsterdam, 2002. K Fægri and K G Dyall, Basis sets for relativistic calculations.

[77] R E Stanton and S Havriliak. Kinetic balance: A partial solution to the problem of variational safety in Dirac calculations. *J. Chem. Phys.* **81**, 1910 (1984).

[78] K. G. Dyall, I. P. Grant, and S. Wilson. Matrix representation of operator products. *J. Phys. B* **17**, 493–503 (1984).

[79] Jan Almlöf. Direct methods in electronic structure theory. In *Modern Electronic Structure Theory, Part I*, edited by D R Yarkony, volume 2, page 110, World Scientific Publishing Co. Pte. Ltd., Singapur, 1995.

[80] Trygve Helgaker and Peter R. Taylor. Gaussian basis sets and molecular integrals. In *Modern Electronic Structure Theory, Part II*, edited by D R Yarkony, volume 2, page 752, World Scientific Publishing Co. Pte. Ltd., Singapur, 1995.

[81] L Visscher, J C Aerts, O Visser, and W C Nieuwpoort. Kinetic Balance in Contracted Basis Sets for Relativistic Calculations. *Int. J. Quantum Chem.: Quantum Chem. Symp.* **25**, 131 (1991).

[82] J Paldus and X Li. A critical assessment of coupled cluster method in quantum chemistry. In *Advances in Chemical Physics*, edited by I Prigogine and S A Rice, volume 110, pages 1–175, John Wiley & Sons, Inc., 1997.

[83] R J Bartlett. Recent advances in coupled cluster methods. In *Recent Advances in Computational Chemistry*, volume 3, World Scientific, Singapore, 1997.

[84] R J Bartlett and M Musial. Coupled-cluster theory in quantum chemistry. *Rev. Mod. Phys.* **79**, 291 (2007).

[85] Lasse K. Sørensen. Konvergens i multireference perturbationstheori. Thesis, Department of Chemistry, University of Aarhus, 2003.

[86] M Heckert, M Kállay, and J Gauss. Molecular equilibrium geometries based on coupled-cluster calculations including quadruple excitations. *Mol. Phys.* **103**, 2109 (2005).

[87] T A Ruden, T Helgaker, P Jørgensen, and J Olsen. Coupled-cluster connected quadruples and quintuples corrections to the harmonic vibrational frequencies and equilibrium bond distances of hf, n-2, f-2, and co. *J. Chem. Phys.* **121**, 5874 (2004).

[88] L Thøgersen and J Olsen. A coupled cluster and full configuration interaction study of cn and cn-. *Chem. Phys. Lett.* **393**, 36 (2004).

[89] A Halkier, W Klopper, T Helgaker, P Jørgensen, and P R Taylor. Basis set convergence of the interaction energy of hydrogen-bonded complexes. *J. Chem. Phys.* **111**, 9157 (1999).

[90] T Helgaker, T A Ruden, P Jørgensen, J Olsen, and W Klopper. A priori calculation of molecular properties to chemical accuracy. *J.Phys. Org. Chem.* **17**, 913 (2004).

[91] Jr T H Dunning. Gaussian basis sets for use in correlated molecular calculations. I. The atoms boron through neon and hydrogen. *J. Chem. Phys.* **90**, 1007 (1989).

[92] R A Kendall, T H Dunning, Jr, and R J Harrison. Electron affinities of the first-row atoms revisited. Systematic basis sets and wave functions. *J. Chem. Phys.* **96**, 6796 (1992).

[93] D E Woon and T H Dunning Jr. Gaussian basis sets for use in correlated molecular calculations. III. The atoms aluminum through argon. *J. Chem. Phys.* **98**, 1358 (1993).

[94] M Heckert, M Kállay, D P Tew, W Klopper, and J Gauss. Basis-set extrapolation techniques for the accurate calculation of molecular equilibrium geometries using coupled-cluster theory. *J. Chem. Phys.* **125**, 44108 (2006).

[95] A Tajti, P G Szalay, A G Császár, M Kállay, J Gauss, E F Valeev, B A Flowers, J Vázquez, and J F Stanton. Heat: High accuracy extrapolated *ab initio* thermochemistry. *J. Chem. Phys.* **121**, 11599 (2004).

[96] Y J Bomble, J Vázquez, M Kállay, C Michauk, P G Szalay, A G Császár, J Gauss, and J F Stanton. High-accuracy extrapolated *ab initio* thermochemistry. || . minor improvements to the protocol and a vital simplification. *J. Chem. Phys.* **125**, 64108 (2006).

[97] M E Harding, J Vázquez, B Ruscic, A K Wilson, J Gauss, and J F Stanton. High-accuracy extrapolated *ab initio* thermochemistry. |||. additional improvement and overview. *J. Chem. Phys.* **128**, 114111 (2008).

[98] S Coriani, D Marchesan, J Gauss, C Hättig, T Helgaker, and P Jørgensen. A priori calculation of molecular properties to chemical accuracy. *J.Phys. Org. Chem.* **17**, 913 (2004).

[99] Jeppe Olsen, 2005. unpublished.

[100] M Nooijen, K R Shamasundar, and D Mukherjee. Reflections on size-extensivity, size-consistency and generalized extensivity in many-body theory. *Mol. Phys.* **103**, 2277 (2005).

[101] V Hurtubise and K F Freed. The algebra of effective hamiltonians and operators: Exact operators. *Adv. Chem. Phys.* , 465 (1993).

[102] V Hurtubise and K F Freed. The algebra of effective hamiltonians and operators: Truncated operators and computational aspects. *J. Chem. Phys.* **99**, 7946 (1993).

[103] B Jeziorski and H J Monkhorst. Coupled-cluster method for multideterminantal reference states. *Phys. Rev. A* **24**, 1668 (1981).

[104] E Eliav, A Borschevsky, K R Shamasundar, S Pal, and U Kaldor. Intermediate hamiltonian hilbert space coupled cluster method: Theory and pilot application. *Int. J. Quantum Chem.* **109**, 2909 (2009).

[105] F. A. Evangelista, A. C. Simmonett, W. D. Allen, H. F. Schaefer, and J. Gauss. Triple excitations in state specific multireference coupled cluster theory. application of mk-mrccsdt and mk-mrccsdt-n methods to model systems. *J. Chem. Phys.* **128**, 124104 (2008).

[106] K Bhaskaran-Nair, O Demel, and J Pittner. Multireference state-specific mukherjee's coupled cluster method with noniterative triexcitations. *J. Chem. Phys.* **129**, 184105 (2008).

[107] D Mukherjee, R K Moitra, and A Mukhopadhyay. Correlation problem in open-shell atoms and molecules a non-perturbative linked cluster formulation. *Mol. Phys.* **30**, 1861 (1975).

[108] L Visscher, E Eliav, and U Kaldor. Formulation and implementation of the relativistic Fock-space coupled-cluster method for molecules. *J. Chem. Phys.* **115**, 9720 (2001).

[109] A Landau, E Eliav, and U Kaldor. Intermediate Hamiltonian Fock-space coupled-cluster method. *Chem. Phys. Lett.* **313**, 399 (1999).

[110] M Musial and R J Bartlett. Fock space multireference coupled cluster method with full inclusion of connected triples for excitation energies. *J. Chem. Phys.* **121**, 1670 (2004).

[111] A Landau, E Eliav, Y Ishikawa, and U Kaldor. Mixed-sector intermediate Hamiltonian Fock-space coupled-cluster approach. *J. Chem. Phys.* **121**, 6634 (2004).

[112] I Lindgren. A coupled-cluster approach to the many-body perturbation theory for open-shell systems. *Int. J. Quantum Chem.* , 33 (1978).

[113] R Chaudhuri, D Mukhopadhyay, and D Mukherjee. Applications of open-shell coupled cluster theory using an eigenvalue-independent partitioning technique: Approximate inclusion of triples in IP calculations. *Chem. Phys. Lett.* **162**, 393 (1989).

[114] E Eliav, M J Vilkas, Y Ishikawa, and U Kaldor. Extrapolated intermediate hamiltonian coupled-cluster approach: Theory and pilot application to electron affinities of alkali atoms. *J. Chem. Phys.* **122**, 224113 (2005).

[115] N Oliphant and L Adamowicz. Multireference coupled-cluster method using a single-reference formalism. *J. Chem. Phys.* **94**, 1229 (1991).

[116] N Oliphant and L Adamowicz. The implementation of the multireference coupled-cluster method based on the single-reference formalism. *J. Chem. Phys.* **96**, 3739 (1991).

[117] L. K. Sørensen, T. Fleig, and J. Olsen. Relativistic 4- and 2-component generalized-active-space coupled cluster, 2009. accepted.

[118] A Köhn and J Olsen. Coupled-cluster with active space selected higher amplitudes: Performance of seminatural orbitals for ground and excited state calculations. *J. Chem. Phys.* **125**, 174110 (2006).

[119] M Kállay and J Gauss. Calculation of excited-state properties using general coupled-cluster and configuration-interaction models. *J. Chem. Phys.* **121**, 9257 (2004).

[120] Y J Bomble, J C Saeh, J F Stanton, P Szalay, M Kállay, and J Gauss. Equation-of-motion coupled-cluster methods for ionized states with an approximate treatment of triple excitations. *J. Chem. Phys.* **122**, 154107 (2005).

[121] A Engels-Putzka and M Hanrath. Multi-reference coupled-cluster study of the potential energy surface of the hydrogen fluoride dissociation including excited states. **902**, 59 (2009).

[122] M Hanrath and A Engels-Putzka. A multi-reference coupled-cluster study on the potential energy surface of N-2 including ground and excited states: spin projections and wavefunction overlaps. *Theoret. Chim. Acta* **122**, 197 (2009).

[123] T Saue, K Fægri, T Helgaker, and O Gropen. Principles of direct 4-component relativistic scf: application to caesium auride. *Mol. Phys.* **91**, 937 (1997).

[124] T Saue and H J Aa Jensen. Quaternion symmetry in relativistic molecular calculations: The Dirac-Hartree-Fock method. *J. Chem. Phys.* **111**, 6211 (1999).

[125] L Visscher, T J Lee, and K G Dyall. Formulation and implementation of a relativistic unrestricted coupled-cluster method including noniterative connected triples. *J. Chem. Phys.* **105**, 8769 (1996).

[126] J D Talman. Minimax Principle for the Dirac Equation. *Phys. Rev. Lett.* **57**, 1091 (1986).

[127] Program LUCIA, a general CI code written by J Olsen, University of Aarhus, with contributions from H. Larsen and M. Fülscher.

[128] 1999, 2002. LUCITA is a direct CI program written by J Olsen, *MOLCAS* interface by T Fleig, 1999, *DIRAC* interface by T Fleig, 2002.

[129] J Olsen, B O Roos, P Jørgensen, and H J Aa Jensen. Determinant based configuration interaction algorithms for complete and restricted configuration interaction spaces. *J. Chem. Phys.* **89**, 2185 (1988).

[130] J. Thyssen, T. Fleig, and H. J. Aa. Jensen. A direct relativistic four-component multi-configuration self-consistent-field method for molecules. *J. Chem. Phys.* **129**, 034109 (2008).

[131] S Knecht, H J Aa Jensen, and T Fleig. Large-scale parallel configuration interaction. II.Four-component double-group general active space implementation with application to BiH, 2009. submitted to *J. Chem. Phys.*.

[132] T Fleig and L K Sørensen. A Relativistic 4-Component Multi-Reference Coupled Cluster Method. Application to the CsLi Molecule. In *NIC Symposium 2006*, edited by G Münster, D Wolf, and M Kremer, volume 32, pages 91–98, NIC Series, ISBN 3-00-017351-X, 2006.

[133] B A Heß. Applicability of the no-pair equation with free-particle projection operators to atomic and molecular structure calculations. *Phys. Rev. A* **32**, 756 (1985).

[134] B A Heß. Relativistic electronic-structure calculations employing a two-component no-pair formalism with external field projection operators. *Phys. Rev. A* **33**, 3742 (1986).

[135] A Wolf, M Reiher, and B A Hess. The generalized Douglas-Kroll transformation. *J. Chem. Phys.* **117**, 9215 (2002).

[136] Written by H. J. Aa. Jensen, T. Saue, L. Visscher with contributions from V. Bakken, E. Eliav, T. Enevoldsen, T. Fleig, O. Fossgaard, T. Helgaker, J. Laerdahl, C. V. Larsen, P. Norman, J. Olsen, M. Pernpointner, J. K. Pedersen, K. Ruud, P. Salek, J. N. P. van Stralen, J. Thyssen, O. Visser, and T. Winther. "DIRAC04, a relativistic ab initio electronic structure program, release dirac04.0 (2004)", 2004.

[137] K Andersson, M Barysz, A Bernhardsson, M R A Blomberg, D L Cooper, T Fleig, M P Fülscher, C de Graaf, B A Hess, G Karlström, R Lindh, P-Å Malmqvist, P Neogrády, J Olsen, B O Roos, A J Sadlej, M Schütz, B Schimmelpfennigand L Seijo, L Serrano-Andrés, P E M Siegbahn, J Stålring, T Thorsteinsson, V Veryazov, and P-O Widmark. molcas version 5., 2000. Lund University, Sweden.

[138] L Visscher, J Styszyński, and W C Nieuwpoort. Relativistic and correlation effects on molecular properties. 2. The hydrogen halides HF, HCl, HBr, HI, and HAt. *J. Chem. Phys.* **105**, 1987 (1996).

[139] K P Huber and G Herzberg. *Molecular Spectra and Molecular Structure, IV, Constants of Diatomic Molecules*. Van Nostrand Reinhold Company, New York, London, Melbourne, 1979.

[140] J Styszyński. Relativistic core-valence correlation effects on molecular properties of the hydrogen halide molecules. *Chem. Phys. Lett.* **317**, 351 (2000).

[141] K G Dyall. Relativistic and nonrelativistic finite nucleus optimized triple-zeta basis sets for the 4 *p* , 5 *p* and 6 *p* elements. *Theoret. Chem. Acc.* **108**, 335 (2002).

[142] K G Dyall. Relativistic quadruple-zeta and revised triple-zeta and double-zeta basis sets for the 4 *p*, 5 *p*, and 6 *p* elements. *Theoret. Chem. Acc.* **115**, 441 (2006).

[143] H Stoll, B Metz, and M Dolg. Relativistic energy-consistent pseudopotentials - recent developments. *J. Comp. Chem.* **23**, 767 (2001).

[144] K Balasubramanian. Relativistic configuration interaction calculations of the low-lying states of bih. *Chem. Phys. Lett.* **114**, 201 (1985).

[145] K Balasubramanian. Relativistic quantum calculations of spectroscopic properties of bih. *J. Mol. Spectrosc.* **115**, 258 (1986).

[146] A B Alekseyev, R J Buenker, HP Liebermann, and G Hirsch. Spin-orbit configuration interaction study of the potential energy curves and radiative lifetimes of the low-lying states of bismuth hydride. *J. Chem. Phys.* **100**, 2989 (1994).

[147] G A DiLabio and P A Christiansen. Low-lying 0^+ states of bismuth hydride. *Chem. Phys. Lett.* **277**, 473 (1997).

[148] B Lindgren and Ch Nilsson. On the spectra of bih and bid. *J. Mol. Spectrosc.* **55**, 407 (1975).

[149] A Heimer. Über das bandenspektrum des wismuthydrids. *Z. Phys.* **95**, 328 (1935).

[150] A Heimer and E Hulthén. Band spectrum of bismuth hydride. *Nature* **127**, 557 (1931).

[151] E Hulthén and A Heimer. Spectrum of bismuth hydride. *Nature* **129**, 399 (1932).

[152] H G Hedderich and P F Bernath. Infrared emission spectroscopy of bismuth monohydride and bismuth monodeuteride. *J. Mol. Spectrosc.* **158**, 170 (1993).

[153] RD Urban, P Polomsky, and H Jones. A reassessment of the ground-state infrared spectrum of bih and bid. *Chem. Phys. Lett.* **181**, 485 (1991).

[154] A M R P Bopegedera, C R Brazier, and P F Bernath. Diode laser spectroscopy of bih and bid. *Chem. Phys. Lett.* **162**, 301 (1989).

[155] G Herzberg. *Molecular Spectra and Molecular Structure.* Krieger Publishing Company, Malabar, Florida, 1989.

[156] A E Leanhardt, T A Pasquini, M Saba, A Schirotzek, Y Shin, D Kielpinski, D E Pritchard, and W Ketterle. Cooling Bose-Einstein Condensates Below 500 Picokelvin. *Science* **301**, 1513 (2003).

[157] J D Weinstein, R deCarvalho, T Guillet, B Friedrich, and J M Doyle. Four-Component Relativistic Coupled Cluster and Configuration Interaction Calculations on the Ground and Excited States of the RbYb molecule. *J. Phys. Chem. A* (2009). DOI: 10.1021/jp904914m.

[158] R González-Férez, M Mayle, and P Schmelcher. Rovibrational dynamics of LiCs dimers in strong electric fields. *Chem. Phys.* **329**, 203 (2006).

[159] M Aymar and O Dulieu. Calculation of accurate permanent dipole moments of the lowest $^{1,3}\Sigma^+$ states of heteronuclear alkali dimers using extended basis sets. *J. Chem. Phys.* **122**, 204302 (2005).

[160] S D Kraft, P Staanum, J Lange, L Vogel, R Wester, and M Weidemüller. Formation of ultracold LiCs molecules. *J. Phys. B* **39**, S993 (2006). DOI: 10.1088/0953-4075/39/19/S13.

[161] J Deiglmayr, A Grochola, M Repp, K Mörtlbauer, C Glück, J Lange, O Dulieu, R Wester, and M Weidemüller. Formation of Ultracold Polar Molecules in the Rovibrational Ground State. *Phys. Rev. Lett.* **101**, 133004 (2008).

[162] A Stein, A Pashov, P F Staanum, H Knöckel, and E Tiemann. The $B^1\Pi$ and $D^1\Pi$ states LiCs studied by Fourier-transform spectroscopy. *Eur. Phys. J. D* **48**, 177 (2008).

[163] P Staanum, A Pashov, H Knöckel, and E Tiemann. $X^1\Sigma^+$ and $a^3\Sigma^+$ states of LiCs studied by Fourier-transform spectroscopy. *Phys. Rev. A* **75**, 042513 (2007).

[164] L Visscher. Approximate molecular relativistic Dirac-Coulomb calculations using a simple Coulombic correction. *Theoret. Chem. Acc.* **98**, 68 (1997).

[165] S F Boys and F Bernardi. The calculation of small molecular interactions by the differences of separate total energies. some procedures with reduced errors. *Mol. Phys.* **19**, 553 (1970).

[166] M Korek, A R Allouche, K Fakhreddine, and A Chaalan. Theoretical study of the electronic structure of LiCs, NaCs, and KCs molecules. *Can. J. Phys.* **78**, 977 (2000).

[167] G Igel-Mann, U Wedig, P Fuentealba, and H Stoll. Ground-state properties of alkali dimers XY (X,Y = Li to Cs). *J. Chem. Phys.* **84**, 5007 (1986).

[168] L. K. Sørensen. A numerical study on the importance of including of outer-core correlation for LiCs and HBr. in preparation.

[169] A Halkier, W Klopper, T Helgaker, and P Jørgensen. Basis-set convergence of the molecular electric dipole moment. *J. Chem. Phys.* **111**, 4424 (1999).

[170] K P Huber and G Herzberg. *Molecular Spectra and Molecular Structure.* Van Nostrand Reinhold Company, New York, London, Melbourne, 1979.

[171] J Deiglmayr, M Aymar, R Wester, M Weidemüller, and O Dulieu. Calculations of static dipole polarizabilities of alkali dimers: Prospect for alignment of ultracold molecules. *J. Chem. Phys.* **129**, 064309 (2008).

[172] J M Amini and H Gould. High precision measurement of the static dipole polarizability of cesium. *Phys. Rev. Lett.* **91**, 153001 (2003).

[173] R W Molof, H L Schwartz, T M Miller, and B Bederson. Measurements of electric dipole polarizabilities of the alkali-metal atoms and the metastable noblegas atoms. *Phys. Rev. A* **10**, 1131 (1974).

[174] L W Wansbeek, B K Sahoo, R G E Timmermans, B. P. Das, and D. Mukherjee. *Ab initio* determination of polarizabilities and van der waals coefficients of li atoms using the relativistic coupled-cluster method. *Phys. Rev. A* **78**, 012515 (2008).

[175] S Tassy, N Nemitz, F Baumer, C Höhl, Batär, and A Görlitz. Sympathetic cooling in a mixture of diamagnetic and paramagnetic atoms. *arXiv:0709.0827v1 [physics.atom-ph],* (2007).

[176] E Eliav, U Kaldor, and Y Ishikawa. Transition energies of ytterbium, lutetium, and lawrencium by the relativistic coupled-cluster method. *Phys. Rev. A* **52**, 291 (1995).

[177] E Eliav, U Kaldor, and Y Ishikawa. Ionization potentials and excitation energies of the alkali-metal atoms by the relativistic coupled-cluster method. *Phys. Rev. A* **50**, 1121 (1994).

[178] J L Tilson, W C Ermler, and R M Pitzer. Parallel spin-orbit coupled configuration interaction. *Comput. Phys. Commun.* **128**, 128 (2000).

[179] S. Knecht, H. J. Aa Jensen, and L. K. Sørensen. Four-component MP2 natural orbitals: An efficient way of selecting appropiate active spaces for coupled cluster and multiconfigurational self-consistent field calculations. in preparation.

[180] A A Auer, G Baumgartner, D E Bernholdt, A Bibireata, V Choppella, D Cociorva, X Gao, R Harrison, S Krishnamoorthyand S Krishnan, C Lam, Q Lu, M Nooijen, R Pitzer, J Ramanujam, P Sadayappan, and A Sibiryakov. Automatic code generation for many-body electronic structure methods: the tensor contraction engine. *Mol. Phys.* **2**, 211 (2006).

[181] S. Knecht and H. J. Aa Jensen. A general-purpose parallel four-component Kramers-restricted CI property module. unpublished work.

[182] A. S. P. Gomes and K. G. Dyall. In preparation. Available from the Dirac web site, http://dirac.chem.sdu.dk.

[183] K.G. Dyall. In preparation. Available from the Dirac web site, http://dirac.chem.sdu.dk.

[184] K. G. Dyall. *Theoret. Chim. Acta* **99**, 366 (1998).

[185] http://old.iupac.org/reports/periodic_table.

[186] I Sioutis and R M Pitzer. Theoretical Investigation of the Binding Energies of the Iodide Ion and Xenon Atom with Decaborane. *J. Phys. Chem. A* **110**, 12528 (2006).

[187] F B van Duijneveldt, J G C M van Duijneveldt-van de Rijdt, and J H van Lenthe. State of the Art in Counterpoise Theory. *Chem. Rev.* **94**, 1873 (1994).

[188] G Chałasiński and M M Szczęśniak. State of the Art and Challenges of the ab Initio Theory of Intermolecular Interactions. *Chem. Rev.* **100**, 4227 (2000).

[189] T J Giese and D M York. High-Level Ab Initio Methods for Calculation of Potential Energy Surfaces of van der Waals Complexes. *Int. J. Quantum Chem.* **98**, 388 (2004).

[190] E F Laschuk, M M Martins, and S Evangelisti. Ab Initio Potentials For Weakly Interacting Systems: Homonuclear Rare Gas Dimers. *Int. J. Quantum Chem.* **95**, 303 (2003).

[191] Ralchenko, Yu; Kramida, A E; Reader, J. and NIST ASD Team (2008). NIST Atomic Spectra Database (version 3.1.5). Available: http://physics.nist.gov/asd3 (2009, May 3). National Institute of Standards and Technology, Gaithersburg, MD.

[192] I S Lim, W C Lee, and Y S Lee. Theoretical investigation of RbCs via two-component spin-orbit pseudopotentials: Spectroscopic constants and permanent dipole moment functions. *J. Chem. Phys.* **124**, 234307 (2006).

[193] Nils Nemitz. *Production and spectroscopy of ultracold YbRb* molecules.* Dissertation, Mathematisch-Naturwissenschaftliche Fakultät, Heinrich-Heine-Universität Düsseldorf, 2008.

[194] E Bodo and F A Gianturco. Ultra low-energy behavior of an ionic replacement reaction $^3He^4He^+ + {}^4He \rightarrow {}^4He_2^+ + {}^3He$. *Phys. Rev. A* **73**, 032702 (2006).

[195] R Côté and A Dalgarno. Ultracold atom-ion collisions. *Phys. Rev. A* **62**, 012709 (2000).

[196] P E Siska. Cold and ultracold ion-neutral inelastic collisions: Spin-orbit relaxation in He + Ne^+. *J. Chem. Phys.* **115**, 4527 (2001).

[197] E Wells, K D Carnes, B D Esry, and I Ben-Itzhak. Charge Transfer and Elastic Scattering in Very Slow H^++D(1s) Half Collisions. *Phys. Rev. Lett.* **86**, 4803 (2001).

[198] O. P. Makarov, R. Côté, H. Michels, and W. W. Smith. Radiative charge-transfer lifetime of the excited state of $(NaCa)^+$. *Phys. Rev. A* **67**, 042705 (2003).

[199] R. Coté, V. Kharchenko, and M. D. Lukin. Mesocopic molecular ions in Bose-Einstein condensates. *Phys. Rev. Lett.* **89**, 093001 (2002).

[200] J. Hecker Denschlag. University of Innsbruck (now University of Ulm), private communication, 2009. Project BaRbIe: An ion in a sea of ultracold neutral atoms, see also http://www.uibk.ac.at/exphys/ultracold/projects/barbi/index.html.

[201] M. Sabidó, J. de Andrés, J. Sogas, M. Alberti, J. M. Bofill, and A. Aguilar. Inelastic electronic excitation and electron transfer processes in collisions between $Mg(3^1S_0)$ atoms and $K^+(^1s_0)$ ions studied by crossed beams in the 0.10-3.80-kev energy range. *J. Chem. Phys.* **123**, 124314 (2005).

[202] M. Sabidó, J. de Andrés, J. Sogas, M. Alberti, J. M. Bofill, and A. Aguilar. Crossed ion-atom beam study of the inelastic collision processes between neutral $Mg(3^1S_0)$ atoms and $Cs^+(^1s_0)$ ions in the 0.05-4.20 kev energy range. *Phys. Chem. Chem. Phys.* **7**, 310 (2005).

[203] Stefan R. Knecht. *Parallel Relativistic Multiconfiguration Methods: New Powerful Tools for Heavy-Element Electronic-Structure Studies.* Dissertation, Mathematisch-Naturwissenschaftliche Fakultät, Heinrich-Heine-Universität Düsseldorf, 2009.

[204] L. K. Sørensen, S. Knecht, T. Fleig, and C. M. Marian. Four-Component Relativistic Coupled Cluster and Configuration Interaction Calculations on the Ground and Excited States of the RbYb Molecule. *J. Phys. Chem. A* **113**, 12607–12614 (2009).

[205] L Visscher and T Saue. Approximate relativistic electronic structure methods based on the quaternion modified Dirac equation. *J. Chem. Phys.* **113**, 3996 (2000).

[206] K.G. Dyall. Relativistic double-zeta, triple-zeta, and quadruple-zeta basis sets for the 4s, 5s, 6s, and 7s elements. *J. Phys. Chem. A* , in press (2009). (8 pages) *Available online*, DOI: 10.1021/jp905057q. Basis sets available from the Dirac web site, http://dirac.chem.sdu.dk.

[207] I. S. Lim, H. Stoll, and P. Schwerdtfeger. Relativistic small-core energy-consistent pseudopotentials for the alkaline-earth elements from Ca to Ra. *J. Chem. Phys.* **124**, 034107 (2006).

[208] Andrzej Sadlej. Program WFFIT. University of Torun.

[209] Jr. C. W. Bauschlicher, S. P. Walch, and H. Partridge. On correlation in the first row transition metal atoms. *J. Chem. Phys.* **76**, 1033–1039 (1982).

[210] A. Landau, E. Eliav, Y. Ishikawa, and U. Kaldor. Intermediate Hamiltonian Fock-space coupled-cluster method: Excitation energies of barium and radium. *J. Chem. Phys.* **113**, 9905–9910 (2000).

[211] A. Landau, E. Eliav, Y. Ishikawa, and U. Kaldor. Intermediate Hamiltonian Fock-space coupled cluster method in the one-hole one-particle sector: Excitation energies of xenon and radon. *J. Chem. Phys.* **115**, 6862–6865 (2001).

[212] Y. Ralchenko, A. E. Kramida, J. Reader, and NIST ASD Team (2008). NIST Atomic Spectra Database (version 3.1.5). Available: http://physics.nist.gov/asd3 (retrieved May 3rd, 2009). National Institute of Standards and Technology, Gaithersburg, MD.

[213] *NIST Chemistry WebBook* (version 69, 2005) National Institute of Standards and Technology, Gaithersburg, MD.

[214] H. J. Aa. Jensen, P. Jørgensen, H. Ågren, and J. Olsen. Second-order Møller-Plesset perturbation theory as a configuration and orbital generator in multiconfiguration self-consistent field calculations. *J. Chem. Phys.* **88**, 3834–3839 (1988).

[215] P Pulay. Analytical derivative techniques and the calculation of vibrational spectra. In *Modern Electronic Structure Theory, Part II*, edited by D R Yarkony, volume 2, page 1191, World Scientific Publishing Co. Pte. Ltd., Singapur, 1995.

List of Abbreviations

BSSE	Basis set superposition error
CAS	Complete active spaces
CC	Coupled Cluster
CCSD	Coupled Cluster Singles Doubles
CCSD(T)	Coupled Cluster Singles Doubles perturbative Triples
CCSDT	Coupled Cluster Singles Doubles Triples
CI	Configuration interaction
CP	Counterpoise
DCHF	Dirac-Coulomb Hartree-Fock
DKH	Douglas-Kroll-Hess
DFT	Density functional theory
FSCC	Fock-space coupled cluster
GAS	Generalized active spaces
GASCI	Generalized active spaces configuration interaction
IHFSCC	Intermediate Hamiltonian Fock-space coupled cluster
KR-MCSCF	Kramers-restricted multiconfigurational self-consistent-field
LL	Lévy-Leblond
MP2	Møller-Plesset second order
MR	Multireference
MRCC	Multireference coupled cluster
MRCI	Multireference configuration interaction
RAS	Restricted active spaces
SF	Spin-free
SFDC	Spin-free Dirac Coulomb
SR	Single-reference

Acknowledgement

Acknowledgment - Vielen Dank ...

... Christel M. Marian, for accepting the ungrateful job of taking over the supervision of my Ph.D. work despite the fact you left this line of research years ago. I am not really sure what the outcome of this work would have been had you not accepted this. I at least hope that you found this trip back to your roots an interesting one. Your knowledge on applications has clearly given me new insights into how this should be performed and discussed.

... Jeppe Olsen, for the co-supervision of my thesis work. I see now that I should have talked to you much sooner about the problems I have experienced during my time as a Ph.D. student. You were clearly the only one with whom this project could be discussed.

... Stefan Knecht, my room mate for the excellent discussions and cooperation we have had during these last years. In particular your technical knowledge and willingness to share this has been a great help for me. I truly look forward to new and interesting projects with you.

... Martin Kleinschmidt, for your technical help, hospitality, good cuisine and your "hail Mary" style of tabletop football. And of course for taking the most of the teaching a load of my shoulder in the last phase of my work.

... Natalie Gilka, whom for a long time was the first and sole author of this manuscript but in the end was left out.

... Peter Taylor, for tips, technical support and encouragement.

... Stephan Raub, for technical support with GAUSS. Always be on good terms with the system administrator.

... Klaus Eifert, my computer is doing something strange. Could you have a look at it?

... Andre Gomes, for programming and showing me how to use the low memory sorter in RELCCSD. Without this the last section of this thesis would not have been possible.

... Mihajlo Etinski, for a solid game of tabletop football. You are up next.
... Karin Schuck, for helping with my paperwork.
... the entire theoretical chemistry group, for making for a friendly working atmosphere.
... the whole DIRAC community for a stimulating annual meeting.

... Susanne, for making it worthwhile for me to have come here to Düsseldorf. Your help and support throughout has been immeasurable. I hope we again will find more time for each other in Denmark since I would really like you also to see my place of origin.
... Moar of far, for jeres støtte og for at lade mig følge mine egne mål.

Dansk tryghed er at have en øloplukker tøjret til sin gyngestol.

Benny Andersen